Non-perturbative study of QCD correlators

Alexey Lokhov

CENTRE DE PHYSIQUE THÉORIQUE - ÉCOLE POLYTECHNIQUE

THÈSE DE DOCTORAT DE L'ÉCOLE POLYTECHNIQUE

Spécialité: **PHYSIQUE THÉORIQUE**

présentée par

Alexey Lokhov

pour obtenir le grade de

Docteur de l'École polytechnique

Sujet:

Étude non-perturbative des corrélateurs en chromodynamique quantique

Soutenue le 8 juin 2006 devant le jury composé de:

MM.	Ulrich Ellwanger,	rapporteur
	Georges Grunberg,	
	Olivier Pène,	
	Silvano Petrarca,	rapporteur
	Claude Roiesnel,	directeur de thèse
	André Rougé,	
&	Jean - Bernard Zuber,	président du jury

Remerciements

Je tiens tout d'abord à exprimer ma gratitude à Olivier Pène et Claude Roiesnel pour m'avoir accepté en thèse, et pour l'avoir dirigée de manière très impliquée. Je suis également très reconnaissant à mes collègues Philippe Boucaud, Damir Bećirević, Jean - Pierre Leroy, Alain Le Yaouanc, Jacques Micheli et Jose Rodríguez - Quintero pour leur disponibilité, leur aide et leur soutien.

Je remercie Patric Mora, Dominique Schiff et Henk Hilhorst de m'avoir accueilli au sein des laboratoires CPHT et LPT qu'ils dirigent.

Je suis reconnaissant à Jean - Bernard Zuber qui m'a fait l'honneur de présider le jury, ainsi qu'à Ulrich Ellwanger et Silvano Petrarca qui ont accépté d'écrire un rapport sur cette thèse. Je remercie très sincèrement les autres membres du jury Georges Grunberg, Olivier Pène, Claude Roiesnel et André Rougé.

J'ai naturellement une pensée pour Vladimir I. Shelest, Yuri L. Bashkatov, Vladimir V. Ivanov, Valery G. Serbo, Ludmila N. Chusovitina, ainsi que Alain Aspet, Costas Bachas, Michel Davier, Pierre Fayet et André Rougé qui ont éveillé ma curiosité scientifique et dont l'enseignement m'a formé en tant que chercheur.

Mes remerciements vont au personnel du secrétariat et aux informaticiens pour leur travail qui assure un fonctionnement idéal du laboratoire.

J'ai partagé beaucoup de moments agréables avec les doctorants (et docteurs) Stéphane Afchain, Nicolas Bernal, Benoît Blossier, Thorsten Brüntjen, Paramita Dey, Pascal Grange, Liguori Jego, François - Xavier Josse - Michaux, Xavier Lacroze, Yacine Mehtar - Tani, Hervé Moutarde, Domenico Orlando, Chloé Papineau, Emmanuel Serié, Mathieu Segond, Ritesh Singh, Cristina Timirgaziu, Barbara Tumpach, Fabien Vignes - Tourneret.

J'ai également une pensé pour mes collègues seniors Igor Anikin, Claude de Calan et Gregory Korchemsky, ainsi que pour mes amis Alexandre, Alexeï K., Alexeï M., Denis, Martijn, Olexandre et Redamy.

Enfin j'exprime toute ma gratitude à ma famille, et particulièrement à ma mère et à Maria, pour leur soutien pendant de nombreuses années.

Contents

Notations and conventions **6**

General introduction **9**

1 Continuum and lattice QCD **11**
1.1 General features of QCD 11
1.1.1 Definitions and symmetries 11
1.1.2 The Gribov ambiguity 13
1.1.3 Schwinger-Dyson equations 15
1.1.4 Slavnov-Taylor identities 18
1.1.5 Renormalisation group equations 19
1.2 Lattice QCD 20
1.2.1 Lattice QCD partition function 20
1.2.2 Fixing the Minimal Landau gauge on the lattice 22

2 Lattice Green functions **27**
2.1 Green functions in Landau gauge 27
2.2 Numerical calculation of the ghost Green functions in Landau gauge 30
2.2.1 Lattice implementation of the Faddeev-Popov operator 30
2.2.2 Numerical inversion of the Faddeev-Popov operator 31
2.2.3 Calculation of the ghost-gluon vertex 33
2.3 Errors of the calculation 34
2.3.1 Estimating the statistical error 34
2.3.2 Handling the discretisation errors 34
2.4 Gribov ambiguity and lattice Green functions 36
2.4.1 The landscape of minima of the gauge-fixing functional . . . 37
2.4.2 Lattice Green functions and the Gribov ambiguity 40

3 The ultraviolet behaviour of Green functions **45**
3.1 Λ_{QCD} and perturbative expressions for Green functions 46
3.2 OPE for the Green functions and dominant power corrections 48
3.2.1 The dominant OPE power correction for the gluon propagator 50
3.2.2 The dominant OPE power correction for the ghost propagator 51
3.2.3 Constraints on the Wilson coefficients from the Slavnov-Taylor identity 52
3.3 Data analysis 53
3.3.1 Fitting the gluon and the ghost propagators 54

3.3.2 Fit of the ratio . . . 56
3.3.3 Comparing the results . . . 59

4 The infrared behaviour of Green functions 61
4.1 Review of today's analytical results . . . 62
4.1.1 Zwanziger's prediction . . . 62
4.1.2 Study of truncated SD and ERG equations . . . 63
4.2 Constraints on the infrared exponents and the Slavnov-Taylor identity 63
4.3 Relation between the infrared exponents . . . 65
4.4 Lattice study of the ghost Schwinger-Dyson equation . . . 68
4.4.1 Complete ghost Schwinger-Dyson equation in the lattice formulation . . . 68
4.4.2 Checking the validity of the tree-level approximation for the ghost-gluon vertex . . . 70
4.5 Direct fits of infrared exponents . . . 72
4.5.1 Testing the relation $2\alpha_F + \alpha_G = 0$. . . . 73
4.5.2 Lattice fits for α_F and α_G. . . . 74

5 Conclusions 79

6 Resumé 83

References 87

A Large momentum behavior of the ghost propagator in $SU(3)$ lattice gauge theory 91

B Non-perturbative power corrections to ghost and gluon propagators 105

C The infrared behaviour of the pure Yang-Mills Green functions 121

D Scaling properties of the probability distribution of lattice Gribov copies 147

E Short comment about the lattice gluon propagator at vanishing momentum 171

F Is the QCD ghost dressing function finite at zero momentum ? 179

Notations and conventions

a	lattice spacing
$\mathcal{A}_\mu = A^a_\mu t^a$	gauge field
$\langle A^2 \rangle$	A^2-condensate
α_F (α_G)	infrared exponent of the ghost (gluon) propagator
$\beta = \frac{2N_c}{g_0^2}$	bare lattice coupling
$\beta(g), \beta_i$	the renormalisation group beta function and its first coefficients
$\gamma(g); \bar{\gamma}, \bar{\gamma}_i$	anomalous dimension; anomalous dimension in a generic MOM scheme and its coefficients
e_μ	a vector in direction μ of norm a
$\tilde{F}^{(2)ab}(p) = \delta^{ab}\frac{\tilde{F}(p)}{p^2}$	ghost propagator
$\tilde{G}^{(2)ab}(p) = \delta^{ab}\frac{\tilde{G}(p)}{p^2}\left(\delta_{\mu\nu} - \frac{p_\mu p_\nu}{p^2}\right)$	gluon propagator
G, Λ	Gribov region and the fundamental modular region
Γ^{abc}_μ	three-gluon vertex
$\widetilde{\Gamma}^{abc}_\mu(p,q;r) = -ig_0 f^{abc} p_\nu \widetilde{\Gamma}_{\nu\mu}(p,q;r)$	ghost-gluon vertex, p is the momentum of the outgoing ghost, r is the gluon momentum.
g_0, g_R	bare coupling, renormalised coupling
$h = g^2/(4\pi)^2$	
L	size of the lattice
$\mathcal{M}_{FP}, \mathcal{M}^{\text{lat}}_{FP}$	Faddeev - Popov operator and its discretized version
N_c	number of colours
$p_\mu = \frac{2\pi}{L} a^{-1} n_\mu$	relation between physical and lattice momenta
$t = \ln \frac{\mu^2}{\Lambda^2_{\text{QCD}}}$	
$U(x, x+e_\mu) \equiv U_\mu(x) =$ $= e^{ig_0 a \mathcal{A}_\mu(x+\frac{a}{2}e_\mu)} \in SU(N_c)$	link variable

V	volume of the lattice
Z_3 ($\widetilde{Z_3}$)	gluon (ghost) field renormalisation factor
$\langle 0 \mid \bullet \mid 0 \rangle$	average with respect to the perturbative vacuum
$\langle \bullet \rangle$	average with respect to the non-perturbative vacuum

Shortenings

b.c	best (Gribov) copy choice
f.c.	first (Gribov) copy choice
ERGE	exact renormalisation group equations
IR	infrared
MOM	momentum substraction renormalisation scheme (see Figures 2.1, 2.2)
RG	renormalisation group
SD	Schwinger-Dyson equations
ST	Slavnov-Taylor identities
UV	ultraviolet
v.e.v.	vacuum expectation values
ZP	zero-point (kinematic configuration, $\widetilde{\text{MOM}}$ renormalisation schemes)

General introduction

"Of course, you can put a theory on the lattice. But then - it is a mess!"
Giorgio Parisi, les Houches

This PhD dissertation is devoted to a non-perturbative study of QCD correlators in Landau gauge. The main tool that we use is lattice QCD. It allows a numerical evaluation of the functional integrals defining vacuum expectation averages of the theory i.e. Green functions. The advantage of this method is that it gives access to the non-perturbative domain and exactly preserves the gauge-invariance allowing to (numerically) study QCD from its first principles. However, the price to pay is the appearance of diverse discretisation artifacts like breakdown of the Lorentz invariance, a necessity to work with the Euclidean formulation of the theory and, in practice, at finite volume. We discuss in details the methods allowing to handle most of the artifacts. Lattice QCD has been successfully used in phenomenology (mass of the charm quark, B- and D-mesons physics, generalised parton distributions, QCD at finite temperature and its phase diagram, etc.). But it can also be used to study the fundamental parameters (like coupling constant) and properties of the theory itself. This is the main goal of the present dissertation. We concentrated our effort on the study of the two-point correlators of the pure Yang - Mills theory in Landau gauge, namely the gluon and the ghost propagators. We are particularly interested in determining the Λ_{QCD} parameter - the fundamental scale of the pure Yang-Mills theory. It is extracted by means of perturbative predictions available up to NNNLO. The related topic is the influence of non-perturbative effects that shows up as appearance of power-corrections to the low-momentum behaviour of the Green functions. We shall see that these corrections are quite important up to energies of the order of 10 GeV.

Another question that we address is the infrared behaviour of the Green functions (in Landau gauge), at momenta of order and below Λ_{QCD}. At low energy the power-law dependence of some Green functions changes considerably, and this is probably related to confinement. The knowledge of the infrared behaviour of the ghost and gluon propagators in Landau gauge is very important, because many confinement scenarii (for example the Gribov-Zwanziger scenario) give predictions for their momentum dependence at very low energies. *Ab initio* simulations on the lattice is a quasi-unique method for testing these predictions and the only way to challenge the underlying models for confinement.

We try to clarify the laws that govern the infrared gluondynamics in order to un-

derstand the radical nature of the changes of the infrared behaviour of some Green functions. Many questions arise: the Gribov ambiguity, the validity of different non-perturbative relations (like Schwinger - Dyson equations, Slavnov - Taylor identities and renormalisation group equations) at low momenta, self-consistency of the lattice approach in this domain. The lattice approach allows to check the predictions of analytical methods because it gives access to non-perturbative correlators. Our main goal thus is to use lattice Green functions as a non-perturbative input for different analytical relations. This allows to control the approximations that are done within the traditional truncation methods for the non-perturbative relations. Such a mixed numerical-analytical analysis of the complete Schwinger - Dyson equation for the ghost propagator provided us with an interesting alternative to the widely spread claim that the gluon dressing function behaves like the inverse squared ghost dressing function, a claim which is at odds with lattice data. According to our analysis the Landau gauge gluon propagator is finite and non-zero at vanishing momentum, and the power-law behaviour of the ghost propagator is the same as in the free case. However, as we shall see, some puzzles remain unsolved.

Chapter 1

Continuum and lattice QCD

In this chapter we recall very briefly the most fundamental ideas of QCD (definitions, symmetries, covariant gauge fixing, Gribov ambiguity). As we are interested in a non-perturbative calculation of different correlators, we also introduce diverse non-perturbative relations between Green functions, namely Schwinger-Dyson equations, Slavnov-Taylor identities and exact renormalisation group equations. After this we shall discuss the lattice formulation of the pure Yang-Mills theories, in particular the procedure of the Landau gauge fixing on the lattice.

1.1 General features of QCD

1.1.1 Definitions and symmetries

Nowadays there is no doubt that Quantum Chromodynamics (QCD) is the theory of the strong interaction. The fundamental principle of this theory is local gauge invariance. This principle, together with general principles of locality, Lorentz invariance and renormalisability, imposes important constraints on the form of the Lagrangian. The simplest form in Euclidean four-dimensional space reads

$$\mathcal{L}_{\mathrm{QCD}} = -\frac{1}{4} F^a_{\mu\nu} F^{a\mu\nu} + \sum_{\psi=u,d,s,c,b,t} \bar{\psi}(iD_\mu \gamma^\mu - m_\psi)\psi \tag{1.1}$$

with (g_0 is the bare coupling)

$$F^a_{\mu\nu} = \partial_\mu A^a_\nu - \partial_\nu A^a_\mu + g_0 f^{abc} A^b_\mu A^c_\nu, \qquad a = 1..N_C^2 - 1 \tag{1.2}$$

$$D_\mu = \partial_\mu - i g_0 t^a A^a_\mu. \tag{1.3}$$

This Lagrangian is invariant under gauge transformations of the fields

$$\mathcal{A}_\mu(x) \mapsto \mathcal{A}^{(u)}_\mu(x) = u(x)\mathcal{A}_\mu(x)u^\dagger(x) + i[\partial_\mu u(x)]u^\dagger(x) \tag{1.4}$$

$$\psi(x) \mapsto \psi^{(u)}(x) = u(x)\psi(x), \tag{1.5}$$

where $u(x) \in SU(N_c)$ and $N_C = 3$ is the number of colours.

In order to quantise QCD using the functional integration formalism one has to

integrate over the quark and the gauge bosons fields. The Grassmannian integral on the quark fields is Gaussian, that is why we discuss only the integration on the gauge boson fields $\mathcal{A}$. The fields $\mathcal{A}^{(u)}$ and $\mathcal{A}$ in the equation (1.4) are related by a gauge transformation, and thus they are physically equivalent. So, in order to quantise a gauge theory one performs an integration over gauge transformation equivalence classes - the **orbits** of the gauge fields. This is the Faddeev - Popov procedure. The integration on the orbits is done by choosing a representative element on every orbit, i.e. fixing the gauge with some relation

$$f[\mathcal{A}] = 0. \tag{1.6}$$

The condition f should define the orbit of the field $\mathcal{A}$ in a unique way. Then the generating functional for Green functions reads

$$Z[j,\overline{\omega},\omega] = \int [\mathcal{D}\mathcal{A}\mathcal{D}\psi\mathcal{D}\overline{\psi}]\,\Delta_f[\mathcal{A}]\,\delta\left(f\left[\mathcal{A}\right]\right)\,e^{-\int d^4x\mathcal{L}_{\mathrm{QCD}}+\int d^4x\left(A^a_\mu j^a_\mu+\overline{\omega}\psi+\overline{\psi}\omega\right)}, \tag{1.7}$$

where all loop integrals are understood to be regularised. We denote the ultraviolet cut-off a^{-1}, $g_0 \equiv g(a^{-1})$. The **Faddeev-Popov determinant** $\Delta_f[\mathcal{A}]$ which appears in this formula is defined by means of invariant integration

$$\Delta_f[\mathcal{A}]\int \mathcal{D}u(x)\prod_x \delta\left(f\left[\mathcal{A}^{(u)}(x)\right]\right) = 1 \tag{1.8}$$

yielding in the general case [1]

$$\Delta_f^{-1}[\mathcal{A}] = \sum_{i:\, f\left[\mathcal{A}^{(g_i)}\right]=0} \det{}^{-1}\frac{\delta f\left[\mathcal{A}^{(g_i)}\right]}{\delta g}. \tag{1.9}$$

Choosing the **Landau gauge** condition

$$f[\mathcal{A}]: \quad \partial_\mu\mathcal{A}_\mu = 0 \tag{1.10}$$

and supposing for the moment that it fixes the gauge in a unique way, one obtains

$$\Delta_{\mathrm{Landau}}[\mathcal{A}] = \det\left(\Delta + ig_0\partial_\mu\mathcal{A}_\mu\right) = \int [\mathcal{D}c\mathcal{D}\bar{c}]\,e^{-\int d^4xd^4y\bar{c}^a(x)\mathcal{M}^{ab}_{FP}(x,y)c^b(y)}. \tag{1.11}$$

The spurious anticommuting fields c and $\bar{c}$ belonging to the adjoint representation of the gauge group are called **Faddeev-Popov ghosts**, and

$$\mathcal{M}^{ab}_{FP}(x,y) = \left(\Delta + ig_0\partial_\mu\mathcal{A}_\mu\right)^{ab}\delta^{(4)}(x-y) \tag{1.12}$$

is the **Faddeev-Popov operator**. The corresponding formula for the generating functional can be easily generalised by choosing for the gauge condition

$$f[\mathcal{A}]: \quad \partial_\mu\mathcal{A}_\mu = \mathfrak{a}(x), \qquad \mathfrak{a}(x) \in \mathfrak{su}(N_C). \tag{1.13}$$

[1] when the condition (1.6) does not fix the gauge in a unique way.

In this case Δ_f remains the same as (1.11), and one can integrate on $\mathfrak{a}(x)$ with some Gaussian weight having a dispersion ξ. This gives for the generating functional

$$Z[j,\bar{\omega},\omega,\bar{\sigma},\sigma] = \int [\mathcal{D}\mathcal{A}\mathcal{D}\psi\mathcal{D}\bar{\psi}\mathcal{D}c\mathcal{D}\bar{c}]\, e^{-\int d^4x \mathcal{L}_{eff}[\mathcal{A},\psi,\bar{\psi},c,\bar{c}]+\Sigma}, \tag{1.14}$$

$$\mathcal{L}_{eff}[\mathcal{A},\psi,\bar{\psi},c,\bar{c}] = \mathcal{L}_{\mathrm{QCD}} - \frac{(\partial_\mu \mathcal{A}_\mu)^2}{2\xi} - \bar{c}^a(x)(\delta^{ab}\Delta + ig_0 f^{abc} A^c_\mu \partial_\mu) c^b(x) \tag{1.15}$$

$$\Sigma = \int d^4x \left(A_\mu j_\mu + \bar{\omega}\psi + \bar{\psi}\omega + \bar{\sigma}c + \bar{c}\sigma\right). \tag{1.16}$$

The choice $\xi = 0$ corresponds to the Landau gauge. The gauge fixing term in (1.14) can be expressed as a result of Gaussian integration on an auxiliary field $B^a(x)$. This gives another form of the Lagrangian $\mathcal{L}_{eff}$:

$$\mathcal{L}_{\mathrm{BRST}} = \mathcal{L}_{QCD} - \frac{\xi}{2}(B^a)^2 + B^a \partial_\mu A^a_\mu + \bar{c}^a(\delta^{ab}\Delta - ig_0 f^{abc}\partial_\mu A^c_\mu) c^b. \tag{1.17}$$

The QCD Lagrangian written in this form is invariant under **BRST transformations**. If λ is a constant infinitesimal Grassmann number these transformations take the form

$$\begin{aligned}
&\delta A^a_\mu = \lambda D^{ac}_\mu c^c \\
&\delta\psi = ig_0\lambda t^a \psi \\
&\delta c^a = -\frac{1}{2} g_0 \lambda f^{abc} c^b c^c \\
&\delta\bar{c}^a = \lambda B^a \\
&\delta B^a = 0.
\end{aligned} \tag{1.18}$$

The virtue of the BRST transformation is its global nature. This simplifies a lot the derivation of the Slavnov-Taylor identities (direct consequence of the gauge invariance). We discuss this question below.

1.1.2 The Gribov ambiguity

A serious theoretical difficulty pointed out by Gribov [1] arises when performing the quantisation of a non-Abelian gauge theory (in covariant gauge) in the case of large field magnitudes. The reason for this is the non-uniqueness of the Landau gauge condition (1.10). Indeed, let us find all the intersections of the gauge orbit with the hypersurface defined by (1.10). Imposing the Landau gauge conditions for both fields $\mathcal{A}_\mu$ and $\mathcal{A}^{(\overline{u})}_\mu$ in (1.4) we obtain the following equation for $\overline{u}(x)$:

$$\left\{ \begin{array}{l} \mathcal{A}_\mu(x) \mapsto \mathcal{A}^{(\overline{u})}_\mu(x) \\ \partial_\mu \mathcal{A}_\mu = 0 \\ \partial_\mu \mathcal{A}^{(\overline{u})}_\mu = 0 \end{array} \right. \quad \rightarrow \quad \partial_\mu \left(\overline{u}(x) D_\mu(x) \overline{u}^\dagger(x) \right) = 0. \tag{1.19}$$

Setting at the leading order

$$\overline{u} \simeq \mathbb{I} + i\overline{\alpha}(x), \quad \overline{u}^{\dagger} \simeq \mathbb{I} - i\overline{\alpha}(x) \qquad \overline{\alpha}(x) \in \mathfrak{su}(N_c) \tag{1.20}$$

we obtain the following equation for $\overline{\alpha}$:

$$\partial_\mu \left(\partial_\mu \overline{\alpha} + i[\mathcal{A}_\mu, \overline{\alpha}] \right) = 0 \quad \longrightarrow \quad \partial_\mu D_\mu \overline{\alpha} = 0. \tag{1.21}$$

But $\partial_\mu D_\mu$ is nothing else but the Faddeev-Popov operator in the covariant gauge. Thus, any non-trivial zero mode of the Faddeev-Popov operator generates an intersection point of the gauge orbit with the hypersurface (1.10). If this point is not unique, we speak about the so called **Gribov copy**. All these secondary gauge configurations correspond to the same physical field $\mathcal{A}_\mu$, and thus they must be removed from the functional integration measure in the partition function.

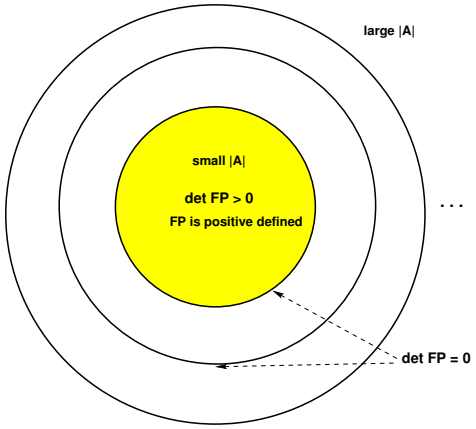

Figure 1.1: *The Gribov region.*

A solution to this problem is to supplement the initial gauge-fixing condition (1.10) with some additional requirement. Gribov's solution consists in restricting the integration measure (for the gluonic field) in (1.14) to the domain where (1.21) has a unique solution, see Fig. 1.1. This domain is called the **Gribov region**, and its boundary (where the Faddeev-Popov determinant vanishes) is called the **Gribov horizon**. It has been argued that some of topological solutions like instantons lie on this boundary [2].

Inside the Gribov region all the eigenvalues of the Faddeev-Popov operator are strictly positive [2]. Hence one can realise the Gribov quantisation by using the Minimal Landau gauge. In this gauge one integrates on the fields satisfying the ordinary Landau gauge and belonging to the set of local minima of the integral

$$\int d^4x \left(A^a_\mu(x) \right)^2 .$$

As we shall see, this ensures that all the proper values of the Faddeev-Popov operator are positive. The Minimal Landau gauge will be discussed in details in the

[2] we recall that in the Euclidean formulation the Faddeev - Popov operator is hermitian.

subsection 1.2.2.

Nowadays it is known that the Gribov quantisation prescription is not exact - there are secondary solutions to (1.19) for some fileds inside the Gribov region. The domain free of them is located inside the Gribov region, and it is called the **fundamental modular region** [3],[4]. This means that the correct quantisation prescription

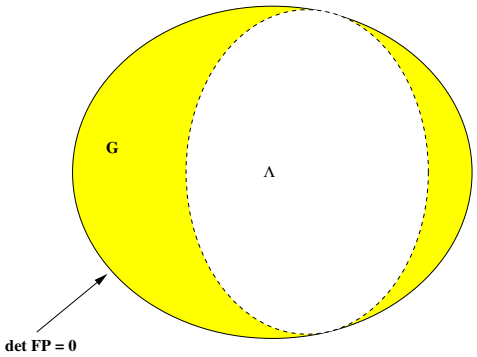

Figure 1.2: *Gribov region and the fundamental modular region.*

consists in restricting the integration in (1.14) to the fundamental modular region Λ instead of the Gribov region G, see figure 1.2. However it is argued in [5] that the expectation values calculated by integration over the Gribov region or the fundamental modular region are equal. So the Gribov quantisation prescription would become in fact exact. We discuss this question in details in the section 2.4.

1.1.3 Schwinger-Dyson equations

The Schwinger-Dyson(SD) equations is a specific class of non-perturbative equations relating Green functions and vertices. They can be easily derived in the functional integration formalism (for a review see [6]). Let $Z[J]$ denote a normalised ($Z[0] = 1$) generating functional (1.14) for the Green functions, and $W[J] = \log Z[J]$ - the one for connected Green functions. Then the effective action, which is a generating functional for one-particle irreducible (1-PI) vertex functions, is obtained by the Legendre transformation

$$\Gamma[\phi^c] = \frac{\delta W[J]}{\delta j_i} j_i - W[J], \qquad \phi_i^c = \frac{\delta W[J]}{\delta j_i}, \tag{1.22}$$

where ϕ_i denotes the generic field ($A_\mu^a, c^a, \ldots$) and j_i is the corresponding source. Then, introducing the action $S = \int d^4x\, \mathcal{L}_{eff}$ and using the quantisation prescription based on the integration over the fundamental modular region, the Schwinger-Dyson equations are obtained from the observation that

$$\int\limits_{\Lambda} [\prod_j \mathcal{D}\phi_j] \frac{\delta}{\delta \phi_i} \left(e^{-S+\phi\cdot j} \right) \equiv \int\limits_{\Lambda} [\prod_j \mathcal{D}\phi_j] e^{-S+\phi\cdot j} \left(-\frac{\delta S}{\delta \phi_i} + j_i \right) = \int\limits_{\partial\Lambda_i} [\prod_j \mathcal{D}\phi_j]\, e^{-S+\phi\cdot j} \tag{1.23}$$

Using the Zwanziger's argument [5] (quoted above) on the equivalence of integrations over Λ and G we restrict the integration domain to the Gribov region. It follows from this that the integral on the boundary vanishes because the Faddeev-Popov determinant present in the integration measure is equal to zero on ∂G (by definition). This allows to write the whole set of the Schwinger-Dyson equations for the Green functions in a compact form

$$\left(-\frac{\delta S[\phi]}{\delta \phi_i}\left[\frac{\delta}{\delta j}\right] + j_i\right) Z[J] = 0. \tag{1.24}$$

We use a generic relation between two smooth functions $f(x)$ and $w(x)$

$$f\left(\frac{d}{dx}\right) e^{w(x)} = e^{w(x)} f\left(\frac{dw(x)}{dx} + \frac{d}{dx}\right) 1, \tag{1.25}$$

that can be applied to (1.24) and yield the equations for the functional W generating the connected Green functions

$$-\frac{\delta S[\phi]}{\delta \phi_i}\left[\frac{\delta}{\delta j} + \frac{\delta W}{\delta j}\right] 1 + j_i = 0. \tag{1.26}$$

Finally, performing a Legendre transformation (1.22), we have

$$-\frac{\delta S[\phi]}{\delta \phi_i}\left[\phi + \frac{\delta^2 W}{\delta j \delta j}\frac{\delta}{\delta \phi}\right] 1 + \frac{\delta \Gamma[\phi]}{\delta \phi_i} = 0, \tag{1.27}$$

corresponding to the full set of Schwinger-Dyson equations for proper functions.

As an example, we derive explicitly the SD equation for the full ghost propagator. Varying S with respect to the antighost field $\bar{c}^a$ we obtain

$$\left\langle -\frac{\delta S}{\delta \bar{c}^a(x)} + \sigma^a(x)\right\rangle_{[j,\bar{\sigma},\sigma]} = 0. \tag{1.28}$$

Varying the last relation with respect to $\sigma^b(y)$ one obtains

$$\left\langle \frac{\delta S}{\delta \bar{c}^a(x)}\bar{c}^b(y)\right\rangle = \delta^{ab}\delta^{(4)}(x-y) = \left\langle \left(\partial_\mu D^{ac}_\mu c^c(x)\right)\bar{c}^b(y)\right\rangle. \tag{1.29}$$

Denoting the full ghost propagator as

$$F^{(2)ab}(x,y) = \left\langle c^a(x)\bar{c}^b(y)\right\rangle, \tag{1.30}$$

we obtain ($\Delta(x,y) \equiv \delta^{(4)}(x-y)\delta$ is the Laplace operator)

$$\delta^{(4)}(x-y) = \Delta(x,z)F^{(2)}(z,y) + ig_0\partial^{(x)}_\mu \left\langle \mathcal{A}_\mu(x)c(x)\bar{c}(y)\right\rangle. \tag{1.31}$$

Note that this equation can be obtained in a simpler way only using the definition of the Faddeev-Popov operator. Indeed, the ghost correlator in the background of a

given gauge field configuration $\mathcal{A}_\mu = A^a_\mu t^a$ is given by

$$F^{(2)}_{1\text{conf}}(\mathcal{A}, x, y) \equiv \mathcal{M}^{1\text{conf}}_{FP}(x, y)^{-1}. \tag{1.32}$$

The subscript means here that the equation is valid for a given gauge configuration. Thus one obviously has

$$\delta^4(x-y) \equiv \mathcal{M}^{1\text{conf}}_{FP}(x, z) F^{(2)}_{1\text{conf}}(\mathcal{A}, z, y), \tag{1.33}$$

where a summation on z is understood. Using the explicit formula (1.12) for $\mathcal{M}_{FP}$ we get

$$\delta(x-y) = \Delta(x,z) F^{(2)}_{1\text{conf}}(z,y) + ig_0\, \partial^{(x)}_\mu \left(\mathcal{A}_\mu(x) F^{(2)}_{1\text{conf}}(\mathcal{A}, x, y) \right), \tag{1.34}$$

valid for *any* gauge field configuration $\mathcal{A}$. Performing the functional integration on $\mathcal{A}$ one gets the mean value on gauge configurations

$$\delta(x-y) = \Delta(x,z) \left\langle F^{(2)}_{1\text{conf}}(z,y) \right\rangle + ig_0 \partial^{(x)}_\mu \left\langle \mathcal{A}_\mu(x) F^{(2)}_{1\text{conf}}(\mathcal{A}, x, y) \right\rangle. \tag{1.35}$$

Using $\left\langle F^{(2)}_{1\text{conf}}(z,y) \right\rangle \equiv F^{(2)}(z,y)$ we find the equation (1.31). The translational invariance of the Green functions allows to replace $\partial^{(x)}_\mu$ by $-\partial^{(y)}_\mu$. Performing the Fourier transform on $(x-y)$, we have finally

$$1 = -p^2 F^{(2)}(p^2) - ig_0 p_\mu \left\langle \mathcal{A}_\mu(0) F^{(2)}_{1\text{conf}}(\mathcal{A}, p) \right\rangle. \tag{1.36}$$

This derivation elucidates the trivial dependence of this equation on the functional integral weight with which we calculate the average $\langle \bullet \rangle$ on the gauge fields $\mathcal{A}$. The form (1.34) allows an explicit discussion of the Gribov copies dependence of the solutions. We address this question below.

Performing the Legendre transformation for the three-point function in (1.31) and introducing the ghost-gluon vertex

$$\widetilde{\Gamma}^{abc}_\mu(-q, k; q-k) = g_0 f^{abc} (iq_{\nu'}) \widetilde{\Gamma}_{\nu'\nu}(-q, k; q-k) \tag{1.37}$$

and the full gluon propagator $G^{(2)ab}_{\mu\nu}(p)$, we write the Schwinger-Dyson equation for the ghost propagator in Fourier space

$$\left(F^{(2)}\right)^{-1}_{ab}(k) = -\delta_{ab}k^2 - g_0^2 f^{acd} f^{ebf} \int \frac{d^4q}{(2\pi)^4} F^{(2)}_{ce}(q) (iq_{\nu'}) \widetilde{\Gamma}_{\nu'\nu}(-q, k; q-k)\, (ik_\mu) \left(G^{(2)}\right)^{fd}_{\mu\nu}(q-k), \tag{1.38}$$

given in a diagrammatic form at Figure 1.3. This equation is much simpler than the one for the gluon propagator, because the last involves complete three- and four-gluon vertices (cf. Figure 1.4). Another virtue of (1.38) is that its *form* is explicitly independent of the choice of the integration domain in the functional integral (1.23), because the equality (1.34) holds valid for *individual* gauge configurations.

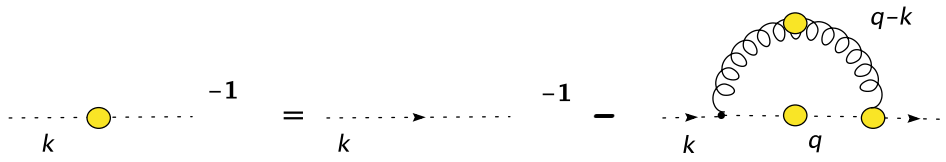

Figure 1.3: *Schwinger-Dyson equation for the ghost propagator in a pure gauge theory, diagrammatically.*

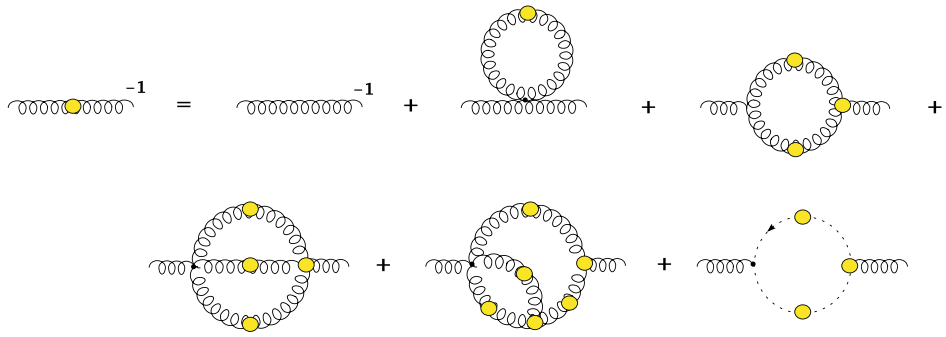

Figure 1.4: *Schwinger-Dyson equation for the gluon propagator in a pure gauge theory, diagrammatically.*

1.1.4 Slavnov-Taylor identities

The Slavnov-Taylor identities ([7],[8]) are Ward identities in the case of a non-Abelian gauge theory. These identities follow directy from the gauge symmetry. We write the generating functional in the case of a general gauge fixing condition (1.6)

$$Z[j] = \int [\mathcal{D}\mathcal{A}] \, \det \mathcal{M}_{FP} \, e^{-\int d^4x \left(\mathcal{L}_{\mathrm{QCD}} - \frac{(f^a[A])^2}{2\xi} + j^a_\mu A^a_\mu \right)}, \tag{1.39}$$

and use the fact that the functional integration measure is invariant under the specific gauge transformations

$$\begin{aligned} \delta A^a_\mu &= D^{ab}_\mu \epsilon^b \\ \delta f^a[\mathcal{A}] &= \mathcal{M}^{ab}_{FP} \epsilon^b. \end{aligned} \tag{1.40}$$

The second equation is just a general definition of the Faddeev-Popov operator. The integration measure times the Faddeev-Popov determinant is invariant with respect to (1.40), and hence

$$Z[j] = \int [\mathcal{D}\mathcal{A}] \, \det \mathcal{M}_{FP} \, e^{-\int d^4x \left(\mathcal{L}_{\mathrm{QCD}} - \frac{(f^a[\mathcal{A}])^2}{2\xi} + j_\mu A_\mu - \frac{1}{\xi} f^a \mathcal{M}^{ab}_{FP} \epsilon^b + j^a_\mu D^{ab}_\mu \epsilon^b \right)}. \tag{1.41}$$

Choosing a particular form for ϵ

$$\epsilon^b = \left(\mathcal{M}^{-1}_{FP} \right)^{bc} \omega^c \tag{1.42}$$

we obtain a functional relation for the generating functional Z

$$\left(\frac{1}{\xi}f^a\left[\frac{\delta}{\delta j}\right] - \int d^4y\, j^b_\mu(y) D^{bc}_\mu\left[\frac{\delta}{\delta j}\right]\left(\mathcal{M}^{-1}_{FP}\right)^{ca}\left[x,y;\frac{\delta}{\delta j}\right]\right) Z[j] = 0. \tag{1.43}$$

In principle, one can use the relation (1.25) in order to obtain an equation for the functional $W[j]$. However, this derivation would lead to a very cumbersome expression. In fact it is much easier to use the Slavnov-Taylor relations obtained within the BRST formalism. The main idea of the derivation remains the same because the BRST transformation is just a specific form of the gauge transformation (1.40), $\mathcal{M}^{-1}_{FP}(x,y)$ being the propagator of the Faddeev-Popov ghost in the background field $\mathcal{A}$. One has using (1.17,1.18) and the BRST invariance of the generating functional $Z[j]$

$$\int d^4x \int [\mathcal{D}\mathcal{A}\mathcal{D}c\mathcal{D}\bar{c}]\, e^{-\int d^4x \mathcal{L}_{eff}} \left(j^a_\mu \cdot D^{ab}_\mu c^b - \frac{1}{\xi}\partial_\mu A^a_\mu \sigma^a - \bar{\sigma}^a \frac{g_0}{2} f^{abc} c^b c^c\right) = 0. \tag{1.44}$$

This equation (1.44) allows to obtain the Slavnov-Taylor identities for the Green functions by differentiating with respect to the sources $j, \sigma, \bar{\sigma}$. Writing (1.44) in terms of generating functionals W and Γ, one obtains (see [9], [7], [8] for details) the general form of Slavnov-Taylor identities between propagators and proper vertices. The relation that we shall use in the following relates the three-gluon vertex $\Gamma_{\lambda\mu\nu}(p,q,r)$ to the ghost-antighost-gluon vertex, and involves the complete ghost and gluon propagators. It reads ([7],[8])

$$\begin{aligned} p^\lambda \Gamma_{\lambda\mu\nu}(p,q,r) = &\frac{p^2 F^{(2)}(p^2)}{r^2 G^{(2)}(r^2)}\left(\delta_{\lambda\nu} r^2 - r_\lambda r_\nu\right)\widetilde{\Gamma}_{\lambda\mu}(r,p;q) - \\ &- \frac{p^2 F^{(2)}(p^2)}{q^2 G^{(2)}(q^2)}\left(\delta_{\lambda\mu} q^2 - q_\lambda q_\mu\right)\widetilde{\Gamma}_{\lambda\nu}(q,p;r). \end{aligned} \tag{1.45}$$

Some remarks regarding the non-perturbative validity of the Slavnov-Taylor identities are in order. The above derivation is invalid when $\mathcal{M}^{-1}_{FP}$ is singular (see (1.40), (1.42) and (1.43)), i.e. for gauge fields lying on the Gribov horizon. However, this transformation is well defined inside the Gribov horizon. Note also that the general form of the Slavnov-Taylor identities does not depend on the choice of the integration domain inside the Gribov horizon (Λ or G). Another argument in favour of non-perturbative validity of the Slavnov-Taylor identities may be given within the stochastic quantisation formalism [5].

1.1.5 Renormalisation group equations

For the sake of completeness we present here another set of non-perturbative relations between the correlators, namely the exact renormalisation group equations (or ERGE, see [10] for a review). Those are flow equations describing the variation of the effective action with the infrared (or ultraviolet) cut-off. The infrared cut-off is

introduced by adding a special term to the action

$$\Delta S_k = \frac{1}{2}\sum_i \int \frac{d^4p}{(2\pi)^4}\,\phi_i(p)R_i(k,p^2)\phi_i(-p), \tag{1.46}$$

where the momentum cut-off function R_i for the field ϕ_i satisfies

$$\begin{cases} R_i(k,p^2) \to 0 & p \gtrsim k \\ R_i(k,p^2) \to k^2 & p \lesssim k. \end{cases} \tag{1.47}$$

The role of ΔS_k is to suppress quantum fluctuations with momenta below k. Then one may show that the partition function satisfies the equation

$$\partial_k Z_k(j) = -\frac{1}{2}\int \frac{d^4p}{(2\pi)^4}\partial_k R(k,p^2)\frac{\delta^2 Z_k(j)}{\delta j(p)\delta j(-p)}. \tag{1.48}$$

The problem that arises within the formalism of the RG equations is the loss of the gauge invariance caused by the cut-off term. However, this problem can be solved by considering a modified set of Slavnov-Taylor identities [11]. One may express the equation (1.48) in terms of the generating functional for proper vertices, that lead to an infinite system of partial differential equations relating different Green functions and the cut-off function (1.47). We shall review some of the results for solutions of the truncated system of such equations in the section 4.1.

1.2 Lattice QCD

1.2.1 Lattice QCD partition function

A fully non-perturbative study from the first principles of QCD phenomenon requires a direct calculation of the functional integral of the type (1.14). These integrals can be approximately evaluated by means of lattice simulations. Another interest in the lattice regularisation is that it preserves the gauge invariance. The inverse lattice spacing a^{-1} plays the role of the ultraviolet cut-off, and we recover the continuum limit theory by sending a to zero.

In what follows we discuss only pure Yang-Mills theories. In practice, when doing a lattice simulation, one considers a theory in a finite volume $V = L^4$ with (most often) periodical boundary conditions; and generates some (quite large) number M of gauge field configurations $\{C_i\}$ distributed according to the probability measure

$$d\mu[\mathcal{A}] = e^{-\int d^4x \mathcal{L}_{\text{Yang-Mills}}(A)}[\mathcal{D}\mathcal{A}]. \tag{1.49}$$

Then one can calculate a Monte-Carlo approximation for any operator $\mathcal{O}$

$$O = \langle \mathcal{O}(\mathcal{A}_\nu)\rangle = \int d\mu \mathcal{O}(\mathcal{A}_\nu) \approx \frac{1}{M}\sum_{i=1}^{M}\mathcal{O}(C_i). \tag{1.50}$$

Let us now discuss the measure $d\mu[A]$ in the discrete case. Gauge fields are defined

on the links of the Euclidean lattice (cf. Figure 1.5), and the fundamental lattice variable for the gauge field is the **link variable**

$$U(x, x+e_\mu) \equiv U_\mu(x) = e^{ig_0 a \mathcal{A}_\mu(x+\frac{a}{2}e_\mu)} \in SU(N_c), \tag{1.51}$$

where e_μ is a vector in direction μ, $\|e_\mu\| = a$. For small values of the lattice spacing

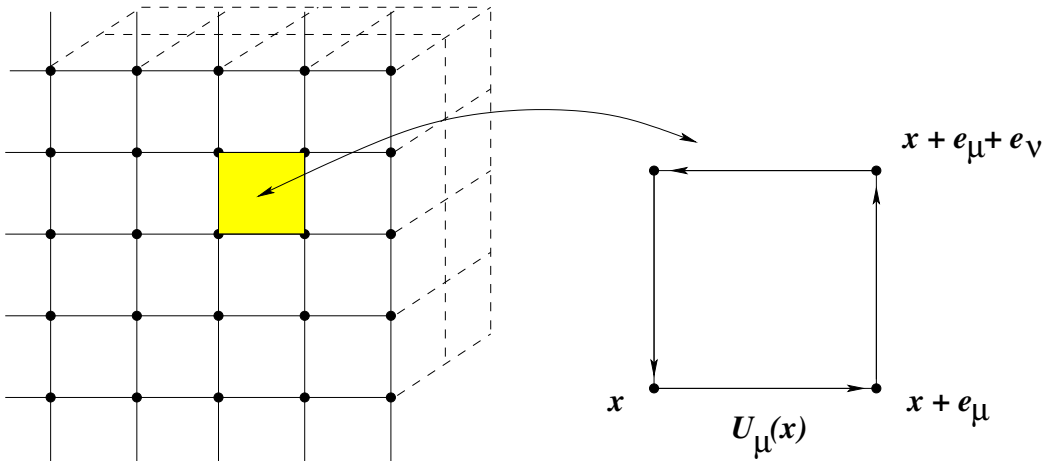

Figure 1.5: *Gauge fields $\mathcal{A}_\mu$ are defined on the links of the lattice ($\|e_\mu\| = a$), and the fermion fields $\psi(x)$ are defined on its sites.*

a we can extract the field $\mathcal{A}_\mu$ using an approximate formula

$$\frac{U_\mu(x) - U_\mu^\dagger(x)}{2iag_0} = \mathcal{A}_\nu\left(x + \frac{e_\mu}{2}\right) + O(a). \tag{1.52}$$

We use this definition of the gluon field in what follows. Then one can define an elementary gauge invariant variable - a **plaquette**

$$U(p) = U_\mu(x)U_\nu(x + ae_\mu)U_\mu^\dagger(x + ae_\nu)U_\nu^\dagger(x). \tag{1.53}$$

Using this variables we can write the simplest action that converges to the pure Yang-Mills' action in the continuum limit ([12], see [13],[14] for a review):

$$S_g[U_\mu(x)] = \beta \sum_x \sum_{\mu,\nu} \left(\mathbb{I} - \frac{1}{N_c}\mathfrak{Re}\mathrm{Tr}\, U(p)\right), \tag{1.54}$$

where the lattice bare coupling is defined by

$$\beta = \frac{2N_c}{g_0^2}. \tag{1.55}$$

Thus, the partition function in the lattice formulation reads

$$Z_{\mathrm{lat}}[U] = \int [\mathcal{D}U_\mu(x)] e^{-S_g[U]}. \tag{1.56}$$

Of course there exist an infinite number of lattice actions giving (1.14) in the continuum limit $a \to 0$. They should all give compatible results when the lattice spacing is small enough and the renormalisation group scaling laws are verified. In practice, one generates the gauge configurations $\{C_i\}, i = 1 \dots M$ according to the probability measure $[\mathcal{D}U_\mu(x)]e^{-S_g[U]}$. In all our simulations we have used the Wilson action (1.54). Usually, the Metropolis or Heatbath algorithms are used for the Monte-Carlo generation. For a detailed review on this topic see [13],[14].

The important question that has not been discussed up to now is the removal of the ultraviolet divergences of the theory in the continuum limit. The regularised lattice partition function contains one parameter - the bare coupling constant g_0 (or, equivalently, the lattice spacing a). When calculating some physical quantity on the lattice, say, the string tension σ, we obtain it as a function of a. If the ultraviolet cut-off a^{-1} is large enough, the calculated quantity obeys the scaling law, and one can compare the result for $\sigma(a)$ of the lattice simulation to the known experimental data σ_{exp}, and thus determine the corresponding physical value of the lattice spacing a by solving the equation $\sigma(a) = \sigma_{\text{exp}}$. In the unquenched case one has to calculate several physical quantities because more non-fixed parameters are involved (the masses of quarks). When all free parameters of the lattice theory are fixed in the scaling region with some experimental inputs, all further calculations [3] are automatically renormalised, and do not contain any divergences. Moreover, all the calculations are now the *predictions* of the theory. Thus, the only limitations of the numerical method *a priori* are discretisation errors and the errors on the experimental inputs. We discuss in details the systematic error of lattice simulations in the section 2.3. In practice one is also often limited by the computer power.

Let us say some words about the strong coupling limit of (1.56), corresponding to the perturbative expansion in the β parameter. The ordinary perturbation expansions in gauge theories (in powers of g_0) are at most asymptotic, but power series of (1.56) in β is proven to have a *finite* radius of convergence [15]. Many interesting results, like the existence of the mass gap and the area law for the Wilson loop, have been analytically proven within this approach. However, it has been argued that the region of the strong coupling is analytically disconnected from the weak-coupling domain, corresponding to the continuum limit of the theory [16]. Lattice gauge theories are believed to possess an essential singularity at some finite value β_{rough}, corresponding to an infinite order phase transition. This phenomenon is well known in statistical physics (roughening transition). Thus it is impossible to know whether the strong-coupling predictions are applicable in the physically interesting weak-coupling regime. In practice, one has to perform numerical simulations with $\beta > \beta_{\text{rough}}$.

1.2.2 Fixing the Minimal Landau gauge on the lattice

The continuum gauge fixing condition (1.6) is modified by the discretization, so one works with its lattice version $f_L(U_\mu) = 0$. A gauge configuration U_{C_0} generated during the simulation process does not satisfy the Landau gauge condition. One has to perform a gauge transformation $u(x)$ on it in order to move the field configuration

[3] of experimentaly observable quantities

along its gauge orbit up to an intersection with the surface $f_L(U_\mu) = 0$. But there is no need to have an explicit form of $u(x)$. Instead we perform an iterative minimisation process that converges to the gauge fixed configuration $U_C^{(u)}$. Let us first illustrate it on the example of the Landau gauge in the continuum limit. For every gauge field $\mathcal{A}$ we calculate the functional

$$F_{\mathcal{A}}[u(x)] = -\mathrm{Tr}\int d^4x \left(\mathcal{A}_\mu^{(u)}(x)\mathcal{A}_\mu^{(u)}(x)\right), \quad u(x) \in SU(N_c). \tag{1.57}$$

Expanding it up to the second order around some element $u_0(x)$ we have ($u = e^X u_0$, $X \in \mathfrak{su}(N_c)$)

$$F_{\mathcal{A}}[u] = F_{\mathcal{A}}[u_0] - 2\int d^4x \mathrm{Tr}\left(X\partial_\mu \mathcal{A}_\mu^{(u_0)}\right) + \int d^4x \mathrm{Tr}\left(X^\dagger \mathcal{M}_{\mathrm{FP}}\left[\mathcal{A}^{(u_0)}\right] X\right) + \ldots, \tag{1.58}$$

where the matrix $\mathcal{M}_{\mathrm{FP}}$ in the quadratic term defines the Faddeev-Popov operator. Obviously, if u_0 is a local minimum of (1.57) then we have a double condition

$$\begin{cases} \partial_\mu \mathcal{A}_\mu^{(u_0)} = 0 \\ \mathcal{M}_{\mathrm{FP}}\left[\mathcal{A}^{(u_0)}\right] \quad \text{is positively defined.} \end{cases} \tag{1.59}$$

Hence, the minimisation of the functional (1.57) allows not only to fix the Landau gauge, but also to obtain a gauge configuration inside the Gribov horizon (because all the eigenvalues of $\mathcal{M}_{\mathrm{FP}}$ are positive). On the lattice, the discretized functional (1.57) reads

$$F_U[u(x)] = -\frac{1}{V}\mathfrak{Re}\mathrm{Tr}\sum_{x,\mu} u(x)U_\mu(x)u^\dagger(x+e_\mu). \tag{1.60}$$

Then at a local minimum u_0 we have a discretized Landau gauge fixing condition

$$\sum_\mu \left[\mathcal{A}_\mu^{(u_0)}\left(x+\frac{e_\mu}{2}\right) - \mathcal{A}_\mu^{(u_0)}\left(x-\frac{e_\mu}{2}\right)\right] = 0 \tag{1.61}$$

that we write in a compact form $\nabla_\mu \mathcal{A}_\mu^{(u_0)} = 0$. Indeed, if $u(x) = u_0(x)e^{s\,\omega(x)}$ where $\omega(x)$ is the element of the algebra $\mathfrak{su}(N_c)$ then

$$\left.\frac{\delta}{\delta u}\right|_{u_0} F(u) \equiv \left.\frac{d}{ds}\right|_{s=0} F(u(s,x)) = 0, \tag{1.62}$$

and hence

$$-\frac{1}{V}\mathfrak{Re}\mathrm{Tr}\sum_{x,\mu}\left(\left[\omega(x+e_\mu) - \omega(x)\right]U_\mu(x)\right) = 0 \qquad \forall\omega(x) \in \mathfrak{su}(N_c). \tag{1.63}$$

Thus

$$\sum_\mu \left[U_\mu(x) - U_\mu^\dagger(x) - U_\mu(x-e_\mu) + U_\mu^\dagger(x-e_\mu)\right] = 0 \tag{1.64}$$

and at leading order in the lattice spacing a (1.52) we obtain (1.61). The second derivative (the equivalent of the second-order term in (1.58)) can be written as

$$\frac{d^2}{ds^2}F\left(u(s,x)\right) = -\frac{1}{V}\left(\omega, \nabla_\mu \mathcal{A}'_\mu\right) \tag{1.65}$$

where

$$\mathcal{A}'_\mu = \frac{1}{2}\left(-\omega(x)U^{(u)}_\mu(x) + U^{(u)}_\mu(x)\omega(x+e_\mu) + \omega(x+e_\mu)U^{(u)\dagger}_\mu(x) - U^{(u)\dagger}_\mu(x)\omega(x)\right). \tag{1.66}$$

This defines a quadratic form

$$\begin{aligned}\left(\omega, \mathcal{M}^{\text{lat}}_{FP}[U]\omega\right) &= -\frac{1}{V}\mathfrak{Re}\text{Tr}\sum_{x,\mu}\left(\left[\omega^2(x+e_\mu) - 2\omega(x+e_\mu)\omega(x) + \omega^2(x)\right]U^{(u_0)}_\mu(x)\right) = \\ &= -\frac{1}{2V}\text{Tr}\sum_{x,\mu}\Big(\left(\omega(x+e_\mu) - \omega(x)\right)^2\left(U^{(u_0)}_\mu(x) + U^{(u_0)\dagger}_\mu(x)\right) - \\ &\qquad - \left[\omega(x+e_\mu), \omega(x)\right]\left(U^{(u_0)}_\mu(x) - U^{(u_0)\dagger}_\mu(x)\right)\Big).\end{aligned} \tag{1.67}$$

The operator $\mathcal{M}^{\text{lat}}_{FP}[U]$ is the lattice version of the Faddeev-Popov operator. It reads

$$\begin{aligned}\left(\mathcal{M}^{\text{lat}}_{FP}[U]\omega\right)^a(x) = \frac{1}{V}\sum_\mu\Big\{ & G^{ab}_\mu(x)\left(\omega^b(x+e_\mu) - \omega^b(x)\right) - (x \leftrightarrow x - e_\mu) \\ & + \frac{1}{2}f^{abc}\left[\omega^b(x+e_\mu)A^c_\mu\left(x + \frac{e_\mu}{2}\right) - \omega^b(x-e_\mu)A^c_\mu\left(x - \frac{e_\mu}{2}\right)\right]\Big\},\end{aligned} \tag{1.68}$$

where

$$G^{ab}_\mu(x) = -\frac{1}{2}\text{Tr}\left(\left\{t^a, t^b\right\}\left(U_\mu(x) + U^\dagger_\mu(x)\right)\right) \tag{1.69}$$

$$A^c_\mu\left(x + \frac{e_\mu}{2}\right) = \text{Tr}\left(t^c\left(U_\mu(x) - U^\dagger_\mu(x)\right)\right). \tag{1.70}$$

For the Minimal Landau gauge fixing in our numerical simulation we have used the Overrelaxation algorithm [17] with $\omega = 1.72$. We stop the iteration process of the minimising algorithm when the following triple condition is fullfield:

$$\begin{aligned}\frac{1}{V(N_c^2-1)}\sum_{x,\mu}\text{Tr}\left[\left(\nabla_\mu \mathcal{A}^{(u^{(n)})}_\mu\right)\left(\nabla_\mu \mathcal{A}^{(u^{(n)})}_\mu\right)^\dagger\right] &\leq \Theta_{\max_x|\partial_\mu A^a_\mu|} = 10^{-18} \\ \frac{1}{V(N_c^2-1)}\left|\sum_x \text{Tr}\left[u^{(n)}(x) - \mathbb{I}\right]\right| &\leq \Theta_{\delta u} = 10^{-9} \\ \forall a, t_1, t_2 \quad \left|\frac{\text{A}^a_0(t_1) - \text{A}^a_0(t_2)}{\text{A}^a_0(t_1) + \text{A}^a_0(t_2)}\right| &\leq \Theta_{\delta \text{A}_0} = 10^{-7}.\end{aligned} \tag{1.71}$$

where $u^{(n)}(x)$ is the matrix of the gauge transformation $u(x)$ at the iteration step n,

and the charge

$$\mathrm{A}_0^a(t) = \int d^3\vec{x} A_0^a(\vec{x}, t) \tag{1.72}$$

must be independent of t in Landau gauge when periodical boundary conditions for the gauge field are used. The choice of numerical values for the stopping parameters is discussed in [18].

Chapter 2

Lattice Green functions

In the functional integral formalism Green functions are defined as mean values of products of fields according to the functional measure, giving as a result the vacuum expectation values of these products. Often one is interested in the Green functions in Fourier space. Here we define the Fourier transformation on the lattice.

If a function $f(x)$ is defined on the *sites* of the four-dimensional lattice with periodical boundary conditions then

$$\begin{aligned} \widetilde{f}(p) &= a^4 \sum_x f(x) e^{-ip\cdot x} \qquad p_\mu = \frac{2\pi}{aL} n_\mu, \quad n_\mu = 0, 1, \ldots, L-1 \\ f(x) &= \frac{1}{V} \sum_p e^{ip\cdot x} \widetilde{f}(p). \end{aligned} \tag{2.1}$$

In the case of the variables defined on the *links* of the lattice one should change the above formulae by $x_\mu \to x_\mu + \frac{e_\mu}{2}$. In the infinite-volume limit $V \to \infty$ we have

$$\frac{1}{V} \sum_p \longrightarrow \frac{1}{(2\pi)^4} \int_{\left[-\frac{\pi}{a}, \frac{\pi}{a}\right]^4} d^4 p. \tag{2.2}$$

We recall in the first part of this chapter the main definitions regarding the lattice two- and three-point Green functions in Landau gauge and the Momentum subtraction renormalisation scheme. Next we describe the details of the numerical calculation of the ghost propagator and discuss different sources of errors of the lattice approach. The last part is devoted to the Gribov ambiguity on the lattice and the influence of Gribov copies on the Green functions.

2.1 Green functions in Landau gauge

The gluon propagator in Landau gauge may be parametrised at all values of momenta as

$$G^{(2)ab}_{\mu\nu}(p, -p) \equiv \left\langle \widetilde{A}^a_\mu(-p) \widetilde{A}^b_\nu(p) \right\rangle = \delta^{ab} \left(\delta_{\mu\nu} - \frac{p_\mu p_\nu}{p^2} \right) G^{(2)}(p^2). \tag{2.3}$$

This implies that the scalar factor $G^{(2)}(p^2)$ may be extracted according to

$$G^{(2)}(p^2) = \frac{1}{3\left(N_C^2-1\right)} \sum_{\mu,a} G^{(2)aa}_{\mu\mu}(p,-p), \qquad p^2 \neq 0 \tag{2.4}$$

completed with

$$G^{(2)}(0) = \frac{1}{4\left(N_C^2-1\right)} \sum_{\mu,a} G^{(2)aa}_{\mu\mu}(0,0), \qquad p^2 = 0. \tag{2.5}$$

The difference in normalisations at zero (2.5) and finite momenta (2.4) is due to an additional degree of freedom related to global gauge transformations on a periodic finite lattice ($p^2 = 0 \leftrightarrow x_\mu \sim x_\mu + L$).

The ghost propagator is parametrised in the common way:

$$F^{(2)ab}(p,-p) \equiv \left\langle \widetilde{c}^a(-p)\widetilde{\bar{c}}^b(p) \right\rangle = \delta^{ab} F^{(2)}(p^2). \tag{2.6}$$

It is not defined at $p^2 = 0$ because in this case the Faddeev-Popov operator is strictly equal to zero and thus it is not invertible.

The renormalisation scheme that is widely used in order to renormalise the lattice Green functions is the so-called Momentum substraction scheme (MOM). The virtue of this scheme is its non-perturbative definition. The renormalisation constants are defined by setting the corresponding Green functions to their tree values at some renormalisation point μ^2. In the case of the two-point Green function the renormalisation constant $Z_3(\mu^2)$ of the gauge field or the one of the ghost field (denoted $\widetilde{Z}_3(\mu^2)$) is unambiguously defined as:

$$Z_3(\mu^2) = \mu^2 G^{(2)}(\mu^2) \tag{2.7}$$

$$\widetilde{Z}_3(\mu^2) = \mu^2 F^{(2)}(\mu^2). \tag{2.8}$$

The coupling constant has also to be renormalised to complete the renormalisation of a pure Yang-Mills theory. It can be defined non-perturbatively by an amputation of a three-point Green-functions from its external propagators. But this requires to fix the kinematic configuration of the three-point Green-function at the normalisation point. On the lattice one usually uses either a fully symmetric kinematic configuration (denoted MOM) or a zero point (ZP) kinematic configuration with one vanishing external momentum (denoted generically $\widetilde{\text{MOM}}$), see Figure 2.1.

Three-gluon vertex: symmetric case

There are only two independent tensors in Landau gauge in the case of the symmetric three-gluon Green function [19]:

$$\mathcal{T}^{[1]}_{\mu_1,\mu_2,\mu_3}(p_1,p_2,p_3) = \delta_{\mu_1\mu_2}(p_1-p_2)_{\mu_3} + \delta_{\mu_2\mu_3}(p_2-p_3)_{\mu_1} + \delta_{\mu_3\mu_1}(p_3-p_1)_{\mu_2} \tag{2.9}$$

$$\mathcal{T}^{[2]}_{\mu_1,\mu_2,\mu_3}(p_1,p_2,p_3) = \frac{(p_1-p_2)_{\mu_3}(p_2-p_3)_{\mu_1}(p_3-p_1)_{\mu_2}}{p^2}. \tag{2.10}$$

Then the three-gluon Green function in MOM scheme ($p_1^2 = p_2^2 = p_3^2 = \mu^2$) can be parametrised as

$$\left\langle \widetilde{A}^a_{\mu_1}(p_1)\widetilde{A}^b_{\mu_2}(p_2)\widetilde{A}^c_{\mu_3}(p_3)\right\rangle = f^{abc}\Big[G^{(3)\mathrm{sym}}(\mu^2)\mathcal{T}^{[1]}_{\mu_1',\mu_2',\mu_3'}(p_1,p_2,p_3)\prod_{i=1,3}\left(\delta_{\mu_i'\mu_i}-\frac{p_{i\mu_i'}p_{i\mu_i}}{\mu^2}\right)+ \\ + H^{(3)}(\mu^2)\mathcal{T}^{[2]}_{\mu_1,\mu_2,\mu_3}(p_1,p_2,p_3)\Big] \tag{2.11}$$

For a non-perturbative MOM definition of the renormalised coupling g_R one need to extract the scalar function $G^{(3)\mathrm{sym}}(\mu^2)$, proportional to the coupling g_0 at the tree order. This is done by the following projection:

$$G^{(3)\mathrm{sym}}(\mu^2) = \left(\mathcal{T}^{[1]}_{\mu_1',\mu_2',\mu_3'}(p_1,p_2,p_3)\prod_{i=1,3}\left(\delta_{\mu_i'\mu_i}-\frac{p_{i\mu_i'}p_{i\mu_i}}{\mu^2}\right)+\frac{1}{2}\mathcal{T}^{[2]}_{\mu_1',\mu_2',\mu_3'}(p_1,p_2,p_3)\right)\times \\ \times\frac{1}{18\mu^2}\frac{f^{abc}}{N_c(N_c^2-1)}\left\langle \widetilde{A}^a_{\mu_1}(p_1)\widetilde{A}^b_{\mu_2}(p_2)\widetilde{A}^c_{\mu_3}(p_3)\right\rangle \tag{2.12}$$

Three-gluon vertex: asymmetric case

The three-gluon Green function with one vanishing external propagator ([20],[19]) can be parametrised as

$$G^{(3)abc}_{\mu\nu\rho}(p,0,-p)\equiv\left\langle \widetilde{A}^a_\mu(-p)\widetilde{A}^b_\nu(p)\widetilde{A}^c_\rho(0)\right\rangle = 2f^{abc}p_\rho\left(\delta_{\mu\nu}-\frac{p_\mu p_\nu}{p^2}\right)G^{(3)\mathrm{asym}}(p^2), \tag{2.13}$$

and thus

$$G^{(3)\mathrm{asym}}(p^2) = \frac{1}{6p^2}\frac{f^{abc}}{N_c(N_c^2-1)}\delta_{\mu\nu}p_\rho G^{(3)abc}_{\mu\nu\rho}(p,0,-p). \tag{2.14}$$

Ghost-gluon vertex

Similar parametrisation may be written in the case of the ghost-ghost-gluon Green function (cf. Figure 2.2). But in this case one obtains two different renormalisation

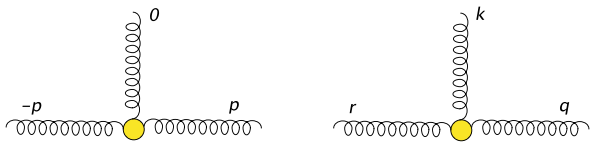

Figure 2.1: *Definitions of the $\widetilde{MOM}$ scheme, $p^2 = \mu^2$ (left) and MOM, $q^2 = r^2 = k^2 = \mu^2$ (right)*

schemes $\widetilde{\mathrm{MOM}}_c$ and $\widetilde{\mathrm{MOM}}_{c0}$ corresponding to the zero-point kinematic configuration with vanishing momentum of, respectively, the gluon and the entering ghost. We denote by $\widetilde{G}^{(3)}_{\mathrm{K}}$ a generic scalar function extracted from a three-point function in

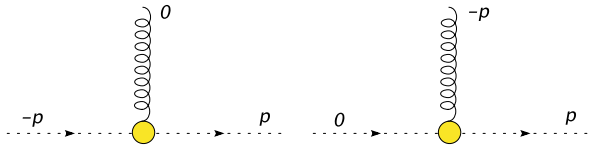

Figure 2.2: *Kinematic configurations of the* $\widetilde{\text{MOM}}_c$, $\widetilde{\text{MOM}}_{c0}$ *schemes,* $p^2 = \mu^2$.

a particular kinematic configuration K. Then the gauge coupling at the renormalisation scale μ^2 is defined by

$$g_R^{(K)}(\mu^2) = \frac{G_{\mathrm{K}}^{(3)}(p_1^2, p_2^2, p_3^2)}{G^{(2)}(p_1^2)G^{(2)}(p_2^2)G^{(2)}(p_3^2)} Z_3^{3/2}(\mu^2) \tag{2.15}$$

in the case of three-gluon vertices, where the choice of p_i determines the renormalisation scheme. For of ghost-ghost-gluon vertices the coupling is defined by

$$\tilde{g}_R^{(K)}(\mu^2) = \frac{\widetilde{G}_{\mathrm{K}}^{(3)}(p_1^2, p_2^2, p_3^2)}{F^{(2)}(p_1^2)F^{(2)}(p_2^2)G^{(2)}(p_3^2)} Z_3^{1/2}(\mu^2)\widetilde{Z}_3(\mu^2). \tag{2.16}$$

where $\widetilde{G}_{\mathrm{K}}^{(3)}(p_1^2, p_2^2, p_3^2)$ is the scalar factor of the ghost-gluon three point function $\left\langle \widetilde{\mathcal{A}}_\mu(p_1)\widetilde{c}(p_2)\widetilde{\bar{c}}(p_3) \right\rangle$. In fact, only the coupling in the $\widetilde{\text{MOM}}_c$ scheme can be defined non-perturbatively for the reasons explained in the following section.

2.2 Numerical calculation of the ghost Green functions in Landau gauge

2.2.1 Lattice implementation of the Faddeev-Popov operator

In order to calculate numerically [21] the ghost propagator

$$F^{(2)}(x-y)\delta^{ab} \equiv \left\langle \left({\mathcal{M}_{FP}^{\mathrm{lat}}}^{-1} \right)_{xy}^{ab} \right\rangle \tag{2.17}$$

one uses the lattice definition (1.68) of the Faddeev-Popov operator. Most lattice implementations of the Faddeev-Popov operator use its explicit component form. But as we have seen the action of the Faddeev-Popov operator on a vector ω can also be written as a lattice divergence

$$\mathcal{M}_{FP}^{\mathrm{lat}}[U]\omega = -\frac{1}{V}\nabla_\mu \mathcal{A}'_\mu \tag{2.18}$$

where $\mathcal{A}'$ is defined by (1.66). This form allows a very efficient lattice implementation which is based on the fast routines coding the group multiplication law:

ω_{in}, ω_{out} *are the ghost fields.*
$U_\mu(x)$ *is the gauge configuration.*
type $SU(N_c)$ $\quad U_\mu(x), dU, W, W_+, W_-$
type $\mathfrak{su}(N_c)$ $\quad \omega_{in}(x), \omega_{out}(x)$
for all x **do**
  $dU = 0.$
  $W = \omega_{in}(x)$
  do $\mu = 1 \ldots 4$
    $W_+ = \omega_{in}(x + e_\mu)$
    $W_- = \omega_{in}(x - e_\mu)$
    $dU = dU + U_\mu(x - e_\mu) * W + W * U_\mu(x)$
      $- U_\mu(x) * W_+ - W_- * U_\mu(x - e_\mu)$
  end do
  $\omega_{out}(x) = dU - dU^\dagger - \frac{1}{N_c}\mathrm{Tr}(dU - dU^\dagger)$
end do

2.2.2 Numerical inversion of the Faddeev-Popov operator

We invert the Faddeev-Popov operator by solving the equation

$$\sum_{y,b} \mathcal{M}^{\mathrm{lat}}_{FP}[U]^{ab}(x,y)\eta^b(y) = S^a(x), \tag{2.19}$$

for some source $S^a(x)$ using an appropriate algorithm (for a review of algorithms see [22]). The operator $\mathcal{M}^{\mathrm{lat}}_{FP}[U]$ has zero-modes, that is why the inversion can only be done in the vector subspace $K^\perp$ orthogonal to the kernel of the operator. The trivial zero-modes are constant fields. If we neglect Gribov copies then the Faddeev-Popov operator has no other zero-modes, and thus the non-zero Fourier modes form a basis of $K^\perp$:

$$\eta(y) = \sum_{p\neq 0} c_p e^{ip\cdot y}, \quad \forall \eta \in K^\perp. \tag{2.20}$$

The inversion in one Fourier mode

Choosing the source for inversion in the form

$$S^a_p(x) = \delta^{ab} e^{ip\cdot x} \tag{2.21}$$

and taking the scalar product of the inverse $\mathcal{M}_{FP}^{\text{lat}}[U]^{-1} S_p^a$ with the source one obtains

$$\left\langle \left(S_p^a \mid \mathcal{M}_{FP}^{\text{lat}\,-1} S_p^a \right) \right\rangle = \sum_{x,y} \left\langle \left(\mathcal{M}_{FP}^{\text{lat}\,-1} \right)_{xy}^{aa} \right\rangle e^{-ip\cdot(x-y)} \tag{2.22}$$

$$= V\, \widetilde{F}^{(2)}(p) \tag{2.23}$$

after averaging over the gauge field configurations. This method requires one matrix inversion for each momentum p. It is suitable only when one is interested in a few values of the ghost propagator.

The inversion in all Fourier modes

One can calculate the ghost propagator for all momenta p doing only one matrix inversion noticing that

$$\delta_{x,y} = \frac{1}{V} + \frac{1}{V} \sum_{p \neq 0} e^{-ip\cdot(x-y)} \tag{2.24}$$

and choosing for the source:

$$S_0^a(x) = \delta^{ab} \left(\delta_{x,0} - \frac{1}{V} \right). \tag{2.25}$$

The Fourier transform of $M^{-1} S_0^a$, averaged over the gauge configurations, yields:

$$\begin{aligned} \sum_x e^{-ip\cdot x} \left\langle \mathcal{M}_{FP}^{\text{lat}\,-1} S_0^a \right\rangle &= \sum_x e^{-ip\cdot x} \left\langle \left(\mathcal{M}_{FP}^{\text{lat}\,-1} \right)_{x0}^{aa} \right\rangle - \frac{1}{V} \sum_{x,y} e^{-ip\cdot x} \left\langle \left(\mathcal{M}_{FP}^{\text{lat}\,-1} \right)_{xy}^{aa} \right\rangle \\ &= \sum_x e^{-ip\cdot x} F^{(2)}(x) - \frac{1}{V} \sum_{x,y} e^{-ip\cdot x} F^{(2)}(x-y) \\ &= \widetilde{F}^{(2)}(p) - \delta(p) \sum_x F^{(2)}(x), \end{aligned} \tag{2.26}$$

where we have used the translational invariance of the ghost propagator. Therefore, with this choice of the source, only one matrix inversion followed by one Fourier transformation of the solution is required to get the ghost propagator for all values of the lattice momenta.

Because in the case of the source (2.25) one inverts in all modes at the same time, some statistical accuracy is lost. However, it turns out to be sufficient for our purposes.

There is one important technical point that should be mentioned. During the inversion process it is mandatory to check, whatever the choice of sources, that rounding errors during the inversion do not destroy the condition that the solution is still orthogonal to the kernel of the Faddeev - Popov operator:

$$\sum_x \left(\mathcal{M}_{FP}^{\text{lat}\,-1} S \right)(x) = 0 \tag{2.27}$$

Indeed, if the zero-mode component of the solution grows beyond some threshold during the inversion of the Faddeev-Popov operator on a gauge configuration, then this component starts to increase exponentially, and a sizeable bias is produced in other components as well. We have observed this phenomenon occasionally, about one gauge configuration every few hundreds, when using the componentwise implementation of the lattice Faddeev-Popov operator based on (1.68). However, we have never observed sizeable deviations from (2.27) using the efficient implementation of the Faddeev-Popov operator exposed in the subsection 2.2.1.

2.2.3 Calculation of the ghost-gluon vertex

In order to calculate the ghost-gluon three-point function in $\widetilde{\text{MOM}}_c$ and $\widetilde{\text{MOM}}_{c0}$ renormalisation schemes one has to calculate the corresponding ghost two-point function:

$$\left\langle \widetilde{\mathcal{A}}_\mu(p_1)\,\underbrace{\widetilde{c}(p_2)\widetilde{\overline{c}}(p_3)}\right\rangle \quad \overset{\text{lattice}}{\longrightarrow} \quad \sum_{\text{conf. } i} \widetilde{\mathcal{A}}_\mu(p_1)\big(\widetilde{\mathcal{M}^{\text{lat}}_{FP}[U_i]^{-1}}\big)(p_2,p_3) \tag{2.28}$$

It is quite easy to calculate this Green function in the $\widetilde{\text{MOM}}_c$ kinematic configuration, because in this case $p_2 = -p, p_3 = p$ and $\big(\widetilde{\mathcal{M}^{\text{lat}}_{FP}[U_i]^{-1}}\big)(-p,p)$ is just a ghost propagator in the background gluon field defined by U_i.

The situation changes when considering the kinematic configurations like $\widetilde{\text{MOM}}_{c0}$, when the momentum of the entering (or of the outgoing) ghost is set to zero. In this case the inversion of the Faddeev-Popov operator has to be performed with the source (2.21). In other words we try to solve the equation

$$\mathcal{M}^{\text{lat}}_{FP}[U]_{xy}\eta_{yz} = e^{ip\cdot(x-z)}. \tag{2.29}$$

The vector $\overline{\eta}_y = \frac{1}{V}\sum_z \eta_{yz}e^{ip\cdot z}$ is the solution of

$$\mathcal{M}^{\text{lat}}_{FP}[U]_{xy}\overline{\eta}_y = e^{ip\cdot x}, \tag{2.30}$$

and

$$\overline{\eta}_y = \frac{1}{V}\sum_z \eta_{yz}e^{ip\cdot z} = \frac{1}{V}\sum_z c(y)\overline{c}(z)e^{ip\cdot z} \equiv c(y)\widetilde{\overline{c}}(p). \tag{2.31}$$

Doing a summation on y we obtain a Fourier transform of the field $c(y)$:

$$\frac{1}{V}\sum_y \overline{\eta}_y = \widetilde{c}(0)\widetilde{\overline{c}}(p). \tag{2.32}$$

But the last equation expresses the orthogonality condition (2.27). Thus we find $\widetilde{c}(0)\widetilde{\overline{c}}(p) = 0$ in this case. That means that (2.28) is also zero, and the vertex function cannot be directly extracted (on the lattice) in the kinematic configuration with vanishing ghost momentum $\widetilde{\text{MOM}}_{c0}$, but only in the $\widetilde{\text{MOM}}_c$ scheme.

2.3 Errors of the calculation

There are three main sources of errors when calculating Green functions on the lattice: the statistical errors of the Monte-Carlo method, the systematic bias coming from the space-time discretisation and finally the error due to the gauge fixing (influence of lattice Gribov copies). The last is discussed in the following section.

2.3.1 Estimating the statistical error

The gauge-field configurations produced via the Monte-Carlo generation process (see [13] for a review) are not completely decorrelated. However, the residual correlations may be neglected. Nevertheless, all data points (as function of momentum p) of a Green function are calculated on the same set of gauge configurations $\{C_i\}$, and in this sense they are not independent. This problem arises when calculating quantities involving functions of mean values, like the coupling constant in a MOM scheme. In order to take in account the bias induced by this correlation one uses a special method (called **Jackknife** [23], [24]) of computation of the error. Generally speaking this method is a standard bootstrap method (of the estimation of the variance in the case of a non-Gaussian distribution) based on a resampling with replacement from the original sample. We start with a Monte-Carlo sample of size M. Our purpose is to calculate the error on the estimation of the mean of this sample. We divide it into $[M/m]$ groups of m elements:

$$\Big[\mathcal{O}(C_1),\ldots,\mathcal{O}(C_m)\Big] \quad \Big[\mathcal{O}(C_{m+1}),\ldots,\mathcal{O}(C_{2m})\Big] \quad \ldots \quad \Big[\ldots,\mathcal{O}(C_M)\Big]. \tag{2.33}$$

Next one defines the partial averages

$$a_k = \frac{\sum_{i=1}^{M}\mathcal{O}(C_i) - \sum_{i=km}^{(k+1)m}\mathcal{O}(C_i)}{M-m}, \quad k = 1\ldots\widetilde{M} = \left[\frac{M}{m}\right], \tag{2.34}$$

and finally obtains the following expression for the error:

$$\Delta_{\text{jackknife}}\langle\mathcal{O}\rangle = \sqrt{\frac{\widetilde{M}-1}{\widetilde{M}}\left(\sum_{k=1}^{\widetilde{M}} a_k^2 - \frac{\left(\sum_{k=1}^{\widetilde{M}} a_k\right)^2}{\widetilde{M}}\right)}. \tag{2.35}$$

This analytical expression differs from the standard formula for the dispersion of the mean value by an additional factor $\sim \widetilde{M}$.

2.3.2 Handling the discretisation errors

Because of discretisation of the space-time, lattice theory [1] looses the rotational symmetry $SO(4)$ inherited from the Lorenz invariance in Minkowski space. This symmetry is replaced by a discret isometry group $H_4 = S_4 \ltimes P_4$ (semiproduct of the

[1] we suppose that the lattice is hypercubic.

permutation and reflection groups) having $4! \cdot 2^4 = 384$ elements. A generic scalar function $\widehat{G}(p)$ extracted form Green functions is thus invariant along the orbit $O(p)$ generated by the action of the group H_4 on the components of the lattice momentum $p \equiv \frac{2\pi}{La} \times (n_1, n_2, n_3, n_4)$. It may be proven in the theory of group invariants that each orbit is characterised by four group invariants

$$p^{[n]} = a^n \sum_\mu p_\mu^n, \quad n = 2, 4, 6, 8 \tag{2.36}$$

One may average on the gauge orbit of the H_4 group in order to increase the statistics:

$$a^2 G_L(p^{[2]}, p^{[4]}, p^{[6]}, p^{[8]}) = \frac{1}{\operatorname{card} O(p)} \sum_{p \in O(p)} \widehat{G}(p), \tag{2.37}$$

where $\operatorname{card} O(p)$ is the number of elements in the orbit $O(p)$. The resulting average is a function of the four invariants $p^{[n]}$. But in the continuum limit any scalar function is a function of the rotational invariant $p^{[2]}$. We will explain how it is possible to remove the dependence on the three other invariants with the example of the free lattice gluon propagator:

$$G_0(p) = \frac{1}{\sum_\mu \widehat{p}_\mu^2}, \quad \text{where} \quad \widehat{p}_\mu = \frac{2}{a} \sin\left(\frac{a p_\mu}{2}\right). \tag{2.38}$$

If all the components of the lattice momentum verify the condition $a p_\mu \ll 1$, then $\sum_\mu \widehat{p}_\mu^2 \simeq p^2 - \frac{1}{12} a^2 p^{[4]}$, and thus one has up to terms of order $\sim a^4$

$$G_0(p) = \frac{1}{p^2} \left(1 + \frac{1}{12} \frac{a^2 p^{[4]}}{p^2} + O(a^4)\right). \tag{2.39}$$

So, taking the continuum limit $a \to 0$ is equivalent to taking the limit $p^{[4]} \to 0$. We apply this idea to (2.37). Making the reasonable hypothesis of regularity near the continuum limit, we expand:

$$G_L(p^{[2]}, p^{[4]}, p^{[6]}, p^{[8]}) \approx G_L(p^{[2]}, 0, 0, 0) + p^{[4]} \frac{\partial G_L}{\partial p^{[4]}}(p^{[2]}, 0, 0, 0) + \cdots \tag{2.40}$$

and $G_L(p^{[2]}, 0, 0, 0)$ is nothing but the scalar factor in the continuum in a finite volume, up to lattice artifacts which do not break $O(4)$ invariance. When several orbits exist with the same p^2, we can remove an important part of the hypercubic artifacts by extrapolating the lattice data towards $G_L(p^{[2]}, 0, 0, 0)$ using a linear regression with respect to $p^{[4]}$ (the other invariants are of higher order in a).

There are vectors p that have only one orbit. In order to include them in the data analysis one should interpolate the slopes obtained in the extrapolation of (2.40). This can be done either numerically or by assuming a functional dependence of the slope with respect to p^2. In principle the p^2 dependence of the slope may be calculated using lattice perturbation theory. A dimensional analysis suggests the

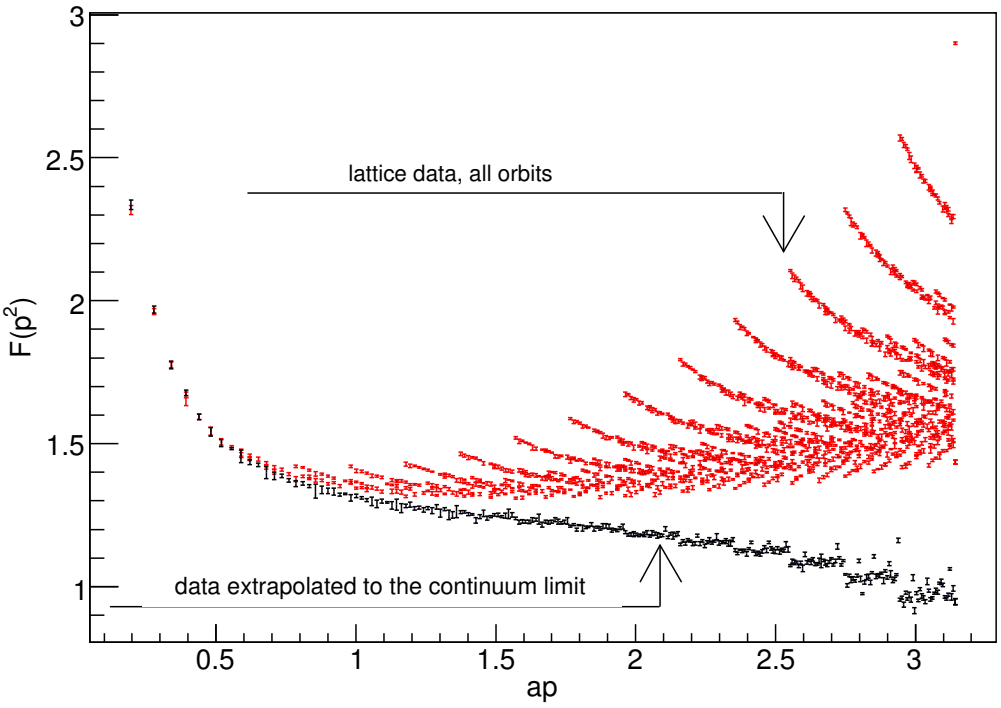

Figure 2.3: *Example of the extrapolation in $p^{[4]}$ for the ghost scalar factor $F(p)$ in the case of the $SU(3)$ gauge group for the lattice volume 32^4 and at $\beta = 6.4$. Red round dots correspond to the bare data, and blue squares to the extrapolated one. In practice we do not consider the moments above $ap = \frac{\pi}{2}$.*

form $\sim \frac{c_1}{(p^2)^2}$. We have used the function

$$\frac{\partial G_L}{\partial p^{[4]}}(p^{[2]},0,0,0) = \frac{1}{\left(p^{[2]}\right)^2}\left(c_1 + c_2 p^{[2]}\right) \tag{2.41}$$

with two fit parameters in order to fit the slopes. The validity of the exposed method is qualitatively checked by the smoothness of the resulting curve. At Figure 2.3 we present an example of removing the hypercubic artifacts. We see that the method works very well, even at large values of ap. In practice we do not consider the momenta above $ap = \frac{\pi}{2}$.

2.4 Gribov ambiguity and lattice Green functions

We have discussed in the previous sections different uncertainties introduced by the discretisation of space-time. Another bias comes from the gauge fixing (see section 1.1.2). As we have already mentioned, the Minimal Landau gauge fixing quantisation is equivalent to realising the Gribov quantisation prescription. Thus lattice Green functions are calculated within this prescription. However, the gauge is not fixed in a unique way. The Gribov ambiguity on the lattice shows up by the non-uniqueness of the minimum (1.59) of the functional (1.60). Indeed, the functional (1.60) has a form similar to the energy of a spin glass which is known to have

exponentially-many metastable states (cf. Figure 2.4). All these lattice Gribov copies are situated inside the Gribov horizon. On a finite lattice one can (in principle) fix the gauge in a unique way. However this is very expensive in terms of computer time.

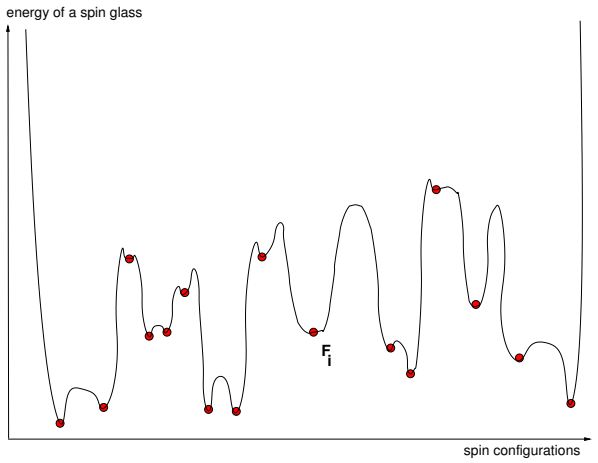

Figure 2.4: *Landscape of minima for a generic spin glass. Circles mark the configurations corresponding to metastable states. Their number grow like* $\exp(const \cdot N)$ *as function of the number of spins* N.

Nevertheless one has to understand the influence of the choice of the minimum of the functional (1.60) on the mean values yielding Green functions. For this purpose we studied the landscape of minima of the gauge-fixing functional [18]. In the following subsection we define a specific probability to find a Gribov copy, as function of the physical momentum. In the next-to-the-following subsection we discuss the influence of these copies on the Green functions, and the Zwanziger's conjecture on the equivalence of the integration over the Gribov region and the fundamental modular region in the infinite volume limit.

2.4.1 The landscape of minima of the gauge-fixing functional

Let us consider the landscape of the functional F_U. One of its characteristics is the distribution of values at minima $F_{\min}$ of F_U. We know that for small magnitudes of the gauge field all the link matrices $U_\mu(x)$ (they play the role of couplings between the "spin" variables) are close to the identity matrix, and thus the minimum is unique. Their number increases when the bare lattice coupling β decreases, because the typical magnitude of the phase of $U_\mu(x)$ grows in this case and thus link matrices move farther from the identity matrix. The number of minima also increases with the number of links (at fixed β) because in this case there are more degrees of freedom in the system.

We can define a probability to find a secondary minimum, as a function of the β parameter. For each orbit we fix the gauge N_{GF} times, each gauge fixing starts after a (periodic) random gauge transformation of the initial field configuration. We thus obtain a distribution of minima $F_{\min}$. This distribution gives us the number of minima $N(F^i)$ as a function of the value of $F^i \equiv F^i_{\min}$. The relative frequency of a

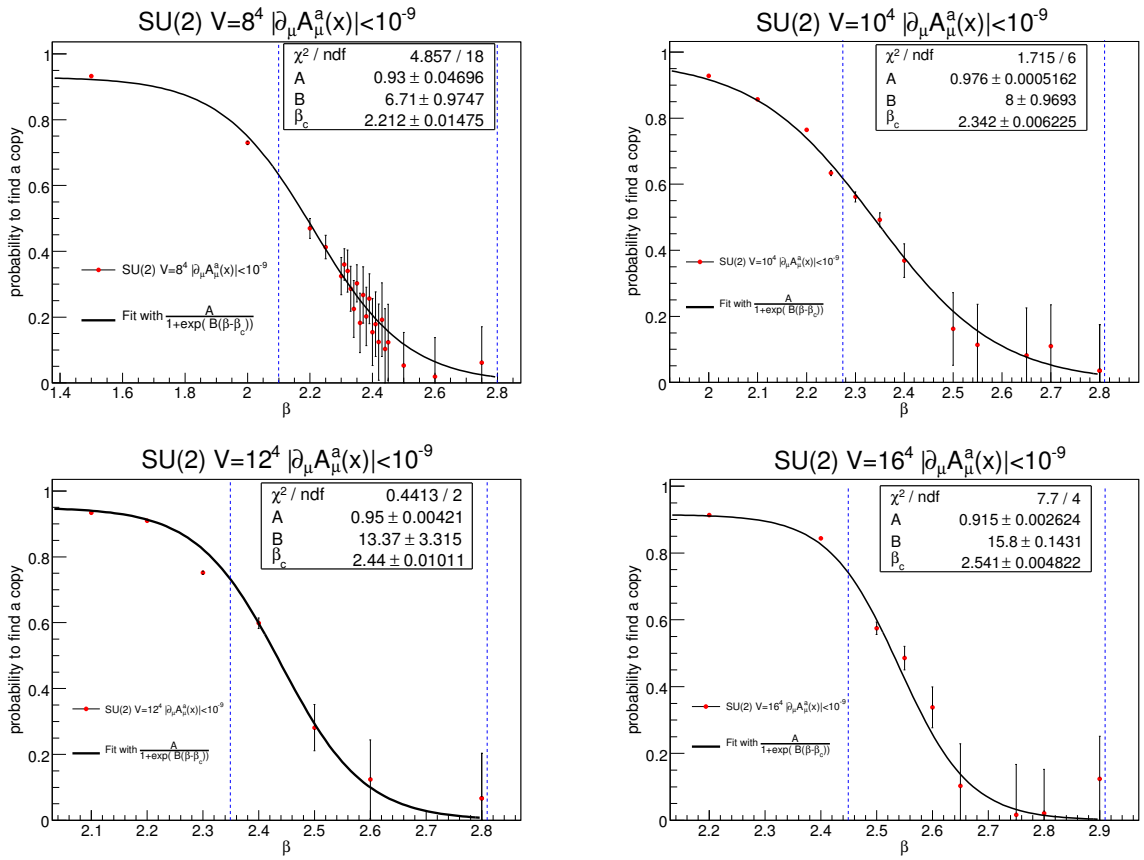

Figure 2.5: *Probability (averaged over gauge orbits) to find a secondary minimum as a function of β at volumes $V = 8^4, 10^4, 12^4, 16^4$. Solid line represents a fit with an empirical formula (2.46). The vertical dashed lines delimit the window of each fit.*

minimum F^i is defined by

$$\omega_i = \frac{N(F^i)}{\sum_i N(F^i)}, \tag{2.42}$$

where $\sum_i N(F^i) = N_{\text{GF}}$. Then the weighted mean number of copies per value of F_{min} is given by

$$\overline{N} = \sum_i \omega_i N(F^i). \tag{2.43}$$

This allows us to define a probability to find a secondary minimum when fixing the Minimal Landau gauge for a given gauge field configuration :

$$p_{1\text{conf}} = 1 - \frac{\overline{N}}{\sum_i N(F^i)}. \tag{2.44}$$

If one finds the same value of F_{min} for all N_{GF} tries then this probability is zero. On the contrary, if all F_i are different then $p_{1\text{conf}}$ is close to one.

Having the probability to find a secondary minimum when fixing the gauge for *one particular* configuration we can calculate the Monte-Carlo *average* $\langle \bullet \rangle$ on gauge orbits, i.e. on "spin couplings" $U_\mu(x)$. We obtain finally the overall probability to

find a secondary minimum during a numerical simulation at given β:

$$P(\beta) \equiv \langle p_{1\text{conf}} \rangle_{\{U_\mu(x)\}} = 1 - \left\langle \frac{\overline{N}}{\sum_i N(F^i)} \right\rangle_{\{U_\mu(x)\}} . \tag{2.45}$$

We have performed simulations in the case of $SU(2)$ latice gauge theory at volumes $V = \{8^4, 10^4, 12^4, 16^4\}$ for β varying from 1.4 to 2.9. For each value of β we generated 100 independent Monte-Carlo gauge configurations, and we fixed the gauge $N_{\text{GF}} = 100$ times for every configuration. Between each gauge fixing a random gauge transformation of the initial gauge configuration was performed, and the minimising algorithm stops when the triple condition (1.71) is satisfied. Examples of the resulting probability to find a secondary minimum are presented at Figure 2.5.

As expected, the probability is small when β is large, and it is close to one when β is small. The dispersion was calculated using the Jackknife method (discussed in the subsection 2.3.1). The physical meaning of this dispersion is the following: when the error is small, all gauge configurations have a similar number of secondary minima. On the contrary, this dispersion is large if there are some exceptional gauge configurations having a different number of copies. At small β almost all gauge configurations have many secondary minima, that is why the dispersion of the probability is small. At large β almost all gauge configurations have a unique minimum, but some of them can have copies. This may considerably increase the dispersion of the probability. The appearance of exceptional gauge configuration possessing a large density of close-to-zero eigenvalues of the Faddeev-Popov operator has been recently reported [25]. Probably these fields are related with those having a lot of secondary minima at large β's, and this correlation deserves a separate study.

We can fit our data (Figure 2.5) for the probability (2.45) with an empirical formula

$$P(\beta) = \frac{A}{1 + e^{B(\beta - \beta_c)}} \tag{2.46}$$

in order to define a characteristic coupling β_c when the probability to find a copy decreases considerably. One can define β_c as corresponding to the semi-heights of the probability function $P(\beta)$. At this value of β an equally probable secondary attractor of the functional F_U appears. The fit has been performed for the points between dashed lines at Figure 2.5, and the results for the fit parameters are given ibidem and in Table 2.1. We see that β_c depends on the volume of the lattice. Let us check whether these values correspond to some physical scale. According to works [26],[27] one has the following expression for the string tension σ for $\beta \geq 2.3$:

$$[\sigma a^2](\beta) \simeq e^{-\frac{4\pi^2}{\beta_0}\beta + \frac{2\beta_1}{\beta_0^2}\log\left(\frac{4\pi^2}{\beta_0}\beta\right) + \frac{4\pi^2}{\beta_0}\frac{d}{\beta} + c} \tag{2.47}$$

with $c = 4.38(9)$ and $d = 1.66(4)$ [2]. Using this formula, we define a characteristic

[2] in this cited formula we kept the original convention for the RG β-function, namely $\beta_0 = 11/3N_C$, $\beta_1 = 17/3N_C^2$. They are different from the one we use in the following.

scale corresponding to the critical values β_c from Figure 2.5 :

$$\lambda_c = a(\beta_c) \cdot L$$

in the string tension units, L is the length of the lattice. In the last column of the Table 2.1 we summarise the results. We see that for the values of β_c in the scaling

L	β_c	χ^2/ndf	λ_c, in units of $1/\sqrt{\sigma}$
8	2.221(14)	0.27	3.85(31)
10	2.342(6)	0.28	3.20(21)
12	2.44(1)	0.22	2.78(20)
16	2.541(5)	1.92	2.68(17)

Table 2.1: *The characteristic length defining the appearance of secondary minima. The errors for λ_c include errors for d and c parameters, and the fitted error for β_c*

regime, when the formula (2.47) is applicable ($\beta \geq 2.3$), we obtain compatible values for the physical length λ_c.

This suggests that in the case of $SU(2)$ gauge theory lattice Gribov copies appear when the physical size of the lattice exceeds a critical value around $2.75/\sqrt{\sigma}$. At first approximation λ_c is scale invariant, but a slight dependence in the lattice spacing remains.

In principle, the parameter β_c can be calculated with good precision. One should do it in the case of $SU(3)$ gauge group, because the dependence of the lattice spacing on the bare coupling is softer, and the scaling of the theory has been better studied than in the case of the $SU(2)$ theory.

A natural question that arises after the study of the distribution of F_{min} is whether the gauge configurations having the same value of F_{min} are equivalent, i.e. they differ only by a global gauge transformation. This can be checked by calculating the two-point gluonic correlation function on the gauge configuration. Indeed, according to the lattice definition of the gauge field that we used (1.52),

$$G^{(2)}_{1\,\text{conf}}(x-y) \propto \text{Tr}\left[\left(U_\mu(x) - U^\dagger_\mu(x)\right) \cdot \left(U_\nu(y) - U^\dagger_\nu(y)\right)\right]. \tag{2.48}$$

Applying a global gauge transformation $U_\mu(x) \to V U_\mu(x) V^\dagger$ we see that the gluon propagator remains unchanged. This is also the case of the ghost propagator scalar function. We have checked numerically that the values of the gluon and the ghost propagators in Fourier space are the same for gauge configurations having the same F_{min}. Thus we conclude that gauge configurations having the same F_{min} are in fact equivalent [18].

2.4.2 Lattice Green functions and the Gribov ambiguity

As we have mentioned in the subsection 1.1.2, there is a conjecture [5] saying that in the infinite volume limit the expectation values calculated by integration over the Gribov region or the fundamental modular region become equal. Let us briefly

recall the argument given in [5]. Let B_μ denote a field lying on the Gribov horizon:

$$\begin{cases} \partial_\mu B_\mu = 0 \\ \mathcal{M}_{FP}(B)\omega_0 = 0, \qquad \omega_0(x) \neq \text{const}, \quad \omega_0(x) \in \mathfrak{su}(N_c). \end{cases} \tag{2.49}$$

We write $F_B(t,\omega)$ for the functional (1.57), with $u(x) = \exp t\omega(x)$. On the boundary one has

$$\begin{cases} F'_B(0,\omega_0) = 0 \\ F''_B(0,\omega_0) = 0 \\ F'''_B(0,\omega_0) \neq 0 \propto \sqrt{V} \\ F''''_B(0,\omega_0) = \frac{3}{2}\int d^4x \left[d_\mu(\omega_0^2)\right]^2 \propto V \end{cases} \tag{2.50}$$

So for small variations of t one has for the functional (1.57)

$$F_B(t) = F_B(0) + \frac{1}{3!}F'''_B(0)t^3 + \frac{1}{4!}F''''_B(0)t^4, \tag{2.51}$$

and the last expression is minimised for $t = \bar{t} \equiv -3F'''_B(0)/F''''_B(0)$. The value that is achieved at this secondary minimum inside the Gribov horizon is

$$F_B(\bar{t}) = F_B(0) - \frac{9}{8}\frac{\left[F'''_B(0)\right]^4}{\left[F''''_B(0)\right]^3}. \tag{2.52}$$

Using the estimations (2.50) and the fact that the third order derivative appears in an even power, one sees that the secondary minimum is *lower* than the one on the boundary, and the difference between them *decreases* with the volume V. The corresponding gauge configuration can be written as

$$B_\mu(x,\bar{t}) = B_\mu(x,0) + \bar{t}\left[D_\mu(B)\omega_0\right](x) = B_\mu(x,0) - 3\frac{F'''_B(0)}{F''''_B(0)}\left[D_\mu(B)\omega_0\right](x). \tag{2.53}$$

When the lattice volume V is large, the integration (over G or Λ) on the gauge configurations is dominated by a small shell near the boundary, because the dimension of the configuration space is large ($2dV(N_C^2-1)$). According to the above argument the configurations near the boundaries ∂G and $\partial\Lambda$ draw together. So, having (2.53) for a typical gauge field configuration, it is natural to suppose that in the infinite volume limit the average calculated by integration over the domains G or Λ become equal. However at a finite lattice this is clearly not the case, that is why it is very important to know what is the influence of lattice Gribov copies on the Green functions. This question that has already been considered by different authors ([28],[29],[30],[31],[32],[33],[25]). To check the dependence of Green functions on the procedure of the choice of the minimum we adopted the same strategy as in above citations : for every of the 100 gauge configurations used to compute Green functions the gauge was fixed 100 times (a periodic random gauge transformation is done after each gauge fixing). The Monte-Carlo average was computed with respect to the "first copy" (fc) found by the minimisation algorithm and the "best copy" (bc), having the smallest value of $F_{\min}$. We have calculated the gluon and the ghost propagators, and also the three-gluon Green functions in symmetric and asymmetric

β	L	n^2	$F_{\rm fc}^{(2)}(p^2) - F_{\rm bc}^{(2)}(p^2)$	$\frac{F_{\rm fc}^{(2)}(p^2) - F_{\rm bc}^{(2)}(p^2)}{F_{\rm bc}^{(2)}}$
2.1	8	1	0.211	0.045
		$\vee$		
2.1	16	$4_{\ n^{[4]}=16}$	0.145	0.033
2.2	8	1	0.078	0.019
		$\vee$		
2.2	16	$4_{\ n^{[4]}=16}$	0.023	0.006
2.3	8	1	0.086	0.024
		$\wedge$		
2.3	16	$4_{\ n^{[4]}=16}$	0.114	0.034

Table 2.2: *Volume dependence of the ghost propagators [18],* $p_\mu = \frac{2\pi}{aL} n_\mu$

β	L	$\overline{\langle F_{\rm min}\rangle}_{\{U\}}$	$\delta\overline{\langle F_{\rm min}\rangle}_{\{U\}}$
2.2	8	-0.8236	0.003744
	10	-0.8262	0.002367
	12	-0.8272	0.001377
	16	-0.8279	0.000802
2.4	8	-0.8642	0.005270
	12	-0.8669	0.002739
	12	-0.8686	0.001849
	16	-0.8702	0.001003

Table 2.3: *Volume dependence of the Monte-Carlo+gauge orbit mean value at minima* F_{min} *and the dispersion of this mean.*

kinematic configurations. The simulations have been performed in the case of the $SU(2)$ group on lattices of volumes 8^4 and 16^4 for $\beta = 2.1, 2.2, 2.3$. According to the results of the subsection 2.4.1, at these values of β we are sure to have lattice Gribov copies. We conclude [18] that no systematic effect could be found for gluonic two- and three-point Green functions, the Monte-Carlo average values in the cases of (fc) and (bc) being compatible within the statistical errors. However the ghost propagator is quite sensitive to the choice of the minimum - in the case of (bc) the infrared divergence is lessened. This dependence has been found to decrease slowly with the volume [33]. The results of the subsection 2.4.1 indicate that the convergence can happen only beyond the critical volume λ_c^4. To check this we compare the fc/bc values of the ghost propagator, at one physical value of the momentum, for the orbit $n^2 = 1$ on a 8^4 lattice and the orbit $n^2 = 4, n^{[4]} = 16$ on the 16^4 lattice [3] at the same β (see Table 2.2). It happens indeed that the decrease is observed only at $\beta = 2.1$ and 2.2, in accordance with Table 2.1. However, these values of β are not in the scaling regime, and thus a study on larger lattices would be welcome. It is not surprising that the ghost propagator depends on the bc/fc choice: the (bc) corresponds to the fields further from the Gribov horizon where the Faddeev-Popov operator has a zero mode, whence the inverse Faddeev-Popov operator (ghost propagator) is expected to be smaller as observed. The correlation between the bc/fc choice and the gluon propagator is not so direct. Another quantity is obviously strongly correlated to the

[3] Remember that the momentum in physical units is equal to $2\pi\, n/(La)$ in our notations.

bc/fc choice: the value of $F_{\min}$. We tested the volume dependence of the Monte-Carlo+gauge orbit mean value of the quantity $F_{\min}$ (see Tab.2.3). According to the argument given in [5], all minima become degenerate in the infinite volume limit, and closer to the absolute minimum (in the fundamental modular region). We see from the Table 2.3 that their average value and dispersion decrease with the volume at fixed β, in agreement with [5].

We finish this section with a brief summary of our results [18] regarding the Gribov ambiguity on the lattice:

1. Lattice Gribov copies appear and their number grows very fast when the physical size of the lattice exceeds some critical value ($\approx 2.75/\sqrt{\sigma}$ in the case of the $SU(2)$ theory). This result is fairly independent of the lattice spacing.

2. The configurations lying on the same gauge orbit and having the same $F_{\min}$ are equivalent, up to a global gauge transformation, and yield the same Green functions. Those corresponding to minima of F_U with different values of $F_{\min}$ differ by a non-trivial gauge transformation, and thus they are not equivalent.

3. We confirm the result ([28],[29],[30],[31],[32],[33],[25]) that the divergence of the ghost propagator is lessened when choosing the “best copy" (corresponding to the choice of the gauge configuration having the smallest value of F_U). We also showed that gluonic Green functions calculated in the “first copy” and “best copy” schemes are compatible within the statistical error, no systematic effect was found (with periodic gauge tranformations).

4. We found that the influence of Gribov copies on the ghost propagator decreases with the volume when the physical lattice size is larger than the critical length discussed above. We also show that the quantity $F_{\min}$ decreases when the volume increases. These two points are in agreement with the Zwanzigers's argument [5] on the equality of the averages over the Gribov region and the fundamental modular region.

Chapter 3

The ultraviolet behaviour of Green functions

The Lagrangian of the Pure Yang-Mills theory in a four-dimensional space-time does not contain any dimensional parameters susceptible to fix an energy scale for dimensionless quantities. However, the spectrum of the corresponding quantum theory contains massive states (glueballs). As a matter of fact, the quantum theory possesses a finite energy scale called Λ_{QCD}, which is generated by the quantisation process followed by the renormalisation. All dimensionful physical quantities are expressed as multiples of powers of this scale, and thus it should be a renormalisation group invariant:

$$\mu\frac{d}{d\mu}\Lambda_{\mathrm{QCD}}\left(\mu, g(\mu^2)\right) = 0 \quad \rightarrow \quad \left[\mu\frac{\partial}{\partial\mu} + \beta\left(g(\mu^2)\right)\frac{\partial}{\partial g}\right]\Lambda_{\mathrm{QCD}}\left(\mu, g(\mu^2)\right) = 0, \tag{3.1}$$

where $\beta\left(g(\mu^2)\right)$ is the renormalisation group beta function and μ is the renormalisation scale. The solution of the above equation reads

$$\Lambda_{\mathrm{QCD}}\left(\mu, g(\mu^2)\right) = \mu\exp\left(-\int_{g_1}^{g(\mu^2)}\frac{dg'}{\beta\left(g'\right)}\right), \tag{3.2}$$

where g_1 is an arbitrary integration constant. Λ_{QCD} is a renormalisation scheme-dependent quantity, although it is a renormalisation group invariant within one particular scheme. So it is not a real physical quantity. Still, its value is important for estimating the lowest bound of the domain of validity of perturbation theory. Knowing several first coefficients of the β-function we find from the equation (3.2):

$$\Lambda_{\mathrm{QCD}}\left(\mu, g(\mu^2)\right) = \mu\exp\left[\frac{1}{2\beta_0}\left(\frac{1}{g_1^2} - \frac{1}{g^2(\mu^2)}\right) + \frac{\beta_1}{2\beta_0^2}\log\frac{g_1^2}{g^2(\mu^2)}\right] + O(g^2). \tag{3.3}$$

We see that there is an essential singularity when $g^2(\mu^2) \to 0$, and thus a perturbative calculation of related quantities (for example, the string tension $\sqrt{\sigma} = c_\sigma\Lambda_{\mathrm{QCD}}$) is impossible. In the following sections we describe the method of calculation of Λ_{QCD} from lattice Green functions in Landau gauge. We start with a review of the

purely perturbative results for Green functions. The momentum range available on the lattice is situated at rather low energies where the non-perturbative power corrections are not negligible. The section 3.2 is devoted to the estimation of the dominant power corrections. At the end of this chapter we present the results of analysis of our lattice data.

3.1 $\Lambda_{\rm QCD}$ and perturbative expressions for Green functions

Different scalar factors of Green functions depend on the $\Lambda_{\rm QCD}$ parameter discussed in the previous subsection. These scalar factors can be calculated non-perturbatively in lattice simulations, and one can extract $\Lambda_{\rm QCD}$ by fitting the lattice data in the ultraviolet domain to the corresponding perturbative formulae. Here we make a review of available perturbative Landau gauge calculations for the ghost and gluon propagators in the MOM schemes.

If $\Gamma^{(N)}_R(p_i, g_R^2, \mu^2)$ is a renormalised proper vertex in Landau gauge, then the corresponding proper bare vertex function is independent of the renormalisation point μ. This fact is reflected by the Callan-Symanzik equation for the renormalised function:

$$\left(\frac{\partial}{\partial \ln \mu^2} + \beta\left(g_R(\mu^2)\right)\frac{\partial}{\partial g} - \frac{N}{2}\gamma\left(g_R(\mu^2)\right)\right)\Gamma^{(N)}_R(p_i, g_R^2, \mu^2) = 0 \tag{3.4}$$

where $\gamma\left(g_R(\mu^2)\right)$ is the anomalous dimension. In the Momentum subtraction schemes, the renormalisation conditions are defined by setting some of the two- and three-point functions to their tree-level values at the renormalisation point. Then (3.4) simplifies to

$$\lim_{a^{-1}\to\infty} \frac{d\ln(Z_{3,\rm MOM}(p^2=\mu^2, a^{-1})}{d\ln\mu^2} = \gamma_{3,\rm MOM}(g_{\rm MOM}) \tag{3.5}$$

in the case of two-point Green functions, where $Z_3(\mu^2)$ is defined in (2.7), a^{-1} stands for the ultraviolet regularisation and $\gamma_{3,\rm MOM}(g_{\rm MOM})$ is the anomalous dimension. A similar expression can be written for the ghost propagator renormalisation factor $\widetilde{Z_3}$. As we have already seen in the section 2.1, there is an infinite number of MOM schemes differing by kinematic configurations at the substraction point. We limit ourselves to the configurations defined by the subtraction of the transverse part of the three-gluon vertex ($\widetilde{\rm MOM}$) and that of the ghost-gluon vertex with vanishing gluon momentum ($\widetilde{\rm MOM}_c$) and vanishing incoming ghost momentum ($\widetilde{\rm MOM}_{c0}$), discussed in the section 2.1.

Both anomalous dimensions for ghost and gluon propagators have been recently

computed ([34], [35]) in the $\overline{\rm MS}$ scheme. The result at four-loop order reads

$$\begin{aligned}
\frac{d\ln(Z_{3,\rm MOM})}{d\ln\mu^2} &= \frac{13}{2}\,h_{\overline{\rm MS}} + \frac{3727}{24}\,h_{\overline{\rm MS}}^2 + \left(\frac{2127823}{288} - \frac{9747}{16}\zeta_3\right) h_{\overline{\rm MS}}^3 \\
&\quad + \left(\frac{3011547563}{6912} - \frac{18987543}{256}\zeta_3 - \frac{1431945}{64}\zeta_5\right) h_{\overline{\rm MS}}^4 \\
\frac{d\ln(\widetilde{Z}_{3,\rm MOM})}{d\ln\mu^2} &= \frac{9}{4}\,h_{\overline{\rm MS}} + \frac{813}{16}\,h_{\overline{\rm MS}}^2 + \left(\frac{157303}{64} - \frac{5697}{32}\zeta_3\right) h_{\overline{\rm MS}}^3 \\
&\quad + \left(\frac{219384137}{1536} - \frac{9207729}{512}\zeta_3 - \frac{221535}{32}\zeta_5\right) h_{\overline{\rm MS}}^4
\end{aligned} \tag{3.6}$$

where $h = g^2/(4\pi)^2$. In order to obtain the coefficients of the anomalous dimensions (3.5) in a MOM scheme one has to express the above expressions in terms of the corresponding coupling. We use the results of the article [34] where the three-loop perturbative substraction of all the three-vertices appearing in the QCD Lagrangian for kinematic configurations with one vanishing momentum are given. In Landau gauge and in the pure Yang-Mills case one has the following relations between the couplings in different MOM schemes and $h_{\overline{\rm MS}}$:

$$\begin{aligned}
h_{\widetilde{\rm MOM}_g} &= h_{\overline{\rm MS}} + \frac{70}{3}h_{\overline{\rm MS}}^2 + \left(\frac{51627}{576} - \frac{153}{4}\zeta(3)\right) h_{\overline{\rm MS}}^3 + \\
&\quad + \left(\frac{304676635}{6912} - \frac{299961}{64}\zeta_3 - \frac{81825}{64}\zeta_5\right) h_{\overline{\rm MS}}^4 \\
h_{\widetilde{\rm MOM}_c} &= h_{\overline{\rm MS}} + \frac{223}{12}h_{\overline{\rm MS}}^2 + \left(\frac{918819}{1296} - \frac{351}{8}\zeta(3)\right) h_{\overline{\rm MS}}^3 + \\
&\quad + \left(\frac{29551181}{864} - \frac{137199}{32}\zeta_3 - \frac{74295}{64}\zeta_5\right) h_{\overline{\rm MS}}^4 \\
h_{\widetilde{\rm MOM}_{c0}} &= h_{\overline{\rm MS}} + \frac{169}{12}h_{\overline{\rm MS}}^2 + \left(\frac{76063}{144} - \frac{153}{4}\zeta(3)\right) h_{\overline{\rm MS}}^3 + \\
&\quad + \left(\frac{42074947}{1728} - \frac{35385}{8}\zeta(3) - \frac{66765}{65}\zeta(5)\right) h_{\overline{\rm MS}}^4.
\end{aligned} \tag{3.7}$$

Thus, inverting (3.7) and substituting in (3.6), we obtain the anomalous dimensions of the gluon and ghost propagator in the three above-mentioned renormalisation schemes. In a MOM scheme, the equations (3.6) may be integrated as functions of h (cf. 3.5) [1]:

$$\begin{aligned}
\ln\left(\frac{Z_{\Gamma,\rm MOM}}{Z_0}\right) &= \log(h)\,\frac{\overline{\gamma}_0}{\beta_0} + h\,\frac{(\beta_0\,\overline{\gamma}_1 - \beta_1\,\overline{\gamma}_0)}{\beta_0^2} \\
&\quad + h^2\,\frac{(\beta_0^2\,\overline{\gamma}_2 - \beta_0\,\beta_1\,\overline{\gamma}_1 - (\beta_0\,\beta_2 - \beta_1^2)\,\overline{\gamma}_0)}{2\beta_0^3} +
\end{aligned}$$

[1] We omit the index specifying the renormalisation scheme both for h and $\Lambda_{\rm QCD}$ in the following formulae

$$+ h^3 \left(\beta_0^3 \overline{\gamma}_3 - \beta_0^2 \beta_1 \overline{\gamma}_2 + (\beta_0 \beta_1^2 - \beta_0^2 \beta_2) \overline{\gamma}_1 + (-\beta_0^2 \beta_3 + 2\beta_0 \beta_1 \beta_2 - \beta_1^3) \overline{\gamma}_0\right) \frac{1}{3\beta_0^4} + \dots \tag{3.8}$$

where $\overline{\gamma}_i$ are the expansion coefficients of the anomalous dimension in a generic MOM type scheme and Z_0 is an integration constant. The knowledge of the β-function

$$\beta(h) = \frac{dh}{d \ln \mu^2} = -\sum_{i=0}^{n} \beta_i h^{i+2} + \mathcal{O}\left(h^{n+3}\right) \tag{3.9}$$

at some order n allows to calculate the momentum dependence of h. At four-loop order one has

$$h(t) = \frac{1}{\beta_0 t}\left(1 - \frac{\beta_1}{\beta_0^2}\frac{\log(t)}{t} + \frac{\beta_1^2}{\beta_0^4}\frac{1}{t^2}\left(\left(\log(t) - \frac{1}{2}\right)^2 + \frac{\beta_2\beta_0}{\beta_1^2} - \frac{5}{4}\right)\right) + \\ + \frac{1}{(\beta_0 t)^4}\left(\frac{\beta_3}{2\beta_0} + \frac{1}{2}\left(\frac{\beta_1}{\beta_0}\right)^3\left(-2\log^3(t) + 5\log^2(t) + \left(4 - 6\frac{\beta_2\beta_0}{\beta_1^2}\right)\log(t) - 1\right)\right), \tag{3.10}$$

where $t = \ln \frac{\mu^2}{\Lambda^2_{\text{QCD}}}$. The last equation together with (3.8) allows us to write the ghost and gluon propagators as functions of the momentum and Λ_{QCD}. The numerical coefficients for the β-function in (3.9) are summarised in the Table 3.1:

	$\widetilde{MOM}$	$\widetilde{MOM}_c$	$\widetilde{MOM}_{c0}$
β_0		11	
β_1		102	
β_2	2412.16	2952.73	3040.48
β_3	84353.8	101484	100541

Table 3.1: *The numerical coefficients for the β-function for different MOM schemes [36]*

3.2 OPE for the Green functions and dominant power corrections

The momentum dependence of the QCD Green functions at low energies is modified by non-perturbative effects. These effects show up by presence of power-corrections to logarithmic series or, in other words, by non-zero values of corresponding condensates. For example, such a non-perturbative object as instanton has a weight $\propto \exp -\frac{8\pi^2}{g^2(p^2)}$, giving at leading order a power correction $\propto \frac{1}{p^2}$. It is argued in ([37],[38]) that non-perturbative lattice gluonic two- and three-point functions include such contributions up to quite large energies of around 10 GeV. For a systematic study of Λ_{QCD} one has to know the influence of power corrections on the Green

functions.

A powerfull tool to study the dependence of Green functions on the non-perturbative condensates is the Operator Product Expansion (OPE) [39]. This method is applicable to the problems having a specific energy hierarchy, or two very different characteristic energy scales. For example, in QCD it may be applied to the study of the influence of some background semi-classical field configurations. We recall here the idea of this method on the example of a two-point correlation function of a generic field ϕ

$$G(x) = \left\langle \phi\left(\frac{x}{2}\right) \phi\left(-\frac{x}{2}\right) \right\rangle . \tag{3.11}$$

It is postulated that when $x \to 0$ the product of the fields may be expanded as

$$\phi\left(\frac{x}{2}\right) \phi\left(-\frac{x}{2}\right) = \sum_{n=0}^{\infty} \sum_{i} w_i^n(x) \mathcal{O}_i^{[2n]}(0), \tag{3.12}$$

where the second sum is performed on all local operators $\mathcal{O}_i^{[2n]}$ of mass dimension $2n$ having the same quantum number than the l.h.s. The OPE suggests that all the features of the short-distance behaviour are stored in the Wilson coefficients

$$w_i^n(x) \sim \left(x^2\right)^{(n-1)} \times \Big[\text{series in } \alpha_s\Big], \tag{3.13}$$

that can be calculated in perturbation theory. In Fourier space they behave as

$$\widetilde{w}_i^n(p) \sim \left(\frac{1}{p^2}\right)^{(n+1)} \times \Big[\text{series in } \alpha_s\Big], \tag{3.14}$$

and thus

$$\widetilde{G}(p) = \sum_{n=0}^{\infty} \sum_{i} \widetilde{v}_i^n \left(\alpha_s, \log\left(p^2/\mu^2\right), a^{-1}\right) \frac{\left\langle \mathcal{O}_i^{[2n]} \right\rangle}{\left(p^2\right)^{n+1}}, \tag{3.15}$$

where the coefficients $\widetilde{v}_i^n$ are computed in perturbation theory, and $\langle \mathcal{O}_i^{[2n]} \rangle$ are **vacuum condensates**. At $n = 0$, corresponding to the trivial basic operator $\mathbb{I}$, we find an ordinary perturbative series for $\widetilde{G}$. But other condensates may lead to the appearance of non-perturbative power corrections. Usually this method is applied to gauge-invariant product of currents, and involves only gauge invariant quantities (for a recent review see [40]). However it can be extended to gauge-dependent operators (like QCD propagators) and involve gauge-variant condensates ([41],[42]). We do not discuss here the subtile question of the renormalisation of condensates and of calculation of their anomalous dimensions. On the lattice the MOM-type renormalisation process is non-ambiguous ([43],[44]), because the non-perturbative value for the l.h.s in (3.15) is available. This allows to define the condensates at fixed ultraviolet cut-off. Then one can apply a MOM renormalisation prescription on the both sides of (3.15) and thus renormalise the condensates $\left\langle \mathcal{O}_i^{[2n]} \right\rangle$.

In the following paragraph we will discuss the dominant power corrections, and corresponding condensates, in the case of the gluon and ghost correlators.

3.2.1 The dominant OPE power correction for the gluon propagator

The basis of operators in the pure Yang-Mills case is

$$\underline{\mathbb{I}} \quad \underline{A^a_\mu} \quad c^a \quad \partial_\mu A^a_\nu \quad \bar{c}^a c^b \quad A^a_\mu c^b \quad \underline{A^a_\mu A^b_\nu} \quad \partial_\mu c^a \quad \bar{c}^a \bar{c}^b \quad c^a c^b \quad \dots \tag{3.16}$$

At the leading order (a $\propto 1/p^2$ power correction compared to perturbation theory) only underlined operators contribute [43] to the gluon propagator, because operators with an odd number of fields cannot satisfy colour and Lorentz invariance and $\bar{c}c$ does not contribute because of the particular structure of the ghost-gluon vertex (cf. Figure 3.1(b)). We write then for the gluon propagator:

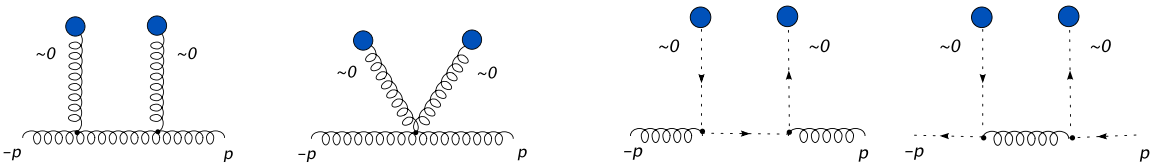

(a) (b)

Figure 3.1: *(a) Contribution of the gluon A^2-condensate (represented as soft external gluons) to the gluon two-point function (b) Contribution of the ghost $\bar{c}c$ condensate (represented as soft external ghosts) to the gluon and ghost two-point functions. These contributions vanish because they are proportional to (∼zero) momentum of the outgoing ghost is the ghost-gluon vertex.*

$$\left(\widetilde{G}^{(2)}\right)^{ab}_{\mu\nu}(p^2) \equiv \left\langle T\left(\widetilde{A}^a_\mu(-p)\widetilde{A}^b_\nu(p)\right)\right\rangle = \\ = (V_0)^{ab}_{\mu\nu}(p^2) + (V_2)^{aba'b'}_{\mu\nu\mu'\nu'}(p^2)\delta^{a'b'}\delta_{\mu'\nu'}\frac{\left\langle : A^c_\rho(0)A^c_\rho(0) :\right\rangle}{4(N_c^2-1)} + \dots, \tag{3.17}$$

where $\langle \bullet \rangle$ is a v.e.v with respect to the non-perturbative vacuum and $: A^c_\rho(0)A^c_\rho(0) :$ is a free-field normal product. In the perturbative vacuum the v.e.v. of all the normal products give zero, and thus only V_0 is non-vanishing. Hence

$$(V_0)^{ab}_{\mu\nu}(p^2) = \left(\widetilde{G}^{(2)}_{\text{pert}}\right)^{ab}_{\mu\nu}(p^2). \tag{3.18}$$

The coefficient V_2 is obtained at the tree-level order from

$$\langle g| : A^c_\rho(0)A^c_\rho(0) : |g\rangle = 2 + O(\alpha_s) \tag{3.19}$$

and

$$\langle g|T\left(\widetilde{A}^a_\mu(-p)\widetilde{A}^b_\nu(p)\right)|g\rangle_{\text{connected}} = (V_2)^{aba'b'}_{\mu\nu\mu'\nu'}(p^2)\langle g| : \widetilde{A}^{a'}_{\mu'}(0)\widetilde{A}^{b'}_{\nu'}(0) : |g\rangle, \tag{3.20}$$

where $|g\rangle$ is a soft gluon state. So, using the LSZ rule to cut the soft external gluons, we obtain

$$(V_2)^{aba'b'}_{\mu\nu\mu'\nu'}(p^2) = \frac{1}{2}\frac{\left\langle \widetilde{A}^t_\tau(0)\widetilde{A}^a_\mu(-p)\widetilde{A}^b_\nu(p)\widetilde{A}^s_\sigma(0)\right\rangle}{\left(G^{(2)}_{\rm pert}(0)\right)^{ta'}_{\tau\mu'}\left(G^{(2)}_{\rm pert}(0)\right)^{sb'}_{\sigma\nu'}}, \tag{3.21}$$

which can be computed in perturbation theory (cf. Figure 3.1(a)). Finally,

$$\left(\widetilde{G}^{(2)}\right)^{ab}_{\mu\nu}(p^2) = \frac{1}{p^2}\left(\delta_{\mu\nu} - \frac{p_\mu p_\nu}{p^2}\right)\left(p^2\widetilde{G}^{(2)}_{\rm pert}(p^2) + N_C\frac{g_0^2\langle A^2\rangle}{4\left(N_C^2-1\right)}\frac{1}{p^2} + O(g^4, p^{-4})\right). \tag{3.22}$$

A MOM-type renormalisation prescription may be defined non-perturbatively. This allows an easy renormalisation procedure for the A^2-condensate [43]. Here we do not include the effects of the anomalous dimension of the A^2 operator [45] and hence we apply the MOM prescription by imposing the tree-level value to the Wilson coefficient at the renormalisation point $p^2 = \mu^2$ for the last equation. This allows to factorise the perturbative gluon propagator giving finally

$$Z_3(\mu^2) \;=\; Z_{3,\rm pert}(\mu^2)\;\left(1 + \frac{N_C}{\mu^2}\frac{g_R^2\langle A^2\rangle_R}{4\left(N_C^2-1\right)} + O(g_R^4, \mu^{-4})\right). \tag{3.23}$$

3.2.2 The dominant OPE power correction for the ghost propagator

In the case of the ghost propagator the set of basic operators is the same, the ghost condensate $\bar{c}c$ does not contribute for the same reasons as for the gluon propagator (cf. Figure 3.1(b)). Thus, applying the OPE to the ghost two-point function, we obtain:

$$\begin{aligned}\widetilde{F}^{(2)ab}(p^2) &= (\widetilde{V}_0)^{ab}(p^2) \;+\; \left(\widetilde{V}_2\right)^{ab\sigma\tau}_{st}(p^2)\langle :A^s_\sigma(0)A^t_\tau(0):\rangle \;+\; \dots \\ &= F^{(2)ab}_{\rm pert}(p^2) \;+\; w^{ab}\,\frac{\langle A^2\rangle}{4(N_c^2-1)} \;+\; \dots\end{aligned} \tag{3.24}$$

where, in analogy with (3.21), the Wilson coefficient reads

$$w^{ab} \;=\; \left(\widetilde{V}_2\right)^{ab\sigma\tau}_{st}\delta^{st}\delta_{\sigma\tau} \;=\; \frac{1}{2}\,\delta^{st}\delta_{\sigma\tau}\frac{\int d^4x e^{ip\cdot x}\,\langle \widetilde{A}^{t'}_{\tau'}(0)\;T\left(c^a\overline{c^b}\right)\;\widetilde{A}^{s'}_{\sigma'}(0)\rangle_{\rm connected}}{G^{(2)\,ss'}_{\sigma\sigma'}(0)G^{(2)\,tt'}_{\tau\tau'}(0)} \tag{3.25}$$

which is equal to twice the diagram represented on the Figure 3.2 that describes the coupling of the ghost propagator to the gluon A^2-condensate. Hence

$$w^{ab} = \frac{1}{2}\delta^{st}\delta_{\sigma\tau}\cdot 2\frac{\delta^{aa_1}}{p^2}\left(ig_0 f^{a_2ta_1}\right)\frac{\delta^{a_2a_3}}{p^2}\left(ig_0 f^{a_4sa_3}\right)\frac{\delta^{a_4b}}{p^2} = N_C\frac{g_0^2}{p^2}\widetilde{F}^{(2)ab}_{\rm tree}(p^2). \tag{3.26}$$

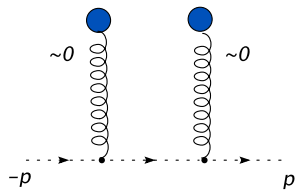

Figure 3.2: *Contribution of the gluon A^2-condensate (external soft gluons) to the ghost propagator*

This gives the leading non-perturbative contribution, because the first Wilson coefficient trivially gives the perturbative ghost propagator. Finally,

$$\widetilde{F}^{(2)ab}(p^2) \;=\; \widetilde{F}^{(2)ab}_{\rm pert}(p^2)\,\left(1+\frac{N_C}{q^2}\,\frac{g_0^2\langle A^2\rangle}{4\left(N_C^2-1\right)}+\,\mathcal{O}\left(g_0^4,q^{-4}\right)\right) \tag{3.27}$$

where all quantities are bare. Performing the MOM renormalisation we obtain for the renormalisation factor:

$$\widetilde{Z_3}(\mu^2) \;=\; \widetilde{Z_{3,\rm pert}}(\mu^2)\,\left(1+\frac{N_C}{\mu^2}\frac{g_R^2\langle A^2\rangle_R}{4\left(N_c^2-1\right)}+O(g_R^4,\mu^{-4})\right)\,, \tag{3.28}$$

where the A^2-condensate is renormalised as in the case of the gluon propagator. We see that the dominant multiplicative correction to the perturbative $\widetilde{Z_{3,\rm pert}}$ is identical to the one obtained in the previous section for the gluon propagator (3.23).

3.2.3 Constraints on the Wilson coefficients from the Slavnov-Taylor identity

The gauge-dependent power corrections due to the $\langle A^2\rangle$-condensate are obviously absent in gauge-invariant quantities. Because of this the Wilson coefficients for the $\langle A^2\rangle$-condensate in different Green functions are not independent. Some relations may be obtained from the Slavnov-Taylor identity (1.45) but their role in the MOM renormalisation constants is not obvious.

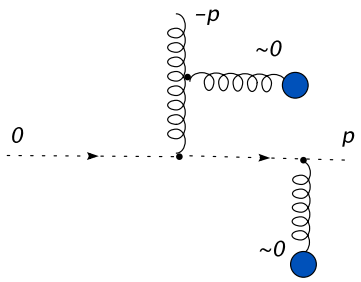

Figure 3.3: *The $\langle A^2\rangle$ contribution to the ghost-gluon vertex with vanishing entering momentum. The above diagram is zero in Landau gauge because of the projector in the gluon propagator.*

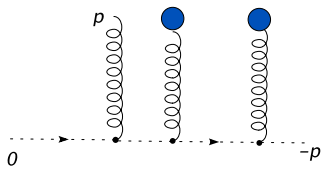

Figure 3.4: *Non-zero dominant $\langle A^2 \rangle$ contribution to the ghost-gluon vertex with vanishing entering momentum. This term contribute to the external ghost propagator.*

It is interesting to know if there are any power corrections to this vertex, because perturbation theory predicts the non-renormalisation of this vertex, i.e. it is equal to 1 to all orders ([8],[34]). If the $\langle A^2 \rangle$ power corrections are present they will constitute the main contribution at low energies. One can directly evaluate the Wilson coefficient to the ghost-gluon vertex $\widetilde{\Gamma}^{abc}_{\mu}(-p, 0; p)$ with vanishing entering ghost momentum.

The only non-zero correction to the ghost-gluon vertex with one vanishing ghost momentum is the one that contributes to the external ghost propagator (see Figure 3.4). But all the diagrams with the condensate interaction attached to different external legs are zero in Landau gauge (see Figure 3.3). Thus the ghost-gluon vertex in this particular kinematic configuration does not contain the $\frac{1}{p^2}$ power-corrections, and thus the non-renormalisation theorem holds at this order. However, this it is not true if the external ghost momentum is not *exactly* zero.

3.3 Data analysis

We calculated, using the techniques described in the chapter 2, the ghost and the gluon propagators of the Landau gauge $SU(3)$ gauge theory at different lattice volumes and different values of the β parameter (cf. Table 3.2) [21]. The lattices marked

β	V	a^{-1} (GeV)	V_{phys} (fm^4)	# Configurations
$\rightarrow$ 6.0	16^4	1.96	6.73	1000
6.0	24^4	1.96	33.17	500
$\rightarrow$ 6.2	24^4	2.75	8.43	500
$\rightarrow$ 6.4	32^4	3.66	8.85	250

Table 3.2: *Lattice setup parameters. The lattice spacings are taken from Table 3 in [46] with a physical unit normalised by $\sqrt{\sigma} = 445$ MeV. The lattices marked by the "$\rightarrow$" symbol have similar physical volume.*

by the "$\rightarrow$" symbol correspond to similar physical volume. The produced data allow us to study the propagators in the momentum range $[\approx 2\text{GeV}, \approx 6.5\text{GeV}]$.

This section is organised in the following way. In the first subsection we present the fits of the ghost and the gluon propagators separately, and compare the fitted values for Λ_{QCD}. Thus we test the self-consistency of the method. Non-perturbative effects are quite important in the energy interval accessible to us. This is why another motivation is to study the asymptoticity of the perturbative series. The latter is done by comparing the results in different renormalisation schemes (R =

$\overline{\text{MS}}, \widetilde{\text{MOM}}, \widetilde{\text{MOM}_c}, \widetilde{\text{MOM}_{c0}}$) and at different orders (from two to four loops). In the second subsection we use the analytical result of the previous section namely that the dominant non-perturbative effects are the same for the ghost and for the gluon propagators, and hence the ratio of the gluon and the ghost dressing functions is better described by perturbation theory at low energies. We shall see that lattice data support this claim.

3.3.1 Fitting the gluon and the ghost propagators

We extracted Λ_{QCD} from the dressing functions of our lattice propagators by fitting them to the formula (3.8) (with h given by (3.10)) in different MOM renormalisation schemes. There are two parameters of the fit - the wanted Λ_{QCD} and the integration constant Z_0. An example of such a fit if presented at Figure 3.5. The obtained value

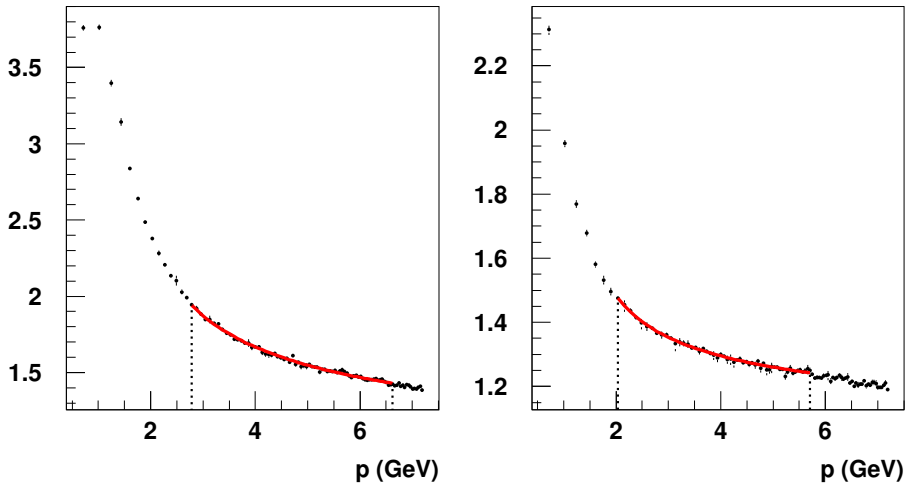

Figure 3.5: *Extrapolated lattice data at $\beta = 6.4$ for $G(p)$ (left) and $F(p)$ (right). The solid line is the fit at four-loop order in the $\overline{MS}$ scheme. The vertical dotted lines delimit the window of each fit.*

of Λ_R in a scheme R is converted to the $\overline{\text{MS}}$ scheme using the exact [2] asymptotic formulae

$$\begin{aligned} \Lambda_{\overline{\text{MS}}} &= 0.346\, \Lambda_{\widetilde{\text{MOM}}} \\ \Lambda_{\overline{\text{MS}}} &= 0.429\, \Lambda_{\widetilde{\text{MOM}_c}} \\ \Lambda_{\overline{\text{MS}}} &= 0.428\, \Lambda_{\widetilde{\text{MOM}_{c0}}} \end{aligned} \tag{3.30}$$

The results in $\overline{\text{MS}}$ are given in Tables 3.3,3.4,3.5. The errors include the statistical error, extrapolation errors and the bias due to the choice of the fit window. We

[2] A relation between the values of Λ_{QCD} in different schemes A and B reads

$$\frac{\Lambda^B}{\Lambda^A} = \exp\left[\frac{1}{2\beta_0}\left(\frac{1}{g_A^2(\mu^2)} - \frac{1}{g_B^2(\mu^2)}\right) + O\left(g^2(\mu^2)\right)\right]. \tag{3.29}$$

If $g_B^2 = g_A^2\left(1 + \zeta\,\frac{g_A^2}{4\pi} + \dots\right)$ then the asymptotic freedom gives $\Lambda^B = \Lambda^A e^{\frac{\zeta}{2\beta_0}}$. Thus the exact conversion coefficient is given by an one-loop calculation [47].

β	$\Lambda^{(3)}_{\overline{\rm MS},gluon}$	$\Lambda^{(3)}_{\overline{\rm MS},ghost}$	$\Lambda^{(4)}_{\overline{\rm MS},gluon}$	$\Lambda^{(4)}_{\overline{\rm MS},ghost}$
6.0	$519(6)^{+12}_{-4}$	$551(12)^{+33}_{-16}$	$441(4)^{+8}_{-4}$	$461(10)^{+29}_{-14}$
6.2	$509(6)^{+17}_{-27}$	$550(8)^{+27}_{-63}$	$435(6)^{+11}_{-19}$	$465(8)^{+33}_{-36}$
6.4	$476(7)^{+44}_{-40}$	$549(7)^{+55}_{-51}$	$410(4)^{+33}_{-29}$	$468(7)^{+48}_{-40}$

Table 3.3: *Three-loop and four-loop physical values of $\Lambda_{\overline{MS}}$ in MeV extracted from fits in the $\overline{MS}$ scheme.*

β	$\Lambda^{(3)}_{\overline{\rm MS},gluon}$	$\Lambda^{(3)}_{\overline{\rm MS},ghost}$	$\Lambda^{(4)}_{\overline{\rm MS},gluon}$	$\Lambda^{(4)}_{\overline{\rm MS},ghost}$
6.0	$324(2)^{+2}_{-5}$	$322(8)^{+20}_{-16}$	—	—
6.2	$320(2)^{+8}_{-14}$	$326(5)^{+26}_{-33}$	—	$331(8)^{+21}_{-16}$
6.4	$312(1)^{+9}_{-25}$	$331(4)^{+42}_{-35}$	$320(4)^{+6}_{-4}$	$353(9)^{+17}_{-38}$

Table 3.4: *Three-loop physical values of $\Lambda_{\overline{MS}}$ in MeV converted from fits in the $\widetilde{MOM}$ scheme.*

β	$\Lambda^{(3)}_{\overline{\rm MS},gluon}$	$\Lambda^{(3)}_{\overline{\rm MS},ghost}$	$\Lambda^{(4)}_{\overline{\rm MS},gluon}$	$\Lambda^{(4)}_{\overline{\rm MS},ghost}$
6.0	$345(3)^{+4}_{-4}$	$369(9)^{+3}_{-2}$	—	—
6.2	$341(2)^{+6}_{-7}$	$364(8)^{+11}_{-19}$	$344(4)^{+9}_{-6}$	$357(10)^{+8}_{-16}$
6.4	$323(2)^{+17}_{-11}$	$354(8)^{+28}_{-20}$	$332(2)^{+14}_{-30}$	$351(8)^{+23}_{-25}$

Table 3.5: *Three-loop physical values of $\Lambda_{\overline{MS}}$ in MeV converted from fits in the $\widetilde{MOM}_c$ scheme.*

see from these tables that at a given order and in a given renormalisation scheme the values obtained from the gluon and ghost propagators are consistent within the error bars, and are quite independent of the ultraviolet cut-off. The results from a direct fit in the $\overline{\rm MS}$ scheme (Table 3.3) confirm the old claim that we are still far from asymtoticity in the considered momentum interval in this scheme [48]. Our analysis suggests that the perturbative series become asymptotic at the NNLO in the case of $\widetilde{\rm MOM}$ and $\widetilde{\rm MOM}_c$ renormalisation schemes. However, the property of asymptoticity is only approximate at considered momenta. To see this one can use the perturbative expression (analogue to (3.3)) for Λ_R in terms of the coupling h_R to the order four

$$2\ln\Lambda_R^{(4)} = \ln\mu^2 - \frac{1}{\beta_0 h_R} - \frac{\beta_1}{\beta_0^2}\ln(\beta_0 h_R) - \frac{\beta_0\beta_2-\beta_1^2}{\beta_0^3}h_R - \frac{\beta_0^2\beta_3 - 2\beta_0\beta_1\beta_2+\beta_1^3}{2\beta_0^4}h_R^2, \tag{3.31}$$

and plot the ratio (Figure 3.6) of the consecutive orders $\frac{\Lambda_R^{(n+1)}}{\Lambda_R^{(n)}}$. There is a qualitative agreement between the ratios presented at Figure 3.6 and our results (see Tables 5-10 in [21]). The influence of truncation, responsible for the differences between different orders and renormalisation schemes, is mostly due to the large value of the effective coupling at considered energies [21]. In fact, as shown in [37], the real value of the coupling constant may be smaller, because of the power correction discussed in the section 3.2. Indeed, according to the OPE analysis the effective coupling constant

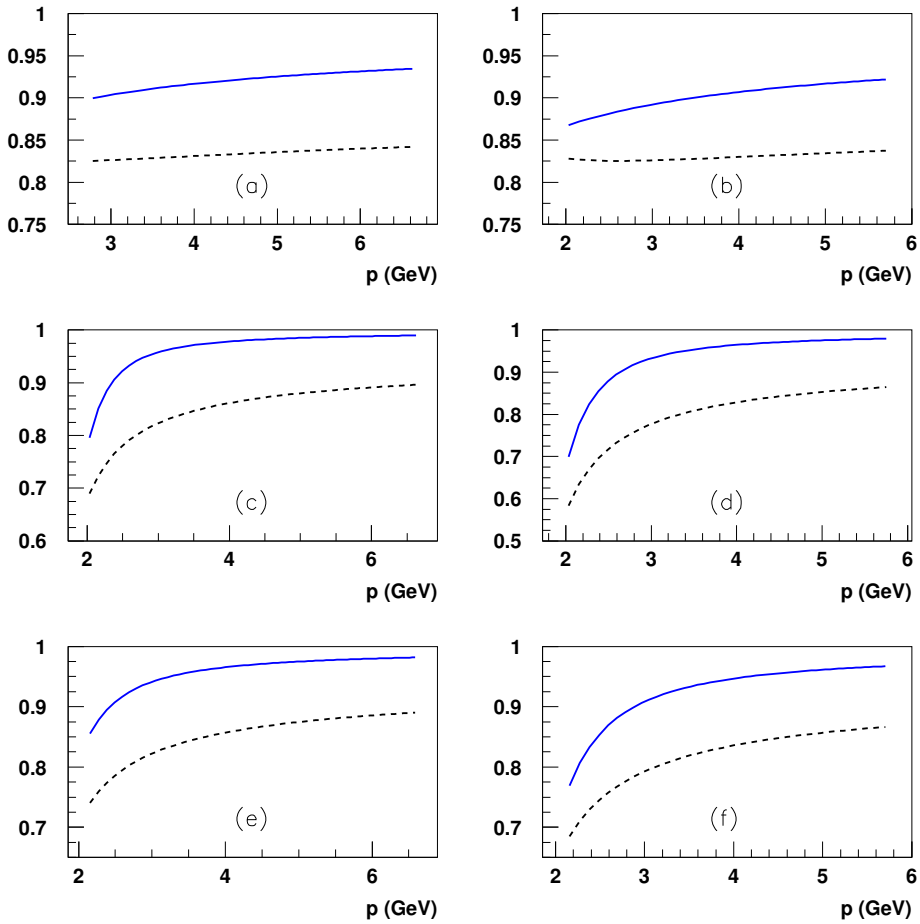

Figure 3.6: $\frac{\Lambda_R^{(n+1)}}{\Lambda_R^{(n)}}$ *for* $n = 2$ *(dashed lines) and* $n = 3$ *(solid lines), for the gluon propagator in the* $\overline{MS}$ *scheme (a),* $\widetilde{MOM}$ *scheme (c) and* $\widetilde{MOM}_c$ *scheme (e), and for the ghost propagator in the* $\overline{MS}$ *scheme (b),* $\widetilde{MOM}$ *scheme (d) and* $\widetilde{MOM}_c$ *scheme (f).*

is modified by a factor

$$\alpha_s \to \alpha_s \left(1 + \text{const} \cdot \frac{\langle A^2 \rangle}{p^2}\right). \tag{3.32}$$

According to the results of the section 3.2, one can eliminate the dominant power correction by considering the ratio of the propagators. In this case one expects a better behaviour of perturbative series at low momenta. We discuss this strategy in the following subsection.

3.3.2 Fit of the ratio

Given that at the leading order the non-perturbative power corrections factorise (3.23),(3.28) and are identical in the case of the ghost and gluon propagators, we

can fit the ratio

$$\frac{\widetilde{Z_3}(q^2,\Lambda_R,\langle A^2\rangle)}{Z_3(q^2,\Lambda_R,\langle A^2\rangle)} = \frac{\widetilde{Z_{3,\mathrm{pert}}}(q^2,\Lambda_R)}{Z_{3,\mathrm{pert}}(q^2,\Lambda_R)}, \tag{3.33}$$

to the ratio of *perturbative* formulae in scheme R given by (3.8), and then convert Λ_R to $\Lambda_{\overline{\mathrm{MS}}}$ using (3.30). It is interesting to notice that non-perturbative corrections cancel out in this ratio even in the unquenched case with $n_f \neq 0$ flavours of dynamical quarks. The Λ_{QCD}-parameter extracted from this ratio is free from non-perturbative power corrections up to contributions related to the operators of dimension four. In Table 3.6 the best-fit parameters for the three schemes are presented and we plot in Figure 3.7 the lattice data and the $\widetilde{\mathrm{MOM}}$ best-fit curve for the ratio (3.33). In Fig-

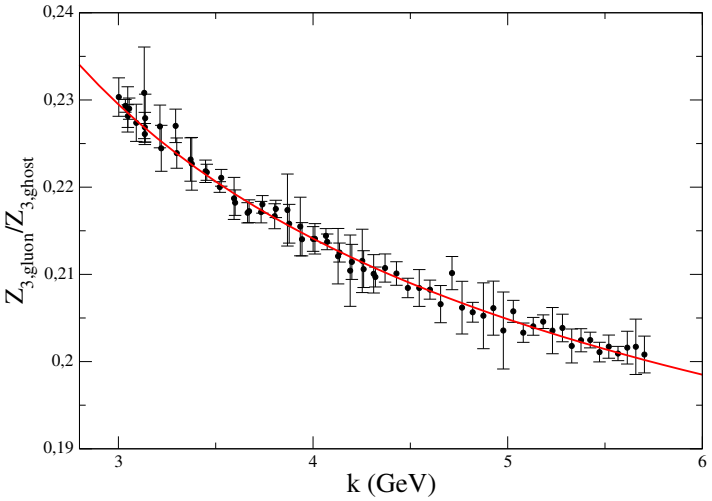

Figure 3.7: *Plot (in the $\widetilde{MOM}$ scheme) of the $\frac{Z_3(p^2)}{\widetilde{Z}_3(p^2)}$ for the best fit parameter $\Lambda_{\overline{MS}} = 269(5)$ MeV.*

scheme	$\Lambda^{(2)}_{\overline{\mathrm{MS}}}$	χ^2/n.d.f	$\Lambda^{(3)}_{\overline{\mathrm{MS}}}$	χ^2/n.d.f	$\Lambda^{4\,\mathrm{loops}}_{\overline{\mathrm{MS}}}$	χ^2/n.d.f
$\widetilde{\mathrm{MOM}}$	324(6)	0.33	269(5)	0.34	282(6)	0.34
$\widetilde{\mathrm{MOM}}_c$	351(6)	0.33	273(5)	0.34	291(6)	0.33
$\widetilde{\mathrm{MOM}}_{c0}$	385(7)	0.33	281(5)	0.34	298(6)	0.33

Table 3.6: *The best-fitted values of $\Lambda_{\overline{MS}}$ for the three considered renormalisation schemes. As discussed in the text, $\widetilde{MOM}_c$ seems to be the one showing the best asymptotic behaviour.*

ure 3.9 we show the evolution of the fitted parameter $\Lambda_{\overline{\mathrm{MS}}}$ when changing the order of perturbation theory used in the fitting formula. One can conclude from Figure 3.9 that the $\widetilde{\mathrm{MOM}}$ scheme at three loops gives the most stable result for $\Lambda_{\overline{\mathrm{MS}}}$. It can also be seen from the ratio of four to three loops contributions (see Figure 3.10) for the

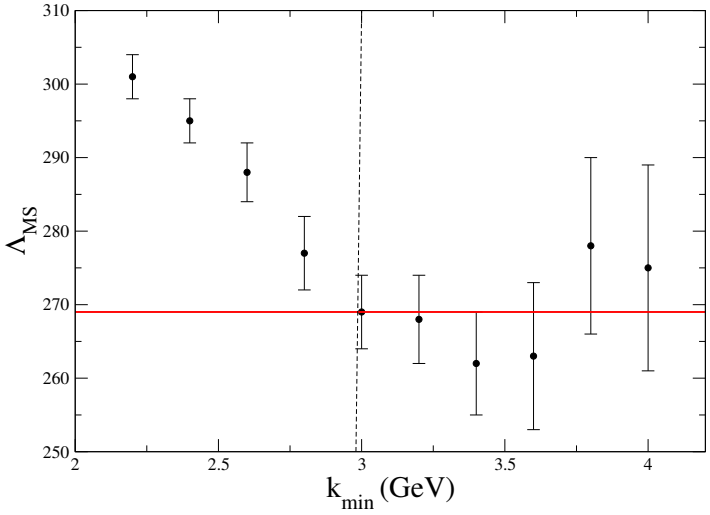

Figure 3.8: *The determination of the optimal window fit (from 3 GeV to $k_{\max}a \leq \pi/2$) results from the search for some "plateau" of $\Lambda_{\overline{MS}}$ when one changes the low bound of the fit window. Fits are done in the $\widetilde{MOM}$ scheme.*

perturbative expansion of $\ln Z_3$,

$$\ln Z_3 \;=\; r_0 \ln h_R + \sum_{i=1} r_i h_R^i \,, \tag{3.34}$$

where the coefficients r_i are to be computed from those in equations (3.6-3.10) using the Table 3.1. The same is done for $\ln \widetilde{Z_3}$.

According to our analysis, and in agreement with the result of the separate fit, three loops seems to be the optimal order for the asymptoticity [3]. Indeed, the values of $\Lambda_{\overline{\rm MS}}$ for the three considered renormalisation schemes practically match each other at three loops (see Figure 3.9). The approximate value

$$\Lambda_{\overline{\rm MS}} = 269(5)^{+12}_{-9} \tag{3.35}$$

could be presented as the result for the fits of the ratio of dressing functions to perturbative formulae.

The results of the previous subsection and [21] suggest that our present systematic uncertainty may be underestimated (narrowness of the momentum interval, truncation of the perturbative series, etc.), that is why we prefer simply to quote $\Lambda_{\overline{\rm MS}} \approx 270$ MeV for future reference. This value is pretty smaller than the value of ≈ 330 MeV obtained by independent fits of dressing functions (see Tables 3.4,3.5). In light of our OPE analysis and previous results [44], this argues in favour of presence of low-order non-perturbative corrections to the ghost and gluon propagators in the momentum range $[2\,\text{GeV}, 6\,\text{GeV}]$.

[3] Note that the the asymptoticity property is better verified in the case of the ratio, see Figure 3.9.

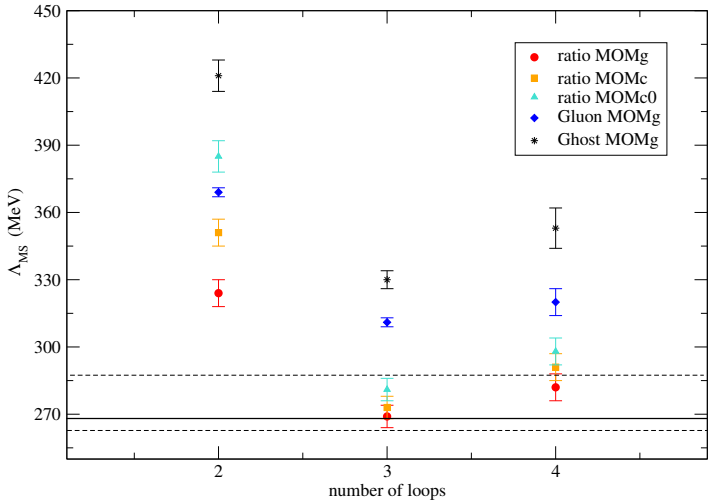

Figure 3.9: *Evolution of the parameter $\Lambda_{\overline{MS}}$, extracted from fits of the ratio 3.33 and propagators alone (rhombus and star markers, extracted from Tables 3.4,3.5 [21]) to perturbative formulae, as function of the order of perturbation theory. The solid line corresponds to the value (3.35). Only statistical error is quoted.*

3.3.3 Comparing the results

We showed that perturbation theory is quite successfull in describing (up to NNNLO) lattice propagators in the momentum range $[2\,\text{GeV}, 6\,\text{GeV}]$, yielding compatible values of Λ_{QCD}. The separate fit of the ghost and gluon propagators, and the fit of their ratio favours the existence of $\propto \frac{1}{p^2}$ power corrections and validates the OPE approach in the case of ghost and gluon propagators. The difference with previous approaches is that we have not introduced any additional fit parameter, and have only used perturbation theory. Our method can also be used to calculate Λ_{QCD} from propagators alone in the unquenched case. In principle, it can be used to estimate the value of the $\langle A^2 \rangle$ condensate.

The main limitation of the application of perturbation theory to lattice Green functions in the accessible energy interval is the lack of asymptoticity and the truncation of the series. In fact, even the conversion formula (3.29) is not exact at considered momenta. We estimate the accuracy of our results at around 10%. It can be improved by performing the simulations at $\beta = 6.6, 6.8$ on the lattices of sizes $48^4, 64^4$, respectively. The choice of parameters is motivated by the necessity to have the same physical volume of the lattice in order to control the finite-size effects.

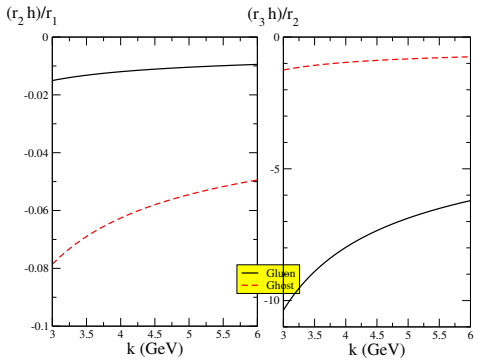

Figure 3.10: *(b) Ratio of four-loop to three-loop contributions (and of three-loop to two-loops for the sake of comparison) for the perturbative expansion of* $\log Z_3$ *and* $\log \widetilde{Z_3}$ *(in* $\widetilde{MOM}$*) in 3.34, plotted versus the momenta inside our fitting window.*

Chapter 4

The infrared behaviour of Green functions

There are compelling reasons to think that confinement is a property of QCD, and does not result from some other theory. One of such indications is a non-zero value of the string tension found in the lattice simulations. As a matter of fact lattice simulations give access to many non-perturbative quantities. We are particularly interested in knowing the Landau gauge Green functions at low momenta, i.e. at energies of order and below than Λ_{QCD}. No free quarks or gluons exist at very small momenta because of confinement. So, a study of gluonic correlation functions in the deep-infrared domain may seem useless. However, in order to study the property of confinement from the first principles one has to understand the change in behaviour of Green functions found at low momenta. Knowing these functions exactly would be a great support for the future development of the theory, because many confinement scenarii (for example the Gribov-Zwanziger scenario) give predictions for low energies momentum dependence of the Green functions in Landau gauge. Lattice simulations allow to test these predictions.

Lattice results for different Green functions of QCD have been successfully tested at large momenta by perturbation theory up to NNNLO (see chapter 3 and [21],[49]). We shall see below that lattice Green functions also satisfy the complete ghost Schwinger-Dyson equation (see Figure 4.2). Thus lattice approach gives consistent results non only in the ultraviolet domain but also in the infrared one. Of course numerical methods could never give us complete Green functions for all possible values of momenta. Nevertheless, lattice gives a *quasi-unique method for testing different analytical approaches*, like study of truncated system of Schwinger-Dyson equations, renormalisation group flow equations and other non-perturbative relations like Slavnov-Taylor identities.

Most of analytical predictions are done for the infrared exponents α_F and α_G that describe power-law deviations from free propagators when $p \to 0$

$$\begin{aligned} p^2 G^{(2)}(p^2) \equiv G(p^2) &\propto \left(\frac{p^2}{\lambda_G^2}\right)^{\alpha_G} \\ p^2 F^{(2)}(p^2) \equiv F(p^2) &\propto \left(\frac{p^2}{\lambda_F^2}\right)^{\alpha_F} \\ &\dots \end{aligned} \tag{4.1}$$

where $\lambda_{G,F}$ are some fixed parameters of dimension one. When p is large, the functions $F(p^2)$ and $G(p^2)$ are logarithmic functions of momentum, and thus $\alpha_{F,G} = 0$. But at low momenta it may not be true. In fact, power-law behaviour is the crudest approximation, allowing to exhibit the most general features of the momentum dependence of the Green functions in the infrared. The real law governing the infrared gluodynamics might be much more complicated. In the following section we review (very briefly) different predictions for the exponents α_G and α_F of, respectively, the gluon and ghost two-point functions. Next we present our analysis of the Slavnov-Taylor identities imposing some limits on these exponents. After this we turn to the study of the ghost Schwinger-Dyson equation and test the widely accepted relation (4.20) between the exponents α_G and α_F. Our conclusion (supported by numerical simulations) is that this relation is not valid. We revisit the usual proof and conclude that either the ghost-gluon vertex behaves unexpectedly in the infrared, or that $\alpha_F = 0$. At the end of the chapter we discuss the results of direct fits of two-point functions, and compare our results with other lattice collaborations.

4.1 Review of today's analytical results

In this section we quote the main analytical results regarding the infrared exponents (4.1). We start with the Zwanziger's prediction obtained for gluonic correlation functions. Next we present the results of other analytical approaches.

4.1.1 Zwanziger's prediction

Zwanziger suggested in [50],[51] that the (Landau gauge) gluon propagator vanishes at zero momentum in the infinite volume limit. The argument is the following. The Faddeev-Popov operator (1.68) is positive definite at a local minimum of the functional (1.60)

$$(\omega, \mathcal{M}^{\text{lat}}_{FP}[U]\omega) \geq 0. \tag{4.2}$$

Choosing a test vector

$$\omega^a(x) = \frac{\exp i\frac{2\pi e_\mu}{L}x}{\sqrt{V}}\chi^a, \tag{4.3}$$

where the normalised colour vector χ^a is an eigenfunction of the "angular momentum" operator $\left(J^b\right)_{ac} = if^{abc}$, one obtains from (1.68) and (4.2) the following limit on the mean colour spin

$$\left| \frac{1}{V}\sum_x A_\mu(x) \right| \leq 2\tan\frac{\pi}{L}. \tag{4.4}$$

Introducing an external colour field H^a_μ source (independent of x), one obtains from (4.4) an estimate for the generating functional

$$\frac{Z(H)}{Z(0)} = \frac{1}{Z(0)}\int [\mathcal{D}\mathcal{A}] e^{-S[\mathcal{A}]+H^a_\mu \sum_x A^a_\mu(x)} \leq e^{2V\sum_\mu |H_\mu| \tan\frac{\pi}{L}}. \tag{4.5}$$

The free energy density $w(H) = \frac{1}{V}\log Z[H]$ is convex and bounded from below ($w(0) = 0$), thus one has

$$0 \leq w(H) \leq 2\sum_{\mu} |H_\mu| \tan\frac{\pi}{L}. \tag{4.6}$$

All connected gluonic Green functions can be obtained by calculating the variations of the free energy with respect to the external sources $H^a_\mu(x)$. The last inequality suggest that in the infinite volume limit all Green functions vanish at zero momentum. However, the inversion of derivation and thermodynamic limit is not supported by a rigorous proof.

4.1.2 Study of truncated SD and ERG equations

Diverse analytical approaches (study of truncated Schwinger-Dyson equations and of renormalisation group equation, see Table 4.1) agree that the infrared divergence of the ghost propagator is enhanced, i.e. $\alpha_F \leq 0$; while they predict different values for α_G, mostly around $\alpha_G \approx 1.2$. This means that the gluon propagator is suppressed in the infrared. However, some groups obtain $\alpha_G \leq 1$, i.e. an infrared-divergent gluon propagator. Lattice simulations confirmed the prediction for the ghost propagator, whereas the lattice gluon propagator seems to remain finite and non-zero in the infrared, i.e. $\alpha_G = 1$. We discuss this question in details in the section 4.5.

Reference	**Method**	$\boldsymbol{\alpha_G}$	$\boldsymbol{\alpha_F}$
Zwanziger [50]	see subsection 4.1.1	> 1	no
Bloch [52]	SD truncation + perturbation theory	$[0.34, 1.06]$	$[-0.53, -0.17]$
von Smekal et al. [53]	SD truncation	1.84	-0.92
Zwanziger [54]	SD truncation + Zwanziger condition	2 or 1.19	-1 or -0.595
Aguilar et al. [55]	SD equation	0.98	-0.04
Kato [56]	ERGE	0.292	-0.146
Pawlowski et al. [57]	ERGE	1.19	-0.595
Fischer et al. [58]	ERGE	1.02	-0.52

Table 4.1: *Summary of various analytical predictions*

4.2 Constraints on the infrared exponents and the Slavnov-Taylor identity

Let us consider the Slavnov-Taylor identity (1.45) relating the three-gluon vertex $\Gamma_{\lambda\mu\nu}$, the ghost-gluon vertex $\widetilde{\Gamma}_{\lambda\mu}(p,q;r)$ and the ghost and gluon propagators:

$$p^\lambda \Gamma_{\lambda\mu\nu}(p,q,r) = \frac{F(p^2)}{G(r^2)}(\delta_{\lambda\nu} r^2 - r_\lambda r_\nu)\widetilde{\Gamma}_{\lambda\mu}(r,p;q) - \frac{F(p^2)}{G(q^2)}(\delta_{\lambda\mu} q^2 - q_\lambda q_\mu)\widetilde{\Gamma}_{\lambda\nu}(q,p;r). \tag{4.7}$$

Taking the limit $r \to 0$ keeping q and p finite, and using the parametrisation $G(r^2) \simeq (r^2)^{\alpha_G}$ valid for $r^2 \ll \Lambda^2_{\rm QCD}$, one finds the following limits on the infrared exponents

$$\begin{cases} \alpha_G < 1 & \text{gluon propagator } \textit{diverges} \text{ in the infrared, and} \\ \alpha_F \leq 0 & \text{the divergence of the ghost propagator is } \textit{unchanged} \text{ or } \textit{enhanced} \text{ in the infrared} \end{cases} \tag{4.8}$$

Let us discuss in details the origin of the limits (4.8). The ghost-gluon vertex $\widetilde{\Gamma}_{\mu\nu}(p,k;q)$ may be parametrised [59] in the most general way as

$$\begin{aligned} \widetilde{\Gamma}^{abc}_{\mu}(p,k;q) &= f^{abc}(-ip_\nu) g_0 \widetilde{\Gamma}_{\nu\mu}(p,k;q) && (4.9) \\ &= f^{abc}(-ip_\nu) g_0 \cdot \big[\delta_{\nu\mu} a(p,k;q) - q_\nu k_\mu b(p,k;q) + p_\nu q_\mu c(p,k;q) + \\ &\qquad + q_\nu p_\mu d(p,k;q) + p_\nu p_\mu e(p,k;q)\big] && (4.10) \end{aligned}$$

We recall that in this formula $-p$ is the momentum of the outgoing ghost, k is the momentum of the incoming one and $q = -p-k$ the momentum of the gluon (all momenta are taken as entering). For some particular kinematic configurations we use the following dense notations

$$\begin{aligned} &a_3(p^2) = a(-p,p;0) \\ &a_1(p^2) = a(0,-p;p), \quad b_1(p^2) = b(0,-p;p), \quad d_1(p^2) = d(0,-p;p). \end{aligned} \tag{4.11}$$

The limit $r^2 \to 0$ leads to an asymmetric kinematic configuration for the three-gluon vertex in the l.h.s. of (4.7). This particular configuration allows a general parametrisation [34]

$$\Gamma_{\mu\nu\rho}(p,-p,0) = \left(2\delta_{\mu\nu}p_\rho - \delta_{\mu\rho}p_\nu - \delta_{\rho\nu}p_\mu\right) T_1(p^2) - \left(\delta_{\mu\nu} - \frac{p_\mu p_\nu}{p^2}\right) p_\rho T_2(p^2) + p_\mu p_\nu p_\rho T_3(p^2). \tag{4.12}$$

with functions $T_{1,2,3}(p^2)$. The scalar function $T_1(p^2)$ is proportional to the gauge coupling in the $\widehat{\rm MOM}$ renormalisation scheme. Now, exhibiting the dominant part of each term in (4.7), we obtain

$$\begin{aligned} &T_1(q^2)\left(q_\mu q_\nu - q^2\delta_{\mu\nu}\right) + q^2 T_3(q^2) q_\mu q_\nu + \eta_{1\mu\nu}(q,r) = \\ &\frac{F\left((q+r)^2\right)}{G(r^2)}\Big[\left(a_1(q^2) + r_1(q,r)\right)\left(\delta_{\mu\nu}r^2 - r_\mu r_\nu\right) + \left(b_1(q^2) + r_2(q,r)\right) q_\mu \left(r^2 q_\nu - (q\cdot r) r_\nu\right) + \\ &\qquad + (b_1(q^2) + d_1(q^2) + r_3(q,r)) r_\mu (r^2 q_\nu - (q\cdot r) r_\nu)\Big] + \\ &\qquad + \frac{F((q+r)^2)}{G(q^2)}\Big[a_3(q^2)(q_\mu q_\nu - q^2\delta_{\mu\nu}) + \eta_{2\mu\nu}(q,r)\Big] \end{aligned} \tag{4.13}$$

with $r_{1,2,3}$ and $\eta_{1,2}$ satisfying

$$\begin{aligned} \lim_{r\to 0} r_1(q,r) = \lim_{r\to 0} r_2(q,r) = \lim_{r\to 0} r_3(q,r) = 0 \\ \lim_{r\to 0} \eta_{1\mu\nu}(q,r) = \lim_{r\to 0} \eta_{2\mu\nu}(q,r) = 0 \end{aligned} \tag{4.14}$$

Identifying the leading terms of the scalar factors multiplying the tensors $q_\mu q_\nu$ and

$\left(q_\mu q_\nu - q^2\delta_{\mu\nu}\right)$ we obtain the usual relations ([34]):

$$\begin{array}{l} T_1(q^2) = \frac{F(q^2)}{G(q^2)} a_3(q^2) \\ T_3(q^2) = 0. \end{array} \tag{4.15}$$

Using these relations in (4.13) we get

$$\lim_{r\to 0} \frac{F(p^2)}{G(r^2)} \left[a_1(q^2) \left(r^2\delta_{\mu\nu} - r_\mu r_\nu \right) + b_1(q^2)(r^2 q_\mu q_\nu - (r\cdot q) q_\mu r_\nu) \right] = 0. \tag{4.16}$$

Thus one sees that if

$$a_1(q^2) \neq 0 \quad \text{or} \quad b_1 \neq 0 \tag{4.17}$$

then (4.7) can only be compatible with the parametrisation (4.1) if

$$\alpha_G < 1. \tag{4.18}$$

The condition (4.17) is satisfied because at large momentum one has to all orders $a_1(p^2) = 1$ (because of the non-renormalisation theorem [8],[34]).

We can also, instead of letting $r \to 0$, take the limit $p \to 0$ of (1.45) as is done in [34]. The dominant part of the l.h.s. of (1.45) is

$$\left(2\delta_{\mu\nu}(p\cdot q) - p_\mu q_\nu - p_\nu q_\mu\right) T_1(q^2) - \left(\delta_{\mu\nu} - \frac{q_\mu q_\nu}{q^2}\right)(p\cdot q) T_2(q^2) + (p\cdot q) q_\mu q_\nu T_3(q^2) \tag{4.19}$$

The r.h.s. is the product of $F(p^2)$ with an expression of at least first order in p. T_1 and T_2 being different from zero we can conclude in this case that $\alpha_F \leq 0$.

Let us repeat here that all these considerations are valid only if all scalar factors of the ghost-ghost-gluon and three-gluons vertices are regular functions when one momentum goes to zero while the others remain finite. Under those quite reasonable hypotheses one obtains important constraints on the gluon and ghost propagators - namely that they are both divergent in the zero momentum limit, and the divergence of the ghost propagator is enhanced.

Let us stress that the limit (4.8) on α_G disagrees with many other analytical predictions quoted in the section 4.1.

4.3 Relation between the infrared exponents

The Schwinger-Dyson equation for the two-point correlation function (and for the quark propagator, but we consider only pure Yang-Mills case here) has the simplest form among other non-perturbative relations between Green functions. It has been used to constrain the the infrared exponents. Even more, there is a a commonly accepted relation between the infrared exponents

$$2\alpha_F + \alpha_G = 0. \tag{4.20}$$

which we shall discus now. The origin of this relation is the dimensional analysis of the Schwinger-Dyson equation for the ghost propagator

$$\frac{1}{F(k)} = 1 + g_0^2 N_c \int \frac{d^4q}{(2\pi)^4} \left(\frac{F(q^2)G((q-k)^2)}{q^2(q-k)^2} \left[\frac{(k\cdot q)^2 - k^2q^2}{k^2(q-k)^2} \right] H_1(q,k) \right), \quad (4.21)$$

where $H_1(q,k)$ is one of the scalar functions defining the ghost-gluon vertex:

$$q_{\nu'} \widetilde{\Gamma}_{\nu'\nu}(-q,k;q-k) = q_\nu H_1(q,k) + (q-k)_\nu H_2(q,k), \quad (4.22)$$

where $H_{1,2}$ are functions of the factors a,b,c,d,e (4.9). The large momentum behaviour ([34],[8]) of this vertex depends on the kinematic configuration:

$$\begin{aligned} &\tfrac{p_\mu p_\nu}{p^2} \cdot \widetilde{\Gamma}^{\overline{\rm MS}}_{\mu\nu}(-p,0;p) = 1 \quad \text{to } \textit{all} \text{ orders} \\ &\tfrac{p_\mu p_\nu}{p^2} \cdot \widetilde{\Gamma}^{\overline{\rm MS}}_{\mu\nu}(-p,p;0) = 1 + \tfrac{9}{16\pi}\alpha_s(p^2) + \dots \end{aligned} \quad (4.23)$$

Note that in the case of the vanishing momentum of the out-going ghost (and only in this case) the non-renormalisation theorem is applicable [8] and hence

$$H_1(q,0) + H_2(q,0) = 1. \quad (4.24)$$

Let us now consider two infrared scales $k_1 \equiv k$ and $k_2 \equiv \kappa k$. Calculating the difference of the Schwinger-Dyson equation (4.21) taken at scales k_1 and k_2 and supposing for the moment that $\alpha_F \neq 0$ one obtains

$$\begin{aligned} \frac{1}{F(k)} - \frac{1}{F(\kappa k)} \propto (1-\kappa^{-2\alpha_F})(k^2)^{-\alpha_F} = g_0^2 N_c \int \frac{d^4q}{(2\pi)^4} \left(\frac{F(q^2)}{q^2} \left(\frac{(k\cdot q)^2}{k^2} - q^2 \right) \times \right. \\ \left. \times \left[\frac{G((q-k)^2)H_1(q,k)}{((q-k)^2)^2} - \frac{G((q-\kappa k)^2)H_1(q,\kappa k)}{((q-\kappa k)^2)^2} \right] \right). \end{aligned} \quad (4.25)$$

This integral equation, as well as the initial equation (4.21), is written in terms of bare Green functions, and the integral may contain ultraviolet divergences. It can be cast into a well-defined renormalised form by multiplying (in (1.38)) $G^{(2)}$ (resp. $F^{(2)}$) by Z_3^{-1} (resp. $\widetilde{Z}_3^{-1}$) and the bare coupling g_0^2 by $Z_g^{-2} = Z_3\widetilde{Z}_3^2$, and finally multiplying the k^2 term by $\widetilde{Z}_3$. However, in the subtracted equation (4.25) all ultraviolet divergences are cancelled, as well as the $\widetilde{Z}_3 k^2$ term. Thus the subtracted Schwinger-Dyson equation holds both in terms of bare and renormalised Green functions without any explicit renormalisation factors.

We now make the hypothesis that there exists a scale q_0 below which the power-law parametrisation is valid

$$G(q^2) \sim (q^2)^{\alpha_G}, \quad F(q^2) \sim (q^2)^{\alpha_F}, \quad \text{for} \quad q^2 \leq q_0^2. \quad (4.26)$$

The equation (4.24) suggests that if *both* functions $H_{1,2}$ are non-singular then one

can suppose $H_1(q,k) \simeq 1$ in (4.25), and (4.20) is straightforward by a dimensional analysis. However, we have a priori no reason to think that the scalar functions $H_1(q,k)$ and $H_2(q,k)$ are *separately* non-singular for all q,k. Writing for example [1]

$$H_1(q,k) \;\sim\; (q^2)^{\alpha_\Gamma}\, h_1\left(\frac{q\cdot k}{q^2}, \frac{k^2}{q^2}\right), \tag{4.27}$$

with a non-singular function h_1, we keep all the generality of the argument admitting a singular behaviour of the scalar factor $H_1(q,k)$. Doing the dimensional analysis of the equation (4.25) *without* putting $H_1(q,k) \simeq 1$, we obtain that the relation (4.20) is satisfied if and only if the following triple condition is verified [60]:

$$2\alpha_F + \alpha_G = 0 \quad \longleftrightarrow \quad \begin{cases} \alpha_F \neq 0 \\ \alpha_\Gamma = 0 \\ \alpha_F + \alpha_G < 1 \end{cases} \tag{4.28}$$

All possible cases and limits obtained from the integral convergence conditions are given in Table 4.2. As we shall see the case 2 is excluded by lattice simulations. The case 4 is particularly interesting, it corresponds to the situation when the power-law infrared behaviour of the ghost propagator is the same as in the free case, and no relation between the infrared exponents follows from the Schwinger - Dyson equation. We shall return to this the discussion of this case in the section 4.5.

case	**1**	**2**	**3**	**4**
	$\alpha_F \neq 0$ $\alpha_F + \alpha_G + \alpha_\Gamma < 1$	$\alpha_F \neq 0$ $\alpha_F + \alpha_G + \alpha_\Gamma \geq 1$	$\alpha_F = 0$ $\alpha_G + \alpha_\Gamma < 1$	$\alpha_F = 0$ $\alpha_G + \alpha_\Gamma \geq 1$
IR convergence conditions	$\alpha_F + \alpha_\Gamma > -2$ $\alpha_G + \alpha_\Gamma > -1$	$\alpha_F + \alpha_\Gamma > -2$ $\alpha_G + \alpha_\Gamma > -1$	$\alpha_\Gamma > -2$ $\alpha_G + \alpha_\Gamma > -1$	$\alpha_\Gamma > -2$ $\alpha_G + \alpha_\Gamma > -1$
SD constraints	$2\alpha_F + \alpha_G + \alpha_\Gamma = 0$	$\alpha_F = -1$	excluded	none

Table 4.2: *Summary of the various cases regarding the α coefficients*

The first and the last conditions (4.28) are compatible with limits coming from the analysis of the Slavnon-Taylor identity (4.8), and are also consistent with lattice simulations (see section 4.5, [60]). If one of the conditions (4.28) is not verified then, according to the Table 4.2, (4.20) should be replaced by

$$2\alpha_F + \alpha_G + \alpha_\Gamma = 0. \tag{4.29}$$

In the following section we present the results of a numerical test of the relation (4.20), and thus we probe the validity of the condition on α_Γ.

One remark regarding the power-law parametrisation is in order. Suppose for the moment that this parametrisation is exact below the scale q_0 defined in (4.26). Then one can differentiate (4.25) n times with respect to κ, keeping q,k finite. We

[1] In fact there are many possible parametrisation. We choose (4.27) in order to illustrate the argument that follows.

obtain

$$\left(k^2\right)^{-2\alpha_F}(-2\alpha_F)\cdot\ldots\cdot(-2\alpha_F-n)\,\kappa^{-2\alpha_F-n}\propto\int d^4q\,\frac{d^n}{d^n\kappa}\left(\frac{G((q-\kappa k)^2)H_1(q,\kappa k)}{((q-\kappa k)^2)^2}\right). \tag{4.30}$$

The r.h.s of the last equation is not equal to zero for finite k, and thus one immediately has

$$\alpha_F\neq-\frac{n}{2},\qquad n=1,2,\ldots. \tag{4.31}$$

Thus any half-integer predictions for α_F should be considered as an indication of incompleteness of the power-law parametrisation (4.1).

4.4 Lattice study of the ghost Schwinger-Dyson equation

4.4.1 Complete ghost Schwinger-Dyson equation in the lattice formulation

In order to derive the discretized version of the ghost Schwinger-Dyson equation we repeat the same steps as in the continuum case (1.32 - 1.36) but for the lattice version of the Faddeev-Popov operator (1.68). We define the covariant Laplacian

$$\Delta_U^{ab}=\sum_\mu\left(G_\mu^{ab}(x)\left(\delta_{x,y}-\delta_{y,x+e_\mu}\right)-G_\mu^{ab}(x-e_\mu)\left(\delta_{y,x-e_\mu}-\delta_{y,x}\right)\right). \tag{4.32}$$

The appearance of Δ_U in (1.68) is due to the appropriate discretisation of the usual Laplacian operator Δ, dictated by the non-locality of derivatives in the lattice formulation, i.e. replacement of the ∇ operator by its covariant version.

Multiplying (1.68) by $F^{(2)}(x,y)$ from the right, one obtains

$$\begin{aligned}\frac{1}{N_c^2-1}\Delta_U^{ab}(y,z)F_{1\text{conf}}^{(2)ba}(U;z,x)=\delta_{y,u}-\\ -\frac{f^{abc}}{2(N_c^2-1)}\left[A_\mu^c(y)F_{1\text{conf}}^{(2)ba}(U;y+e_\mu,x)-A_\mu^c(y-e_\mu)F_{1\text{conf}}^{(2)ba}(U;y-e_\mu,x)\right].\end{aligned} \tag{4.33}$$

This is an exact mathematical identity for each gauge configuration U, and thus the consequences that can be derived from this relation are free of any ambiguity originating from the presence of Gribov copies. Performing an averaging $\langle\bullet\rangle$ over the configurations U one gets

$$\begin{aligned}\frac{1}{N_c^2-1}\mathrm{Tr}\left\langle\Delta_U(y,z)F_{1\text{conf}}^{(2)}(z,x)\right\rangle=\delta_{y,x}-\\ -\frac{f^{abc}}{2(N_c^2-1)}\left\langle A_\mu^c(y)F_{1\text{conf}}^{(2)ba}(U,y+e_\mu,x)-A_\mu^c(y-e_\mu)F_{1\text{conf}}^{(2)ba}(U,y-e_\mu,x)\right\rangle\end{aligned} \tag{4.34}$$

This averaging procedure depends on the way chosen to treat the Gribov problem:

the particular set of configurations over which it is performed depends on the prescription which is adopted (fc/bc procedures on the lattice, restriction to the fundamental modular region; see the subsection 2.4.2 for details). Consequently, the Green functions may vary but they must in any case satisfy the above equation, even when the volume of the lattice is finite.

Like in the continuum case, we perform a Fourier transform and obtain:

$$\frac{1}{N_c^2-1}\mathrm{Tr}\sum_x e^{ip\cdot x}\left\langle \Delta_U(0,z)F^{(2)}_{1\mathrm{conf}}(U,z,x)\right\rangle = 1 - i\sin(p_\mu)\frac{f^{abc}}{(N_c^2-1)}\left\langle A^c_\mu(0)\tilde{F}^{(2)ba}_{1\mathrm{conf}}(U,p)\right\rangle \tag{4.35}$$

Although the equations (4.33) and (4.34) have to be exactly verified by lattice data, the relation (4.35) does only approximately (within statistical errors) since it relies on translational invariance, which could be guaranteed only if we used an infinite number of Monte-Carlo configurations.

The presence of Δ_U in the last equation is due to non-zero lattice spacing effects. Indeed, lattice perturbation theory possesses an infinite number of ghost-gluon vertices depending on the lattice spacing a, giving tadpole contributions like the one presented at the Figure 4.1. Such tadpole contributions may be estimated by a mean

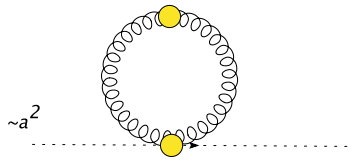

Figure 4.1: *Example of the terms in the Schwinger-Dyson equation on the lattice.*

field method [61]. Using the average plaquette $\langle P\rangle$ (for $\beta = 6.0$ $\langle P\rangle \simeq 0.5937$) one predicts a tadpole correction factor $\propto \langle P\rangle^{-(1/4)} \simeq 1.14$. These terms disappear in the continuum limit, but they do so only very slowly : the tadpole corrections (1 - plaquette) vanish only as an inverse logarithm with the lattice spacing. This is to be contrasted with the corrections arising in the r.h.s which are expected to be of order a^2. Our lattice calculation [60] gives

$$\Delta_U \simeq \Delta/\left(1.16 \pm 0.01\right), \tag{4.36}$$

almost independently of the momentum. This is in good agreement with the correction factor 1.14 quoted above.

We see from Figure 4.2 that the lattice Green functions match pretty well the SD equation (4.35) in both the ultraviolet and infrared regions. Lattice propagators were successfully checked by the perturbation theory at large momentum, and they satisfy the ghost Schwinger-Dyson equation. This means that lattice approach gives consistent results also in the infrared.

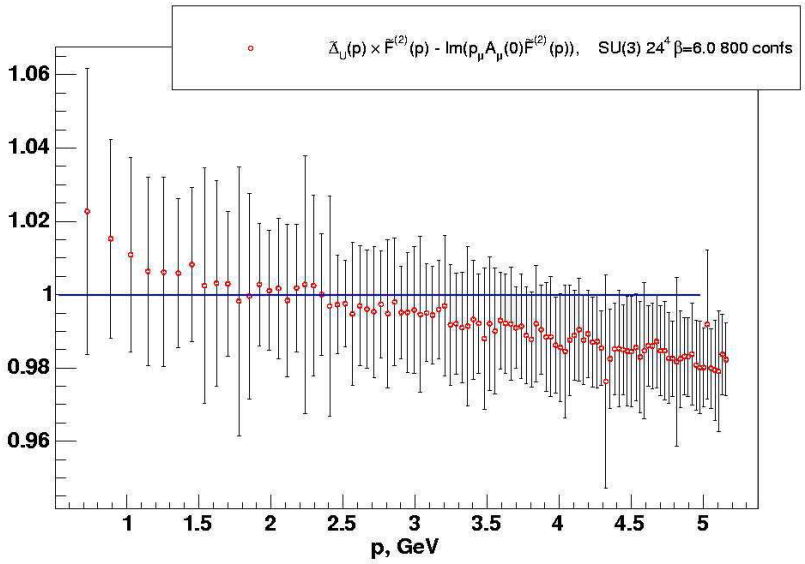

Figure 4.2: *Checking that lattice Green functions satisfy the ghost SD equation (4.35). We plot* $\frac{1}{1.16}\widetilde{F}(p^2) - g_0 \frac{p_\mu}{N_c^2-1} f^{abc} \langle A_\mu^c(0)\, \widetilde{F}^{(2)ba}_{1conf}(\mathcal{A}, p)\rangle$ *compared to* 1.

4.4.2 Checking the validity of the tree-level approximation for the ghost-gluon vertex

The simplest approximation (used by many authors, see section 4.1) of the ghost Schwinger - Dyson equation (4.21) corresponds to the case

$$H_1(q,k) = 1 \quad \forall q,k, \tag{4.37}$$

an approximation motivated by the non-renormalisation theorem (4.24) valid for the sum $H_1(q,k) + H_2(q,k)$ when $k = 0$. This gives

$$\frac{1}{F(k)} = 1 + \frac{g_0^2 N_c}{k^2} \int \frac{d^4q}{(2\pi)^4} \Big(\frac{F(q^2)G((k-q)^2)}{q^2(k-q)^2} \frac{(k\cdot q)^2 - k^2q^2}{(q-k)^2} \cdot 1 \Big). \tag{4.38}$$

Strictly speaking this equation, written in this way, is meaningless since it involves UV-divergent quantities. However it is well defined at fixed ultraviolet cut-off.

We want to check whether lattice propagators satisfy it. According to perturbation theory, it should be approximately true at large k. Lattice propagators are discrete functions of momentum and thus one has to handle the problem of the numerical evaluation of the loop integral I in (4.38). Let us express the integrand solely in terms of q^2 and $(k-q)^2$

$$I = \int \frac{d^4q}{(2\pi)^4} \frac{F^2(q)G(k-q)}{q^2(k-q)^2} \Big[\frac{(k-q)^2}{4} + \frac{(k^2)^2 + (q^2)^2 - 2k^2q^2}{4(k-q)^2} - \frac{q^2+k^2}{2} \Big]. \tag{4.39}$$

Then we write

$$I = I_1 + I_2 + I_3 + I_4 + I_5 + I_6, \tag{4.40}$$

each I_i corresponds to one term in (4.39). All these integrals have the form

$$I_i = C_i(k) \int \frac{d^4q}{(2\pi)^4} f_i(q) h_i(k-q). \tag{4.41}$$

The convolution in the r.h.s. is just the Fourier transform of the product at the same point in configuration space:

$$\int \frac{d^4q}{(2\pi)^4} f_i(q) h_i(k-q) = \mathrm{F}_+\Big(\mathrm{F}_-(f_i)[x]\mathrm{F}_-(h_i)[x]\Big)(k), \tag{4.42}$$

where $\mathrm{F}_-(\hat{f})(x)$ is an inverse and $\mathrm{F}_+(f)(k)$ a direct Fourier transform. Thus, in order to calculate the integral I from discrete lattice propagators one proceeds as follows:

1. calculate $\{f_i\}(p)$ and $\{h_i\}(p)$ as functions of $F(p), G(p), p^2$ for all i
2. apply the inverse Fourier transform F_- to all these functions and get $f_i(x)$ and $h_i(x)$
3. compute the product at the same point $f_i(x) \cdot h_i(x)$
4. apply the direct Fourier transform F_+ to $f_i(x) \cdot h_i(x)$

The integrands in (4.39) depend only on the squared norms q^2 and $(k-q)^2$, and thus the angular part may be integrated out, giving the four-dimensional Hankel transformation

$$\begin{aligned} \widehat{f(|x|)}[p] &= \frac{1}{|p|} \int_0^\infty J_1(|p|r) r^2 f(r) dr \\ f(r) &= \frac{1}{(2\pi)^2} \frac{1}{r} \int_0^\infty J_1(\rho r) \rho^2 \widehat{f(|x|)}[\rho] d\rho. \end{aligned} \tag{4.43}$$

These integrals are evaluated numerically by means of the Riemann sum

$$f(r) = (2\pi)^{-2} |r|^{-1} \sum_{i=1}^{N} J_1(r\rho_i) \rho_i^2 \frac{\hat{f}[\rho_i] + \hat{f}[\rho_{i-1}]}{2} (\rho_i - \rho_{i-1}), \qquad \rho_0 = 0, \tag{4.44}$$

where N is the number of data points. The inverse transformation is done in the similar way. In practice, because of the lattice artifacts (see subsection 2.3.2) which become important at large ρ the summation has to be restricted to $\rho < \rho_{max} \simeq 2.2$ instead of the maximal value 2π.

Now we are ready to check the approximate equation (4.38) on the lattice. We still have to face the same problem we have already encountered in the previous subsection, namely that the lattice Faddeev-Popov operator involves the non trivial discretisation Δ_U of the Laplacian operator. This is taken into account by means of the substitution of $\widetilde{\Delta_U}(p^2)/p^2$ to the "1" term in the l.h.s of equation (4.38) We present on Figure 4.3 the result of the numerical integration described above. We have chosen for this purpose the data set from the simulation with the gauge group

$SU(3)$ at $\beta = 6.4, V = 32^4, a^{-1} \approx 3.6$ GeV. One sees that the equality is achieved at large momenta, but in the infrared the naive approximation of the ghost Schwinger-Dyson equation fails. The errors on Figure 4.3 include statistical Monte-Carlo errors

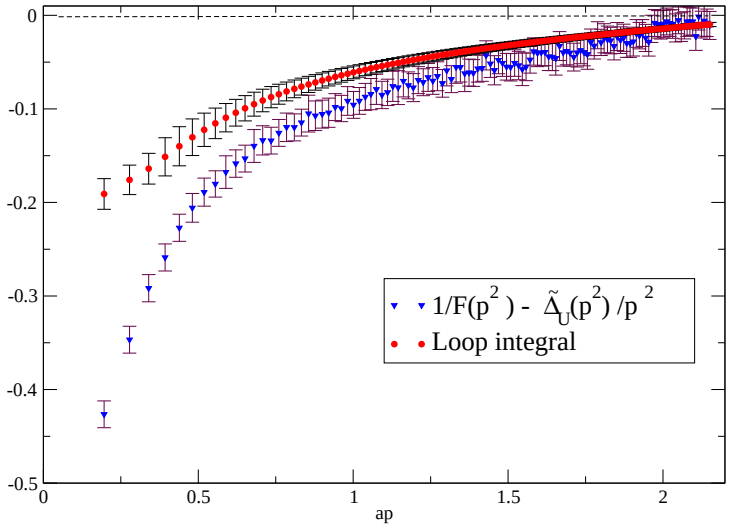

Figure 4.3: *Checking whether lattice Green functions satisfy the ghost SD equation (4.21) with an assumption* $H_1(q,k) = 1$. *The upper line(circles) correspond to the loop integral in (4.21), and the down line (triangles) corresponds to* $1/F(p^2) - 1$. *In this plot* $a^{-1} \approx 3.6$ *GeV.*

for $F(q^2)$ and $G(q^2)$ and the bias coming from the UV cut-off of the integral I.

We see that at small momenta (below $\approx$ 3 GeV) the ghost Schwinger-Dyson equation with the assumption $H_1(q,k) = 1$ is not satisfied. However, it is quite difficult to establish whether this disagreement is due to the infrared or ultraviolet dependencies of $H_1(q,k)$. To check this one has to know $H_1(q,k)$ for all values of q, k. Unfortunately this information is not available. Thus the main conclusion of the present subsection is that the scalar function $H_1(q,k)$ plays an important role in the infrared gluodynamics, and it cannot be set to one.

4.5 Direct fits of infrared exponents

We have seen in the previous section that lattice simulations give consistent results for the Green functions at all momenta. Another interesting feature that we have established is the important role of the scalar factor $H_1(q,k)$ coming from the complete ghost-gluon vertex (4.22). In this section we present numerical results allowing to check the relation (4.20). After this we present our results for direct fits of the exponents α_F and α_G, and compare them to the results of other lattice collaborations.

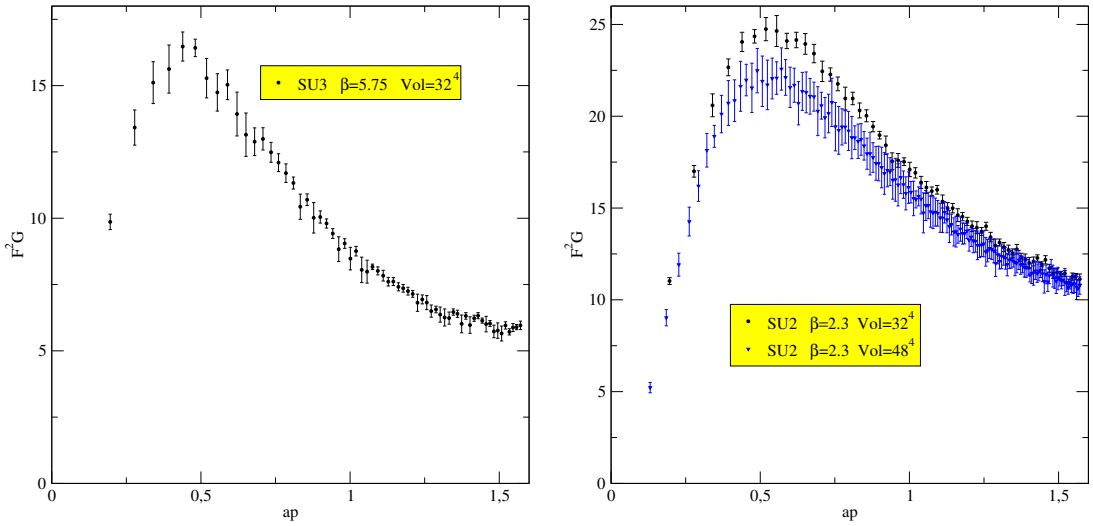

Figure 4.4: *Direct test of the relation* $2\alpha_F + \alpha_G = 0$. *If the last is true* F^2G *has to be constant in the infrared. We see that it is clearly not the case. In these plots* $a^{-1} \approx 1.2$ *GeV, so the peak is located at* ≈ 600 *MeV.*

4.5.1 Testing the relation $2\alpha_F + \alpha_G = 0$.

In order to test the relation (4.20) we plot at Figure 4.4 the quantity $F^2(p^2)G(p^2)$. If all the conditions (4.28) are satisfied this quantity should be constant in the infrared (or slightly varying). We see from Figure 4.4 that in the infrared (below ≈ 600 MeV) the quantity F^2G is not constant, and thus one of the conditions (4.28) is not verified. We have seen that the conditions $\alpha_F \neq 0$ and $\alpha_F + \alpha_G < 1$ are consistent with the limits (4.8) from the Slavnov-Taylor identity (4.7). We have also seen (cf. Figures 4.2 and 4.3) that neglecting the momentum dependence of the vertex is not possible in the infrared, because in this case the ghost Schwinger-Dyson equation is no longer satisfied by lattice propagators. Thus the only possibility is to admit that $H_1(q,k)$ plays an important role, and that the relation (4.20) is not verified. If $\alpha_F \neq 0$ then the modified form (4.29) that takes in account the singularity of $H_1(q,k)$ should be considered (according to Fig.4.3), with $\alpha_\Gamma < 0$ in our parametrisation. This singularity is probably related to the non-perturbative power corrections to the vertex discussed in the subsection 3.2.3.

Another reason to think that the relation (4.20) is not exact is the dependence of α_F and α_G on the choice of the Gribov copy. We have seen in the section 2.4 that the low-momentum dependence of the gluon propagator is not sensitive to the bc/fc choice while the infrared behaviour of the ghost propagator depends on it. But the Schwinger - Dyson equation for the ghost propagator is independent of the choice of the copy, because it is valid exactly for every gauge configuration, even on a finite lattice (see equations (1.36) and (4.34)). Hence if there is a relation between the infrared exponents α_F and α_G resulting from the ghost Schwinger - Dyson equation then it could not depend on the choice of the copy. Thus it is not possible to have a relation with α_F and α_G alone. This above argument is not directly applicable in the case $\alpha_F = 0$.

According to the analysis performed in the section 4.3, and given (see next sub-

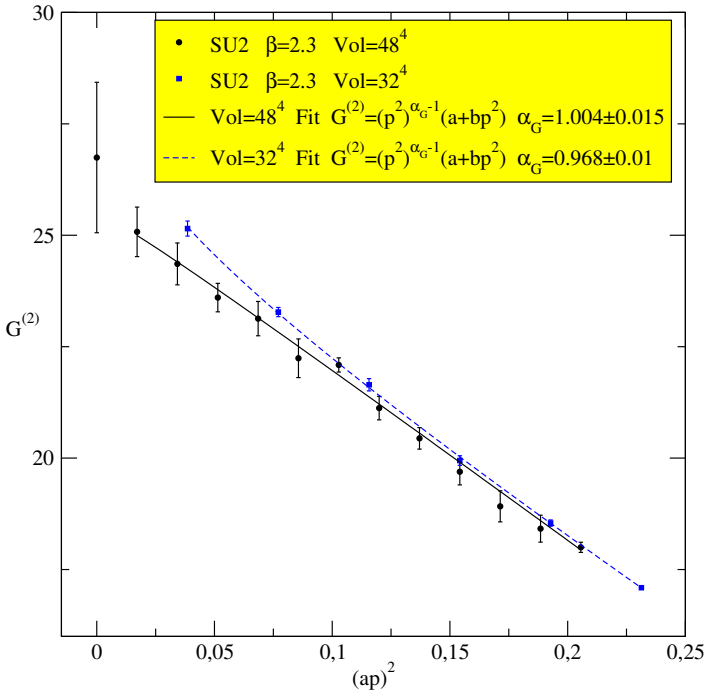

Figure 4.5: $G^{(2)}(p^2)$ *from lattice simulation for* $SU(2)$ *(left).* $\beta_{SU(2)} = 2.3$ *and* $\beta_{SU(3)} = 5.75$. *The volumes are* 32^4 *and* 48^4 *for* $SU(2)$. *In these plots* $a^{-1} \approx 1.2$ *GeV.*

section) that the case 2 of the Table 4.2 is excluded by lattice simulations the following explanations of the non-validity of the relation $2\alpha_F + \alpha_G = 0$ are possible:

1. The ghost-gluon vertex contains scalar factors that are singular in the infrared, i.e. $\alpha_\Gamma \neq 0$ in the equation 4.27.

2. The case 4 of the Table 4.2 is realised [62] and hence there exists *no* relation between the infrared exponents. Let us recall that in the above case one has $\alpha_F = 0$ and $\alpha_G + \alpha_\Gamma \geq 1$. If the ghost-gluon vertex is regular in the infrared then one has
$$\begin{cases} \alpha_F = 0 \\ \alpha_G \geq 1. \end{cases} \tag{4.45}$$

4.5.2 Lattice fits for α_F and α_G.

Let us now discuss the direct fits for the infrared exponents α_G and α_F. The examples of such fits of lattice data are presented on Figure 4.5. The errors are quite large, leading to an instability in the fit results. That is why we fit both propagators in the infrared to the formula
$$(q^2)^\alpha(\lambda + \mu q^2) \tag{4.46}$$
where we added an additional term of the form μq^2 in order to describe a situation like the one at Figure 4.5(left) where $G^{(2)}(p^2)$ seems to go to a finite limit when p goes to zero. The obtained values for $\alpha_{F,G}$ are summarised in Table 4.3. For $SU(2)$

Group	Volume	β	α_G	α_F
$SU(2)$	48^4	2.3	1.004(15)	−0.087(15)
$SU(2)$	32^4	2.3	0.968(11)	−0.109(14)

Table 4.3: Summary of the fit results for the F and G functions

and the larger lattice volume the value obtained for α_G is compatible with 1.We also take into account our experience from previous studies of the gluon propagator where we have always observed that the gluon propagator goes continuously to a finite limit in the infrared region (see Figure 4.6). However, the fits are quite instable,

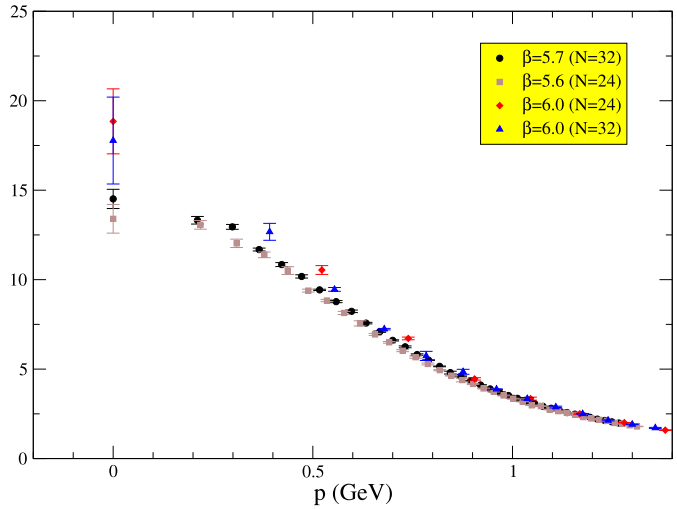

Figure 4.6: *The continuity of the lattice gluon propagator in the infrared.*

and depend a lot on the choice of the fit formula that can considerably change the result. The main problem is the lack of data points at low momenta.

Regarding the gluon propagator another strategy may be taken. It consist in extrapolating the available data to the infinite volume limit. A very detailed study of the gluon dressing function and specially of its volume dependence at $k = 0$ has already been performed in [63]. This study shows that a value $\alpha_G = 1$ is compatible with the data (the dressing function shows no signal of discontinuity in the neighbourhood of zero) and that no pathology shows up as the volume goes to infinity. Let us compare all available lattice results for the point $G^{(2)}(0)$ and check whether there is an agreement between the data. Following [63] we renormalise the gluon propagator in the MOM scheme at 4 GeV and use the suggested extrapolation formula

$$G_R^{(2)}(0, \mu = 4\,\mathrm{GeV}) = G_{R\,\infty}^{(2)}(0, \mu = 4\,\mathrm{GeV}) + \frac{c}{V}. \tag{4.47}$$

We compare the results of [63],[64] and our data from the Table 4.4. The results for

the fit parameters $G^{(2)}_{R\,\infty}(0)$ and c are presented in the Table 4.5. We are aware that not

β	V in units of a	bare propagator $G^{(2)}(p)$	$1/aL$ in GeV
5.7	16^4	16.81 ± 0.13	0.0672
5.7	24^4	15.06 ± 0.29	0.0448
5.8	16^4	19.12 ± 0.16	0.0841
5.9	24^4	18.12 ± 0.30	0.0685
6.0	32^4	17.70 ± 0.59	0.0615
6.0	24^4	19.67 ± 0.35	0.0821

Table 4.4: *Physical lattice sizes and raw data for the gluon propagator at zero momentum $G^{(2)}(p)$ from our old data.*

reference	$G^{(2)}_R(0, \mu = 4\,\mathrm{GeV})$ in GeV^{-2}	c in GeV^{-2} fm^4	max vol in fm^4
[63]	7.95 ± 0.13	245 ± 22	2000
Table 4.4	9.1 ± 0.3	140 ± 50	90
[64]	$10.9 - 11.3$	$47 - 65$	110s

Table 4.5: *Summary of the infinite volume zero momentum propagator and its slope in terms of $1/V$ for three different simulations. The largest volume used in the fit is also indicated. The statistical error is not quoted in [64].*

all systematic errors are taken into account: $O(a)$ effects, effect due to different lattice shape, insufficiently large volumes (for the second and third lines), uncertainty in the estimate of the lattice spacing in physical units, etc. However, it seems that not only there is a clear indication in favour of a finite non vanishing zero momentum gluon propagator, but that different lattice collaborations agree on the value. Of course a more extensive study is necessary to check this statement. The other free parameter of the fit - the slope c - is clearly different, but still all the values are in agreement in the order of magnitude.

We conclude [65] thus that all available numerical results point towards a finite non-vanishing and zero momentum renormalised lattice gluon propagator in the infinite volume limit. This suggests that $\alpha_G = 1$. An additional study at much larger lattices is needed to get a reliable result for this infrared exponent.

This last result is in conflict with the limits found from the study of the Slavnov - Taylor identity (4.8), and contradicts the Zwanzigers's prediction that the gluon propagator is infrared suppressed. However, it is very close to the results presented in [55].

Let us finally discuss the gauge-dependence of the parameter α_G. This is still an open question. However, the results of works [66],[67] suggest that the value of α_G does not change drastically (see Figure 4.8) when changing the gauge parameter ξ. This question deserves a separate study.

To finish this chapter, let us summarise the lattice results. We have found that α_F is very close to 0 (see Figure 4.7), α_G is close to 1 and the widely used relation $2\alpha_F + \alpha_G = 0$ is not true. Going back to the possibilities given in the Table 4.2 we find that the cases 2 and 3 are not realised. We are left with the cases 1 and 4, and

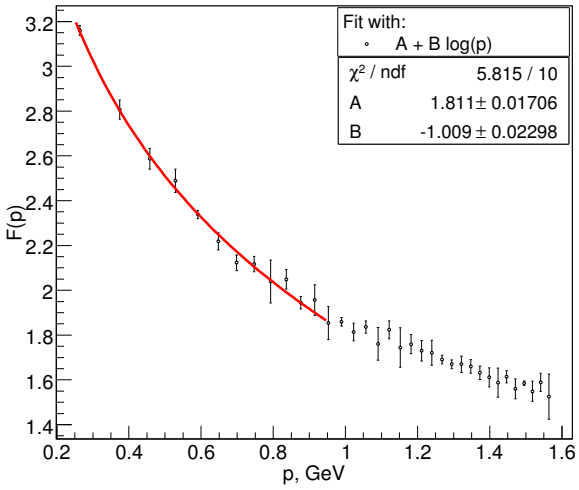

Figure 4.7: *The fit of the ghost scalar factor $F(p)$ to the formula $A + B \log p$. It suggests that the infrared divergence of $F(p)$ is very slow. Hence α_F is close to zero [62]. The simulations was performed on a $V = 32^4$ lattice at $\beta = 5.8$. The Landau gauge was fixed using the f.c. choice for the Gribov copies.*

for the moment lattice simulations cannot say which possibility is true. However, all numerical results are better explained by the possibility (4.45) corresponding to the case 4 of the Table 4.2 supplied with an hypothesis of the regularity of the scalar factors entering the ghost-gluon vertex. We recall that in this case one has:

$$\begin{cases} \alpha_F = 0 \\ \alpha_G \geq 1. \\ \text{no relation between } \alpha_F \text{ and } \alpha_G \text{ follows from the ghost SD equation.} \end{cases} \tag{4.48}$$

Note that it is still in conflict with the constraints coming from the Slavnov - Taylor identity (4.8). Thus the essential question today is to understand whether $\alpha_F = 0$ or not [62]. And, of course, a study on larger lattices is necessary to perform better fits of the infrared exponents.

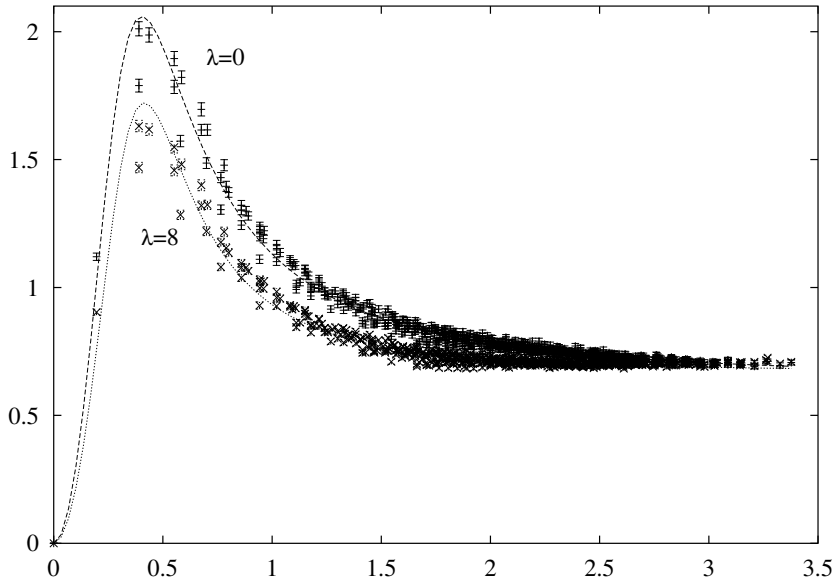

Figure 4.8: *Transverse part of the gluon propagator $p^2G^{(2)}(p)$ in covariant gauges as a function of p. The two sets of data refer to ($\xi = \lambda$) $\xi = 0$ (Landau gauge) and $\xi = 8$, 221 thermalized $SU(3)$ configurations at $\beta = 6.0$ with a volume $V \times T = 16^3 \times 32$. Extracted from [66].*

Chapter 5

Conclusions

In this chapter we discuss the conclusions of the present dissertation. Lattice simulations is a great tool to study the non-perturbative effects in QCD. The main goal of this dissertation is to exhibit how these effects influence the momentum behaviour of different Green functions in Landau gauge. Our hope is that the knowledge of the change in momentum behaviour at low momenta can help in the understanding of one of the most difficult puzzles of QCD - the mechanism of confinement.

In the chapter 3 the large momentum behaviour of the ghost and the gluon propagator of a pure Yang-Mills theory in Landau gauge is investigated. The main parameter under study is the scale $\Lambda_{\rm QCD}$. We show that the values of $\Lambda_{\rm QCD}$ fitted from the ghost and the gluon propagator are consistent. However, the available momentum range (from ≈ 2 to ≈ 6.5 GeV) is situated in the zone where non-perturbative effects cannot be neglected. So at first glance the agreement between $\Lambda_{\rm QCD}$ extracted from different Green function may seem strange. An explanation of this fact comes from the OPE analysis allowing to estimate the influence of dominant non-perturbative power corrections. We found that these corrections are the same in the case of the ghost and gluon propagators, that is why the values of $\Lambda_{\rm QCD}$ are compatible. According to the OPE calculation, the value of $\Lambda_{\rm QCD}$ that is extracted from the propagators is modified by the non-perturbative effects. We used the fact that the equivalence of the leading power corrections implies that their ratio is free of power corrections at the considered order. Thus the ratio of the ghost and gluon propagators is a quantity which is better described by perturbation theory in the considered energy interval than the propagators themselves. Indeed, our analysis of the lattice data showed that the fit of the ratio gives a smaller value for $\Lambda_{\rm QCD}$ (≈ 270 MeV in the $\overline{\rm MS}$ renormalisation scheme) compared to the value obtained from the separate fits of the propagators ($\Lambda_{\overline{\rm MS}} \approx 330$ MeV). Both fits are performed on the same data samples. This speaks in favour of a presence of non-perturbative power corrections in the interval $[2\ {\rm GeV}, 6.5\ {\rm GeV}]$, in agreement with the OPE predictions and the results of previous investigations.

One can use the Slavnov - Taylor identities in order to find other relations between the Wilson coefficients in different Green functions. For example we found that the dominant $\propto \frac{1}{p^2}$ power corrections are the same in the case of the three gluon vertex and the ghost-gluon vertex in asymmetric kinematic configurations (with the

gluon momentum set to zero). We have also shown that the power correction to the ghost-gluon vertex with vanishing momentum of the entering ghost is equal to zero (in Landau gauge). However, this is not true if the momentum of the entering ghost is not *exactly* equal to zero. In this case the vertex has an $\propto \frac{1}{p^2}$ power correction that becomes quite important at low momenta.

As a partial conclusion we stress the attention of the reader on the fact that lattice simulations are very successfull in describing the Green functions at large momentum, the results are consistent with the predictions of perturbation theory, completed with the OPE calculation of the power corrections, up to NNNLO.

In the chapter 4 we turn to the study of very low momentum behaviour (of order and below Λ_{QCD}) of the Green functions. One of the very interesting puzzles in the infrared is the problem of the Gribov ambiguity. The lattice method has an advantage to explicitly perform the Gribov quantisation. However, the gauge is not fixed in a unique way and there are Gribov copies on the lattice. We showed that the probability to find a secondary Gribov copy possess the property of scaling. This probability increases significantly when the physical volume of the lattice excesses some critical volume (of around $(2.75/\sqrt{\sigma})^4$ in the case of $SU(2)$ gauge theory). Our conclusion is that in order to study the non-perturbative effects one has to work at lattices with physical volume larger then the critical one that we found.

Our first step in the study of low-momentum behaviour of Green functions is to check that lattice simulations can give reliable results in the infrared. For this purpose we verified (numerically, see Figure 4.2) that lattice Green functions satisfy the complete ghost Schwinger - Dyson equation (1.38) for all considered momenta. These tests allow us to conclude that numerical simulation on the lattice give relevant results not only in the ultraviolet domain, but also in the infrared one.

The quantitative parameters we are interested in are the infrared exponents α_F and α_G describing the power-law deviation (this is a crudest approximation) from free propagators (ghost and gluon respectively) in the deep infrared. Our analysis of the Slavnov-Taylor identity relating the three-gluon vertex, the ghost-gluon vertex and the propagators showed that the power-law infrared divergence of the ghost propagator is unchanged or enhanced in the infrared (compared to the free case), and that the gluon propagator must diverge in the infrared. The latter limit is in conflict with today's lattice results yelding a finite non-zero gluon propagator at zero momentum, and with most present analytical estimations that we quote in the section 4.1, that support a vanishing gluon propagator in the infrared.

Another analytical relation imposing constraints on the infrared exponents is the ghost Schwinger-Dyson equation. We revisited the commonly accepted relation (4.20) between these exponents saying that $2\alpha_F + \alpha_G = 0$. According to our analysis this relation is true only if the ghost-gluon vertex contains no singularity, in none of the scalar functions defining the vertex. Our numerical studies showed that the relation in question is not valid, because F^2G is infrared suppressed, and hence $2\alpha_F + \alpha_G > 0$. This statement is supported by the fact that lattice propagators do not match the reduced Schwinger - Dyson equation (see Figure 4.3), whereas the complete one is perfectly verified, Figure 4.2. There are even more reasons to think that the relation (4.20) is not true. First, we have seen that the non-perturbative

ghost-gluon vertex contains singular contributions from the $\langle A^2 \rangle$ condensate for most kinematic configurations. However, it is difficult to estimate the role of such contributions at very low momenta. Second, we have seen that the infrared behaviour of the ghost and gluon propagator seem to vary differently with the choice of the Gribov copy (bc or fc). We have seen that the form of the complete ghost Schwinger - Dyson equation does not depend on the choice of the Gribov copy. If $\alpha_F \neq 0$ and it depends on the choice of the copy, it is impossible to have an exact relation between α_F and α_G alone, and to satisfy the condition of independence of the choice of the copy.

The direct fit of the propagators in the infrared supports the prediction that the infrared behaviour of the ghost propagator is enhanced in the infrared. But this enhancement is very slight. The gluon propagator is found to be infrared finite. This last result is in conflict with the limit found from the analysis of the Slavnov - Taylor identity. For the moment we have no explanation regarding this disagreement.

Summarising the numerical results, we found that the gluon propagator is finite in the infrared ($\alpha_G \approx 1$), that the infrared divergence of the ghost propagator is almost the same as in the free case ($\alpha_F \approx 0$) and that the commonly accepted relation $2\alpha_F + \alpha_G = 0$ is not true. Going back to the analysis of the ghost Schwinger - Dyson equation (see Table 4.2), two solutions are possible:

1. The infrared exponent of the ghost propagator α_F is *strictly* equal to zero, i.e. the power-law infrared dependence is the same as at large momenta. This implies that *no* relation between α_F and α_G follows from the ghost Schwinger - Dyson equation. If we now suppose that the ghost-gluon vertex contains no (infrared) singular components then all our lattice results are perfectly described.

2. The infrared exponent of the ghost propagator $\alpha_F \neq 0$, then there is a relation between α_F, α_G and α_Γ following from the ghost Schwinger - Dyson equation. The fact that the relation $2\alpha_F + \alpha_G = 0$ is not verified on the lattice suggests that there is a singularity in one of the scalar factors defining the ghost-gluon vertex i.e. $\alpha_\Gamma \neq 0$.

The today's lattice results speak in favour of the first possibility, but calculations at larger lattices are necessary in order to conclude.

Chapitre 6

Resumé

Nous présentons dans ce chapitre les conclusions essentielles de la présente thèse. Notre objectif est d'étudier les fonctions de corrélation de la théorie Yang - Mills pure. Plus précisément, nous cherchons à comprendre les différents effets non-perturbatifs qui déterminent le comportement des fonctions de Green dans la jauge de Landau aux basses énergies.

L'outil principal utilisé est la simulation numérique de la Chromodynamique Quantique, appelée la QCD sur réseau. Il permet d'évaluer numériquement les intégrales fonctionnelles définissant les valeurs moyennes de produits des champs dans le vide, autrement dit les fonctions de Green. L'avantage de cette méthode est qu'elle préserve explicitement l'invariance de jauge, ce qui permet une étude non-perturbative à toutes les échelles d'énergie à partir des seul principes premiers. Toutefois, il est obligatoire de travailler sur un réseau discret (ce qui brise l'invariance de Lorentz) de taille finie et dans une formulation euclidienne. Cependant, aujourd'hui il existe des méthodes de traitement des divers artefacts causés par la discrétisation. La QCD sur réseau a fait ses preuves : la masse du quark charmé a été calculée ainsi que les diverses propriétés des mésons lourds, la température de déconfinement, etc. Mais les simulations numériques peuvent aussi être utilisée afin d'étudier les paramètres fondamentaux de la théorie tels que la constante de couplage, l'échelle Λ_{QCD}, etc. Ceci est le but principal de cette thèse.

I

Nous commençons par une étude du comportement des propagateurs du gluon et du fantôme de Faddeev - Popov dans l'intervalle d'énergie d'environ 2.5 GeV à 6.5 GeV. Le paramètre qui nous intéresse est Λ_{QCD}. Ce paramètre est très important car il fixe une échelle caractéristique de la théorie. Il est intéressant de noter que le lagrangien de la théorie Yang - Mills pure ne contient pas de paramètres dimensionnés, la valeur non nulle de Λ_{QCD} étant générée par le processus de la quantification suivi par la renormalisation. Λ_{QCD} n'est pas une vraie quantité physique, car il dépend du schéma de renormalisation. Cependant, la valeur de ce paramètre non-perturbatif dans un schéma donné est très importante car elle permet d'estimer la portée d'autres méthodes : calculs perturbatifs, règles de resommations, etc.

Sur réseau, on peut obtenir Λ_{QCD} à l'aide des prédictions de la théorie des perturbations (jusqu'à l'ordre NNNLO) pour les propagateurs que nous avons considérés. Nous avons

montré [21] que les valeurs de Λ_{QCD} extraites séparément du propagateur du gluon et de celui du fantôme sont compatibles. Cet accord peut paraître surprenant car on s'attendrait plutôt à des effets non-perturbatifs importants dans le domaine d'énergie considérée. L'estimation OPE (développement en produit d'opérateurs) des corrections non-perturbatives [49] montre qu'elles sont identiques pour les deux propagateurs ce qui explique l'accord sur la valeur de Λ_{QCD}. L'égalité des corrections multiplicatives dominantes aux propagateurs du gluon et du fantôme implique que leur rapport n'en contient pas (à l'ordre dominant). Par conséquent, ce rapport est mieux décrit par la théorie des perturbations que ne le sont les propagateurs séparément. En effet, notre analyse a montré que la valeur de Λ_{QCD} extraite du rapport ($\Lambda_{\overline{MS}}^{n_f=0} \approx 270$ MeV) est plus petite que celle obtenue à partir des propagateurs ($\Lambda_{\overline{MS}}^{n_f=0} \approx 330$ MeV). Puisque dans les deux cas nous avons utilisé les mêmes données numériques, cette différence indique la présence de corrections en puissance dans l'intervalle d'énergie considéré, ce qui est en accord avec les prédictions de l'OPE faites par le passé.

On peut utiliser les identités de Slavnov - Taylor pour établir un lien entre les coefficients de Wilson pour des fonctions de Green différentes. On peut par exemple s'assurer que les corrections dominantes au vertex fantôme-gluon et au vertex à trois gluons (dans la configuration cinématique avec le moment du gluon mis à zéro) sont très liées. Malheureusement, on ne peut pas trouver une relation entre la correction dominante au vertex gluon-gluon dans la configuration cinématique avec un fantôme ayant le moment nul et les corrections aux autres fonctions de Green. Mais un calcul direct suggère que ce vertex n'a pas de correction en $\frac{1}{p^2}$. Ce cas est particulièrement intéressant car la non-renormalisation du vertex fantôme-gluon implique qu'il est égal à 1 en jauge de Landau à tout ordre de la théorie des perturbations. Il semblerait donc que le théorème de non-renormalisation du vertex soit aussi vérifié par des corrections non-perturbatives dues à la présence du condensat $\langle A^2 \rangle$. Cependant, si l'impulsion du fantôme entrant n'est pas exactement égale à zéro, le vertex possède des corrections en $\frac{1}{p^2}$ qui deviennent importantes aux petites énergies.

Nous retiendrons en tant que conclusion partielle que les simulations numériques donnent une estimation très fiables des fonctions de Green aux grandes énergies, les résultats étant compatibles avec les prédictions de la théorie de perturbations (complétée par un calcul OPE des corrections en puissance) jusqu'à l'ordre de NNNLO.

II

La deuxième partie de la thèse est consacrée à l'étude du comportement infrarouge des propagateurs fondamentaux [60]. Il a été observé que ce comportement change de manière radicale aux énergies de l'ordre de Λ_{QCD}. Cela est probablement lié au confinement, ce qui explique notre intérêt pour ce problème.

Un des problèmes les plus délicats est l'ambiguïté de Gribov. L'avantage de la QCD sur réseau est que dans le cadre de cette méthode on réalise explicitement la prescription de quantification à la Gribov. Toutefois, la jauge n'est pas fixé de manière unique et il y a donc des copies de Gribov sur réseau. Nous avons montré que la probabilité de touver une copie de Gribov, pour une configuration de jauge donnée, possède la propriété de scaling. Cette

probabilité croît considérablement quand le volume physique du réseau excède une valeur critique (de $\left(2.75/\sqrt{\sigma}\right)^4$ dans le cas de la théorie $SU(2)$ en jauge de Landau), au-delà de laquelle presque chaque configuration du champ de jauge possède des copies de Gribov. Notons qu'un effet similaire a déjà été observé pour les fonctions de Green dans la jauge Maximale Abélienne. Nous en concluons que pour étudier les effets non-perturbatifs l'utilisation de réseaux dont le volume est supérieur au volume critique est indispensable. Nous sommes ainsi amené à sélectionner une copie. D'après notre analyse (et celle d'autres collaborations) les fonctions gluoniques sont insensibles au choix de la copie (l'effet étant plus petit que les erreurs statistiques), tandis que le propagateur du fantôme a une légère dépendance.

Avant de commencer l'étude de fonctions de Green dans l'infrarouge (aux énergies de l'ordre de ou inférieures à Λ_{QCD}), nous voulons nous assurer que les simulations sur réseau permettent d'étudier les fonctions de Green à basse énergie. Pour cela nous avons vérifié numériquement que les propagateurs obtenus sur réseau satisfont l'équation de Schwinger - Dyson pour le propagateur du fantôme. Nous avons aussi vu que les propagateurs ont été testés par la théorie des perturbations jusqu'à l'ordre NNNLO aux grandes énergies. La QCD sur réseau est donc une bonne méthode pour étudier les fonctions de Green dans l'infrarouge.

Lors d'une étude des fonctions de Green à basse énergie, nous sommes principalement intéressés par le changement de la loi en puissance des corrélateurs [60]. Ceci est l'approximation la plus grossière. Notre analyse de l'identité de Slavnov - Taylor a abouti à des contraintes sur les exposants infrarouges des propagateurs. Ces contraintes imposent que le propagateur du gluon diverge à basse énergie, et que le propagateur du fantôme a la même divergeance ou bien diverge plus vite que dans le cas libre. Une étude analytique de l'équation de Schwinger - Dyson a suggéré plusieurs cas possibles pour les valeurs et relations entre les exposants infrarouges. Les simulations numériques favorisent un propagateur du gluon fini non-nul dans l'infrarouge [65], et indiquent que le propagateur du fantôme diverge légèrement plus vite que dans le cas libre. Ces résultats permettent de conclure que la relation entre les exposants infrarouges obtenue avec des méthodes approximatives de résolution des équations de Schwinger - Dyson n'est en fait pas valable. Le résultat pour le propagateur du gluon est en désaccord avec la borne trouvée à partir de l'identité de Slavnov - Taylor. Pour l'instant nous n'avons pas trouvé d'explication à ce phénomène. Si l'on compare les résultats numériques pour les exposants infrarouges et l'étude analytique de l'équation de Schwinger - Dyson pour le propagateur du fantôme, deux possibilités sont envisageables :

1. *le comportement en puissance (dans l'infrarouge) du propagateur du fantôme est le même que dans le cas libre. Dans ce cas il ne peut exister de relation entre les exposant infrarouges (en tout cas, pas à partir de l'équation de Schwinger - Dyson pour le propagateur du fantôme). Si de plus on suppose que le vertex fantôme-gluon ne contient pas de facteur scalaire singulier à basse énergie, tous les résultats numériques peuvent alors être expliqués ;*
2. *si le comportement en puissance (dans l'infrarouge) du propagateur du fantôme est différent de celui du cas libre, alors il y a nécessairement des facteurs singuliers dans le vertex fantôme-gluon. Il existe aussi une relation entre certains exposants infrarouges qui découle de l'équation de Schwinger - Dyson.*

La première solution semble être favorisée par les simulations numériques, mais pour conclure, nous devons étudier le propagateur du fantôme sur des réseaux plus grands que ceux dispo-

nibles à l'heure actuelle.

Bibliographie

[1] V. N. Gribov. Quantization of non-abelian gauge theories. *Nucl. Phys.*, B139 :1, 1978.

[2] Axel Maas. On the spectrum of the Faddeev-Popov operator in topological background fields. 2005, hep-th/0511307.

[3] M. Semenov-Tyan-Shanskii and V. Franke. All gauge orbits and some Gribov copies encompassed by the Gribov horizon. *Zap. Nauch. Sem. Leningrad. Otdeleniya Matematicheskogo Instituta im. V. A. Steklova, AN SSSR*, vol. 120 :159, 1982. (English translation :New York, Plenum Press 1986).

[4] Pierre van Baal. More (thoughts on) Gribov copies. *Nucl. Phys.*, B369 :259–275, 1992.

[5] Daniel Zwanziger. Non-perturbative Faddeev-Popov formula and infrared limit of QCD. *Phys. Rev.*, D69 :016002, 2004, hep-ph/0303028.

[6] Reinhard Alkofer and Lorenz von Smekal. The infrared behavior of QCD Green's functions : Confinement, dynamical symmetry breaking, and hadrons as relativistic bound states. *Phys. Rept.*, 353 :281, 2001, hep-ph/0007355.

[7] A. A. Slavnov. Ward identities in gauge theories. *Theor. Math. Phys.*, 10 :99–107, 1972.

[8] J. C. Taylor. Ward identities and charge renormalization of the Yang-Mills field. *Nucl. Phys.*, B33 :436–444, 1971.

[9] J. C. Taylor. Gauge theories of weak interactions. Cambridge 1976, 167p.

[10] C. Bagnuls and C. Bervillier. Exact renormalization group equations : An introductory review. *Phys. Rept.*, 348 :91, 2001, hep-th/0002034.

[11] Ulrich Ellwanger, Manfred Hirsch, and Axel Weber. The heavy quark potential from Wilson's exact renormalization group. *Eur. Phys. J.*, C1 :563–578, 1998, hep-ph/9606468.

[12] Kenneth G. Wilson. Confinement of quarks. *Phys. Rev.*, D10 :2445–2459, 1974.

[13] I. Montvay and G. Munster. Quantum fields on a lattice. Cambridge, UK : Univ. Pr. (1994) 491 p. (Cambridge monographs on mathematical physics).

[14] J. Smit. Introduction to Quantum Fields on a lattice : A robust mate. *Cambridge Lect. Notes Phys.*, 15 :1–271, 2002.

[15] K. Osterwalder and E. Seiler. Gauge field theories on the lattice. *Ann. Phys.*, 110 :440, 1978.

[16] C. Itzykson, Michael E. Peskin, and J. B. Zuber. Roughening of Wilson's surface. *Phys. Lett.*, B95 :259, 1980.

[17] Stephen L. Adler. Overrelaxation algorithms for lattice field theories. *Phys. Rev.*, D37 :458, 1988.

[18] A. Y. Lokhov, O. Pene, and C. Roiesnel. Scaling properties of the probability distribution of lattice Gribov copies. 2005, hep-lat/0511049.

[19] P. Boucaud, J. P. Leroy, J. Micheli, O. Pene, and C. Roiesnel. Lattice calculation of alpha(s) in momentum scheme. *JHEP*, 10 :017, 1998, hep-ph/9810322.

[20] B. Alles et al. α_s from the nonperturbatively renormalised lattice three gluon vertex. *Nucl. Phys.*, B502 :325–342, 1997, hep-lat/9605033.

[21] Ph. Boucaud et al. Large momentum behavior of the ghost propagator in SU(3) lattice gauge theory. *Phys. Rev.*, D72 :114503, 2005, hep-lat/0506031.

[22] Yousef Saad. Iterative methods for sparse linear systems. PWS Publishing, New York, 1996.

[23] B. Efron. Bootstrap methods : Another look at the jackknife. *The Annals of Statistics*, 7 :1–26, 1979.

[24] A. C. Davison and D. V. Hinkley. Bootstrap methods and their applications. *Monographs on Statistics and Applied Probability 57, Chapman and Hall/CRC*, (1994).

[25] A. Sternbeck, E. M. Ilgenfritz, and M. Mueller-Preussker. Spectral properties of the Landau gauge Faddeev-Popov operator in lattice gluodynamics. *Phys. Rev.*, D73 (2006) 014502, hep-lat/0510109.

[26] Jacques C. R. Bloch, Attilio Cucchieri, Kurt Langfeld, and Tereza Mendes. Propagators and running coupling from SU(2) lattice gauge theory. *Nucl. Phys.*, B687 :76–100, 2004, hep-lat/0312036.

[27] J. Fingberg, Urs M. Heller, and F. Karsch. Scaling and asymptotic scaling in the SU(2) gauge theory. *Nucl. Phys.*, B392 :493–517, 1993, hep-lat/9208012.

[28] Attilio Cucchieri. Gribov copies in the Minimal Landau gauge : The influence on gluon and ghost propagators. *Nucl. Phys.*, B508 :353–370, 1997, hep-lat/9705005.

[29] T. D. Bakeev, Ernst-Michael Ilgenfritz, V. K. Mitrjushkin, and M. Mueller-Preussker. On practical problems to compute the ghost propagator in SU(2) lattice gauge theory. *Phys. Rev.*, D69 :074507, 2004, hep-lat/0311041.

[30] A. Sternbeck, E. M. Ilgenfritz, M. Muller-Preussker, and A. Schiller. The influence of Gribov copies on the gluon and ghost propagator. *AIP Conf. Proc.*, 756 :284–286, 2005, hep-lat/0412011.

[31] A. Sternbeck, E. M. Ilgenfritz, M. Muller-Preussker, and A. Schiller. The gluon and ghost propagator and the influence of Gribov copies. *Nucl. Phys. Proc. Suppl.*, 140 :653–655, 2005, hep-lat/0409125.

[32] P. J. Silva and O. Oliveira. Gribov copies, lattice QCD and the gluon propagator. *Nucl. Phys.*, B690 :177–198, 2004, hep-lat/0403026.

[33] A. Sternbeck, E. M. Ilgenfritz, M. Mueller-Preussker, and A. Schiller. Towards the infrared limit in SU(3) Landau gauge lattice gluodynamics. *Phys. Rev.*, D72 :014507, 2005, hep-lat/0506007.

[34] K. G. Chetyrkin and A. Retey. Three-loop three-linear vertices and four-loop mom beta functions in massless QCD. 2000, hep-ph/0007088.

[35] K. G. Chetyrkin. Four-loop renormalization of QCD : Full set of renormalization constants and anomalous dimensions. *Nucl. Phys.*, B710 :499–510, 2005, hep-ph/0405193.

[36] T. van Ritbergen, J. A. M. Vermaseren, and S. A. Larin. The four-loop beta function in Quantum chromodynamics. *Phys. Lett.*, B400 :379–384, 1997, hep-ph/9701390.

[37] P. Boucaud et al. Lattice calculation of $1/p^2$ corrections to α_S and of $\Lambda_{\rm QCD}$ in the $\widetilde{MOM}$ scheme. *JHEP*, 04 :006, 2000, hep-ph/0003020.

[38] P. Boucaud et al. Preliminary calculation of α_S from Green functions with dynamical quarks. *JHEP*, 01 :046, 2002, hep-ph/0107278.

[39] Kenneth G. Wilson. Nonlagrangian models of current algebra. *Phys. Rev.*, 179 :1499–1512, 1969.

[40] B. L. Ioffe. Condensates in Quantum chromodynamics. *Phys. Atom. Nucl.*, 66 :30–43, 2003, hep-ph/0207191.

[41] Martin Lavelle and Michael Oleszczuk. The Operator Product Expansion of the QCD propagators. *Mod. Phys. Lett.*, A7 :3617–3630, 1992.

[42] Jorg Ahlbach, Martin Lavelle, Martin Schaden, and Andreas Streibl. Propagators and four-dimensional condensates in pure QCD. *Phys. Lett.*, B275 :124–128, 1992.

[43] P. Boucaud et al. Consistent OPE description of gluon two point and three point green function ? *Phys. Lett.*, B493 :315–324, 2000, hep-ph/0008043.

[44] Ph. Boucaud et al. Testing Landau gauge ope on the lattice with a condensate. *Phys. Rev.*, D63 :114003, 2001, hep-ph/0101302.

[45] P. Boucaud et al. A transparent expression of the $\langle A^2 \rangle$-condensate's renormalization. *Phys. Rev.*, D67 :074027, 2003, hep-ph/0208008.

[46] Gunnar S. Bali and Klaus Schilling. Running coupling and the lambda parameter from SU(3) lattice simulations. *Phys. Rev.*, D47 :661–672, 1993, hep-lat/9208028.

[47] William Celmaster and Richard J. Gonsalves. The renormalization prescription dependence of the QCD coupling constant. *Phys. Rev.*, D20 :1420, 1979.

[48] D. Becirevic et al. Asymptotic scaling of the gluon propagator on the lattice. *Phys. Rev.*, D61 :114508, 2000, hep-ph/9910204.

[49] Ph. Boucaud et al. Non-perturbative power corrections to ghost and gluon propagators. *JHEP*, 01 :037, 2006, hep-lat/0507005.

[50] Daniel Zwanziger. Vanishing color magnetization in lattice Landau and Coulomb gauges. *Phys. Lett.*, B257 :168–172, 1991.

[51] D. Zwanziger. Vanishing of zero momentum lattice gluon propagator and color confinement. *Nucl. Phys.*, B364 :127–161, 1991.

[52] J. C. R. Bloch. Two-loop improved truncation of the ghost-gluon Dyson-Schwinger equations : Multiplicatively renormalizable propagators and non-perturbative running coupling. *Few Body Syst.*, 33 :111–152, 2003, hep-ph/0303125.

[53] Lorenz von Smekal, Andreas Hauck, and Reinhard Alkofer. A solution to coupled Dyson-Schwinger equations for gluons and ghosts in Landau gauge. *Ann. Phys.*, 267 :1, 1998, hep-ph/9707327.

[54] Daniel Zwanziger. Non-perturbative Landau gauge and infrared critical exponents in QCD. *Phys. Rev.*, D65 :094039, 2002, hep-th/0109224.

[55] A. C. Aguilar and A. A. Natale. A dynamical gluon mass solution in a coupled system of the Schwinger-Dyson equations. *JHEP*, 08 :057, 2004, hep-ph/0408254.

[56] Junya Kato. Infrared non-perturbative propagators of gluon and ghost via exact renormalization group. 2004, hep-th/0401068.

[57] Jan M. Pawlowski, Daniel F. Litim, Sergei Nedelko, and Lorenz von Smekal. Infrared behaviour and fixed points in Landau gauge QCD. *Phys. Rev. Lett.*, 93 :152002, 2004, hep-th/0312324.

[58] Christian S. Fischer and Holger Gies. Renormalization flow of Yang-Mills propagators. *JHEP*, 10 :048, 2004, hep-ph/0408089.

[59] James S. Ball and Ting-Wai Chiu. Analytic properties of the vertex function in gauge theories. 2. *Phys. Rev.*, D22 :2550, 1980.

[60] Ph. Boucaud et al. The infrared behaviour of the pure Yang-Mills Green functions. 2005, hep-ph/0507104.

[61] G. Peter Lepage and Paul B. Mackenzie. On the viability of lattice perturbation theory. *Phys. Rev.*, D48 :2250–2264, 1993, hep-lat/9209022.

[62] J.P. Leroy A. Le Yaouanc A.Y. Lokhov J. Micheli O. Pene J. Rodriguez-Quintero Ph. Boucaud, Th. Bruntjen. Is the QCD ghost dressing function finite at zero momentum ? *JHEP* 0606, 001 (2006), hep-ph/0604056.

[63] Frederic D. R. Bonnet, Patrick O. Bowman, Derek B. Leinweber, Anthony G. Williams, and James M. Zanotti. Infinite volume and continuum limits of the Landau-gauge gluon propagator. *Phys. Rev.*, D64 :034501, 2001, hep-lat/0101013.

[64] Orlando Oliveira and Paulo J. Silva. Finite volume effects in the gluon propagator. *PoS*, LAT2005 :287, 2005, hep-lat/0509037.

[65] Ph. Boucaud et al. Short comment about the lattice gluon propagator at vanishing momentum. 2006, hep-lat/0602006.

[66] L. Giusti, M. L. Paciello, S. Petrarca, C. Rebbi, and B. Taglienti. Results on the gluon propagator in lattice covariant gauges. *Nucl. Phys. Proc. Suppl.*, 94 :805–808, 2001, hep-lat/0010080.

[67] L. Giusti, M. L. Paciello, S. Petrarca, B. Taglienti, and N. Tantalo. Quark and gluon propagators in covariant gauges. *Nucl. Phys. Proc. Suppl.*, 106 :995–997, 2002, hep-lat/0110040.

Annexe A

Large momentum behavior of the ghost propagator in $SU(3)$ lattice gauge theory

Phys.Rev. **D72** (2005) 114503

hep-lat/0506031

PHYSICAL REVIEW D **72,** 114503 (2005)

Large momentum behavior of the ghost propagator in SU(3) lattice gauge theory

Ph. Boucaud,[1] J. P. Leroy,[1] A. Le Yaouanc,[1] A. Y. Lokhov,[2] J. Micheli,[1] O. Pène,[1] J. Rodríguez-Quintero,[3] and C. Roiesnel[2]

[1]*Laboratoire de Physique Théorique et Hautes Energies,* Université de Paris XI, Bâtiment 211, 91405 Orsay Cedex, France*

[2]*Centre de Physique Théorique† de l'Ecole Polytechnique, F91128 Palaiseau cedex, France*

[3]*Departamento Física Aplicada, Facultad Ciencias Experimentales, Universidad de Huelva, 21071 Huelva, Spain*

(Received 30 June 2005; published 7 December 2005)

We study the large momentum behavior of the ghost propagator in the quenched SU(3) lattice gauge theory with Wilson action. The study is performed on lattices with a physical volume fixed around 1.6 fm and different lattice spacings: 0.100, 0.070, and 0.055 fm. We implement an efficient algorithm for computing the Faddeev-Popov operator on the lattice. We are able to extrapolate the lattice data for the ghost propagator towards the continuum and to show that the extrapolated data on each lattice can be described up to four-loop perturbation theory from 2.0 to 6.0 GeV. The three-loop values are consistent with those extracted from previous perturbative studies of the gluon propagator. However the effective $\Lambda_{\overline{\mathrm{MS}}}$ scale which reproduces the data depends strongly upon the order of perturbation theory and on the renormalization scheme used in the parametrization. We show how the truncation of the perturbative series can account for the magnitude of the dependency in this energy range. The contribution of nonperturbative corrections will be discussed elsewhere.

DOI: 10.1103/PhysRevD.72.114503 PACS numbers: 12.38.Gc

I. INTRODUCTION

Whereas lattice gauge theory (LGT) has been initially formulated to study gauge-invariant quantities in the nonperturbative regime, it has long been recognized that LGT could be a useful tool for studying gauge-variant quantities such as Green functions, both in the nonperturbative and in the perturbative regimes. The SU(3) gluon propagator in momentum space was first considered [1] to gain some insight into the physics of confinement. Much work was then devoted to the study of its infrared behavior (for a review see [2]). Subsequent studies [3,4] were focused on the ultraviolet behavior and have been able to compare quantitatively the large momentum dependence of the lattice gluon propagator with perturbative predictions beyond one-loop order. The result for $\Lambda_{\overline{\mathrm{MS}}}$ was found to depend strongly upon the order of the perturbation theory and upon the renormalization scheme used in the parametrization. This strong dependence raised the question whether the energy windows in these calculations were large enough for perturbative QCD to be a valid approximation.

On the other hand, as shown by Gribov [5], the infrared behavior of the gluon propagator is closely related to the singularity structure of the ghost propagator inferred from the gauge-fixing ambiguities. As is well known, the Landau gauge, which is presently the only covariant gauge for which there exists effective local gauge-fixing algorithms on the lattice, suffers from these ambiguities. The infrared behaviors of the ghost and gluon propagators have been extensively studied within the Schwinger-Dyson approach [6]. The comprehensive theoretical study by Zwanziger [7] of the Faddeev-Popov operator on the lattice in Landau gauge spurred the first numerical study of the ghost propagator [8] in SU(2) and SU(3) gauge theories. Most subsequent activity has been dedicated to the SU(2) lattice gauge theory in the infrared region, mainly for technical reasons as we shall explain below. There are relatively few numerical studies of the SU(3) ghost propagator which are either more focused on the infrared region and the Gribov copy problem [9–11] or have only performed a qualitative perturbative description in the quenched approximation [12,13] and, quite recently, in the unquenched case also [14].

It is important to make the study of the SU(3) ghost propagator in the ultraviolet region more quantitative for comparison purposes with the gluon propagator. Lattice results at small distances may be described by perturbation theory and the independent extraction of the Λ_{QCD} scale from the two propagators would provide a self-consistency test of the analysis and of the lattice approach. It would be particularly significant to confirm or not, from the study of the lattice propagators alone, the need for the nonperturbative power corrections found in the study of the three-gluon coupling on the lattice [15].

The paper is organized as follows. We will begin by recalling in Sec. II the method used to relate lattice data for the ghost propagator to its perturbative renormalization description. Then we proceed by exhibiting in Sec. III the salient features of our lattice calculation, particularly of our implementation of the Faddeev-Popov operator on the lattice. The following section outlines the general method that we devised previously [3,4] to eliminate hypercubic artifacts from two-point functions and extrapolate the lattice data towards the continuum. This extrapolation is crucial to succeed in a quantitative description. The

*Unité Mixte de Recherche 8627 du Centre National de la Recherche Scientifique.

†Unité Mixte de Recherche 7644 du Centre National de la Recherche Scientifique.

results are discussed in Sec. V which contains several subsections where the analysis is performed in different renormalization schemes up to four-loop order. In particular the scheme dependence is thoroughly investigated and used to probe the effects of the truncation of the perturbative series. We conclude in Sec. VI with a comparison of the different methods to compute the $\Lambda_{\rm QCD}$ scale on the lattice.

II. RENORMALIZATION DESCRIPTION OF THE GHOST PROPAGATOR

Let $\Gamma_B^{(n)}$ be some gauge-fixed multiplicatively renormalizable one-particle irreducible n-point bare Green function defined in Euclidean momentum space and in some regularization scheme with cutoff Λ. Let s denote some polarization state and kinematical configuration of the external particles contributing to $\Gamma_B^{(n)}$. Let p denote a scale transformation on s and g_B denote the bare coupling. It is well known that, in any renormalization scheme R defined by some renormalization conditions on state s at the renormalization point $p = \mu$, we have

$$\Gamma_B^{(n)}(p, s, g_B, \Lambda) = Z_{\Gamma,R}(\mu, s, g_R, \Lambda)\Gamma_R^{(n)}(p, s, g_R, \mu) + \mathcal{O}(\Lambda^{-1}), \tag{1}$$

where $Z_{\Gamma,R}$ is the renormalization constant in scheme R, $\Gamma_R^{(n)}$ is the renormalized Green function, and $g_R(\mu)$ is the renormalized coupling. We omit the dependence on the gauge parameter for simplicity of notation since we will specialize to the Landau gauge.

The explicit dependence on μ drops out of the renormalized Green function $\Gamma_R^{(n)}$ at the renormalization point $p = \mu$. It follows that

$$\lim_{\Lambda\to\infty} \frac{d\ln(\Gamma_B^{(n)}(\mu, s, g_B, \Lambda))}{d\ln\mu^2} = \lim_{\Lambda\to\infty} \frac{d\ln(Z_{\Gamma,R}(\mu, s, g_R, \Lambda))}{d\ln\mu^2} + \frac{d\ln(\Gamma_R^n(s, g_R))}{d\ln\mu^2} \equiv \gamma_{\Gamma,R}(g_R) + \frac{dg_R}{d\ln\mu^2}\frac{\partial\ln\Gamma_R^n}{\partial g_R}. \tag{2}$$

The arbitrariness in the choice of the renormalization scheme R has prompted attempts at determining the "best" schemes for describing the q^2 evolution of bare Green functions on the lattice. Clearly it is always possible to find a change of coupling which will be a best approximation of a set of data at a given order of perturbation theory, within some prescribed criteria. Rather than pursuing this route, we will follow the standard wisdom which consists of choosing renormalization conditions appropriate to the continuum quantity under scrutiny.

Momentum substraction schemes have long been used to define renormalization conditions befitted to the description of the renormalization dependence of "physical" quantities. They are defined by setting some of the 2- and 3-point functions to their tree values. In the $\widetilde{\rm MOM}$ schemes, for these Green functions, Eq. (2) simplifies to

$$\lim_{\Lambda\to\infty} \frac{d\ln(\Gamma_B^{(n)}(\mu, s, g_B, \Lambda))}{d\ln\mu^2} = \frac{d\ln(Z_{\Gamma,\rm MOM})}{d\ln\mu^2} = \gamma_{\Gamma,\rm MOM}(g_{\rm MOM}). \tag{3}$$

Infinitely many MOM schemes can be defined which differ by the substraction point of the vertices. We have shown in [3] that the $\widetilde{\rm MOM}$g scheme, defined by substracting the transversal part of the three-gluon vertex at the asymmetric point where one external momentum vanishes, appears to provide a much better estimate of the asymptotic behavior of the gluon propagator in Landau gauge than the $\overline{\rm MS}$ scheme. For the study of the asymptotic behavior of the ghost propagator in Landau gauge, it seems therefore natural to use a $\widetilde{\rm MOM}$c scheme defined by substracting the ghost-gluon vertex at the asymmetric point where the momentum of the external gluon vanishes (Fig. 1). Comparison of the two $\widetilde{\rm MOM}$ schemes should provide us with an estimate of the systematic error entailed in the truncation of the perturbation theory.

The perturbative calculation of the gluon, ghost, and quark self-energies and all 3-vertices appearing in the QCD Lagrangian have been done at three-loop order in the $\overline{\rm MS}$ scheme and in a general covariant gauge at the asymmetric point with one vanishing momentum [16]. These three-loop results allow one to relate the coupling constants of any $\widetilde{\rm MOM}$-like scheme to the $\overline{\rm MS}$ scheme at three-loop order. For the $\widetilde{\rm MOM}$g and $\widetilde{\rm MOM}$c schemes defined above these relations read, respectively, in Landau gauge and in the quenched approximation ($n_f = 0$), with $h = g^2/16\pi^2$:

$$h_{\widetilde{\rm MOMg}} = h_{\overline{\rm MS}} + \frac{70}{3}h_{\overline{\rm MS}}^2 + \left(\frac{516\,217}{576} - \frac{153}{4}\zeta_3\right)h_{\overline{\rm MS}}^3 + \left(\frac{304\,676\,635}{6912} - \frac{299\,961}{64}\zeta_3 - \frac{81\,825}{64}\zeta_5\right)h_{\overline{\rm MS}}^4, \tag{4}$$

$$h_{\widetilde{\rm MOMc}} = h_{\overline{\rm MS}} + \frac{223}{12}h_{\overline{\rm MS}}^2 + \left(\frac{918\,819}{1296} - \frac{351}{8}\zeta_3\right)h_{\overline{\rm MS}}^3 + \left(\frac{29\,551\,181}{864} - \frac{137\,199}{32}\zeta_3 - \frac{74\,295}{64}\zeta_5\right)h_{\overline{\rm MS}}^4, \tag{5}$$

where $\zeta_3 = 1.202\,056\,9$ and $\zeta_5 = 1.036\,927\,7$ are the Riemann zeta coefficients. The very large coefficients of these perturbative expansions explain the difficulties met by the $\overline{\rm MS}$ scheme to approach asymptotic scaling below 10 GeV.

The recent calculation [17] of the anomalous dimensions in the $\overline{\text{MS}}$ scheme of the gluon and ghost fields at four-loop order, together with the knowledge of the β function [18,19], makes it possible to perform the analysis of the lattice data for the gluon and ghost propagators up to four-loop order also in the $\widetilde{\text{MOM}}$g and $\widetilde{\text{MOM}}$c schemes. The numerical coefficients of the β function defined as

$$\beta(h) = \frac{dh}{d\ln\mu^2} = -\sum_{i=0}^{n} \beta_i h^{i+2} + \mathcal{O}(h^{n+3}) \tag{6}$$

are

$$\begin{aligned} \beta_2^{\widetilde{\text{MOMg}}} &= 2412.16, & \beta_2^{\widetilde{\text{MOMc}}} &= 2952.73, \\ \beta_3^{\widetilde{\text{MOMg}}} &= 84\,353.8, & \beta_3^{\widetilde{\text{MOMc}}} &= 101\,484.0. \end{aligned} \tag{7}$$

For completeness we also give the expansion coefficients of the renormalization constants of the gluon and ghost fields in the MOM schemes with respect to the renormalized coupling of the $\overline{\text{MS}}$ scheme up to four-loop order:

$$\begin{aligned} \frac{d\ln(Z_{3,\text{MOM}})}{d\ln\mu^2} &= \frac{13}{2}h_{\overline{\text{MS}}} + \frac{3727}{24}h_{\overline{\text{MS}}}^2 + \left(\frac{2\,127\,823}{288}\right. \\ &\quad \left. - \frac{9747}{16}\zeta_3\right)h_{\overline{\text{MS}}}^3 + \left(\frac{3\,011\,547\,563}{6912}\right. \\ &\quad \left. - \frac{18\,987\,543}{256}\zeta_3 - \frac{1\,431\,945}{64}\zeta_5\right)h_{\overline{\text{MS}}}^4, \end{aligned} \tag{8}$$

$$\begin{aligned} \frac{d\ln(\tilde{Z}_{3,\text{MOM}})}{d\ln\mu^2} &= \frac{9}{4}h_{\overline{\text{MS}}} + \frac{813}{16}h_{\overline{\text{MS}}}^2 + \left(\frac{157\,303}{64}\right. \\ &\quad \left. - \frac{5697}{32}\zeta_3\right)h_{\overline{\text{MS}}}^3 + \left(\frac{219\,384\,137}{1536}\right. \\ &\quad \left. - \frac{9\,207\,729}{512}\zeta_3 - \frac{221\,535}{32}\zeta_5\right)h_{\overline{\text{MS}}}^4. \end{aligned} \tag{9}$$

III. LATTICE CALCULATION

A. Faddeev-Popov operator on the lattice

The ghost propagator is defined on the lattice as

$$G(x-y)\delta^{ab} \equiv \langle (M^{-1})_{xy}^{ab} \rangle, \tag{10}$$

where the action of the Faddeev-Popov operator M on an arbitrary element η of the Lie algebra $\mathcal{SU}(N)$ of the gauge group SU(N), in a Landau gauge-fixed configuration, is given by [7]

TABLE I. Pseudocode of our implementation of the Faddeev-Popov operator.

```
!η_in, η_out are the ghost fields.
!U is the gauge configuration.
type (SUN) U(*), dU, W, W_+, W_-
type (SUN) η_in(*), η_out(*)
for all x:
   dU = 0.
   W = η_in(x)
do μ = 1, 4
   W_+ = η_in(x + μ̂)
   W_- = η_in(x - μ̂)
   dU = dU + U_μ(x - μ̂) × W + W × U_μ(x)
        - U_μ(x) × W_+ - W_- × U_μ(x - μ̂)
enddo
η_out(x) = dU - dU† - (1/N) Tr(dU - dU†)
```

$$\begin{aligned} (M\eta)^a(x) &= \frac{1}{N}\sum_\mu \{G_\mu^{ab}(x)(\eta^b(x+\hat{\mu}) - \eta^b(x)) \\ &\quad - (x \leftrightarrow x-\hat{\mu}) + \frac{1}{2}f^{abc}(\eta^b(x+\hat{\mu})A_\mu^c(x) \\ &\quad - \eta^b(x-\hat{\mu})A_\mu^c(x-\hat{\mu}))\}, \end{aligned} \tag{11}$$

and where, with anti-Hermitian generators T^a,

$$G_\mu^{ab}(x) = \tfrac{1}{2}\,\text{Tr}(\{T^a, T^b\}(U_\mu(x) + U_\mu^\dagger(x))), \tag{12}$$

$$A_\mu^c(x) = -\text{Tr}(T^c(U_\mu(x) - U_\mu^\dagger(x))). \tag{13}$$

Most lattice implementations of the Faddeev-Popov operator have followed closely the componentwise Eqs. (11)–(13). But the derivation in [7] shows that the Faddev-Popov operator can also be written as a lattice divergence:

$$M(U) = -\frac{1}{N}\nabla\cdot\tilde{D}(U), \tag{14}$$

where the operator $\tilde{D}$ reads

$$\begin{aligned} \tilde{D}_\mu(U)\eta(x) &= \tfrac{1}{2}(U_\mu(x)\eta(x+\hat{\mu}) - \eta(x)U_\mu(x) \\ &\quad + \eta(x+\hat{\mu})U_\mu^\dagger(x) - U_\mu^\dagger(x)\eta(x)). \end{aligned} \tag{15}$$

Using conversion routines between the Lie algebra and the Lie group, Eqs. (14) and (15) allow for a very efficient lattice implementation, sketched in Table I, which is based on the fast routines coding the group multiplication law.

B. Inversion of the Faddeev-Popov operator

Constant fields are zero modes of the Faddeev-Popov operator. This operator can be inverted only in the vector subspace $K^\perp$ orthogonal to its kernel. If the Faddeev-Popov operator has no other zero modes than constant fields, then the nonzero Fourier modes form a basis of $K^\perp$:

$$\eta(x) = \sum_{p\neq 0} c_p e^{ip\cdot x}, \qquad \forall\ \eta \in K^\perp. \tag{16}$$

The standard procedure has been to invert the Faddev-Popov operator with one nonzero Fourier mode as a source

$$S^a_p(x) = \delta^{ab} e^{ip\cdot x} \tag{17}$$

and to take the scalar product of $M^{-1}S^a_p$ with the source:

$$(S^a_p \mid M^{-1}S^a_p) = \sum_{x,y} (M^{-1})^{aa}_{xy} e^{-ip\cdot(x-y)} \tag{18}$$

$$= V\hat{G}(p) \tag{19}$$

after averaging over the gauge field configurations. This method requires one matrix inversion for each value of the ghost propagator in momentum space. It is suitable only when one is interested in a few values of the ghost propagator.

However, the study of the ultraviolet behavior of the ghost propagator in the continuum requires its calculation at many lattice momenta to control the spacing artifacts, as we shall see in the next section. This can be done very economically by noting that

$$\delta(x, y) = \frac{1}{V} + \frac{1}{V}\sum_{p\neq 0} e^{-ip\cdot(x-y)} \tag{20}$$

and choosing as a source

$$S^a_0(x) = \delta^{ab}\left(\delta(x, 0) - \frac{1}{V}\right). \tag{21}$$

The Fourier transform of $M^{-1}S^a_0$, averaged over the gauge configurations, yields

$$\begin{aligned}\sum_x e^{-ip\cdot x}\langle M^{-1}S^a_0\rangle &= \sum_x e^{-ip\cdot x}\langle (M^{-1})^{aa}_{x0}\rangle \\ &\quad - \frac{1}{V}\sum_{x,y} e^{-ip\cdot x}\langle (M^{-1})^{aa}_{xy}\rangle \\ &= \sum_x e^{-ip\cdot x}G(x) - \frac{1}{V}\sum_{x,y} e^{-ip\cdot x}G(x-y) \\ &= \hat{G}(p) - \delta(p)\sum_x G(x)\end{aligned} \tag{22}$$

as a consequence of the translation invariance of the ghost propagator. Therefore, with this choice of source, only one matrix inversion followed by one Fourier transformation of the solution is required to get the full ghost propagator on the lattice.

There is of course a price to pay, as can be read off Eq. (22) which lacks the factor V present in Eq. (19). The statistical accuracy with the source S^a_p is better, especially at high momentum p. However the statistical accuracy with the source S^a_0 turns out to be sufficient for our purpose.

There is one final point we want to make and which has never been raised to the best of our knowledge. It is mandatory to check, whatever the choice of sources, that rounding errors during the inversion do not destroy the condition that the solution belongs to $K^\perp$:

$$\sum_x (M^{-1}S)(x) = 0. \tag{23}$$

Indeed, if the zero-mode component of the solution grows beyond some threshold during the inversion of the Faddeev-Popov operator on some gauge configuration, then that component starts to increase exponentially and a sizable bias is produced in other components as well. We have observed this phenomenon occasionally, about one gauge configuration every few hundreds, when using the implementation of the lattice Faddeev-Popov operator based on Eqs. (11)–(13). But the systematic bias which is induced on the averages over gauge field configurations can be uncomfortably close to those ascribed to the Gribov copies.

Another virtue of the algorithm described in Table I is its numerical stability which is improved by several orders of magnitude. We have never observed sizable deviations from Eq. (23) with this algorithm.

C. The simulation

We ran simulations of the SU(3) lattice gauge theory with the Wilson action in the quenched approximation on several hypercubic lattices, whose parameters are summarized in Table II. All lattices have roughly the same physical volume except the 24^4 lattice at $\beta = 6.0$ which has been included to check out finite-volume effects. The SU(3) gauge configurations were generated using a hybrid algorithm of the Cabibbo-Marinari heat bath and Creutz overrelaxation steps. Ten thousand lattice updates were discarded for thermalization and the configurations were analyzed every 100/200/500 sweeps on the $16^4/24^4/32^4$ lattices.

Landau gauge fixing was carried out by minimizing the functional

$$F_U[g] = \mathrm{Re}\sum_x\sum_\mu\left(1 - \frac{1}{N}g(x)U_\mu(x)g^\dagger(x+\hat{\mu})\right) \tag{24}$$

by use of a standard overrelaxation algorithm driving the gauge configuration to a local minimum of $F_U[g]$. We did not try to reach the fundamental modular region Λ, defined as the set of absolute minima of $F_U[g]$ on all gauge orbits. Indeed there have been numerous studies, in SU(2) [21,22] and in SU(3) [9,10], of the effect of Gribov copies on the ghost propagator. The consensus is that noticeable system-

TABLE II. Run parameters. The lattice spacings are taken from Table 3 in [20] with a physical unit normalized by $\sqrt{\sigma} =$ 445 MeV.

β	V	a^{-1} (GeV)	No. of configurations
6.0	16^4	1.96	1000
6.0	24^4	1.96	500
6.2	24^4	2.75	500
6.4	32^4	3.66	250

atic errors, beyond statistical errors, are only found for the smallest p^2, much smaller than the squared momenta that we used to study the asymptotic behavior of the ghost propagator.

Then the ghost propagator $G(p)$ is extracted from Eq. (22) for all $p \neq 0$. The required matrix inversion, with a conjugate-gradient algorithm without any preconditioning, and the Fourier transform consume on average less than half the computing time of the Landau gauge fixing.

IV. HYPERCUBIC ARTIFACTS

The ghost propagator $\hat{G}(p)$ is a scalar invariant on the lattice which means that it is invariant along the orbit $O(p)$ generated by the action of the isometry group $H(4)$ of hypercubic lattices on the discrete momentum $p \equiv \frac{2\pi}{La} \times (n_1, n_2, n_3, n_4)$ where the n_μ's are integers, L is the lattice size, and a the lattice spacing. The general structure of polynomials invariant under a finite group is known from group-invariant theory. Indeed it can be shown that any polynomial function of p which is invariant under the action of $H(4)$ is a polynomial function of the 4 invariants $p^{[n]} = a^n \sum_\mu p_\mu^n$, $n = 2, 4, 6, 8$ which index the set of orbits.

Our analysis program uses these 4 invariants to average the ghost propagator over the orbits of $H(4)$ to increase the statistical accuracy:

$$a^2 G_L(p^{[2]}, p^{[4]}, p^{[6]}, p^{[8]}) = \frac{1}{\|O(p)\|} \sum_{p \in O(p)} \hat{G}(p), \quad (25)$$

where $\|O(p)\|$ is the cardinal number of the orbit $O(p)$. By the same token, one should always take the following *real* source:

$$\overline{S}^a_p(x) = \delta^{ab} \sum_{p \in O(p)} \cos(p \cdot x) \quad (26)$$

rather than a single complex Fourier mode for studies of the ghost propagator in the infrared region. Indeed, after averaging over the gauge configurations and use of the translational invariance, one gets

$$\langle (\overline{S}^a_p \,|\, M^{-1} \overline{S}^a_p) \rangle = \sum_{p, p' \in O(p)} \sum_{x,y} \langle (M^{-1})^{aa}_{xy} \rangle e^{-ip' \cdot x + ip \cdot y} = V \|O(p)\| a^2 G_L(p^{[2]}, p^{[4]}, p^{[6]}, p^{[8]}). \quad (27)$$

By analogy with the free lattice propagator

$$G_0(p) = \frac{1}{\sum_\mu \hat{p}_\mu^2} = \frac{a^2}{p^{[2]}} \left(1 + \frac{1}{12} \frac{p^{[4]}}{p^{[2]}} + \cdots \right), \quad (28)$$

where $\hat{p}_\mu = \frac{2}{a} \sin\left(\frac{a p_\mu}{2} \right)$

it is natural to make the hypothesis that the lattice ghost propagator is a smooth function of the discrete invariants near the continuum limit, when $a p_\mu \ll 1$, $\forall\ \mu$,

$$G_L(p^{[2]}, p^{[4]}, p^{[6]}, p^{[8]}) \approx G_L(p^{[2]}, 0, 0, 0) + p^{[4]} \frac{\partial G_L}{\partial p^{[4]}} \times (p^{[2]}, 0, 0, 0) + \cdots \quad (29)$$

and $G_L(p^{[2]}, 0, 0, 0)$ is nothing but the propagator of the continuum in a finite volume, up to lattice artifacts which do not break $O(4)$ invariance. When several orbits exist with the same p^2, the simplest method to reduce the hypercubic artifacts is to extrapolate the lattice data towards $G_L(p^{[2]}, 0, 0, 0)$ by making a linear regression at fixed p^2 with respect to the invariant $p^{[4]}$ since the other invariants are of higher order in the lattice spacing. The range of validity of this linear approximation can be checked *a posteriori* from the smoothness of the extrapolated data with respect to p^2.

Choosing the variables $\hat{p}_\mu$ appropriate to the parametrization of a lattice propagator with periodic boundary conditions provides an independent check of the extrapolation. Indeed we can write as well

$$G_L(p^{[2]}, p^{[4]}, p^{[6]}, p^{[8]}) \equiv \hat{G}_L(\hat{p}^{[2]}, \hat{p}^{[4]}, \hat{p}^{[6]}, \hat{p}^{[8]}) \quad (30)$$

with the new invariants, again hierachically suppressed with respect to the lattice spacing,

$$\hat{p}^{\,[n]} = a^n \sum_\mu \hat{p}_\mu^n. \quad (31)$$

G_L and $\hat{G}_L$ are two different parametrizations of the same lattice data, but near the continuum limit one must also have

$$\hat{G}_L(\hat{p}^{[2]}, \hat{p}^{[4]}, \hat{p}^{[6]}, \hat{p}^{[8]}) \approx \hat{G}_L(\hat{p}^{[2]}, 0, 0, 0) + \hat{p}^{[4]} \frac{\partial \hat{G}_L}{\partial \hat{p}^{[4]}} \times (\hat{p}^{[2]}, 0, 0, 0) + \cdots, \quad (32)$$

where $G_L(p^{[2]}, 0, 0, 0)$ and $\hat{G}_L(\hat{p}^{[2]}, 0, 0, 0)$ have the same value, the propagator of the continuum [again up to lattice artifacts which do not break $O(4)$ invariance].

If one wants to include in the data analysis the points with a single orbit at fixed p^2, one must interpolate the slopes extracted from Eqs. (29) or (32). This interpolation can be done either numerically or by assuming a functional dependence of the slope with respect to p^2 based on dimensional arguments. The simplest ansatz is to assume that the slope has the same leading behavior as for a free lattice propagator:

$$\frac{\partial G_L}{\partial p^{[4]}}(p^{[2]}, 0, 0, 0) = \frac{1}{(p^{[2]})^2}(c_1 + c_2 p^{[2]}). \quad (33)$$

The inclusion of $O(4)$-invariant lattice spacing corrections is required to get fits with a reasonable χ^2. The quality of such two-parameter fits to the slopes, and the extension of the fitting window in p^2, supplies still another independent check of the validity of the extrapolations.

TABLE III. Cuts on the lattice data for the gluon propagator. $[ap_{\min}, ap_{\max}]$ is the momentum window of a fit in lattice units and N_{points} is the number of data points in that window.

β	V	N_{points}	$ap_{\min}$	$ap_{\max}$	χ^2
6.0	16^4	>10	≤ 1.30	≤ 1.82	≤ 1.4
6.2	24^4	>12	≤ 1.30	≤ 1.82	≤ 1.1
6.4	32^4	>20	≤ 1.40	≤ 1.82	≤ 1.3

TABLE IV. Cuts on the lattice data for the ghost propagator. The columns have the same meaning as in Table III.

β	V	N_{points}	$ap_{\min}$	$ap_{\max}$	χ^2
6.0	16^4	>10	≤ 1.30	≤ 1.57	≤ 1.0
6.2	24^4	>20	≤ 1.30	≤ 1.57	≤ 1.0
6.4	32^4	>20	≤ 1.00	≤ 1.57	≤ 1.0

We have used Eqs. (29) and (33) to extrapolate our lattice data towards the continuum and determined the range of validity in p^2 of the extrapolations from the consistency of the different checks within our statistical errors. The errors on the extrapolated points have been computed with the jackknife method. Tables III and IV summarize the cuts that have been applied to the data for the estimation of the systematic errors in the analysis of the next section. We have repeated the analysis of the gluon propagator [4] to study the sensitivity of the results with respect to the window in p^2 which has been enlarged considerably in our new data. The cuts for the lattice ghost propagator are stronger than for the gluon lattice propagator because the statistical errors of the former are 2 to 3 times larger which make the continuum extrapolations less controllable.

The number of distinct orbits at each p^2 increases with the lattice size and, eventually, a linear extrapolation limited to the single invariant $p^{[4]}$ breaks down. However it is of course possible to include higher-order invariants in a systematic way and to extend the range of validity of the extrapolations (e.g. as in [23]). Various empirical recipes have been put forward for the treatment of hypercubic artifacts. A detailed comparison of our method, which has been largely ignored in the literature, with the popular ''democratic'' method [24] has been done for the gluon propagator [3]. The outcome is very much the same for the ghost propagator which has a similar behavior in the ultraviolet regime.

V. DATA ANALYSIS

The evolution equation of the renormalization constants of the gluon or ghost fields in a MOM scheme, with respect to the coupling constant h in an arbitrary scheme R (the index R is omitted but understood everywhere), can be written generically up to four-loop order:

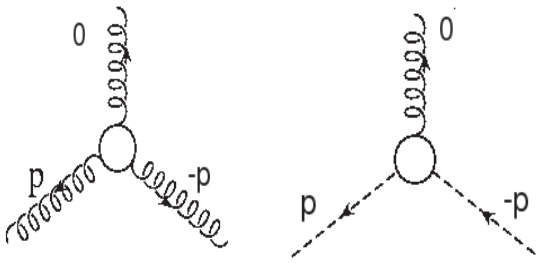

FIG. 1. $\widetilde{\text{MOM}}$g scheme (left) and $\widetilde{\text{MOM}}$c scheme (right).

$$\frac{d\ln(Z_{\Gamma,\text{MOM}})}{d\ln\mu^2} = \overline{\gamma}_0 h + \overline{\gamma}_1 h^2 + \overline{\gamma}_2 h^3 + \overline{\gamma}_3 h^4 \qquad (34)$$

and the perturbative integration of Eq. (34) yields, to the same order,

$$\begin{aligned}\ln\left(\frac{Z_{\Gamma,\text{MOM}}}{Z_0}\right) = \log(h)\frac{\overline{\gamma}_0}{\beta_0} + h\frac{(\beta_0\overline{\gamma}_1 - \beta_1\overline{\gamma}_0)}{\beta_0^2} \\ + h^2\frac{(\beta_0^2\overline{\gamma}_2 - \beta_0\beta_1\overline{\gamma}_1 - (\beta_0\beta_2 - \beta_1^2)\overline{\gamma}_0)}{2\beta_0^3} \\ + h^3(\beta_0^3\overline{\gamma}_3 - \beta_0^2\beta_1\overline{\gamma}_2 + (\beta_0\beta_1^2 - \beta_0^2\beta_2)\overline{\gamma}_1 \\ + (-\beta_0^2\beta_3 + 2\beta_0\beta_1\beta_2 - \beta_1^3)\overline{\gamma}_0)\frac{1}{3\beta_0^4} \qquad (35)\end{aligned}$$

with the standard four-loop formula for the running coupling

$$\begin{aligned}h(t) = \frac{1}{\beta_0 t}\left(1 - \frac{\beta_1}{\beta_0^2}\frac{\log(t)}{t} + \frac{\beta_1^2}{\beta_0^4}\frac{1}{t^2}\left(\left(\log(t) - \frac{1}{2}\right)^2\right.\right. \\ \left.\left. + \frac{\beta_2\beta_0}{\beta_1^2} - \frac{5}{4}\right)\right) + \frac{1}{(\beta_0 t)^4}\left(\frac{\beta_3}{2\beta_0} + \frac{1}{2}\left(\frac{\beta_1}{\beta_0}\right)^3\right. \\ \times\left(-2\log^3(t) + 5\log^2(t)\right. \\ \left.\left. + \left(4 - 6\frac{\beta_2\beta_0}{\beta_1^2}\right)\log(t) - 1\right)\right) \qquad (36)\end{aligned}$$

and $t = \log(\mu^2/\Lambda^2)$.

We now consider in turn the three renormalization schemes $\overline{\text{MS}}$, $\widetilde{\text{MOM}}$g, and $\widetilde{\text{MOM}}$c and fit the two parameters of Eqs. (35) and (36) to our extrapolated lattice data. Figure 2 illustrates the typical quality of such fits.

A. $\overline{\text{MS}}$ scheme

The analysis in the $\overline{\text{MS}}$ scheme is summarized in Table V. The statistical error is at the level of 1% for the gluon propagator and 2%–3% for the ghost propagator, whereas the systematic error due to the extrapolations is around 3%–5% and 5%–10%, respectively. The values of $\Lambda_{\overline{\text{MS}}}$ extracted from the gluon and the ghost propagators are consistent within these errors and within each order of perturbation theory.

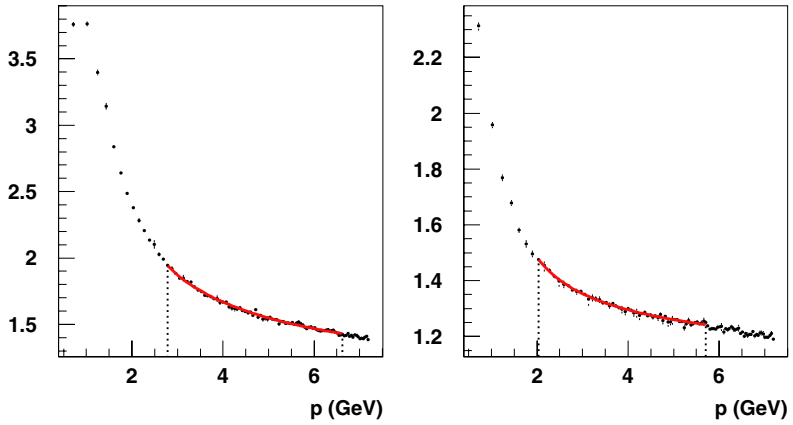

FIG. 2 (color online). Extrapolated lattice data at $\beta = 6.4$ for Z_3 (left panel) and $\tilde{Z}_3$ (right panel). The solid line is the fit at four-loop order in the $\overline{\text{MS}}$ scheme. The vertical dotted lines delimit the window of each fit.

TABLE V. Fits of $\Lambda_{\overline{\text{MS}}}$ from the gluon and ghost lattice propagators. The error in parentheses is the statistical error corresponding to a window $[ap_{\text{min}}, ap_{\text{max}}]$ with the ap_{min} quoted in the Table and the upper bound for ap_{max} quoted in Tables III and IV, respectively.

β	L	ap_{min}	$a\Lambda^{(2)}_{\overline{\text{MS}},\text{gluon}}$	χ^2	$a\Lambda^{(3)}_{\overline{\text{MS}},\text{gluon}}$	χ^2	$a\Lambda^{(4)}_{\overline{\text{MS}},\text{gluon}}$	χ^2
6.0	16	1.111	$0.336(3)^{+8}_{-4}$	1.3	$0.265(3)^{+6}_{-2}$	1.0	$0.225(2)^{+4}_{-2}$	1.1
	24	1.111	$0.332(3)^{+8}_{-12}$	0.6	$0.262(3)^{+6}_{-8}$	0.5	$0.222(2)^{+5}_{-8}$	0.6
6.2	24	0.907	$0.240(2)^{+6}_{-9}$	0.8	$0.185(2)^{+6}_{-10}$	0.8	$0.158(2)^{+4}_{-7}$	0.8
6.4	32	0.760	$0.171(2)^{+10}_{-11}$	1.4	$0.130(2)^{+12}_{-11}$	1.4	$0.112(1)^{+9}_{-8}$	1.4
β	L	ap_{min}	$a\Lambda^{(2)}_{\overline{\text{MS}},\text{ghost}}$	χ^2	$a\Lambda^{(3)}_{\overline{\text{MS}},\text{ghost}}$	χ^2	$a\Lambda^{(4)}_{\overline{\text{MS}},\text{ghost}}$	χ^2
6.0	16	1.039	$0.354(7)^{+23}_{-13}$	0.5	$0.281(6)^{+17}_{-8}$	0.5	$0.235(5)^{+15}_{-7}$	0.5
	24	0.785	$0.325(6)^{+13}_{-20}$	0.2	$0.259(5)^{+10}_{-18}$	0.2	$0.217(4)^{+8}_{-13}$	0.2
6.2	24	0.693	$0.254(4)^{+20}_{-20}$	0.4	$0.200(3)^{+10}_{-23}$	0.4	$0.169(3)^{+12}_{-13}$	0.4
6.4	32	0.555	$0.193(2)^{+22}_{-14}$	0.8	$0.150(2)^{+15}_{-14}$	0.8	$0.128(2)^{+13}_{-11}$	0.8

However, the three-loop and four-loop values, which are displayed in Table VI with the physical units of Table II, clearly confirm our previous result [3] that we are still far from asymptoticity in that scheme.

B. $\widetilde{\text{MOM}}$g scheme

Table VII, which summarizes the analysis in the $\widetilde{\text{MOM}}$g scheme, shows that, at the lower β's, we were not able to describe both lattice propagators at four-loop order with reasonable cuts and χ^2. This could be interpreted as a hint that perturbation theory has some problems of convergence beyond three-loop order below 3–4 GeV.

TABLE VI. Three-loop and four-loop physical values of $\Lambda_{\overline{\text{MS}}}$ in MeV extracted from Table V.

β	$\Lambda^{(3)}_{\overline{\text{MS}},\text{gluon}}$	$\Lambda^{(3)}_{\overline{\text{MS}},\text{ghost}}$	$\Lambda^{(4)}_{\overline{\text{MS}},\text{gluon}}$	$\Lambda^{(4)}_{\overline{\text{MS}},\text{ghost}}$
6.0	$519(6)^{+12}_{-4}$	$551(12)^{+33}_{-16}$	$441(4)^{+8}_{-4}$	$461(10)^{+29}_{-14}$
6.2	$509(6)^{+17}_{-27}$	$550(8)^{+27}_{-63}$	$435(6)^{+11}_{-19}$	$465(8)^{+33}_{-36}$
6.4	$476(7)^{+44}_{-40}$	$549(7)^{+55}_{-51}$	$410(4)^{+33}_{-29}$	$468(7)^{+48}_{-40}$

If we select the three-loop result as the best perturbative estimate of $\Lambda_{\widetilde{\text{MOMg}}}$ and convert it to the $\overline{\text{MS}}$ scheme with the asymptotic one-loop formula, $\Lambda_{\overline{\text{MS}}} = 0.346\Lambda_{\widetilde{\text{MOMg}}}$, then we get the physical values quoted in Table VIII which agree completely with previous values [4].

C. $\widetilde{\text{MOM}}$c scheme

The results of the analysis in the $\widetilde{\text{MOM}}$c scheme are displayed in Table IX. We still find that the three-loop and four-loop values of $\Lambda^{(3)}_{\widetilde{\text{MOMc}}}$ are very much the same for both the gluon propagator and for the ghost propagator. Thus the perturbative series seems again to become asymptotic at three-loop order in that scheme.

Selecting the three-loop result as the best perturbative estimate of $\Lambda_{\widetilde{\text{MOMc}}}$ and converting it to the $\overline{\text{MS}}$ scheme

TABLE VII. Fits of $\Lambda \underset{\text{MOMg}}{\sim}$ from the gluon and ghost lattice propagators. The notations are the same as in Table V.

β	L	$ap_{\min}$	$a\Lambda^{(2)}_{\text{MOMg,gluon}}$	χ^2	$a\Lambda^{(3)}_{\text{MOMg,gluon}}$	χ^2	$a\Lambda^{(4)}_{\text{MOMg,gluon}}$	χ^2
6.0	16	1.039	$0.551(3)^{+8}_{-8}$	1.0	$0.477(3)^{+5}_{-8}$	1.2	...	...
	24	1.014	$0.536(4)^{+14}_{-19}$	0.9	$0.464(3)^{+10}_{-11}$	0.9	...	...
6.2	24	0.693	$0.396(2)^{+19}_{-12}$	1.0	$0.336(2)^{+8}_{-15}$	0.9	...	...
6.4	32	0.555	$0.292(1)^{+15}_{-14}$	1.3	$0.246(1)^{+7}_{-20}$	1.4	$0.253(3)^{+5}_{-3}$	1.6
β	L	$ap_{\min}$	$a\Lambda^{(2)}_{\text{MOMg,ghost}}$	χ^2	$a\Lambda^{(3)}_{\text{MOMg,ghost}}$	χ^2	$a\Lambda^{(4)}_{\text{MOMg,ghost}}$	χ^2
6.0	16	1.039	$0.660(40)^{+24}_{-29}$	0.4	$0.475(12)^{+29}_{-24}$	0.5	...	...
	24	1.014	$0.559(22)^{+25}_{-20}$	0.2	$0.438(12)^{+14}_{-25}$	0.2	$0.408(17)^{+20}_{-18}$	0.9
6.2	24	0.693	$0.455(11)^{+9}_{-17}$	0.3	$0.342(5)^{+27}_{-34}$	0.6	$0.348(8)^{+23}_{-17}$	1.0
6.4	32	0.555	$0.333(4)^{+36}_{-26}$	1.2	$0.261(3)^{+33}_{-28}$	0.9	$0.279(7)^{+14}_{-30}$	0.8

TABLE VIII. Three-loop physical values of $\Lambda_{\overline{\text{MS}}}$ in MeV extracted from Table VII.

β	$\Lambda^{(3)}_{\overline{\text{MS}},\text{gluon}}$	$\Lambda^{(3)}_{\overline{\text{MS}},\text{ghost}}$
6.0	$324(2)^{+2}_{-5}$	$322(8)^{+20}_{-16}$
6.2	$320(2)^{+8}_{-14}$	$326(5)^{+26}_{-33}$
6.4	$312(1)^{+9}_{-25}$	$331(4)^{+42}_{-35}$

with the asymptotic formula, $\Lambda_{\overline{\text{MS}}} = 0.429\Lambda \underset{\text{MOMc}}{\sim}$, we get the physical values quoted in Table X.

D. Scheme dependence

The puzzling feature of Tables VI, VIII, and X is the rather large dependence of the Λ_{QCD} scale upon the loop order and the renormalization scheme whereas, within any scheme, the values from the ghost and gluon propagators are rather consistent at each loop order and pretty independent of the lattice spacing.

Let us consider again the evolution equation of the renormalization constants of the gluon or ghost fields in a MOM scheme, with respect to the coupling h_R in an arbitrary scheme R. We have

$$\frac{d\ln(Z_{\Gamma,\text{MOM}})}{d\ln\mu^2} = \overline{\gamma}_R(h_R) = -\frac{1}{2}\frac{d\ln(Z_{\Gamma,\text{MOM}})}{d\ln\Lambda_R}, \tag{37}$$

where Λ_R is the scale in scheme R. If we truncate the perturbative expansion at order n

$$\ln\left(\frac{Z_{\Gamma,\text{MOM}}}{Z_0}\right) = c_{R,0}\ln(h_R) + \sum_{k=1}^{n-1} c_{R,k}h_R^k \tag{38}$$

the change in the effective scale $\Lambda_R^{(n)}$, or equivalently, the change in the coupling h_R, induced by adding the contribution at order $n+1$ is typically

$$\frac{\Delta\Lambda_R^{(n)}}{\Lambda_R^{(n)}} \approx -\frac{c_{R,n}h_R^n}{2\gamma_R(h_R)}. \tag{39}$$

Now the dependence of the effective scale Λ_R upon the coupling h_R is given up to order 4

TABLE IX. Fits of $\Lambda \underset{\text{MOMc}}{\sim}$ from the gluon and ghost lattice propagators. The notations are the same as in Table V.

β	L	$ap_{\min}$	$a\Lambda^{(2)}_{\text{MOMc,gluon}}$	χ^2	$a\Lambda^{(3)}_{\text{MOMc,gluon}}$	χ^2	$a\Lambda^{(4)}_{\text{MOMc,gluon}}$	χ^2
6.0	16	1.178	0.482(6)	1.3	$0.408(3)^{+4}_{-4}$	1.0	...	...
	24	1.111	$0.468(5)^{+6}_{-5}$	0.5	$0.394(3)^{+11}_{-6}$	0.8	$0.411(7)^{+3}_{-2}$	1.1
6.2	24	0.907	$0.345(3)^{+17}_{-10}$	0.9	$0.288(2)^{+5}_{-6}$	0.9	$0.292(3)^{+8}_{-5}$	0.8
6.4	32	0.589	$0.255(1)^{+12}_{-15}$	1.5	$0.205(1)^{+11}_{-7}$	1.6	$0.212(1)^{+9}_{-17}$	1.6
β	L	$ap_{\min}$	$a\Lambda^{(2)}_{\text{MOMc,ghost}}$	χ^2	$a\Lambda^{(3)}_{\text{MOMc,ghost}}$	χ^2	$a\Lambda^{(4)}_{\text{MOMc,ghost}}$	χ^2
6.0	16	0.962	$0.489(6)^{+10}_{-6}$	0.8	$0.437(11)^{+6}_{-2}$	0.4	...	...
	24	1.047	$0.459(6)^{+15}_{-15}$	0.5	$0.408(8)^{+6}_{-5}$	0.5	$0.398(14)^{+13}_{-20}$	0.3
6.2	24	0.740	$0.367(7)^{+21}_{-33}$	0.4	$0.308(7)^{+9}_{-16}$	0.2	$0.303(9)^{+7}_{-14}$	0.2
6.4	32	0.589	$0.280(5)^{+28}_{-23}$	0.6	$0.225(5)^{+18}_{-13}$	0.6	$0.224(5)^{+15}_{-16}$	0.6

TABLE X. Three-loop physical values of $\Lambda_{\overline{\rm MS}}$ in MeV extracted from Table IX.

β	$\Lambda^{(3)}_{\overline{\rm MS},\rm gluon}$	$\Lambda^{(3)}_{\overline{\rm MS},\rm ghost}$
6.0	$345(3)^{+4}_{-4}$	$369(9)^{+3}_{-2}$
6.2	$341(2)^{+6}_{-7}$	$364(8)^{+11}_{-19}$
6.4	$323(2)^{+17}_{-11}$	$354(8)^{+28}_{-20}$

$$2\ln\Lambda_R^{(4)} = \ln\mu^2 - \frac{1}{\beta_0 h_R} - \frac{\beta_1}{\beta_0^2}\ln(\beta_0 h_R) - \frac{\beta_0\beta_2 - \beta_1^2}{\beta_0^3}h_R - \frac{\beta_0^2\beta_3 - 2\beta_0\beta_1\beta_2 + \beta_1^3}{2\beta_0^4}h_R^2, \quad (40)$$

and, denoting the coefficient of order h_R^{n-2} in that equation by $-\rho_{R,n-1}$, the effective scales which describe a same coupling at order n and $n+1$ are related by

$$\ln\frac{\Lambda_R^{(n+1)}}{\Lambda_R^{(n)}} \equiv -\frac{1}{2}\rho_{R,n-1}h_R^{n-1}. \quad (41)$$

Combining Eqs. (39) and (41) gives the relation between the effective scales which describe the renormalization constants of the gluon or ghost fields in a MOM scheme at order n and $n+1$

$$\frac{\Lambda_R^{(n+1)}}{\Lambda_R^{(n)}} = \exp-\frac{1}{2}\left(\rho_{R,n-1} + \frac{c_{R,n}h_R}{\gamma_R(h_R)}\right)h_R^{n-1}. \quad (42)$$

Figure 3 displays the behavior of this ratio for the gluon and ghost propagators in the three schemes as a function of the momentum p for $n=2$ and $n=3$. The couplings are taken from the fits at $\beta = 6.4$. There is a pretty good qualitative agreement with Tables VI, VIII, and X, which confirms the overall consistency with perturbation theory of the lattice data for the gluon and ghost propagators *within* any renormalization scheme.

The scheme dependence of the $\Lambda_{\rm QCD}$ scale can also be analyzed with Eq. (40):

$$\frac{\Lambda_{R_2}^{(n)}}{\Lambda_{R_1}^{(n)}} = \exp\left\{\frac{1}{2\beta_0}\left(\frac{1}{h_{R_1}} - \frac{1}{h_{R_2}}\right) + \frac{\beta_1}{2\beta_0^2}\ln\frac{h_{R_1}}{h_{R_2}} + \cdots\right\}. \quad (43)$$

Figure 4 shows the behavior of the ratios $\Lambda^{(n)}_{\overline{\rm MS}}/\Lambda^{(n)}_{\widetilde{\rm MOMg}}$ and

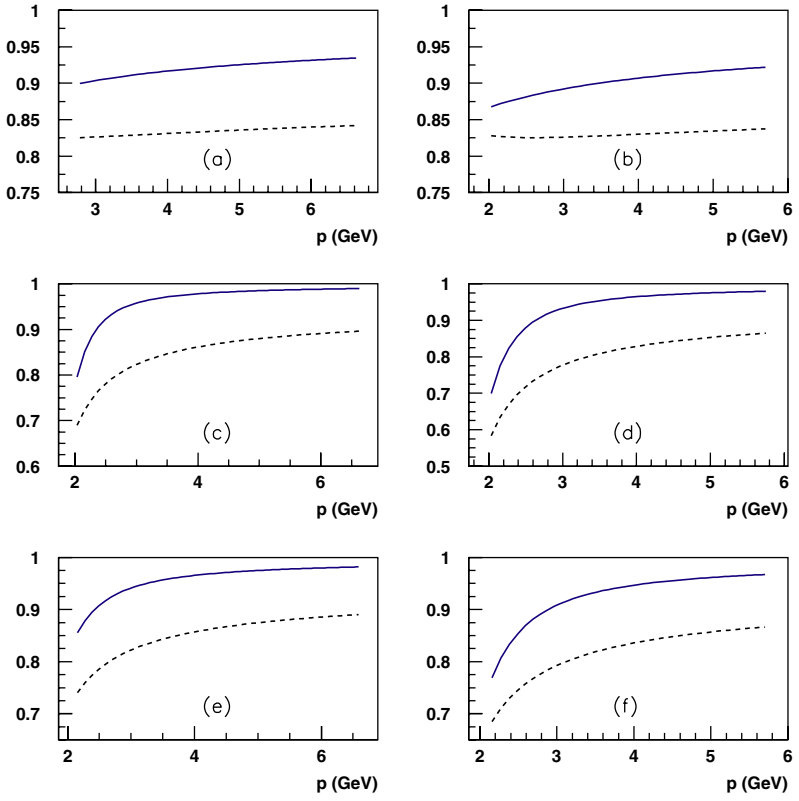

FIG. 3 (color online). $\Lambda_R^{(n+1)}/\Lambda_R^{(n)}$ for $n=2$ (dashed lines) and $n=3$ (solid lines), for the gluon propagator in the $\overline{\rm MS}$ scheme (a), $\widetilde{\rm MOMg}$ scheme (c) and $\widetilde{\rm MOMc}$ scheme (e), and for the ghost propagator in the $\overline{\rm MS}$ scheme (b), $\widetilde{\rm MOMg}$ scheme (d) and $\widetilde{\rm MOMc}$ scheme (f).

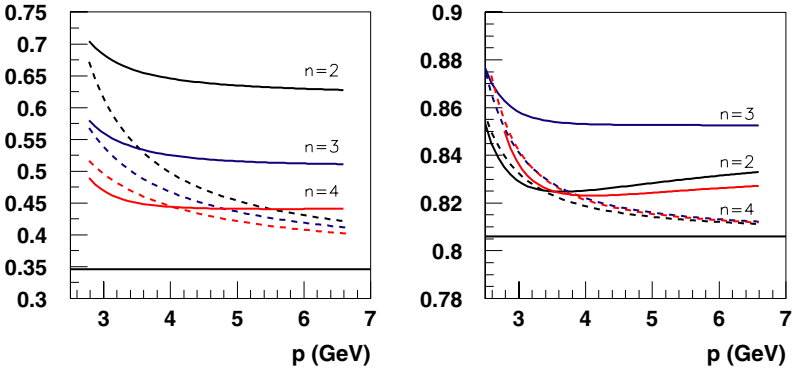

FIG. 4 (color online). $\Lambda^{(n)}_{\overline{\rm MS}}/\Lambda^{(n)}_{\widetilde{\rm MOMg}}$ (left panel) and $\Lambda^{(n)}_{\widetilde{\rm MOMc}}/\Lambda^{(n)}_{\widetilde{\rm MOMg}}$ (right panel) for $n = 2$, $n = 3$, and $n = 4$. The solid lines are the plots of Eq. (43) with the fitted couplings whereas the dashed lines are the plots with Eq. (44). Horizontal lines are the asymptotic values.

$\Lambda^{(n)}_{\widetilde{\rm MOMc}}/\Lambda^{(n)}_{\widetilde{\rm MOMg}}$, as a function of the momentum p at each order of perturbation theory. The couplings are taken from the fits of the gluon propagator at $\beta = 6.4$.

Clearly, the limiting values of these ratios are not the asymptotic values. If we replace in Eq. (43) the coupling h_{R_2} by its perturbative expansion with respect to h_{R_1}

$$h_{R_2} = h_{R_1} + \sum_{k=1}^{n-1} r_k h_{R_1}^{k+1} \tag{44}$$

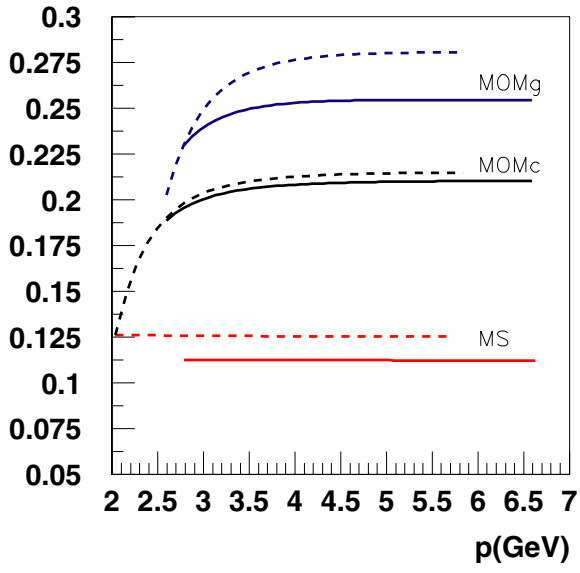

FIG. 5 (color online). $a\Lambda^{(4)}_{\overline{\rm MS}}$, $a\Lambda^{(4)}_{\widetilde{\rm MOMg}}$, and $a\Lambda^{(4)}_{\widetilde{\rm MOMc}}$ from the gluon propagator (solid lines) and from the ghost propagator (dashed lines) at $\beta = 6.4$, as a function of the momentum through Eq. (40).

then the ratios do of course tend towards the asymptotic values $\exp\{r_1/2\beta_0\}$. The disagreement with respect to the perturbative expansion is not a problem with the lattice data or with the numerical analysis. Indeed the fits do a very good job at extracting a well-behaved coupling as illustrated in Fig. 5 which displays the dimensionless scales $a\Lambda^{(4)}_{\overline{\rm MS}}$, $a\Lambda^{(4)}_{\widetilde{\rm MOMg}}$, and $a\Lambda^{(4)}_{\widetilde{\rm MOMc}}$ as a function of the momentum p, using Eq. (40) with the fitted couplings at $\beta = 6.4$ from the ghost and gluon propagators. Z_0, the other fitted parameter of Eq. (35), is nearly independent, within a few percent, of the renormalization scheme as it should in the absence of truncations. It follows that the difficulty to reproduce the asymptotic ratios between the scales of different renormalization schemes is mainly a consequence of the truncation of the perturbative series of the renormalization constants of the gluon and ghost propagators.

We can substantiate this claim, and estimate the rate of convergence, by the following exercise. We solve h_{R_2} in terms of h_{R_1} using Eq. (38) at four-loop order

$$\ln\left(\frac{Z_{\Gamma,\rm MOM}}{Z_0}\right) = c_{R_2,0}\ln(h_{R_2}) + \sum_{k=1}^{3} c_{R_2,k} h_{R_2}^k = c_{R_1,0}\ln(h_{R_1}) + \sum_{k=1}^{3} c_{R_1,k} h_{R_1}^k. \tag{45}$$

Then we plug the solution into Eq. (43). Figure 6 shows the behavior of the corresponding ratios, $\Lambda^{(4)}_{\overline{\rm MS}}/\Lambda^{(4)}_{\widetilde{\rm MOMg}}$ and $\Lambda^{(4)}_{\widetilde{\rm MOMc}}/\Lambda^{(4)}_{\widetilde{\rm MOMg}}$, as a function of the coupling $h_{\overline{\rm MS}}$ and $h_{\widetilde{\rm MOMc}}$, respectively. The effect of the truncation of the perturbative series is manifest for the $\overline{\rm MS}$ scheme and gives the right order of magnitude of what is actually measured in Tables V and VII.

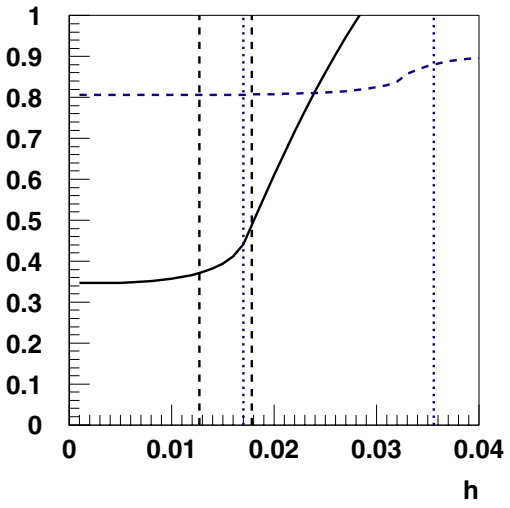

FIG. 6 (color online). $\Lambda^{(4)}_{\overline{\rm MS}}/\Lambda^{(4)}_{\widetilde{\rm MOMg}}$ (solid line) as a function of $h_{\overline{\rm MS}}$ and $\Lambda^{(4)}_{\widetilde{\rm MOMc}}/\Lambda^{(4)}_{\widetilde{\rm MOMg}}$ (dashed lines) as a function of $h_{\widetilde{\rm MOMc}}$. The vertical lines delimit the values spanned by $h_{\overline{\rm MS}}$ (dashed) and $h_{\widetilde{\rm MOMc}}$ (dotted) in the fits of the gluon propagator at $\beta = 6.4$.

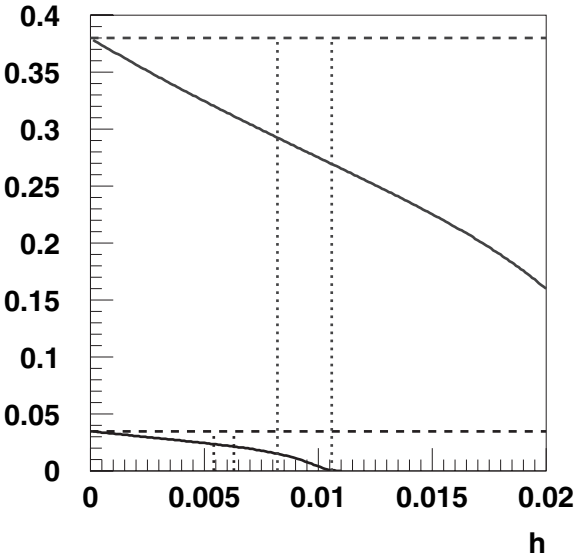

FIG. 7. $\Lambda^{(3)}_{\rm L}/\Lambda^{(3)}_{\overline{\rm MS}}$ (lower solid line) as a function of h_L and $\Lambda^{(3)}_{\Box}/\Lambda^{(3)}_{\overline{\rm MS}}$ (upper solid line) as a function of $h_{\Box}$. The vertical lines (dotted) delimit the values spanned by h_L and $h_{\Box}$ in the simulations of [29] ($5.7 \leq \beta \leq 6.9$). The dashed horizontal lines are the asymptotic values.

VI. CONCLUSION

We have shown that the lattice formulation of the ghost propagator has the expected perturbative behavior up to four-loop order from 2 to 6 GeV. We have been able to go beyond the qualitative level and to produce quantitative results for the scale $\Lambda_{\overline{\rm MS}}$ which are pretty consistent with the values extracted from the lattice gluon propagator. We have understood the strong dependence of the effective $\Lambda_{\overline{\rm MS}}$ scale upon the order of perturbation theory and upon the renormalization scheme used for the parametrization of the data. The perturbative series of the $\widetilde{\rm MOM}$ schemes seem to be asymptotic at three-loop order in the energy range we have probed whereas the $\overline{\rm MS}$ scheme converges very slowly. If we assume that all perturbative series remain well behaved beyond four-loop above 4 GeV, then we get $\Lambda_{\overline{\rm MS}} \approx 320$ MeV with a 10% systematic uncertainty. The statistical errors are at the 1% level. This value is also in pretty good agreement with the values of $\Lambda_{\overline{\rm MS}}$ extracted from the three-gluon vertex in a $\widetilde{\rm MOM}$ scheme at three-loop order [25], at the same β's and with the same lattice sizes. On the other hand it exceeds by 20% the value obtained from the same vertex at $\beta = 6.8$ on a 24^4 lattice. This discrepancy motivated the introduction of power corrections which are successful in describing the combined data of the three-gluon vertex [15]. We will show in a forthcoming paper how the power corrections can be unraveled from the lattice propagators alone.

The value quoted above exceeds also by about 30% the previous determinations of the QCD scale in the quenched approximation based on gauge-invariant definitions of the strong coupling constant [26,27] (take note, for comparison purposes, that our physical unit corresponds to the force parameter r_0 [28] set approximately to 0.53 fm). However there is also an uncertainty due to the use of the asymptotic one-loop relation between $\Lambda_{\overline{\rm MS}}$ and the Λ_L's. For illustration, let us consider the determination of $\Lambda_{\overline{\rm MS}}$ using lattice perturbation theory up to three-loop order with the Wilson action [29]. It is possible to estimate the rate of convergence of the ratio $\Lambda^{(3)}_L/\Lambda^{(3)}_{\overline{\rm MS}}$ as a function of the bare lattice coupling $h_L = 6/(4\pi)^2\beta$ by inserting the perturbative expansion of $h_{\overline{\rm MS}}$ into Eq. (43). Figure 7 displays the evolution of this ratio and also of the ratio $\Lambda^{(3)}_{\Box}/\Lambda^{(3)}_{\overline{\rm MS}}$ for the so-called "boosted" lattice scheme which reexpresses the lattice perturbative series as a function of the coupling $h_{\Box} = h_L/\langle plaq\rangle$. The mere truncation of the perturbative series introduces an uncertainty on the absolute scale of the lattice schemes which could be as large as 30% in the range of β studied in these simulations.

No strategy can fix the scale $\Lambda_{\rm QCD}$ to an accuracy better than the uncertainty entailed by the truncation of the perturbative series in the conversion to the $\overline{\rm MS}$ scheme. We have shown that this error can be larger than the main well-known sources of systematic errors which come from setting the scale a^{-1} and from the continuum extrapolation. If we aim at reducing below 10% the error in the conversion of the $\widetilde{\rm MOM}$ schemes to the $\overline{\rm MS}$ scheme, then a

look at Fig. 6 shows that we need to apply a cut at 6 GeV. Such an analysis would require simulations at $\beta = 6.6$ and $\beta = 6.8$ on 48^4 and 64^4 lattices, respectively, to work at fixed volume and minimize finite-size effects. The existence of several lattice observables, gluon propagator, ghost propagator, three-gluon vertex, from which one can extract independent values of the scale $\Lambda_{\rm QCD}$, an advantage of the Green function approach, should then allow one to disentangle unambiguously the effects of the truncation of the perturbative series from the nonperturbative corrections, and to get a value of $\Lambda_{\overline{\rm MS}}$ at a true 10% accuracy.

[1] C. Bernard, C. Parrinello, and A. Soni, Phys. Rev. D **49**, 1585 (1994).
[2] J. E. Mandula, Phys. Rep. **315**, 273 (1999).
[3] D. Becirevic, P. Boucaud, J. P. Leroy, J. Micheli, O. Pène, J. Rodríguez-Quintero, and C. Roiesnel, Phys. Rev. D **60**, 094509 (1999).
[4] D. Becirevic, P. Boucaud, J. P. Leroy, J. Micheli, O. Pène, J. Rodríguez-Quintero, and C. Roiesnel, Phys. Rev. D **61**, 114508 (2000).
[5] V. N. Gribov, Nucl. Phys. **B139**, 1 (1978).
[6] R. Alkofer and L. von Smekal, Phys. Rep. **353**, 281 (2001).
[7] D. Zwanziger, Nucl. Phys. **B412**, 657 (1994).
[8] H. Suman and K. Schilling, Phys. Lett. B **373**, 314 (1996).
[9] A. Sternbeck, E.-M. Ilgenfritz, M. Mueller-Preussker, and A. Schiller, Nucl. Phys. B, Proc. Suppl. **140**, 653 (2005)
[10] A. Sternbeck, E.-M. Ilgenfritz, M. Mueller-Preussker, and A. Schiller, AIP Conf. Proc. **756**, 284 (2005).
[11] A. Sternbeck, E.-M. Ilgenfritz, M. Mueller-Preussker, and A. Schiller, Phys. Rev. D **72**, 014507 (2005).
[12] S. Furui and H. Nakajima, Phys. Rev. D **69**, 074505 (2004).
[13] S. Furui and H. Nakajima, Phys. Rev. D **70**, 094504 (2004).
[14] S. Furui and H. Nakajima, hep-lat/0503029.
[15] P. Boucaud *et al.*, J. High Energy Phys. 04 (2000) 006.
[16] K. G. Chetyrkin and A. Rétey, hep-ph/0007088.
[17] K. G. Chetyrkin, Nucl. Phys. **B710**, 499 (2005).
[18] T. van Ritbergen, J. A. M. Vermaseren, and S. A. Larin, Phys. Lett. B **400**, 379 (1997).
[19] M. Czakon, Nucl. Phys. **B710**, 485 (2005).
[20] G. S. Bali and K. Schilling, Phys. Rev. D **47**, 661 (1993).
[21] A. Cucchieri, Nucl. Phys. **B508**, 353 (1997).
[22] T. D. Bakeev, E. M Ilgenfritz, M. Muller-Preussker, and V. K. Mitrjushkin, Phys. Rev. D **69**, 074507 (2004).
[23] P. Boucaud *et al.*, Phys. Lett. B **575**, 256 (2003).
[24] D. B. Leinweber, C. Parrinello, J. I. Skullerud, and A. G. Williams, Phys. Rev. D **58**, 031501 (1998).
[25] P. Boucaud, J. P. Leroy, J. Micheli, O. Pène, and C. Roiesnel, J. High Energy Phys. 10 (1998) 017.
[26] S. Capitani, M. Lüscher, R. Sommer, and H. Wittig, Nucl. Phys. **B544**, 669 (1999).
[27] S. Booth *et al.*, Phys. Lett. B **519**, 229 (2001).
[28] S. Necco and R. Sommer, Nucl. Phys. **B622**, 328 (2002).
[29] M. Göckeler *et al.*, hep-ph/0502212.

Annexe B

Non-perturbative power corrections to ghost and gluon propagators

JHEP **0601**, 037 (2006)

hep-lat/0507005

Published by Institute of Physics Publishing for SISSA

Received: *July 7, 2005*
Revised: *October 10, 2005*
Accepted: *December 7, 2005*
Published: *January 10, 2006*

Non-perturbative power corrections to ghost and gluon propagators

Philippe Boucaud,[a] **Jean-Pierre Leroy,**[a] **Alain Le Yaouanc,**[a] **Alexey Lokhov,**[b] **Jacques Micheli,**[a] **Olivier Pène,**[a] **Jose Rodríguez-Quintero**[c] **and Claude Roiesnel**[b]

[a] *Laboratoire de Physique Théorique et Hautes Energies*[*]
Université de Paris XI
Bâtiment 211, 91405 Orsay Cedex, France
[b] *Centre de Physique Théorique*[†] *de l'Ecole Polytechnique*
F91128 Palaiseau cedex, France
[c] *Dpto. Física Aplicada, Fac. Ciencias Experimentales, Universidad de Huelva*
21071 Huelva, Spain
E-mail: Philippe.boucaud@th.u-psud.fr, Jean-Pierre.Leroy@th.u-psud.fr, Alain.Le-Yaouanc@th.u-psud.fr, lokhov@cpht.polytechnique.fr, micheli@th.u-psud.fr, pene@th.u-psud.fr, jose.rodriguez@dfaie.uhu.es, Claude.Roiesnel@cpht.polytechnique.fr

Abstract: We study the dominant non-perturbative power corrections to the ghost and gluon propagators in Landau gauge pure Yang-Mills theory using OPE and lattice simulations. The leading order Wilson coefficients are proven to be the same for both propagators. The ratio of the ghost and gluon propagators is thus free from this dominant power correction. Indeed, a purely perturbative fit of this ratio gives smaller value ($\simeq$ 270MeV) of $\Lambda_{\overline{\rm MS}}$ than the one obtained from the propagators separately($\simeq$ 320MeV). This argues in favour of significant non-perturbative $\sim 1/q^2$ power corrections in the ghost and gluon propagators. We check the self-consistency of the method.

Keywords: Non-perturbative Effects, Lattice QCD.

[*] Unité Mixte de Recherche 8627 du Centre National de la Recherche Scientifique
[†] Unité Mixte de Recherche 7644 du Centre National de la Recherche Scientifique.

http://jhep.sissa.it/archive/papers/jhep012006037/jhep012006037.pdf

JHEP01(2006)037

Contents

1. Introduction **1**

2. The analytical inputs **2**
2.1 Pure perturbation theory 2
2.2 OPE power corrections for ghost and gluon propagators 4

3. Data Analysis **6**
3.1 Lattice setup 6
3.2 Extracting Λ_{QCD} from lattice data 6
3.3 Estimating the value of the $\langle A^2 \rangle$ gluon condensate 8

4. Conclusions **9**

A. Fitting $\Lambda_{\overline{\rm MS}}$ from separate data samples **9**

1. Introduction

A non-zero value of different QCD condensates leads to non-perturbative power corrections to propagators. The one being intensively studied during last years is the A^2-condensate in Landau gauge [1 – 6] (extended to a gauge-invariant non-local operator, [7]), that is responsible for $\sim 1/q^2$ corrections to the gluonic propagator compared to perturbation theory. In this paper we investigate the rôle of such corrections in the ghost propagator, and present a method that allows to test numerically that power corrections of $\sim 1/q^2$ type really exist using only ghost and gluon lattice propagators, and ordinary perturbation theory.

The study of the asymptotic behaviour of the ghost propagator in Landau gauge in the $SU(3)$ quenched lattice gauge theory with Wilson action was the object of a previous work [8]. The lattice definition and the algorithm for the inversion of the Faddeev-Popov operator, as well as the procedure of eliminating specific lattice artifacts, are exposed there. A perturbative analysis, up to four-loop order ([9, 10]), has been accomplished over the whole available momentum window [2GeV $\leftrightarrow$ 6GeV]. However, a lesson we retained after a careful study of the gluon propagator performed in the past [11, 12, 2] is that non-perturbative low-order power corrections and high-order perturbative logarithms give comparable contributions over momentum windows of such a width. Both appear to be hardly distinguishable, and thus - because of the narrowness of the fit window - the power-correction contribution could lead to some enhancement of the $\Lambda_{\rm QCD}$ parameter. Conversely, higher perturbative orders could borrow something to the non-perturbative

JHEP01(2006)037

condensate fitted from the power correction term. So, the quality of the fits (the value of χ^2/d.o.f) of lattice data is not a sufficient criterion when interpreting the results. A solution to the problem is to use several lattice data samples in order to increase the number of points in the fit window. This presumably brings another bias: the rescaling of the lattice data from different simulations (with different values of the ultraviolet(UV) cut-off *i.e.* the lattice spacing a). Nevertheless, we have to assume anyhow that the dependence on UV cut-off approximatively factorises [1] in order to fit lattice data to any continuum formula. Such an assumption will be furthermore under control provided that, as it happens in practice, our lattice data from different simulations match each other after rescaling.

In the present paper we will follow the approach presented in refs. [2, 3] and do a fully consistent analysis of ghost and gluon propagators in the pure Yang-Mills theory based on the OPE description of the non-perturbative power corrections in Landau gauge. As far as our lattice correlation functions are computed in Landau gauge, the leading non-perturbative contribution is expected to be attached to the *v.e.v.* of the local A^2 operator. This condensate generates a $1/q^2$-correcting term, still sizeable for our considered momenta, and that, as will be seen, gives *identical power corrections to both gluon and ghost propagators*. This result allows to separate the dominant power-correction term from the perturbative contribution, and suggests a new strategy for analysing the asymptotic behaviour of ghost and gluon propagators, even in the case of a small fit window.

In the present letter we use this strategy to extract the $\Lambda_{\rm QCD}$-parameter from ghost and gluon propagators.

2. The analytical inputs

The present section is devoted to briefly overview the analytical (perturbative and non-perturbative) tools we have implemented to analyse our gluon and ghost lattice propagators.

2.1 Pure perturbation theory

In the so-called Momentum subtraction (MOM) schemes, the renormalisation conditions are defined by setting some of the two- and three-point functions to their tree-level values at the renormalisation point. Then, in Landau gauge,

$$\lim_{\Lambda\to\infty} \frac{d\ln(Z_{3,\rm MOM}(p^2=\mu^2,\Lambda)}{d\ln\mu^2} = \gamma_{3,\rm MOM}(g_{\rm MOM}) \tag{2.1}$$

where Λ is some regularisation parameter (a^{-1} if we specialise to lattice regularisation) and [2]

$$Z_{3,\rm MOM}(p^2=\mu^2,\Lambda) = \frac{1}{3\left(N_C^2-1\right)}\cdot p^2\cdot\delta_{ab}\left(\delta_{\mu\nu}-\frac{p_\mu p_\nu}{p^2}\right)\ \langle\widetilde{A^a_\mu}(-p)\widetilde{A^b_\nu}(p)\rangle\ . \tag{2.2}$$

[1] This is the case of any renormalisation scheme where one drops any regular term depending on the cut-off away from renormalisation constants [13].

[2] In Euclidean space.

A similar expression can be written for the ghost propagator renormalisation factor $\widetilde{Z_3}$. Both anomalous dimensions for ghost and gluon propagators have been recently computed [9] in the $\overline{\rm MS}$ scheme. At four-loop order we have

$$\begin{aligned}
\frac{d\ln(Z_{3,MOM})}{d\ln\mu^2} &= \frac{13}{2}\,h_{\overline{\rm MS}} + \frac{3727}{24}\,h^2_{\overline{\rm MS}} + \left(\frac{2127823}{288} - \frac{9747}{16}\zeta_3\right) h^3_{\overline{\rm MS}} + \\
&+ \left(\frac{3011547563}{6912} - \frac{18987543}{256}\zeta_3 - \frac{1431945}{64}\zeta_5\right) h^4_{\overline{\rm MS}} \\
\frac{d\ln(\widetilde{Z}_{3,MOM})}{d\ln\mu^2} &= \frac{9}{4}\,h_{\overline{\rm MS}} + \frac{813}{16}\,h^2_{\overline{\rm MS}} + \left(\frac{157303}{64} - \frac{5697}{32}\zeta_3\right) h^3_{\overline{\rm MS}} + \\
&+ \left(\frac{219384137}{1536} - \frac{9207729}{512}\zeta_3 - \frac{221535}{32}\zeta_5\right) h^4_{\overline{\rm MS}}
\end{aligned} \tag{2.3}$$

where $h = g^2/(4\pi)^2$. However, the definition of a MOM scheme still needs the definition of the MOM coupling constant. Once chosen a three-particle vertex, the polarisations and momenta of the particles at the subtraction point, there is a standard procedure to extract the vertex and to define the corresponding MOM coupling constant. This may be performed in several ways. In fact, infinitely many MOM schemes can be defined. In ref. [14], the three-loop perturbative substraction of all the three-vertices appearing in the QCD Lagrangian for kinematical configurations with one vanishing momentum have been performed. In particular, the three schemes defined by the subtraction of the transversal part of the three-gluon vertex ($\widetilde{\rm MOMg}$) [3] and that of the ghost-gluon vertex with vanishing gluon momentum ($\widetilde{\rm MOMc}$) and vanishing incoming ghost momentum ($\widetilde{\rm MOMc0}$) will be used in the following. In Landau gauge and in the pure Yang-Mills case ($n_f = 0$) one has

$$\begin{aligned}
h_{\widetilde{\rm MOM}_g} =& h_{\overline{\rm MS}} + \frac{70}{3}h^2_{\overline{\rm MS}} + \left(\frac{51627}{576} - \frac{153}{4}\zeta_3\right) h^3_{\overline{\rm MS}} + \\
&+ \left(\frac{304676635}{6912} - \frac{299961}{64}\zeta_3 - \frac{81825}{64}\zeta_5\right) h^4_{\overline{\rm MS}} \\
h_{\widetilde{\rm MOM}_c} =& h_{\overline{\rm MS}} + \frac{223}{12}h^2_{\overline{\rm MS}} + \left(\frac{918819}{1296} - \frac{351}{8}\zeta_3\right) h^3_{\overline{\rm MS}} + \\
&+ \left(\frac{29551181}{864} - \frac{137199}{32}\zeta_3 - \frac{74295}{64}\zeta_5\right) h^4_{\overline{\rm MS}} \\
h_{\widetilde{\rm MOM}_{c0}} =& h_{\overline{\rm MS}} + \frac{169}{12}h^2_{\overline{\rm MS}} + \left(\frac{76063}{144} - \frac{153}{4}\zeta_3\right) h^3_{\overline{\rm MS}} + \\
&+ \left(\frac{42074947}{1728} - \frac{35385}{8}\zeta_3 - \frac{66765}{65}\zeta_5\right) h^4_{\overline{\rm MS}}.
\end{aligned} \tag{2.4}$$

Thus, inverting Eq. (2.4) and substituting in Eq. (2.3), we obtain the gluon and ghost propagator anomalous dimensions in the three above-mentioned renormalisation schemes. The knowledge of the β-function

$$\beta(h) \;= \frac{d}{d\ln\mu^2}\;h = -\sum_{i=1}^{n}\beta_i\;h^{i+2} \;+\; \mathcal{O}\left(h^{n+3}\right)\;, \tag{2.5}$$

[3] It corresponds to $\widetilde{\rm MOMgg}$ in [14].

makes possible the perturbative integration of the three equations obtained from Eq. (2.3). The integration and perturbative inversion of Eq. (2.5) at four-loop order gives an expression for the running coupling:

$$h(t) = \frac{1}{\beta_0 t}\left(1 - \frac{\beta_1}{\beta_0^2}\frac{\log(t)}{t} + \frac{\beta_1^2}{\beta_0^4}\frac{1}{t^2}\left(\left(\log(t) - \frac{1}{2}\right)^2 + \frac{\beta_2\beta_0}{\beta_1^2} - \frac{5}{4}\right)\right) + \\ + \frac{1}{(\beta_0 t)^4}\left(\frac{\beta_3}{2\beta_0} + \frac{1}{2}\left(\frac{\beta_1}{\beta_0}\right)^3\left(-2\log^3(t) + 5\log^2(t) + \left(4 - 6\frac{\beta_2\beta_0}{\beta_1^2}\right)\log(t) - 1\right)\right), \tag{2.6}$$

where $t = \ln\frac{\mu^2}{\Lambda^2_{\rm QCD}}$. We omit the index specifying the renormalisation scheme both for h and $\Lambda_{\rm QCD}$.

The last equation allows us to write the ghost and gluon propagators as functions of the momentum. The numerical coefficients for the β-function in Eq. (2.5) are [15]:

$$\beta_0 = 11, \qquad \beta_1 = 102,$$
$$\beta_2^{\widetilde{\rm MOM}_{c0}} = 3040.48, \qquad \beta_2^{\widetilde{\rm MOM}_g} = 2412.16, \qquad \beta_2^{\widetilde{\rm MOM}_c} = 2952.73,$$
$$\beta_3^{\widetilde{\rm MOM}_{c0}} = 100541, \qquad \beta_3^{\widetilde{\rm MOM}_g} = 84353.8, \qquad \beta_3^{\widetilde{\rm MOM}_c} = 101484.$$

2.2 OPE power corrections for ghost and gluon propagators

The dominant OPE power correction for the gluon propagator has been calculated in ([2, 3]), and it has the form

$$Z_3(q^2) \;=\; Z_{3,\rm pert}(q^2)\;\left(1 + \frac{3}{q^2}\frac{g_R^2\langle A^2\rangle_R}{4(N_C^2-1)}\right). \tag{2.7}$$

In this section we present the calculation of the analogous correction to the ghost propagator. The leading power contribution to the ghost propagator

$$F^{ab}(q^2) = \int d^4x e^{iq\cdot x}\langle\, T\left(c^a(x)\overline{c^b}(0)\right)\,\rangle, \tag{2.8}$$

as in refs. [2, 3] for gluon two- and three-point Green functions, can be computed using the operator product expansion [16]:

$$T\left(c^a(x)\overline{c^b}(0)\right) = \sum_t (c_t)^{ab}(x)\; O_t(0) \tag{2.9}$$

where O_t is a local operator, regular when $x \to 0$, and where the Wilson coefficient c_t contains the short-distance singularity. In fact, up to operators of dimension two, nothing but $\mathbf{1}$ and $:A^a_\mu A^b_\nu:$ contribute to Eq. (2.8) in Landau gauge [4]. Then, applying (2.9) to

[4] Those operators with an odd number of fields ($\partial_\mu A$ and $\partial_\mu\overline{c}$) cannot satisfy colour and Lorentz invariance and do not contribute with a non-null non-perturbative expectation value, neither $\overline{c}c$ contributes because of the particular tensorial structure of the ghost-gluon vertex

(2.8), we obtain:

$$\begin{aligned} F^{ab}(q^2) &= (c_0)^{ab}(q^2) \;+\; (c_2)^{ab\sigma\tau}_{st}\,(q^2)\langle :\, A^s_\sigma(0) A^t_\tau(0)\, :\rangle \;+\; \cdots \\ &= F^{ab}_{\rm pert}(q^2) \;+\; w^{ab}\;\frac{\langle A^2\rangle}{4(N_C^2-1)} \;+\; \cdots \end{aligned} \tag{2.10}$$

where

$$w^{ab} \;=\; (c_2)^{ab\sigma\tau}_{st}\,\delta^{st}g_{\sigma\tau} \;=\; \frac{1}{2}\,\delta^{st}g_{\sigma\tau}\frac{\int d^4x e^{iq\cdot x}\;\langle \widetilde{A}^{t'}_{\tau'}(0)\;T\left(c^a\overline{c^b}\right)\;\widetilde{A}^{s'}_{\sigma'}(0)\rangle_{\rm connected}}{G^{(2)}{}^{ss'}_{\sigma\sigma'}G^{(2)}{}^{tt'}_{\tau\tau'}}$$

$= 2 \times$ 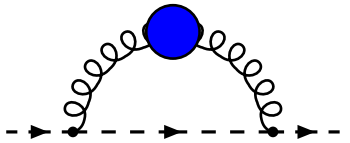 ,

(2.11)

and the SVZ sum rule [17] is invoked to compute the Wilson coefficients. Thus, one should compute the "*sunset*" diagram in the last line of Eq. (2.11), that couples the ghost propagator to the gluon A^2-condensate, to obtain the leading non-perturbative contribution (the first Wilson coefficient trivially gives the perturbative propagator). Finally,

$$F^{ab}(q^2) \;=\; F^{ab}_{\rm pert}(q^2)\;\left(1+\frac{3}{q^2}\;\frac{g_R^2\langle A^2\rangle_R}{4(N_C^2-1)}\right) \;+\; \mathcal{O}\left(g^4, q^{-4}\right) \tag{2.12}$$

where the A^2-condensate is renormalised, according to the MOM scheme definition, by imposing the tree-level value to the Wilson coefficient at the renormalisation point, [2]. As far as we do not include the effects of the anomalous dimension of the A^2 operator (see ref. [3]), we can factorise the perturbative ghost propagator. Then, doing the transverse projection, one obtains the following expression for the ghost dressing function:

$$\widetilde{Z_3}(q^2) \;=\; \widetilde{Z_{3,{\rm pert}}}(q^2)\;\left(1+\frac{3}{q^2}\frac{g_R^2\langle A^2\rangle_R}{4(N_C^2-1)}\right)\;. \tag{2.13}$$

We see that the multiplicative correction to the perturbative $\widetilde{Z_{3,{\rm pert}}}$ is identical to that obtained in ref. [2] for the gluon propagator (Eq. (2.7)).

We do not know whether there is a deep reason for the equality of the Wilson coefficients at one loop for the gluon and ghost propagators. Is it a consequence of the absence of (gauge-dependant) $\langle A^2\rangle$ contributions in gauge-invariant quantities? In principle, this could be proven either by a direct calculation of some gauge-invariant quantity or by analysing a Slavnov-Taylor identity [18] that relates the ghost and gluon propagators with the three-gluon and the ghost-gluon vertices. In both cases one has to evaluate the $\langle A^2\rangle$ corrections to these vertices, and this is a delicate question (because of soft external legs, [19]). The understanding of the mechanism of compensation of diverse gauge-dependent OPE contributions deserves a separate study, and we do not address this question in the present paper.

β	Volume	a^{-1} (GeV)	Number of conf.
6.0	16^4	1.96	1000
6.0	24^4	1.96	500
6.2	24^4	2.75	500
6.4	32^4	3.66	250

Table 1: Run parameters of the exploited data ([8]).

3. Data Analysis

3.1 Lattice setup

The lattice data that we exploit in this letter were previously presented in ref. [8]. We refer to this work for all the details on the lattice simulation (algorithms, action, Faddeev-Popov operator inversion) and on the treatment of the lattice artifacts (extrapolation to the continuum limit, etc). The parameters of the whole set of simulations used are described in table 1.

Our strategy for the analysis will be, after rescaling and combining the data from each particular simulation, to try global fits over a momentum window as large as possible. As will be seen, after such a multiplicative rescaling, all the data match each other from $\sim$ 2 GeV to $\sim$ 6 GeV (cf. figure 1). For the sake of completeness, we have furthermore performed an independent analysis (at fixed lattice spacing) for all simulations from table 1. The results of this analysis are given in appendix A.

3.2 Extracting Λ_{QCD} from lattice data

Given that at the leading order the non-perturbative power corrections factorise as in Eq. (2.13) and are identical in the case of the ghost and gluon [2] propagators, our strategy to extract Λ_{QCD} is to fit the ratio

$$\frac{\widetilde{Z_3}(q^2,\Lambda_R,\langle A^2\rangle)}{Z_3(q^2,\Lambda_R),\langle A^2\rangle)} = \frac{\widetilde{Z_{3,\mathrm{pert}}}(q^2,\Lambda_R)}{Z_{3,\mathrm{pert}}(q^2,\Lambda_R)}, \tag{3.1}$$

to the ratio of three-loop *perturbative* formulae in scheme R obtained in section 2.1, and then convert Λ_R to $\Lambda_{\overline{\mathrm{MS}}}$ ([8]). It is interesting to notice that non-perturbative corrections cancel out in this ratio even in the case $n_f \neq 0$. The Λ_{QCD}-parameter extracted from this ratio is free from non-perturbative power corrections up to operators of dimension four, while the dressing functions themselves are corrected by the dimension two A^2-condensate. In table. 2, the best-fit parameters for the three schemes are presented and we plot in figure 1 the lattice data and the $\widetilde{\mathrm{MOM}}_g$ best-fit curve for the ratio in Eq. (3.1).

In figure 2*a* we show the evolution of the fitted parameter $\Lambda_{\overline{\mathrm{MS}}}$ when changing the order of the perturbation theory used in the fitting formula. One can conclude from figure 2*a* and appendix A that $\widetilde{\mathrm{MOM}}_g$ scheme at three loops gives the most stable results for $\Lambda_{\overline{\mathrm{MS}}}$. It can also be seen from the ratio of four to three loops contributions (see figure 2*b*) for the

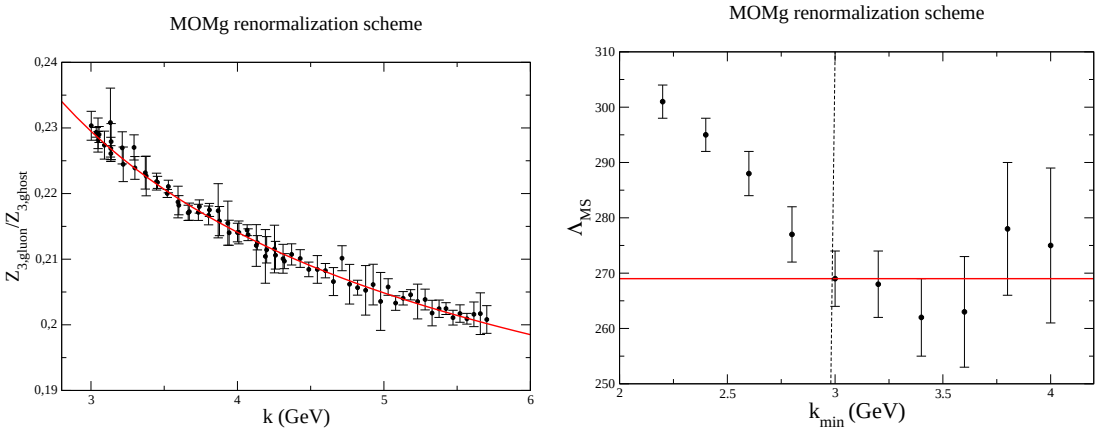

(a) (b)

Figure 1: (a) Plot of the $\frac{Z_3(p^2)}{\widetilde{Z}_3(p^2)}$ for the best fit parameter $\Lambda_{\overline{\rm MS}} = 269(5)$ MeV. (b) The determination of the optimal window fit (from 3 GeV to $k_{\rm max}a \leq \pi/2$) results from the search for some "plateau" of $\Lambda_{\overline{\rm MS}}$ when one changes the low bound of the fit window.

scheme	$\Lambda^{2\text{ loops}}_{\overline{\rm MS}}$	χ^2/d.o.f	$\Lambda^{3\text{ loops}}_{\overline{\rm MS}}$	χ^2/d.o.f	$\Lambda^{4\text{ loops}}_{\overline{\rm MS}}$	χ^2/d.o.f
$\widetilde{\rm MOM}_g$	324(6)	0.33	269(5)	0.34	282(6)	0.34
$\widetilde{\rm MOM}_c$	351(6)	0.33	273(5)	0.34	291(6)	0.33
$\widetilde{\rm MOM}_{c0}$	385(7)	0.33	281(5)	0.34	298(6)	0.33

Table 2: The best-fitted values of $\Lambda_{\overline{\rm MS}}$ for the three considered renormalisation schemes. As discussed in the text, $\widetilde{\rm MOM}_g$ seems to be the one showing the best asymptotic behaviour.

perturbative expansion of $\log Z_3$,

$$\ln(Z_3) \;=\; r_0 \ln(h_R) + \sum_{i=1} r_i h_R^i \;, \tag{3.2}$$

where the coefficients r_i are to be computed from those in eqs. (2.3)–(2.7) and R stands for any renormalisation scheme ($R = \widetilde{\rm MOM}_g$ in figure 2b). The same is done for $\log \widetilde{Z}_3$.

According to our analysis, *three loops seems to be the optimal order for asymptoticity. Indeed, the values of $\Lambda_{\overline{MS}}$ for the three considered renormalisation schemes practically match each other at three loops.* Finally,

$$\Lambda_{\overline{\rm MS}} = 269(5)^{+12}_{-9} \tag{3.3}$$

could be presented as the result for the fits of the ratio of dressing functions to perturbative formulae, where we take into account the bias due to the choice of the fitting window (see figure 1b and appendix A).

However, there are indications (appendix A and [8]) that our present systematic uncertainty may be underestimated, and we prefer simply to quote $\Lambda_{\overline{\rm MS}} \approx 270$ MeV . This value is considerably smaller than the value of ≈ 320 MeV obtained by independent fits of

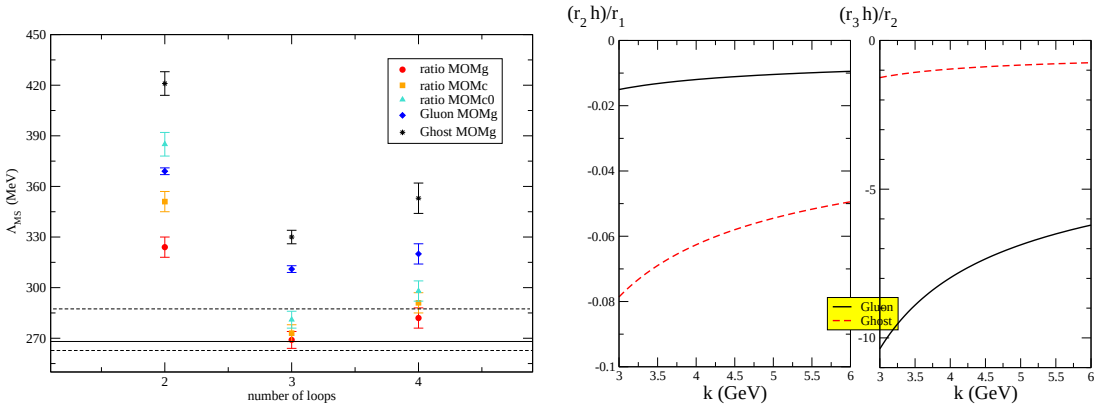

(a) (b)

Figure 2: (a) Evolution of the parameter $\Lambda_{\overline{\rm MS}}$, extracted from fits of the ratio eq. (3.1) and propagators alone (rhombus and star markers, extracted from table 7 of [8]) to perturbative formulae, as function of the order of the perturbation theory. Only statistical error is quoted. (b) Ratio of four-loop to three-loop contributions (and of three-loop to two-loops for the sake of comparison) for the perturbative expansion of $\log Z_3$ and $\log \widetilde{Z_3}$ (in $\widetilde{\rm MOM}_g$) in eq. (3.2), plotted versus the momenta inside our fitting window.

	Z_3	$\widetilde{Z_3}$
$g_R^2\langle A^2\rangle$ (GeV^2)	2.7(4)	2.7(2)

Table 3: The best-fitted values of $g_R^2\langle A^2\rangle$ for $\widetilde{\rm MOM}_g$ obtained from fitting lattice data to a three-loop perturbative formula + non-perturbative power correction with $\Lambda_{\overline{\rm MS}} = 270$ MeV. We only quote statistical errors.

dressing functions ([8]), and with fitting windows independently determined for each lattice sample (see figure 2a). This argues in favour of presence of low-order non-perturbative corrections to the ghost and gluon propagators.

3.3 Estimating the value of the $\langle A^2\rangle$ gluon condensate

Knowing $\Lambda_{\overline{\rm MS}}$ we can fit ghost and gluon dressing functions using eqs. (2.7), (2.13). The free parameter in this case is $g_R^2\langle A^2\rangle$. According to the theoretical argument given in 2.2, the results obtained from these fits have to be compatible. We have performed this analysis for the rough value $\Lambda_{\overline{\rm MS}} \approx 270$ MeV, (see table 3). Indeed, we find that the resulting values agree. It is worth to emphasise the meaning of this result: *a fully self-consistent description of gluon and ghost propagators computed from the same sample of lattice configuration (same $\Lambda_{\overline{MS}}$ and same $\langle A^2\rangle$) is obtained.*

The values of the gluon condensate presented in table 3 are smaller than those obtained from the previous analysis of the gluon propagator [2]. The reason for this is the larger value of $\Lambda_{\overline{\rm MS}}$ we have found. Had we taken $\Lambda_{\overline{\rm MS}} \simeq 240$ MeV, we would obtain similar results to those previously presented. Of course, this discrepancy have to be included in the present systematical uncertainty of our analysis of the ghost propagator lattice data. However, the

JHEP01(2006)037

purpose of this paper is not to present a precise determination of the dimension-two gluon condensate, but only to show that ghost and gluon propagators analysis strongly indicates its existence. The precision could be improved by increasing the Monte-Carlo statistics and by performing new simulations at larger β.

Another source of discrepancy are renormalon-type contributions that can also be of the order of $\sim 1/q^2$. In fact, our OPE study does not include the analysis of such corrections. However, the numerical equality (cf. table 3) of $\sim 1/q^2$ power corrections at fixed $\Lambda_{\overline{\rm MS}}$ suggests that the ratio (3.1) is free of such corrections, in agreement with the common belief that the renormalon ambiguities are compensated by condensate contributions. The estimate for $\Lambda_{\overline{\rm MS}}$ obtained from this ratio is thus not affected by the renormalon-type contributions. But the dependence of the value of these corrections on $\Lambda_{\overline{\rm MS}}$ speaks in favour of the presence of renormalon-type contributions in Z_3 and $\widetilde{Z_3}$ separately.

4. Conclusions

We have analysed non-perturbative low-order power corrections to the ghost propagator in Landau gauge pure Yang-Mills theory using OPE. We found that these corrections are the *same* as those for the gluon propagator at leading order. This means that their ratio does not contain low-order power corrections ($\sim 1/q^2$), and can be described (up to terms of order $\sim 1/q^4$) by the perturbation theory. Fitting the ratio of propagators calculated on the lattice we have extracted the $\Lambda_{\overline{\rm MS}}$ parameter using three- and four-loop perturbation theory. The value $\Lambda_{\overline{\rm MS}} \approx 270$ MeV extracted from the ratio is quite small compared to the one obtained in fits of gluon and ghost propagator ($\Lambda_{\overline{\rm MS}}^{\rm pert} \approx 320$ MeV, [8]) separately. Indeed, $\Lambda_{\overline{\rm MS}} \approx 270$ MeV extracted from the ratio of ghost and gluon dressing functions is closer to the value calculated in the past with power-corrections taken into account ($\Lambda_{\overline{\rm MS}}^{\text{with } A^2} \approx 250$ MeV, [3, 4]) than to the purely perturbative result . This study within perturbation theory confirms the validity of our OPE analysis, and argues in favour of a non-zero value of non-perturbative A^2-condensate. We are not able at the moment to give a precise value of the A^2-condensate using this strategy. More lattice data and detailed analysis of diverse systematic uncertainties are needed for this. But the method exposed in this letter can in principle be used for this purpose, both in quenched and unquenched cases.

A. Fitting $\Lambda_{\overline{\rm MS}}$ from separate data samples

In this appendix we present results for $\Lambda_{\rm QCD}$ extracted by fitting the ratio $\frac{\widetilde{Z}_3(p^2)}{Z_3(p^2)}$ using two, three and four-loop perturbation theory. But we do not mix data samples obtained in different lattice simulations. This allows to control the effects of several lattice artifacts and of the uncertainty on the lattice spacing calculation on the resulting value of $\Lambda_{\rm QCD}$. Fits have been performed in $\widetilde{\rm MOM}_c, \widetilde{\rm MOM}_{c0}, \widetilde{\rm MOM}_g$ renormalisation schemes (cf. tables 4–9). In each case we chose the best fit from several fitting windows, having the smallest χ^2/d.o.f.; the statistical error corresponds to that fit. The systematic error is calculated from different fit windows.

V	β	Left, GeV	Right,GeV	$a\Lambda^{(2)}_{\frac{\widetilde{Z}_3}{Z_3},\widetilde{\mathrm{MOM}_g}}$	conversion to $\Lambda^{(2)\overline{\mathrm{MS}}}$, MeV	$\chi 2$/d.o.f.
16^4	6.0	2.54	4.32	$529(17)^{+4}_{-2}$	$359(12)^{+2}_{-1}$	0.21
24^4	6.0	3.14	4.12	$513(15)^{+16}_{-16}$	$348(10)^{+11}_{-11}$	0.10
24^4	6.2	3.02	4.95	$377(24)_{-11}$	$358(22)_{-10}$	0.14
32^4	6.4	3.66	5.85	$257(21)^{+1}_{-4}$	$325(26)^{+3}_{-5}$	0.17

Table 4: Perturbative fit of $\frac{\widetilde{Z}_3(p2)}{Z_3(p2)}$ at 2 loops in $\widetilde{\mathrm{MOM}_g}$ scheme and further conversion to $\overline{\mathrm{MS}}$.

V	β	Left, GeV	Right,GeV	$a\Lambda^{(2)}_{\frac{\widetilde{Z}_3}{Z_3},\widetilde{\mathrm{MOM}_c}}$	conversion to $\Lambda^{(2)\overline{\mathrm{MS}}}$, MeV	$\chi 2$/d.o.f.
16^4	6.0	2.15	4.12	$445(6)_{-6}$	$375(5)_{-5}$	0.14
24^4	6.0	3.14	4.12	$398(53)^{+16}_{-1}$	$335(45)^{+11}_{-1}$	0.10
24^4	6.2	3.02	4.95	$313(19)_{-22}$	$369(22)_{-26}$	0.13
32^4	6.4	3.66	5.85	$215(17)^{+2}_{-2}$	$337(26)^{+3}_{-3}$	0.17

Table 5: Perturbative fit of $\frac{\widetilde{Z}_3(p2)}{Z_3(p2)}$ at 2 loops in $\widetilde{\mathrm{MOM}_c}$ scheme and further conversion to $\overline{\mathrm{MS}}$.

V	β	Left, GeV	Right,GeV	$a\Lambda^{(2)}_{\frac{\widetilde{Z}_3}{Z_3},\widetilde{\mathrm{MOM}_{c0}}}$	conversion to $\Lambda^{(2)\overline{\mathrm{MS}}}$, MeV	$\chi 2$/d.o.f.
16^4	6.0	1.97	4.11	$400(6)_{-5}$	$413(6)_{-5}$	0.15
24^4	6.0	3.13	4.12	$354(49)^{+26}$	$367(41)^{+27}$	0.11
24^4	6.2	3.02	4.95	$280(17)^{+1}_{-12}$	$367(24)^{+1}_{-17}$	0.11
32^4	6.4	3.66	5.85	$190(16)^{+2}_{-3}$	$366(30)^{+4}_{-6}$	0.16

Table 6: Perturbative fit of $\frac{\widetilde{Z}_3(p2)}{Z_3(p2)}$ at 2 loops in $\widetilde{\mathrm{MOM}_{c0}}$ scheme and further conversion to $\overline{\mathrm{MS}}$.

V	β	Left, GeV	Right,GeV	$a\Lambda^{(3)}_{\frac{\widetilde{Z}_3}{Z_3},\widetilde{\mathrm{MOM}_c}}$	conversion to $\Lambda^{(3)\overline{\mathrm{MS}}}$, MeV	χ^2/d.o.f.
16^4	6.0	2.54	4.31	$354(12)^{+5}_{-5}$	$297(10)^{+4}_{-4}$	0.23
24^4	6.0	3.13	4.12	$312(48)^{+30}$	$261(40)^{+25}$	0.10
24^4	6.2	3.14	4.95	$247(20)_{-22}$	$289(23)_{-26}$	0.14
$26\ 32^4$	6.4	3.66	5.86	$163(15)^{+2}_{-1}$	$254(24)^{+3}_{-2}$	0.16

Table 7: Perturbative fit of $\frac{\widetilde{Z}_3(p^2)}{Z_3(p^2)}$ at 3 loops in $\widetilde{\mathrm{MOM}_c}$ scheme and further conversion to $\overline{\mathrm{MS}}$.

One can see from these fits that the values for $\Lambda_{\overline{\mathrm{MS}}}$ are small at three and four loops when fitting at energies $\geq$ 3GeV. All results are rather stable in this domain, and thus the fitting of combined data from the simulations with different lattice spacings, presented in the main part of the present letter, is safe and well defined.

References

[1] K.G. Chetyrkin, S. Narison and V.I. Zakharov, *Short-distance tachyonic gluon mass and 1/Q^2 corrections*, *Nucl. Phys.* **B 550** (1999) 353 [hep-ph/9811275];

V	β	Left, GeV	Right,GeV	$a\Lambda^{(3)}_{\frac{\widetilde{Z}_3}{Z_3},\widetilde{\mathrm{MOM}_g}}$	conversion to $\Lambda^{(3)\overline{\mathrm{MS}}}$, MeV	χ^2/d.o.f.
16^4	6.0	2.06	3.44	$453(18)_{-5}$	$307(12)_{-4}$	0.16
24^4	6.0	2.06	3.53	$451(16)^{+2}_{-10}$	$306(11)^{+1}_{-7}$	0.1
24^4	6.2	2.80	4.81	$295(20)^{+15}$	$282(19)^{+14}$	0.13
32^4	6.4	3.79	5.59	$216(25)_{-13}$	$270(31)_{-16}$	0.13

Table 8: Perturbative fit of $\frac{\widetilde{Z}_3(p^2)}{Z_3(p^2)}$ at 3 loops in $\widetilde{\mathrm{MOM}_g}$ scheme and further conversion to $\overline{\mathrm{MS}}$.

V	β	Left, GeV	Right,GeV	$a\Lambda^{(3)}_{\frac{\widetilde{Z}_3}{Z_3},\widetilde{\mathrm{MOM}_{c0}}}$	conversion to $\Lambda^{(3)\overline{\mathrm{MS}}}$, MeV	χ^2/d.o.f.
16^4	6.0	2.16	3.53	$312(11)_{-17}$	$323(11)_{-18}$	0.11
24^4	6.0	3.21	4.11	$252(47)^{+36}$	$260(48)^{+37}$	0.10
24^4	6.2	3.13	4.95	$205(16)_{-18}$	$297(23)_{-26}$	0.14
32^4	6.4	3.66	5.86	$136(12)^{+1}_{-2}$	$262(23)^{+2}_{-2}$	0.17

Table 9: Perturbative fit of $\frac{\widetilde{Z}_3(p^2)}{Z_3(p^2)}$ at 3 loops in $\widetilde{\mathrm{MOM}_{c0}}$ scheme and further conversion to $\overline{\mathrm{MS}}$.

V	β	Left, GeV	Right,GeV	$a\Lambda^{(4)}_{\frac{\widetilde{Z}_3}{Z_3},\widetilde{\mathrm{MOM}_g}}$	conversion to $\Lambda^{(4)\overline{\mathrm{MS}}}$, MeV	$\chi 2$/d.o.f.
16^4	6.0	–	–	–	–	–
24^4	6.0	3.14	4.12	$365(13)^{+18}$	$248(8)^{+12}$	0.10
24^4	6.2	3.02	4.95	$288(17)^{+1}_{-4}$	$274(16)^{+1}_{-4}$	0.13
32^4	6.4	3.66	5.85	$199(15)^{+5}$	$252(19)^{+6}$	0.17

Table 10: Perturbative fit of $\frac{\widetilde{Z}_3(p2)}{Z_3(p2)}$ at 4 loops in $\widetilde{\mathrm{MOM}_g}$ scheme and further conversion to $\overline{\mathrm{MS}}$.

V	β	Left, GeV	Right,GeV	$a\Lambda^{(4)}_{\frac{\widetilde{Z}_3}{Z_3},\widetilde{\mathrm{MOM}_c}}$	conversion to $\Lambda^{(4)\overline{\mathrm{MS}}}$, MeV	$\chi 2$/d.o.f.
16^4	6.0	–	–	–	–	–
24^4	6.0	–	–	–	–	–
24^4	6.2	–	–	–	–	–
32^4	6.4	3.66	5.85	$175(15)^{+1}_{-2}$	$274(23)^{+2}_{-4}$	0.17

Table 11: Perturbative fit of $\frac{\widetilde{Z}_3(p2)}{Z_3(p2)}$ at 4 loops in $\widetilde{\mathrm{MOM}_c}$ scheme and further conversion to $\overline{\mathrm{MS}}$.

L. Stodolsky, P. van Baal and V.I. Zakharov, *Defining $\langle a^2\rangle$ in the finite volume hamiltonian formalism*, *Phys. Lett.* **B 552** (2003) 214 [hep-th/0210204].

[2] P. Boucaud et al., *Consistent ope description of gluon two point and three point green function?*, *Phys. Lett.* **B 493** (2000) 315 [hep-ph/0008043].

[3] P. Boucaud et al., *Testing Landau gauge ope on the lattice with a $\langle a^2\rangle$ condensate*, *Phys. Rev.* **D 63** (2001) 114003 [hep-ph/0101302].

[4] P. Boucaud et al., *Lattice calculation of $1/p^2$ corrections to α_s and of lambda(QCD) in the MOM scheme*, *JHEP* **04** (2000) 006 [hep-ph/0003020];

V	β	Left, GeV	Right,GeV	$a\Lambda^{(4)}_{\frac{\widetilde{Z}_3}{Z_3},\widetilde{\mathrm{MOM}_{c0}}}$	conversion to $\Lambda^{(4)\overline{\mathrm{MS}}}$, MeV	$\chi 2$/d.o.f.
16^4	6.0	–	–	–	–	–
24^4	6.0	2.95	4.12	$299(29)_{-26}$	$309(30)_{-27}$	0.11
24^4	6.2	3.02	4.95	$225(14)^{+1}_{-4}$	$326(20)^{+1}_{-6}$	0.13
32^4	6.4	3.66	5.85	$152(13)^{+1}_{-2}$	$293(25)^{+2}_{-4}$	0.16

Table 12: Perturbative fit of $\frac{\widetilde{Z}_3(p2)}{Z_3(p2)}$ at 4 loops in $\widetilde{\mathrm{MOM}_{c0}}$ scheme and further conversion to $\overline{\mathrm{MS}}$.

F. De Soto and J. Rodriguez-Quintero, *Notes on the determination of the Landau gauge ope for the asymmetric three gluon vertex*, *Phys. Rev.* **D 64** (2001) 114003 [hep-ph/0105063];
P. Boucaud et al., *Instantons and A2 condensate*, *Phys. Rev.* **D 66** (2002) 034504 [hep-ph/0203119];
P. Boucaud et al., *A transparent expression of the A^2-condensate's renormalization*, *Phys. Rev.* **D 67** (2003) 074027 [hep-ph/0208008].

[5] D. Dudal, H. Verschelde and S.P. Sorella, *The anomalous dimension of the composite operator A^2 in the Landau gauge*, *Phys. Lett.* **B 555** (2003) 126 [hep-th/0212182];
D. Dudal, R.F. Sobreiro, S.P. Sorella and H. Verschelde, *The Gribov parameter and the dimension two gluon condensate in euclidean Yang-Mills theories in the Landau gauge*, *Phys. Rev.* **D 72** (2005) 014016 [hep-th/0502183].

[6] K.I. Kondo, *A physical meaning of mixed gluon-ghost condensate of mass dimension two*, *Phys. Lett.* **B 572** (2003) 210 [hep-th/0306195].

[7] F.V. Gubarev, L. Stodolsky and V.I. Zakharov, *On the significance of the quantity A^2*, *Phys. Rev. Lett.* **86** (2001) 2220 [hep-ph/0010057];
K.I. Kondo, *Vacuum condensate of mass dimension 2 as the origin of mass gap and quark confinement*, *Phys. Lett.* **B 514** (2001) 335 [hep-th/0105299].

[8] P. Boucaud et al., *Large momentum behavior of the ghost propagator in* SU(3) *lattice gauge theory*, *Phys. Rev.* **D 72** (2005) 114503 [hep-lat/0506031].

[9] K.G. Chetyrkin, *Four-loop renormalization of QCD: full set of renormalization constants and anomalous dimensions*, *Nucl. Phys.* **B 710** (2005) 499 [hep-ph/0405193].

[10] M. Czakon, *The four-loop QCD beta-function and anomalous dimensions*, *Nucl. Phys.* **B 710** (2005) 485 [hep-ph/0411261].

[11] D. Becirevic et al., *Asymptotic behaviour of the gluon propagator from lattice QCD*, *Phys. Rev.* **D 60** (1999) 094509 [hep-ph/9903364].

[12] D. Becirevic et al., *Asymptotic scaling of the gluon propagator on the lattice*, *Phys. Rev.* **D 61** (2000) 114508 [hep-ph/9910204].

[13] G. Grunberg, *Renormalization scheme independent QCD and QED: the method of effective charges*, *Phys. Rev.* **D 29** (1984) 2315.

[14] K.G. Chetyrkin and A. Retey, *Three-loop three-linear vertices and four-loop mom beta functions in massless QCD*, hep-ph/0007088.

[15] T. van Ritbergen, J.A.M. Vermaseren and S.A. Larin, *The four-loop beta function in quantum chromodynamics*, *Phys. Lett.* **B 400** (1997) 379 [hep-ph/9701390].

JHEP01(2006)037

[16] R. Wilson, *Phys. Rev.* **179** (1969) 1499.

[17] M.A. Shifman, A.I. Vainshtein and V.I. Zakharov, *QCD and resonance physics. sum rules*, *Nucl. Phys.* **B 147** (1979) 385; *Nucl. Phys.* **B 147** (1979) 447*QCD and resonance physics. The ρ-ω mixing*, *Nucl. Phys.* **B 147** (1979) 519;
M.A. Shifman, A.I. Vainshtein, M.B. Voloshin and V.I. Zakharov, *$\eta(c)$ puzzle in quantum chromodynamics*, *Phys. Lett.* **B 77** (1978) 80.

[18] J. C. Taylor, *Ward identities and charge renormalization of the Yang-Mills field*, *Nucl. Phys.* **B 33** (1971) 2;
A. A. Slavnov, *Ward identities in gauge theories*, *Theor. Math. Phys.* **10** (1972) 99 [*Teor. Mat. Fiz.* **10** (1972) 153].

[19] F. De Soto and J. Rodriguez-Quintero, *Notes on the determination of the Landau gauge OPE for the asymmetric three gluon vertex*, *Phys. Rev.* **D 64** (2001) 114003 [hep-ph/0105063].

Annexe C

The infrared behaviour of the pure Yang-Mills Green functions

submitted to Phys. Rev. D

hep-lat/0507104

The Infrared Behaviour of the Pure Yang-Mills Green Functions

Ph. Boucaud[a], J.P. Leroy[a], A. Le Yaouanc[a], A.Y. Lokhov[b], J. Micheli[a], O. Pène[a], J. Rodríguez-Quintero[c] and C. Roiesnel[b]

[a]Laboratoire de Physique Théorique et Hautes Energies[1]
Université de Paris XI, Bâtiment 211, 91405 Orsay Cedex, France
[b] Centre de Physique Théorique[2]de l'Ecole Polytechnique
F91128 Palaiseau cedex, France
[c] Dpto. Física Aplicada, Fac. Ciencias Experimentales,
Universidad de Huelva, 21071 Huelva, Spain.

Abstract

We study the infrared behaviour of the pure Yang-Mills correlators using relations that are well defined in the non-perturbative domain. These are the Slavnov-Taylor identity for three-gluon vertex and the Schwinger-Dyson equation for ghost propagator in the Landau gauge. We also use several inputs from lattice simulations. We show that lattice data are in serious conflict with a widely spread analytical relation between the gluon and ghost infrared critical exponeessencnts. We conjecture that this is explained by a singular behaviour of the ghost-ghost-gluon vertex function in the infrared. We show that, anyhow, this discrepancy is not due to some lattice artefact since lattice Green functions satisfy the ghost propagator Schwinger-Dyson equation. We also report on a puzzle concerning the infrared gluon propagator: lattice data seem to favor a constant non vanishing zero momentum gluon propagator, while the Slavnov-Taylor identity (complemented with some regularity hypothesis of scalar functions) implies that it should diverge.

UHU-FP/05-12
CPHT RR 038.0605
LPT-Orsay/05-38

[1]Unité Mixte de Recherche 8627 du Centre National de la Recherche Scientifique
[2]Unité Mixte de Recherche 7644 du Centre National de la Recherche Scientifique

1 Introduction

1.1 Generalities

The whole set of correlation functions fully describes a Quantum Field Theory, as it is related to the S-matrix elements. In QCD or pure Yang-Mills theories Green functions are most often gauge dependent quantities which have no direct relationship with physical observables, the latter being necessarily gauge invariant. However, their indirect physical relevance is well known. In particular, long distance (or small momentum) Green functions will hopefully shed some light on the deepest mysteries of QCD such as confinement, spontaneous chiral symmetry breaking, etc. In this paper we concentrate our efforts on the study of the gluon and ghost Green functions at small momentum in a pure Yang-Mills theory. Our tools will be Slavnov-Taylor (ST) identities, Schwinger-Dyson (SD) equations and also several inputs from lattice QCD.

The infrared behaviour of Green functions has been extensively studied using different techniques, such as Schwinger-Dyson equations (see *e.g.* [3, 5, 24, 25] and references therein), renormalization group methods [26], stochastic quantization [4, 27]. These equations are exact consequences of QCD and can be easily derived using the path integral formalism. However their practical use reveals in most cases very difficult and one has to resort to a truncation which lessens the rigour of the method. One of the noticeable exceptions is the Schwinger-Dyson equation for the ghost propagator which contains only one integral and thus needs no truncation; this is the only one which we shall use in what follows. On the other hand, in order to exploit it in practice, one usually has to make appropriate *ansätze* for the gluon propagator and the ghost-ghost-gluon vertex.

We shall also use the Slavnov-Taylor identity which relates the three-gluons vertex to the ghost-ghost-gluon vertex in covariant gauges. Applying this relation in the non-perturbative domain will lead, under some assumptions about the infrared regularity of the dressing functions, to non trivial and surprising conclusions.

Lattice simulations are, of course, another major tool to study small momentum Green functions. However this paper is not meant to be a standard "lattice paper". We aim at using SD and ST to derive properties of the small momentum Green functions and we will use lattice simulations as valuable inputs in our theoretical discussion and as a check of some hypotheses. As we shall see, the outcome proves to be quite surprising and undermines some widely spread beliefs.

In what follows we work in the Landau gauge, but some of the results we present are actually valid in any covariant gauge. Our notations are the following :

$$(F^{(2)})^{ab}(k) = -\delta^{ab}\frac{F(k^2)}{k^2} \quad (1)$$

$$(G^{(2)}_{\mu\nu})^{ab}(k) = \delta^{ab}\frac{G(k^2)}{k^2}\left(\delta_{\mu\nu} - \frac{k_\mu k_\nu}{k^2}\right) \quad (2)$$

$$\Gamma^{abc}_{\mu\nu\rho}(p,q,r) = f^{abc}\Gamma_{\mu\nu\rho}(p,q,r) \quad (3)$$

$$\begin{aligned}\Gamma^{abc}_{\mu}(p,k;q) &= f^{abc}(-ip_\nu)g_0\widetilde{\Gamma}_{\nu\mu}(p,k;q) \\ &= f^{abc}(-ip_\nu)g_0 \\ &\quad \cdot[\delta_{\nu\mu}a(p,k;q) - q_\nu k_\mu b(p,k;q) + p_\nu q_\mu c(p,k;q) + q_\nu p_\mu d(p,k;q) \\ &\quad + p_\nu p_\mu e(p,k;q)]\end{aligned} \tag{4}$$

respectively for the ghost propagator, the gluon propagator, the three-gluons vertex and the ghost-ghost-gluon vertex[3]. All momenta are taken as entering. In eq. (4) $-p$ is the momentum of the outgoing ghost, k the momentum of the incoming one and $q = -p - k$ the momentum of the gluon. $F(p^2)$ and $G(p^2)$ are the dressing functions of the ghost and gluon propagators respectively. We parameterise the propagators in the infrared by setting at leading order

$$\begin{aligned}G(p^2) &= \left(\frac{p^2}{\lambda^2}\right)^{\alpha_G} \\ F(p^2) &= \left(\frac{p^2}{\eta^2}\right)^{\alpha_F}, \quad \text{when } p^2 \text{ is small,}\end{aligned} \tag{5}$$

where λ, η are some dimensional parameters.

Let us make a brief and partial summary of the present predictions for $\alpha_{F,G}$ ([3–5, 24–26, 28, 29]). We refer, for a very complete list of references, to the review by Alkofer and von Smekal [3]. All those references assume the relation $2\alpha_F + \alpha_G = 0$ and parameterise α_F and α_G as

$$\begin{aligned}\alpha_F &= -\kappa_{\mathrm{SD}} \\ \alpha_G &= 2\kappa_{\mathrm{SD}}.\end{aligned} \tag{6}$$

Different truncation schemes for the Schwinger-Dyson equations give ([3, 5, 24–26, 28, 29])

$$\begin{array}{ll}\kappa_{\mathrm{SD}} = 0.92 & [29] \\ \kappa_{\mathrm{SD}} \in [0.17, 0.53] & [5]\ \text{, using a 2-loop perturbative input}\end{array}$$

while another approach, ([4, 26]), predicts two possible solutions

$$\begin{aligned}\kappa_{\mathrm{SD}} &= 1, \quad \text{or} \\ \kappa_{\mathrm{SD}} &= 0.59\end{aligned}$$

Lattice simulations give $\alpha_G \simeq 1$. Note that $\alpha_G = 1$ corresponds to the gluon propagator being finite and non-zero at vanishing momentum; in other words, among the numbers we have just quoted, only the ones given in ref. [5] lead to a divergent infrared gluon propagator while the other values correspond to a vanishing one[4].

1.2 Numerical setup of the lattice simulations

In this part we briefly describe the technical details of our numerical lattice simulations.

[3] We stick to the decomposition given in ref. [19] *except for the arguments of the scalar functions, for which we keep the same order as in* Γ *itself*

[4] After the completion of this paper our attention was drawn on ref. [6] which also predicts an IR-divergent gluon propagator and on refs. [7, 8] which lead to a finite non-zero one.

We use the standard Wilson action. For the $SU(2)$ gauge group we have used lattices of size 32^4 and 48^4 with $\beta = 2.3$. This value of β corresponds to $\beta_{\mathrm{SU(3)}} \approx 5.75$. In the case of the $SU(3)$ gauge group the simulation has been done on 32^4, 24^4 and smaller lattices with $\beta = 5.75$ and $\beta = 6.0$. Those rather low values of β have been chosen because they allow measurements at small momenta. We have used periodical boundary conditions for the gauge field. The gluon propagator is defined as a mean value over gauge field configurations :

$$< A^a_\mu(x) A^b_\nu(y) > .$$

The ghost propagator is calculated by the inversion of the discretised Faddeev-Popov operator (cf eq. 27). For this purpose we have used the conjugate gradient algorithm with the source

$$\left(1 - \frac{1}{V}, \frac{1}{V}, \ldots, \frac{1}{V}\right)$$

where V is the number of lattice points. The rôle of the $1/V$ terms is to eliminate the zero modes of the Faddeev-Popov operator (corresponding to global gauge transformations) in order to allow its inversion in the orthogonal subspace (cf ref. [2]). All lattice data have been extrapolated to the continuum as described in ref. ([2]). A detailed report on all numerical results is presented in the same reference.

2 Constraints on α_F and α_G from the ghost Schwinger - Dyson equation

There is a widely used relation between α_F and α_G, referred to in the following as $\mathbf{R}_\alpha$, which comes from the scaling analysis of the Schwinger-Dyson equation for the ghost propagator ([4]) and states that in four-dimensional space one has $2\alpha_F + \alpha_G = 0$.

We have attempted to test this relation on lattices with the characteristics indicated above. We plot in fig. 1 the quantity $F^2(p)G(p)$ as a function of p. If the relation $\mathbf{R}_\alpha$ was true, this quantity should be constant in the infrared domain. One can see that *it is not the case: F^2G goes to zero at small momenta*. On the other hand the ultraviolet (UV) behaviour is exactly the expected one. The same trend is already visible at β's larger than ours : in refs. ([12, 13]) it is mentioned that F^2G might decrease as the momentum approaches zero[5] at $\beta = 6.0$ and $\beta = 6.4$. The same authors have even reported on the same effect in the unquenched case [11]. Very recently Ilgenfritz et al. have published in ref. [16] results which go in the same direction (although the conclusions they draw thereof differ from ours).

It was suggested in [13] that Gribov copies might induce significant changes in the infrared behaviour of the ghost propagator. Could this explain our findings for F^2G ? In ref. [17] the accurate lattice gauge fixing (choosing the "best copy", corresponding to the lowest value of $\|A^{(g)}\|$) seems to lessen the infrared divergence of the ghost propagator [14, 15, 17], implying a further increase of the drop of F^2G in the infrared, while the gluon propagator is known to be only slightly affected by the presence of

[5]In ref. [12] it is assumed that the vertex function stays constant in the zero momentum limit, in which case F^2G is proportional to the strong coupling constant $\tilde{\alpha}_s$ in the MOM scheme based on ghost-ghost-gluon vertex.

lattice Gribov copies. Furthermore, we shall see that the SD equation is closely related to a lattice-SD equation which is a mathematical identity, valid independently of the choice of the Gribov copy. Thus the possible influence of Gribov copies on propagators cannot explain the behaviour of F^2G at small momenta.

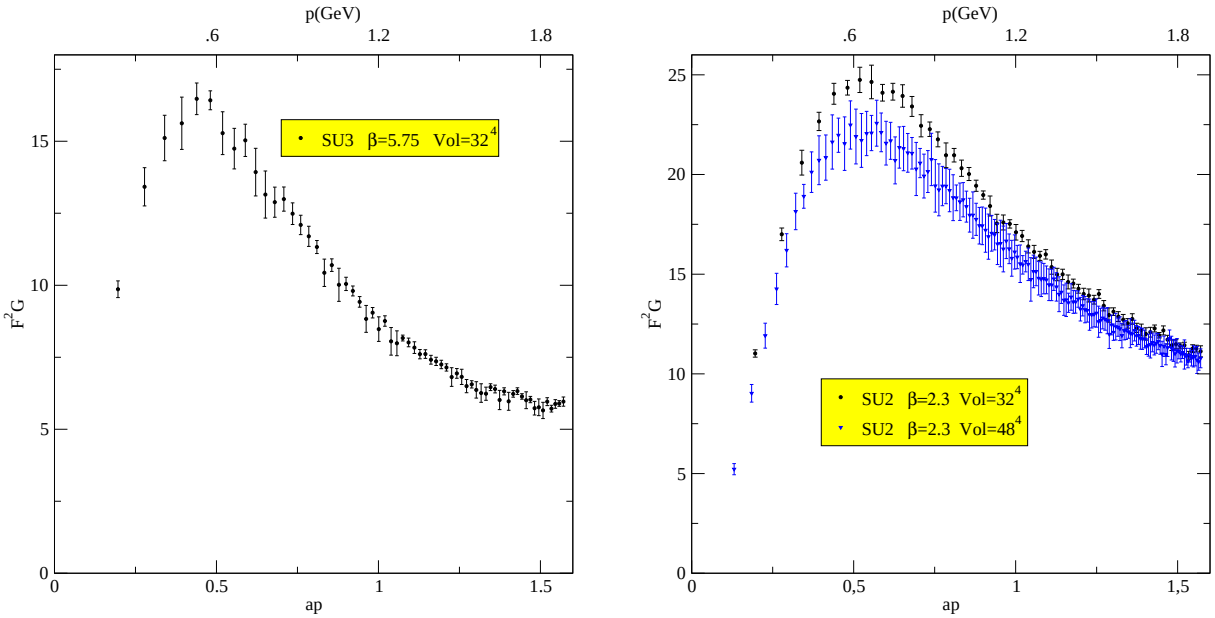

Figure 1: F^2G from lattice simulation for the $SU(3)$ (left, $32^4, \beta = 5.75$) and $SU(2)$ (right, 32^4 and $48^4, \beta_{SU(2)} = 2.3$) gauge groups. The β's are chosen so as to give the same lattice spacings : 1.2 GeV^{-1}. If the relation $2\alpha_F + \alpha_G = 0$ was true this quantity should be constant in the infrared domain. One clearly does not see this behaviour.

The rest of this section is aimed at understanding this disagreement between lattice simulations and the theoretical claim ($\mathbf{R}_\alpha$). We will first revisit the proof of the latter in order to identify all the hypotheses needed and submit each of them to a critical analysis. In the next-to-following section we will discuss a special writing of the ghost Schwinger-Dyson equation, in a form which involves only Green functions instead of vertices and can thus be directly tested on the lattice.

2.1 Revisiting the relation between α_F and α_G

We will examine to what extent the proof of $\mathbf{R}_\alpha$ is compelling, using the Schwinger-Dyson equation for the bare ghost propagator which can be written diagrammatically as

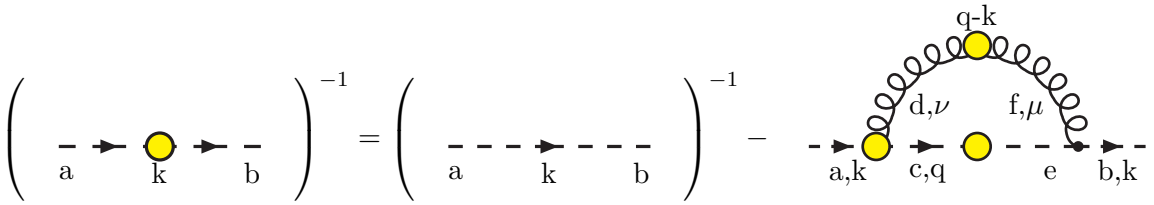

i.e.

$$
\begin{aligned}
(F^{(2)})^{-1}_{ab}(k) &= -\delta_{ab}k^2 \qquad (7)\\
&\quad -g_0^2 f_{acd}f_{ebf}\int \frac{d^4q}{(2\pi^4)} F^{(2)}_{ce}(q)(iq_{\nu'})\Gamma_{\nu'\nu}(-q,k;q-k)(ik_\mu)(G^{(2)})^{fd}_{\mu\nu}(q-k),
\end{aligned}
$$

where we use the notations of eqs. (1-5) and g_0 is the bare coupling constant. This integral equation is written in terms of bare Green functions. It can be cast into a renormalized form by multiplying $G^{(2)}$ (resp. $F^{(2)}, \Gamma$) by Z_3^{-1} (resp. $\widetilde{Z}_3^{-1}, \widetilde{Z}_1$) and g_0^2 by $Z_g^{-2} = Z_3\frac{\widetilde{Z}_3^2}{\widetilde{Z}_1^2}$ and multiplying the k^2 term by $\widetilde{Z}_3$. The integral therein is ultraviolet divergent but one can check that the cut-off dependence is matched by the cut-off dependence of Z_g and of the $\widetilde{Z}_3$ factor multiplying k^2. Later on we will only use *subtracted* SD equations such that the UV divergence is cancelled as well as the $\widetilde{Z}_3 k^2$ term. These subtracted SD equations hold both in terms of bare and renormalized Green functions without any explicit renormalization factor.

Let us now consider (7) at small momenta k. The ghost-gluon vertex may be expressed as

$$
q_{\nu'}\widetilde{\Gamma}_{\nu'\nu}(-q,k;q-k) = q_\nu H_1(q,k) + (q-k)_\nu H_2(q,k) \qquad (8)
$$

where, using the decomposition (4), one gets:

$$
\begin{aligned}
H_1(q,k) &= a(-q,k;q-k) - (q^2 - q\cdot k)\,(b(-q,k;q-k)\\
&\quad + d(-q,k;q-k)) + q^2 e(-q,k;q-k)) \simeq\\
&\overset{k\to 0}{\simeq} a(-q,k;q-k) - q^2\,(b(-q,k;q-k) + d(-q,k;q-k) - e(-q,k;q-k))\\
H_2(q,k) &= (q^2 - q\cdot k)\,b(-q,k;q-k) - q^2\,c(-q,k;q-k) \qquad (9)
\end{aligned}
$$

In the Landau gauge, because of the transversality condition, H_2 does not contribute. Thus, dividing both sides of eq. (7) by k^2 and omitting colour indices, one obtains

$$
\frac{1}{F(k)} = 1 + g_0^2 N_c \int \frac{d^4q}{(2\pi)^4}\left(\frac{F(q^2)G((q-k)^2)}{q^2(q-k)^2}\left[\frac{\frac{(k\cdot q)^2}{k^2} - q^2}{(q-k)^2}\right] H_1(q,k)\right). \qquad (10)
$$

2.2 What does the "non-renormalization theorem" exactly say?

A widely used statement, known as the "non-renormalization theorem", claims that, in the Landau gauge, the renormalization constant $\tilde{Z}_1$ of the ghost gluon vertex is exactly one. Note that there is no reference to a particular renormalisation scheme. Formulated in this way, this claim is wrong. Let us first state and then explain below what is true in our opinion :

1) There is a true and very clear statement which can be extracted from Taylor's paper (the argument is given below), ref. [1].

$$
\widetilde{\Gamma^{abc,Bare}_{\mu}}(-p,0;p) = -if^{abc}p_\mu \qquad (11)
$$

i.e. there is no radiative correction in this particular momentum configuration (with zero momentum of the ingoing ghost)

2) This entails that $\widetilde{\Gamma}_{\mu}^{abc,Bare}(p,k;q)$ is *finite* whatever the external momenta, and that therefore $\widetilde{Z_1}^{\overline{\rm MS}} = 1$. In addition, we get also trivially $\tilde{Z}_1^{\ {\rm MOM}_h} = 1$, where ${\rm MOM}_h$ refers to the configuration of momenta in equation (11). In general, in other schemes, *there is* a finite renormalisation, and this is why we do not adopt the misleading expression "non-renormalization theorem".

3) In particular, one finds in the very extensive calculations of radiative corrections at least two cases of MOM schemes where there is a finite renormalisation (and certainly many more) : ${\rm MOM}_g$ in the notations of ref. [19], and the *symmetric* MOM scheme. For the latter, we give the proof below.

The essence of Taylor's argument is actually very simple. In a kinematical situation where the incoming ghost momentum is zero, consider any perturbative contribution to the ghost-gluon vertex. Following the ghost line in the direction of the flow, the first vertex will be proportional to the outgoing ghost momentum p_μ, i.e. to the gluon momentum $-p_\mu$. In the Landau gauge this contribution will thus give 0 upon contraction with the gluon propagator $D_{\mu\nu}(p)$. Therefore the only contribution to remain is the tree-level one. In other words the bare ghost-gluon vertex is shown to be equal to its tree-level value in these kinematics : $\widetilde{\Gamma_{\mu}^{abc,Bare}}(-p,0;p) = -if^{abc}p_\mu$. This result has been checked by means of a direct evaluation to three loops in perturbation theory by Chetyrkin. In our notations :

$$H_1(p,0) + H_2(p,0) = 1.$$

Note that in the Schwinger-Dyson equation 10, only H_1 is present, and the theorem of Taylor does not tell that $H_1(p,0) = 1$, as seems assumed in many Schwinger-Dyson calculations, where it plays a crucial rôle in the proof of $\mathbf{R}_\alpha$.

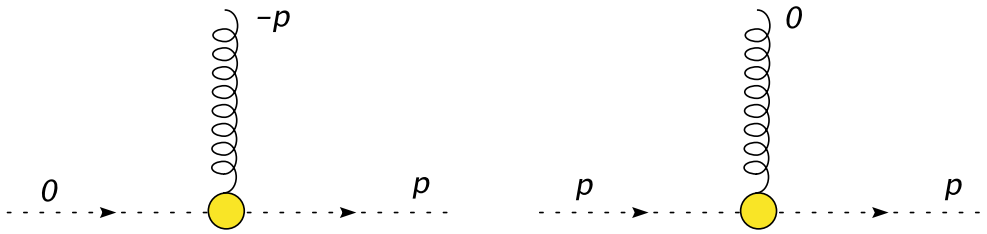

Figure 2: The kinematical situations considered below. The left diagram (0-momentum incoming ghost) corresponds to Γ_h below which is known to be equal to one. The right one (0-momentum gluon) corresponds to Γ_g and leads to a non-trivial p^2-dependence

As an illustration of our point 3), let us quote the formulas from the appendix of ref. [19], reduced to the situation we are interested in ($\xi_L = 0, n_f = 0$). The two dressing functions $\tilde{\Gamma}_h$ (resp. $\tilde{\Gamma}_g$) are defined by $\widetilde{\Gamma}_{\mu}^{abc}(-p,0,p) = -if^{abc}\tilde{\Gamma}_h(p)$ (resp. $\widetilde{\Gamma}_{\mu}^{abc}(-p,p,0) = -if^{abc}\tilde{\Gamma}_g(p)$) and correspond to the kinematical situations depicted in the left (resp. right) part of fig. (2). We have already mentionned that Γ_h is exactly

one, but this does not hold for Γ_g and, indeed, one has at three loops :

$$\tilde{\Gamma}_{\rm g}^{\overline{\rm MS}}|_{p^2=\mu^2} = 1 + \frac{3}{4}\frac{\alpha_s}{4\pi}C_A + \frac{599}{96}(\frac{\alpha_s}{4\pi})^2C_A^2 + \left[\frac{43273}{432}+\frac{783}{64}\zeta_3-\frac{875}{64}\zeta_5\right](\frac{\alpha_s}{4\pi})^3C_A^3 + \left[\frac{27}{4}-\frac{639}{16}\zeta_3+\frac{225}{8}\zeta_5\right](\frac{\alpha_s}{4\pi})^3C_A^2C_F\ . \quad (12)$$

It is then easy to find the p^2-dependence :

$$\tilde{\Gamma}_{\rm g} = \widetilde{\Gamma}_{\rm g}^{\overline{\rm MS}}|_{p^2=\mu^2} + \left[\frac{11}{4}C_A^2(\frac{\alpha_s}{4\pi})^2 + \frac{7813}{144}C_A^3(\frac{\alpha_s}{4\pi})^3+\cdots\right]\log(\frac{\mu^2}{-p^2})+\cdots$$

In ref. [28] the non -renormalization theorem is understood as the statement that the vertex reduces to its tree-level form at all symmetric-momenta points in a symmetric subtraction scheme. However this statement is not supported by a direct evaluation. Using the one-loop results of Davydychev (ref. [20]) one gets in a symmetric configuration the value

$$\widetilde{\Gamma}_\mu^{abc}(p,k;q)|_{p^2=k^2=q^2=\mu^2} = -if^{abc}\left\{p_\mu\left(1+\frac{\alpha_s}{4\pi}\frac{C_A}{12}(9+\frac{5}{2}\phi)\right)+q_\mu\frac{\alpha_s}{4\pi}\frac{C_A}{12}(3+\frac{5}{4}\phi)\right\} \quad (13)$$

with $\phi=\frac{4}{\sqrt{3}}Cl_2(\frac{\pi}{3}), Cl_2(\frac{\pi}{3})=1.049\cdots$.

According to ref. [28] the coefficient of p_μ should be one. The presence of α_s in the above formulas implies on the contrary that the vertex will in general depend on the momenta : using the results given in the appendices of ref. [19] one finds for the leading p^2-dependence $-if^{abc}\left\{\frac{11}{3}\frac{C_A^2}{12}(\frac{\alpha_s}{4\pi})^2\log(\frac{p^2}{\mu 2})\left((9+\frac{5}{2}\phi)p_\mu+(3+\frac{5}{4}\phi)q_\mu\right)\right\}$. This dependence is logarithmic, as is expected in a perturbative approach. Furthermore, in ref. ([28]) it is supposed that the vertex function takes the form $(q^2)^\ell(k^2)^m((q-k)^2)^n$ with the restriction $\ell+m+n=0$. One should note that this last condition corresponds in our notations to $\alpha_\Gamma=0$ (cf. section (2.3) below). This restriction comes from the assumption that the *s*ymmetric vertex is equal to 1 for any p^2, which, as we have just seen, is actually not the case. Therefore we shall adopt a more general point of view and keep open the possibility of a non perturbative effect leading to a singular or vanishing limit of H_1 when $q\to 0$. We should mention that the problem of the p^2-dependence of the ghost-gluon vertex has already been addressed in refs. [33, 34]. However these authors work under the condition $\mathbf{R}_\alpha$ which appears not to be satisfied by our lattice data.

2.3 A subtracted Schwinger-Dyson equation

Let us now consider two infrared scales $k_1\equiv k$ and $k_2\equiv\kappa k$. Calculating the difference of eq. (10) taken at scales k_1 and k_2 and supposing for the moment that $\alpha_F\neq 0$ one obtains

$$\frac{1}{F(k)}-\frac{1}{F(\kappa k)}\propto(1-\kappa^{-2\alpha_F})(k^2)^{-\alpha_F} = g_0^2N_c\int\frac{d^4q}{(2\pi)^4}\left(\frac{F(q^2)}{q^2}\left(\frac{(k\cdot q)^2}{k^2}-q^2\right)\times\left[\frac{G((q-k)^2)H_1(q,k)}{((q-k)^2)^2}-\frac{G((q-\kappa k)^2)H_1(q,\kappa k)}{((q-\kappa k)^2)^2}\right]\right). \quad (14)$$

We now make the hypothesis that there exists a scale q_0 such that

$$G(q^2) \sim (q^2)^{\alpha_G}, \quad F(q^2) \sim (q^2)^{\alpha_F}, \quad \text{for} \quad q^2 \leq q_0^2.$$

Similarly, we suppose that H_1 can be written for $q^2, k^2 \leq q_0^2$ as

$$H_1(q,k) \sim (q^2)^{\alpha_\Gamma} \, h_1\left(\frac{q\cdot k}{q^2}, \frac{k^2}{q^2}\right)$$

or as

$$H_1(q,k) \sim ((q-k)^2)^{\alpha_\Gamma} \, h_2\left(\frac{q\cdot k}{q^2}, \frac{k^2}{q^2}\right)$$

where the scalar functions $h_{1,2}$ are supposed to be regular enough (i.e. free of singularities worse than logarithmic) and expandable in Taylor series for $k \to 0$ They are obviously invariant under any simultaneous rescaling of both q and k. The exponent α_Γ gives the leading critical behaviour of H_1 on q.

Thus we rewrite (14) by rescaling $k \to \lambda k$ with λ chosen so that $(\lambda k)^2 \ll q_0^2$ and splitting the integral in the r.h.s. into two parts

$$I_1(\lambda) = \int_{q^2<q_0^2} \frac{d^4q}{(2\pi)^4}\Big[\dots\Big], \qquad I_2(\lambda) = \int_{q^2>q_0^2} \frac{d^4q}{(2\pi)^4}\Big[\dots\Big]. \tag{15}$$

In I_1, since $(\lambda k)^2 \ll q_0^2$, we can substitute the infrared approximations (5) for G and F . I_1 is infrared convergent if :

$$\begin{aligned} \alpha_F + \alpha_\Gamma &> -2 \qquad \text{IR convergence at } q^2 = 0 \\ \alpha_G + \alpha_\Gamma &> -1 \qquad \text{IR convergence at } (q-k)^2 = 0 \text{ and } (q-\kappa k)^2 = 0 \end{aligned} \tag{16}$$

We shall suppose in the following that these conditions are verified. We then obtain, performing the change of variable $q \to \lambda q$ and writing generically h for $h_{1,2}$:

$$\begin{aligned} I_1(\lambda) \approx \lambda^{2(\alpha_F+\alpha_G+\alpha_\Gamma)} \int_{q^2<\frac{q_0^2}{\lambda^2}} \frac{d^4q}{(2\pi)^4} \Bigg(& (q^2)^{\alpha_F+\alpha_\Gamma-1} \left(\frac{(k\cdot q)^2}{k^2} - q^2\right) \\ & \times \left[((q-k)^2)^{\alpha_G-2} \, h\left(\tfrac{q\cdot k}{q^2}, \tfrac{k^2}{q^2}\right) - ((q-\kappa k)^2)^{\alpha_G-2} \, h\left(\kappa\tfrac{q\cdot k}{q^2}, \kappa^2\tfrac{k^2}{q^2}\right)\right] \Bigg) \ . \end{aligned} \tag{17}$$

The point we have to keep in mind is the fact that the upper bound of the integral goes to infinity when $\lambda \to 0$. This potentially induces a dependence on λ whose interplay with the behaviour explicitly shown in (17) we must check. In this limit, the convergence of the integral depends on the asymptotic behaviour of the whole integrand for large q. In particular, the leading contribution of the square bracket in eq. (17) behaves as

$$(q^2)^{\alpha_G-2}\left(\frac{k^2}{q^2}\right) \sim q^{2\alpha_G-6} \ ,$$

because the terms in $q\cdot k$, being odd under $q_\mu \to -q_\mu$, give a null contribution under the angular integration in eq. (17). Thus, assuming the conditions (16) are satisfied

Case	$\alpha_F \neq 0$ $\alpha_F+\alpha_G+\alpha_\Gamma<1$	$\alpha_F \neq 0$ $\alpha_F+\alpha_G+\alpha_\Gamma\geq 1$	$\alpha_F = 0$ $\alpha_G+\alpha_\Gamma<1$	$\alpha_F = 0$ $\alpha_G+\alpha_\Gamma\geq 1$
IR Convergence Conditions	$\alpha_F+\alpha_\Gamma>-2$ $\alpha_G+\alpha_\Gamma>-1$	$\alpha_F+\alpha_\Gamma>-2$ $\alpha_G+\alpha_\Gamma>-1$	$\alpha_\Gamma>-2$ $\alpha_G+\alpha_\Gamma>-1$	$\alpha_\Gamma>-2$ $\alpha_G+\alpha_\Gamma>-1$
SD constraints	$2\alpha_F+\alpha_G+\alpha_\Gamma=0$	$\alpha_F=-1$	excluded	none

Table 1: Summary of the various cases regarding the α coefficients

the integral $I_1(\lambda)$ is guaranteed to be convergent when $q \to 0$ (or $k \to q$) and its asymptotics for small λ is given by

$$I_1(\lambda) \sim \begin{cases} \lambda^{2(\alpha_G+\alpha_F+\alpha_\Gamma)} \int_0^{q_0/\lambda} dq\; q^{2(\alpha_F+\alpha_G+\alpha_\Gamma)-3} \;\sim\; \lambda^{2(\alpha_G+\alpha_F+\alpha_\Gamma)} \\ \qquad\qquad\qquad\qquad\qquad\qquad\qquad\qquad \text{if}\;\; \alpha_G+\alpha_F+\alpha_\Gamma<1 \\ \lambda^2 \int_0^{q_0} dq\; q^{2(\alpha_F+\alpha_G+\alpha_\Gamma)-3} \;\sim\; \lambda^2 \qquad\qquad \text{if}\;\; \alpha_G+\alpha_F+\alpha_\Gamma\geq 1 \end{cases} \tag{18}$$

because in both cases the integral on the momentum q is finite and does not depend on λ in the limit $\lambda \to 0$.

Let us now consider I_2. Its dependence on λ is explicit in the factor

$$\frac{G\left((q-\lambda k)^2\right) H(q,\lambda k)}{\left((q-\lambda k)^2\right)^2} - \frac{G\left((q-\lambda\kappa k)^2\right) H(q,\lambda\kappa k)}{\left((q-\lambda\kappa k)^2\right)^2}$$

which stems from the substitution $k \to \lambda k$ in (14). Clearly, this quantity can only be even in λ : any odd power of λ would imply an odd power of $q\cdot k$ whose angular integral is zero. Since the integrand is identically zero at $\lambda = 0$ and the integral is ultraviolet convergent, it is proportional to λ^2 (unless some accidental cancellation forces it to behave as a higher even power of λ).

So, if the first of the conditions (18) is verified, it follows $I_1 + I_2 \approx \lambda^{2(\alpha_F+\alpha_G+\alpha_\Gamma)}$, else $I_1 + I_2 \approx \lambda^2$. Comparing this to the left hand side of eq. (10)

$$\frac{1}{F(\lambda k)} - \frac{1}{F(\lambda\kappa k)} \sim \lambda^{-2(\alpha_F)} \tag{19}$$

we then conclude :

$$\begin{aligned} \alpha_F+\alpha_G+\alpha_\Gamma \;&<1 \quad\Longrightarrow\; 2\alpha_F+\alpha_G+\alpha_\Gamma=0 \\ \alpha_F+\alpha_G+\alpha_\Gamma \;&\geq 1 \quad\Longrightarrow\; \alpha_F=-1 \end{aligned} \tag{20}$$

In the particular case $\alpha_F = 0$ the leading term in the l.h.s. of eq. (14) is identically zero. We are left with the subleading one which, pursuing the same argumentation, we suppose to be proportional to k^2. Then the argument is the same as in the previous case except for the power of λ in the r.h.s. of eq. (19) which becomes equal to 2. It results that the case $\alpha_G+\alpha_\Gamma<1$ is now excluded while the case $\alpha_G+\alpha_\Gamma\geq 1$ provides no extra constraint.

The various possibilities which have appeared in this discussion are summarised in table 1. From this table it appears that *only the triple condition that*

$$\alpha_F \neq 0, \quad \alpha_\Gamma = 0, \quad \alpha_F+\alpha_G<1$$

does actually imply the *standard statement that* $2\alpha_F + \alpha_G = 0$. However, the plot in Fig.1 indicates a behaviour $2\alpha_F + \alpha_G > 0$, indicating that at least one of these conditions is not fulfilled.

Let us assume for the moment that $\alpha_F + \alpha_G \geq 1$ and $\alpha_\Gamma = 0$. Then $2\alpha_F + \alpha_G \geq 0$, in agreement with fig.1, and $\alpha_G \geq 2$. However the possibility that α_G be greater than 2 is unambiguously excluded by the lattice simulations so that the hypothesis has to be rejected. Furthermore, as we shall see, one can derive from the Slavnov-Taylor identity relating the three-gluons and ghost-ghost-gluon vertices the inequality $\alpha_G < 1$ if one assumes that some of the scalar form factors of these vertices are regular when one momentum goes to zero.

We now consider the hypothesis $2\alpha_F + \alpha_G + \alpha_\Gamma = 0$ with $\alpha_\Gamma < 0$ to comply with the lattice indications of fig.1. This implies that some of the scalar factors of the ghost-ghost-gluon vertex are singular in the infrared. We shall turn back to this possibility in the concluding remarks of this section (2.4.4). The question is whether a non-perturbative effect could generate a non vanishing α_Γ.

A direct lattice estimate of the ghost-ghost-gluon vertex would be welcome. However this is a difficult task. A direct measurement implying a zero momentum ghost is impossible since the corresponding Green functions are singular because of the zero modes of the Faddeev-Popov operator. A careful limiting procedure implying very small external momenta has to be performed. This study is under way. In between we propose a simpler check based on another writing of the SD equation (7) in terms of a pinched Green function which can be directly checked on the lattice. This will also allow to control the lattice artefacts and to rule out the hypothesis that the problem encountered in fig. 1 is simply due to a lattice artefact.

2.4 Green function formulation of the ghost SD equation

We will now rewrite the ghost SD equation using only propagators and the ghost-ghost-gluon Green function. In this form, its validity can be tested on the lattice, because what one directly calculates in lattice simulations are *Green functions*, not *vertex functions*. If we consider the loop integral in Eq. (7) we can see that it is nothing else but a ghost-ghost-gluon Green function in which the left ghost leg has been cut and where the gluon and right-hand ghost have been pinched onto the same point in configuration space. We shall see that this quantity is directly accessible from lattice data *without making any specific assumption about the behaviour of the vertex function.*

The interest of this approach is that it will help us to throw a closer look at the compatibility of the lattice simulations and the SD equations. Indeed, as we have just seen, we are facing a contradiction between, on the one hand the lattice estimate of $F^2\,G$ (fig. 1) and, on the other hand, the relation $\mathbf{R}_\alpha$ which is derived from the SD equation (7) complemented by a regularity assumption ($\alpha_\Gamma = 0$) suggested by perturbation theory. Therefore we feel the need to directly confront lattice calculations with SD. The form of SD which is presented in this subsection allows such a direct confrontation and, this form being closely related to a lattice SD equation which is just a mathematical identity, we are in a good position to trace back any discrepancy.

In the next subsection we present the continuum limit derivation of the Green

function formulation of the ghost SD, as well as its lattice derivation.

2.4.1 Continuum limit case

For a given gauge field configuration $\mathcal{A}_\mu = A^a_\mu t^a$, the Faddeev-Popov operator in covariant gauges is given by

$$M(x,y)_{1\text{conf}} = (\partial_\mu D_\mu)\delta(x-y) = (\Delta + ig_0\partial_\mu\mathcal{A}_\mu)\,\delta^4(x-y) \equiv {F^{(2)}_{1\text{conf}}}^{-1}(\mathcal{A},x,y), \quad (21)$$

and it is equal to the inverse of the ghost correlator in the background of the gluon field $\mathcal{A}$, $F^{(2)}_{1\text{conf}}$. The subscript means here that the equation is valid for any given gauge configuration. This can be written

$$\delta^4(x-y) \equiv M_{1\text{conf}}(x,z)F^{(2)}_{1\text{conf}}(\mathcal{A},z,y), \quad (22)$$

where a summation on z is understood. Expanding M according to (21) we get

$$\delta(x-y) = \Delta(x,z)F^{(2)}_{1\text{conf}}(z,y) + ig_0\,\partial^{(x)}_\mu\Big(\mathcal{A}_\mu(x)F^{(2)}_{1\text{conf}}(\mathcal{A},x,y)\Big), \quad (23)$$

valid for *any* gauge field configuration. Performing the path integral one gets the mean value on gauge configurations

$$\delta(x-y) = \Delta(x,z)\langle F^{(2)}_{1\text{conf}}(z,y)\rangle + ig_0\partial^{(x)}_\mu\langle\mathcal{A}_\mu(x)F^{(2)}_{1\text{conf}}(\mathcal{A},x,y)\rangle. \quad (24)$$

Of course $\langle F^{(2)}_{1\text{conf}}(z,y)\rangle$ is nothing else but the ghost propagator defined in equation (1).

The averages $\langle F^{(2)}(x,y)\rangle$ and $\partial^{(x)}_\mu\langle\mathcal{A}_\mu(x)F^{(2)}(x,y)\rangle$ are invariant under translations so that one can replace the derivative $\partial^{(x)}_\mu \to -\partial^{(y)}_\mu$. We take $x=0$ and perform the Fourier transform on the y variable (note that there is no tilde on $\mathcal{A}_\mu(0)$)

$$1 = -p^2\tilde{F}^2(p) - g_0 p_\mu\langle\mathcal{A}_\mu(0)\tilde{F}^{(2)}_{1\text{conf}}(\mathcal{A},p)\rangle. \quad (25)$$

Finally we get

$$F(p^2) = 1 + g_0\frac{p_\mu}{N_c^2-1}f^{abc}\langle A^c_\mu(0)\tilde{F}^{(2)ba}_{1\text{conf}}(\mathcal{A},p)\rangle. \quad (26)$$

One caveat is in order here. Eq. (7) implies an ultraviolet divergent integral which is matched by renormalization constants. This divergence is of course also present in eq. (24) via the local product of operators at x. In section 2.1 this divergence was canceled by subtracting two terms as is apparent in eq. (14). In the following this divergence is regularised by the lattice cut-off. To perform the connection with the discussion in section 2.1 it will be necessary to perform an analogous subtraction when using the form (26).

2.4.2 Lattice case

We now repeat the same steps as in the preceding paragraph for the lattice version of the Faddeev-Popov operator

$$M^{ab}_{xy} \equiv F^{(2)}_{1\text{conf}}(U,x,y)^{-1} = \sum_\mu\Big[S^{ab}_\mu(x)\left(\delta_{x,y}-\delta_{y,x+e_\mu}\right) - S^{ab}_\mu(x-e_\mu)\left(\delta_{y,x-e_\mu}-\delta_{y,x}\right) + \\ + \frac{1}{2}f^{abc}\left[A^c_\mu(x)\delta_{y,x+e_\mu} - A^c_\mu(x-e_\mu)\delta_{y,x-e_\mu}\right]\Big], \quad (27)$$

where

$$\begin{array}{l} S_\mu^{ab}(x) = -\frac{1}{2}\mathrm{Tr}\left[\{t^a,t^b\}\left(U_\mu(x)+U_\mu^\dagger(x)\right)\right] \\ A_\mu(x) = \frac{U_\mu(x)-U_\mu^\dagger(x)}{2} - \frac{1}{N}\mathrm{Tr}\frac{U_\mu(x)-U_\mu^\dagger(x)}{2}, \end{array} \tag{28}$$

in which $U_\mu(x)$ denotes a standard link variable[6], and e_μ is a unitary vector in direction μ. We define

$$\Delta_U = \sum_\mu \left(S_\mu^{ab}(x)\left(\delta_{x,y}-\delta_{y,x+e_\mu}\right) - S_\mu^{ab}(x-e_\mu)\left(\delta_{y,x-e_\mu}-\delta_{y,x}\right)\right). \tag{29}$$

The appearance of Δ_U as the appropriate discretisation of the usual Laplacian operator Δ is dictated by the gauge invariance of the original Yang-Mills action, which imposes that the standard ∇ operator be replaced by its *covariant* version and by the specific form – $\mathfrak{Re}\mathrm{Tr}(\sum_{\mathrm{links}} U^g)$ – of the functional to be minimized in order to fix the Landau gauge.
Then, multiplying M_{xy}^{ab} by $F^{(2)}(x,y)$ from the right, one obtains :

$$\begin{array}{l} \frac{1}{N_c^2-1}\mathrm{Tr}\Delta_U(y,z)F_{1\mathrm{conf}}^{(2)}(U;z,u) = \delta_{y,u} - \\ -\frac{f^{abc}}{2(N_c^2-1)}\left[A_\mu^c(y)F_{1\mathrm{conf}}^{(2)ba}(U;y+e_\mu,u) - A_\mu^c(y-e_\mu)F_{1\mathrm{conf}}^{(2)ba}(U;y-e_\mu,u)\right], \end{array} \tag{30}$$

This is an exact mathematical identity for each gauge configuration which must actually be fulfilled by our lattice data since our $F_{1\mathrm{conf}}^{(2)}$ are computed by means of an explicit inversion of the Faddeev-Popov operator. From this fact results an important feature which we wish to stress : *since eq. 30 is valid in any configuration, its consequences are free of any ambiguity originating from the presence of Gribov copies.* Upon averaging over the configurations one gets

$$\begin{array}{l} \frac{1}{N_c^2-1}\mathrm{Tr}\langle\Delta_U(y,z)F_{1\mathrm{conf}}^{(2)}(z,u)\rangle = \delta_{y,u} - \\ -\frac{f^{abc}}{2(N_c^2-1)}\left[\langle A_\mu^c(y)F_{1\mathrm{conf}}^{(2)ba}(U,y+e_\mu,u) - A_\mu^c(y-e_\mu)F_{1\mathrm{conf}}^{(2)ba}(U,y-e_\mu,u)\rangle\right] \end{array} \tag{31}$$

Of course, this averaging procedure depends on the way chosen to treat Gribov's problem : the particular set of configurations over which it is performed depends on the prescription which is adopted (choice of any local minimum of A^2, restriction to the fundamental modular region...) and, consequently, the Green functions will vary but *they will in any case satisfy the above equation.* Like in the continuum case, after setting y to zero, a Fourier transformation with respect to u gives:

$$\begin{array}{l} \frac{1}{N_c^2-1}\mathrm{Tr}\sum_u e^{ip\cdot u}\langle\Delta_U(0,z)F_{1\mathrm{conf}}^{(2)}(U,z,u)\rangle = 1 - \\ -i\sin(p_\mu)\frac{f^{abc}}{(N_c^2-1)}\langle A_\mu^c(0)\tilde{F}_{1\mathrm{conf}}^{(2)ba}(U,p)\rangle \end{array} \tag{32}$$

Note that although eqs. (30) and (31) have to be exactly verified by lattice data eq. (32) does only approximately (within statistical errors) since it relies on translational invariance, which could be guaranteed only if we used an infinite number of configurations.

[6]Note that the definition of A_μ given in (28) differs from the naïve one by a factor ig_0. This is the reason for the presence of i and the absence of g_0 in eq. (31) as compared to eq. (10).

Eq. (32) is a discretised version of (26). Therefore any lattice correlator, satisfying (32), should also satisfy (26) *up to non-zero lattice spacing effects*. Among the various sources for such effects the use of the specific Δ_U discretisation of the Laplacian operator in the l.h.s. deserves some comments. The gauge fields present in the $S^{ab}_{\mu}(x)$ terms in eq. (29) generate in Δ_U the so-called "tadpole" diagrams such as in fig. 3. According

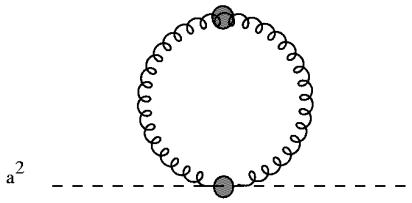

Figure 3: Example of the terms in the Schwinger-Dyson equation on the lattice.

to the philosophy developed by Lepage and Mackenzie in ref. ([23]) the tadpole contribution can be estimated by a mean field method. Using the average plaquette P (for $\beta = 6.0\, P \simeq 0.5937$) one predicts a tadpole correction factor $\propto P^{-(1/4)} \simeq 1.14$. These terms disappear in the continuum limit but they do so only very slowly : the tadpole corrections (1 - plaquette) vanish only as an inverse logarithm with the lattice spacing. This is to be contrasted with the corrections arising in the r.h.s which are expected to be of order a^2.

2.4.3 Checking the validity of the SD equation on the lattice

Since, as we have just mentionned, eqs. (30) and (31) are mathematical identities, there is in principle little –if any– to learn from a verification of eq. (32), except for the verification that our configurations are actually in the Landau gauge. On the other hand one thing we wish to be reassured about is the possible role of lattice artefacts in the discrepancies we have noticed.

We begin with a comparison of the continuum r.h.s of eq. (26) with the l.h.s. of (32). Both sides are plotted in fig. (4).

The agreement is impressive. Should we on the contrary use eq. (26) itself we observe a clear disagreement between the two sides of the equation. What we thus learn is that the major part of the discretization artefact comes from Δ_U. In fact, our lattice data show that $\Delta_U \simeq \Delta/1.16$ *almost independently of the momentum*, see fig. 5. This is in good agreement with the correction factor of 1.14 obtained from Lepage-Mackenzie's mechanism [23]. To conclude the tadpole effect explains almost all of the discrepancy observed when trying to verify (26). One can also understand why this discretisation artefact is so large : this is due to the slow logarithmic vanishing of the tadpole corrections.

It results from this discussion that the lattice artefacts cannot be blamed for the violation of the relation $\mathbf{R}_\alpha$ observed in fig. (1) : the tadpole effect has been seen to produce a corrective factor almost constant in p, thus unable to explain an error in the power behaviour.

2.4.4 Concluding remarks

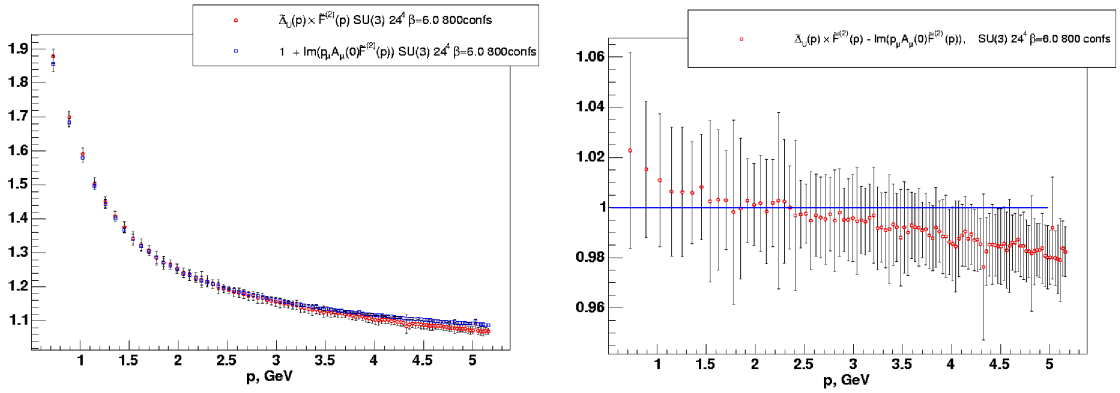

Figure 4: Check of the validity of the SD equation on the lattice. Left : $\frac{1}{N_c^2-1}\langle\Delta_U(p)\mathrm{Tr}\,\tilde{F}^{(2)}_{1\mathrm{conf}}(p)\rangle$ (circles) is plotted vs. $1+g_0\frac{p_\mu}{N_c^2-1}f^{abc}\langle A^c_\mu(0)\tilde{F}^{(2)ba}_{1\mathrm{conf}}(\mathcal{A},p)\rangle$ (squares). Right : $\frac{1}{N_c^2-1}\langle\Delta_U(p)\mathrm{Tr}\,\tilde{F}^{(2)}(p)\rangle - g_0\frac{p_\mu}{N_c^2-1}f^{abc}\langle A^c_\mu(0)\tilde{F}^{(2)ba}_{1\mathrm{conf}}(\mathcal{A},p)\rangle$ is compared to 1.

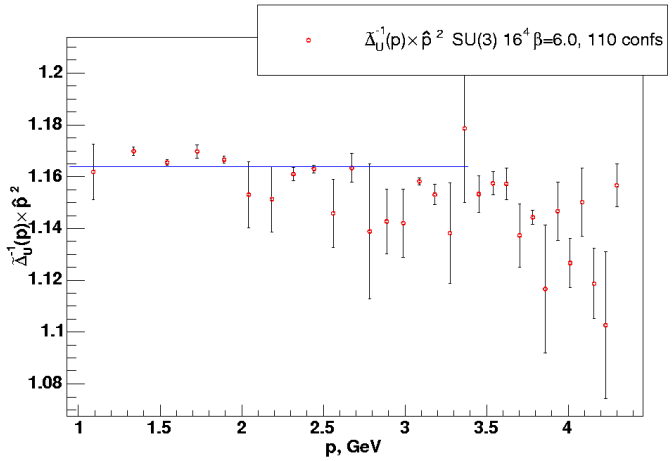

Figure 5: Lattice computation of Δ/Δ_U in Fourier space as a function of the momentum. The statistics is poor for technical reasons. Note also that the region above $\pi/2$ ($\sim 3\,\mathrm{GeV}$) is affected by strong discretisation effects.

We want to emphasize at this stage that our lattice data both *satisfy* the properly discretised SD equation and *violate* the relation $\mathbf{R}_\alpha$. The most likely way out we can think of is that the hypothesis $\alpha_\Gamma = 0$ is not verified, i.e. that H_1 is singular when all momenta are small. One more argument in favour of this explanation is provided by a direct numerical examination which shows that, in the eventuality of neglecting the momentum dependence of H_1, the SD equation is satisfied in the UV but badly violated in the IR. The results of this comparison are given in fig. 6 . The details of the method can be found in the appendix.

The possibility of a singular behaviour of H_1 in the infrared has already been considered by various authors, for example in ref. [21] in the framework of exact renormalization group equations. It is known from perturbation theory ([1]), that the sum $H_1 + H_2$ (cf eq. (9)) is exactly equal to 1 at $k = 0$ (this has been checked explicitly in perturbation theory up to fourth order in ref. [19]). This is the argument which is usually called for when advocating $\alpha_\Gamma = 0$. However it does not prevent the contribu-

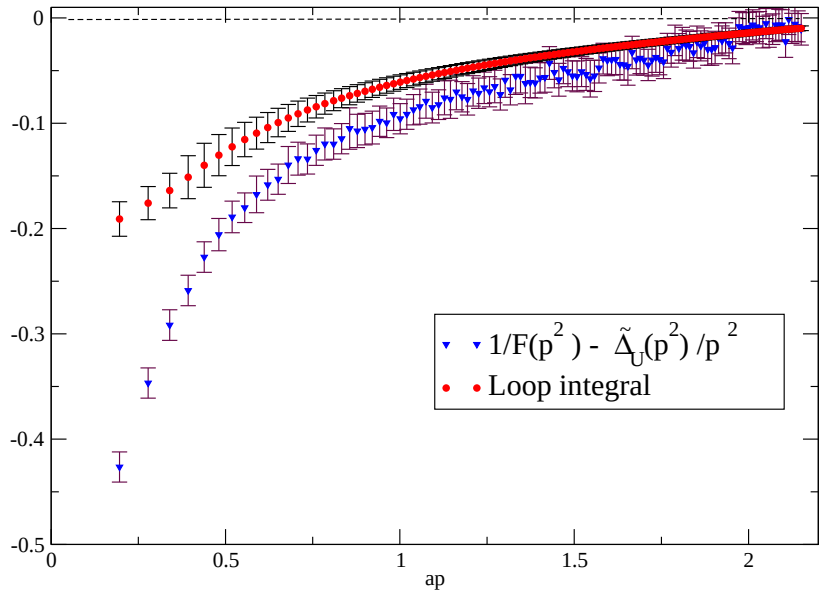

Figure 6: Testing the truncated ghost SD equation on the lattice. The data correspond to a $SU(3)$ simulation at $\beta = 6.4$ and $V = 32^4$, ($a^{-1} = 3.66$ GeV).

tions of the scalar function b to H_1 and H_2, which cancel out in the sum, from being singular in this limit. Actually, from dimensional considerations, one concludes that b must be of dimension -2. At $k = 0$ the only dimensional quantity involved (at the perturbative level) is q, which means $b(q, 0; -q) \propto 1/q^2$. This singularity is removed by the kinematical factor in front of b in H_1 and H_2, but this would no longer be the case for $k \neq 0$ if one had more generally $b(q, k; -q - k) \propto 1/q^2$. *In any case our results appear to plead in favour of a divergent ghost-ghost-gluon vertex in the infrared domain.*

3 Slavnov-Taylor identity and the infrared behaviour of the gluon propagator

Another non-perturbative relation that can be exploited is the Slavnov-Taylor identity. It can be used to constrain (under some hypotheses) the infrared exponent for the gluon dressing function. In the preceding section we have explored the consequences of the very strong assumption that H_1 is regular when all its arguments go to zero and we have shown that this assumption is not tenable when the lattice data are taken into account. We shall now make the weaker hypothesis that the scalar factors present in the decomposition (4) of the ghost-ghost-gluon vertex are regular when one of their arguments go to zero while the others are kept finite and exploit the Slavnov-Taylor identity under this assumption to derive constraints on α_F and α_G.

The Slavnov-Taylor ([1]) identity for the three-gluon function reads

$$\begin{aligned} p^\lambda \Gamma_{\lambda\mu\nu}(p,q,r) = \frac{F(p^2)}{G(r^2)}(\delta_{\lambda\nu} r^2 - r_\lambda r_\nu)\widetilde{\Gamma}_{\lambda\mu}(r,p;q) - \\ - \frac{F(p^2)}{G(q^2)}(\delta_{\lambda\mu} q^2 - q_\lambda q_\mu)\widetilde{\Gamma}_{\lambda\nu}(q,p;r). \end{aligned} \tag{33}$$

One then takes the limit $r \to 0$ while keeping q and p finite. The tensor structure of $\widetilde{\Gamma}_{\mu\nu}(p,k;q)$ has been recalled in eq. (4). We adopt the following notations for particular kinematic configurations:

$$\begin{aligned} &a_3(p^2) = a(-p,p;0) \\ &a_1(p^2) = a(0,-p;p), \quad b_1(p^2) = b(0,-p;p), \quad d_1(p^2) = d(0,-p;p). \end{aligned} \tag{34}$$

In the present case of one zero momentum the three-gluon vertex may be parameterised in the general way as ([19])

$$\Gamma_{\mu\nu\rho}(p,-p,0) = (2\delta_{\mu\nu}p_\rho - \delta_{\mu\rho}p_\nu - \delta_{\rho\nu}p_\mu)\, T_1(p^2) - \left(\delta_{\mu\nu} - \frac{p_\mu p_\nu}{p^2}\right) p_\rho T_2(p^2) + p_\mu p_\nu p_\rho T_3(p^2). \tag{35}$$

Now, exhibiting the dominant part of each term of eq.(33) we obtain:

$$\begin{aligned} T_1(q^2)(q_\mu q_\nu - q^2\delta_{\mu\nu}) + q^2 T_3(q^2) q_\mu q_\nu + \eta_{1\mu\nu}(q,r) = \\ \tfrac{F((q+r)^2)}{G(r^2)}\Big[(a_1(q^2) + r_1(q,r))(\delta_{\mu\nu}r^2 - r_\mu r_\nu)1 + +(b_1(q^2) + r_2(q,r))q_\mu(r^2 q_\nu - q.r r_\nu) \\ +(b_1(q^2) + d_1(q^2) + r_3(q,r))r_\mu(r^2 q_\nu - q.r r_\nu)\Big] + \\ + \tfrac{F((q+r)^2)}{G(q^2)}\Big[a_3(q^2)(q_\mu q_\nu - q^2\delta_{\mu\nu}) + \eta_{2\mu\nu}(q,r)\Big] \end{aligned} \tag{36}$$

where $r_{1,2,3}$ and $\eta_{1,2}$ verify

$$\begin{aligned} &\lim_{r\to 0} r_1(q,r) = \lim_{r\to 0} r_2(q,r) = \lim_{r\to 0} r_3(q,r) = 0 \\ &\lim_{r\to 0} \eta_{1\mu\nu}(q,r) = \lim_{r\to 0} \eta_{2\mu\nu}(q,r) = 0 \end{aligned} \tag{37}$$

Identifying the leading terms of the scalar factors multiplying the tensors $q_\mu q_\nu$ and $q_\mu q_\nu - q^2\delta_{\mu\nu}$ we obtain the usual relations ([19]):

$$\begin{aligned} &T_1(q^2) = \tfrac{F(q^2)}{G(q^2)} a_3(q^2) \\ &T_3(q^2) = 0. \end{aligned} \tag{38}$$

Using these relations we see that Eq.(36) implies:

$$\lim_{r\to 0} \frac{F(p^2)}{G(r^2)}\Big[a_1(q^2)(r^2\delta_{\mu\nu} - r_\mu r_\nu) + b_1(q^2)(r^2 q_\mu q_\nu - r.q q_\mu r_\nu)\Big] = 0 \tag{39}$$

Thus one sees that if $a_1(q^2) \neq 0$ or $b_1 \neq 0$ (and, indeed, one knows from perturbation theory that at large momenta $a_1 = 1$, cf. [1,19]) (33) can only be compatible with the parameterisation (5) if

$$\alpha_G < 1. \tag{40}$$

We can also, instead of letting $r \to 0$, take the limit $p \to 0$ of Eq.(33) as is done in [19]. The dominant part of the l.h.s. of (33) is :

$$(2\delta_{\mu\nu}p.q - p_\mu q_\nu - p_\nu q_\mu)T_1(q^2) - (\delta_{\mu\nu} - \frac{q_\mu q_\nu}{q^2})p.qT_2(q^2) + p.qq_\mu q_\nu T_3(q^2)$$

The r.h.s. is the product of $F(p^2)$ with an expression of at least first order in p. T_1 and T_2 being different from zero we can conclude in this case that $\alpha_F \leq 0$.

Let us repeat here that all these considerations are valid only if all scalar factors of the ghost-ghost-gluon and three-gluons vertices are regular functions when one momentum goes to zero while the others remain finite. Under those hypotheses one obtains important constraints on the gluon and ghost propagators - namely that they are divergent in the zero momentum limit.

3.1 Lattice results

The results for α_G and α_F from lattice simulations are presented in figs. (1) and (7). We present in Table 2 the values of the coefficients for a fit of the form[7] $(q^2)^\alpha(\lambda + \mu q^2)$.

Group	Volume	β	α_G	α_F
SU(2)	48^4	2.3	1.004 ± 0.015	-0.087 ± 0.015
SU(2)	32^4	2.3	0.968 ± 0.011	-0.109 ± 0.014
SU(3)	32^4	5.75	0.864 ± 0.016	-0.153 ± 0.022

Table 2: Summary of the fitting parameters for the F and G functions

The fits have been performed without using the point $p^2 = 0$ even in the case of the gluon propagator where it is known. Its inclusion would have *forced* α_G to be equal to 1. In any case one sees on fig. 7 that the point at $p^2 = 0$ available in the $SU(2), 32^4$ case is compatible with the fit.

For SU(2) and the larger volume the value obtained for α_G is compatible with 1. The situation is less clear for SU(3), but in this case data with the larger volume (48^4) are lacking. Moreover we have to take into account our experience from previous studies of the gluon propagator where we have always observed that the gluon propagator goes continuously to a finite limit in the infrared region. A very detailed study of the gluon dressing function and specially of its volume dependence at $k = 0$ has been performed by Bonnet et al. (cf ref. [30]). This study shows that a value $\alpha_G = 1$ is compatible with the data (the dressing function shows no signal of discontinuity in the neighbourhood of zero) and that no pathology shows up as the volume goes to infinity.

We conclude that lattice data seem to contradict Zwanziger's result ($G^{(2)}(0) = 0$), [22] and most probably also the predictions derived from the Slavnov-Taylor identity ($G^{(2)}(0)$ infinite). Like in the preceding section a possible way out of this contradiction could consist in dropping the regularity assumptions which have been made in the course of the proof.

[7] A term of the form μq^2 is clearly needed in order to describe a situation like the one in fig. (7 left) where $G^{(2)}(p^2)$ seems to go to a finite limit when p goes to zero

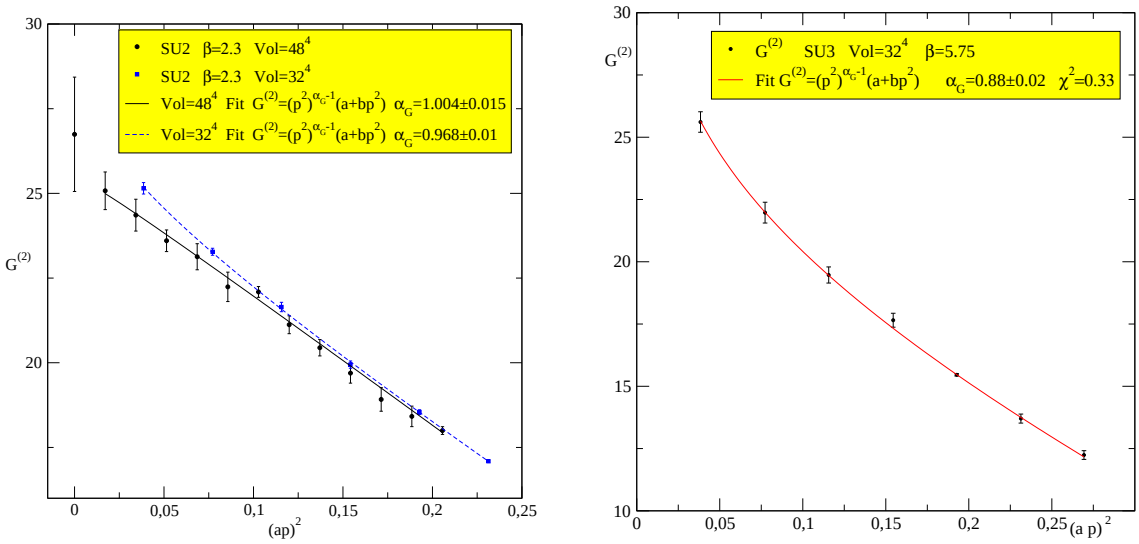

Figure 7: $G^{(2)}(p^2)$ from lattice simulation for $SU(2)$ (left) and $SU(3)$ (right) . $\beta_{\mathrm{SU(2)}} = 2.3$ and $\beta_{\mathrm{SU(3)}} = 5.75$. the volumes are 32^4 and48^4 for $SU(2)$ and 32^4 for $SU(3)$.

4 Discussion and Conclusions

4.1 Discussion of the validity of SD and ST equations in the infrared

Schwinger-Dyson equations and Slavnov-Taylor identities are valid non-perturbatively. However some care is needed mainly due to Gribov ambiguities in the gauge fixing procedure. One needs a well defined QCD partition function for a given gauge (in the following we concentrate on Landau gauge). Many different non-perturbative prescriptions for the quantisation of non-abelian theories have been suggested : integration only over the absolute minima of the $\int A^2$ functional (Gribov fundamental modular region) [22], summing of copies with signed Faddeev-Popov determinant [9], stochastic quantisation [31], etc. All these prescriptions correspond to different valid gauge fixing procedures.

In lattice numerical simulations two main methods are of practical use: The algorithm which minimises the functional is stopped at its first solution, which is a local minimum, or one takes the smallest local minimum among a given number of trials on the same gauge orbit. One is sure to be inside the Gribov region, never to be inside the fundamental modular region.

The question is whether SD and ST relations are valid in these gauge fixing schemes. It is argued in ([4]) that the Schwinger - Dyson equations are valid under different quantisation prescriptions provided that the Faddeev-Popov determinant vanishes on the boundary of the integration domain. However, the partition functions will differ and hence, the Green functions will be in general different solutions of the the SD equations.

The Slavnov-Taylor identities may be derived from the QCD partition function

using the gauge invariance of the action and stating that the gauge fixed path integral is invariant after a change of variables which corresponds to a gauge transformation. It is then clear that the Slavnov-Taylor identities remain valid whichever gauge fixing procedure has been followed. However this proof has to be taken with care in the presence of singularities of the partition function or of Green functions.

One more general comment is in order. As we have already stated, no Green function with a vanishing ghost momentum can be defined on the lattice since the zero modes of the Faddeev-Popov operator are discarded. For the same reason no source term for the zero mode ghost field is allowed. More generally we do not know of any non perturbative way to define such Green functions. We cannot prove that this means a divergence of the Green functions with one ghost momentum going to zero, but we can suspect that it is the case as lattice indicates for the ghost propagator [8]. Indeed the close-to-zero modes of the Faddeev-Popov operator are strongly influenced by the Gribov horizon and, for sure, very different from any perturbative result. This casts also some doubt about the use of ST identities or SD equations in the case of a zero ghost momentum.

4.2 Conclusions

We have tried in this work to put together various inputs in order to clarify our understanding of the infrared behaviour of the pure Yang-Mills Green functions. Our findings can be summarised as follows :

1. The lattice Green functions contradict the common *lore* according to which $2\alpha_F + \alpha_G = 0$. The present situation is that $2\alpha_F+\alpha_G > 0$, i.e., the product $F^2(k^2)\, G(k^2)$ tends to 0 for $k \to 0$. From what we observe concerning the evolution of the curves with the size of the lattice, it is difficult to imagine how a further increase of the volume could eventually revert this tendency.

2. The result $2\alpha_F + \alpha_G = 0$ ($\mathbf{R}_\alpha$) which is contradicted by lattice data, is usually claimed to be derived from the ghost SD equation. Our results seem to cast some doubt on the validity of these derivations, based on the assumption of a trivial ghost-ghost-gluon vertex ("naïve approximation"). Indeed, we do verify that the *properly discretised* SD ghost equation on the lattice is well satisfied. We conclude that the lattice data seem to prove that this "naïve approximation" is invalid, and that there exists in the ghost-ghost-gluon vertex a non-perturbative infrared singularity of the form $(k^2)^{\alpha_\Gamma}$ which has been neglected in the standard analysis and which leads to the replacement of $\mathbf{R}_\alpha$ by $2\alpha_F+\alpha_G+\alpha_\Gamma = 0$ ($\alpha_\Gamma < 0$).

3. Regarding the ghost correlator it results from its very definition that it cannot be defined at zero momentum. Its lattice values at low momentum appear to be in favour of a divergent dressing function ($\alpha_F < 0$), as is also suggested by the above theoretical arguments. However the divergence is much slower ($\alpha_F \in [-.15, -.1]$) than what is usually reported. This is in agreement with the conclusions one can draw from the Slavnov Taylor identity.

4. In relation with points 2) and 3) above it is worth insisting on the fact that the Schwinger -Dyson equation by itself is not sufficient to determine the behaviour of

[8] Notice that we cannot claim anything about the behaviour of vertex functions when one ghost momentum goes to zero.

the ghost-propagator and of the ghost-ghost-gluon vertex. Different treatments of the Gribov copies lead to different infrared solutions (se also ref [17] in this respect), *all of which fulfill the SD equation.*

5. As for the gluon propagator the situation is much less clear. Three sources of information are available and give contradictory results.

   - The Slavnov Taylor identity, supplemented by regularity assumptions for the ghost-ghost-gluon vertex functions, points towards a *divergent* infrared behaviour.
   - Our lattice data indicate a finite limit when the momentum goes to zero. This trend is very clear in the $SU(2)$ case although less compelling for $SU(3)$. The fit has been performed by excluding the point at $p = 0$ but the latter, when known, is compatible with the extrapolated value. These results agree with the ones of our previous studies as well as with the findings of the other lattice groups who have studied this matter ([30]) which include the point $p = 0$ and impose therefore $\alpha_G = 1$.
   - Zwanziger's result [22] states that the gluon propagator vanishes at k=0 but a fully satisfactory proof of a *continuous* vanishing as $k \to 0$ is still lacking.

   We are unable for the moment to settle this point in a totally unambiguous way.

This set of conclusions raises some questions. First of all further studies are still under way in order to fix the issues related to point 4). As to point 2), a direct lattice study of the ghost-ghost-gluon vertex at low momenta is desirable, although difficult. Such a study has recently been performed for $SU(2)$ in a specific kinematical situation (zero-momentum gluon) ([32]). The precise relevance of this special case to the points we have considered remains to be clarified.

Note added

After the completion of this work we realised that the particular situation ($\alpha_F = 0$) which we have mentionned in the fourth column of table 1 but not fully investigated might provide a good agreement with the lattice data while complying with the constraints stemming from the SD equation. This possibility is discussed in a further publication ([35]) . Let us stress that this solution too is compatible with the non-vanishing of $2\alpha_F + \alpha_G$.

5 Acknowledgements

We wish to thank N. Wschebor and U. Ellwanger for illuminating discussions.

6 Appendix: Testing the naive approximation of the ghost SD equation

The simplest approximation of the ghost SD equation (10) corresponds to the case $H_1(q,k) = 1\,\forall q,k$:

$$\frac{1}{F(k)} = 1 + \frac{g_0^2 N_c}{k^2}\int \frac{d^4q}{(2\pi)^4}\Big(\frac{F(q^2)G((k-q)^2)}{q^2(k-q)^2}\frac{(k\cdot q)^2 - k^2q^2}{(q-k)^2}\Big]\Big) \tag{41}$$

Strictly speaking this equation, written in this way, is meaningless since it involves UV divergent quantities but a corresponding meaningful renormalized version can be given (see the caveats about eq (7) in subsection (2.1)). We want to check whether lattice propagators satisfy it. According to perturbation theory, it should be true at large k. Lattice propagators are discrete functions, and thus one has to handle the problem of the numerical evaluation of the loop integral I in (41). Let us express the integrand in terms of q^2 and $(k-q)^2$

$$I = \int \frac{d^4q}{(2\pi)^4}\frac{F^2(q)G(k-q)}{q^2(k-q)^2}\Big[\frac{(k-q)^2}{4} + \frac{(k^2)^2 + (q^2)^2 - 2k^2q^2}{4(k-q)^2} - \frac{q^2+k^2}{2}\Big]. \tag{42}$$

Then we write

$$I = I_1 + I_2 + I_3 + I_4 + I_5 + I_6,$$

each I_i corresponds to one term in (42).

All these integrals have the form

$$I_i = C_i(k)\int \frac{d^4q}{(2\pi)^4} f_i(q)h_i(k-q).$$

The convolution in the r.h.s. is just the Fourier transform of the product at the same point in configuration space:

$$\int \frac{d^4q}{(2\pi)^4} f_i(q)h_i(k-q) = \mathrm{F}_+\Big(\mathrm{F}_-(f_i)[x]\mathrm{F}_-(h_i)[x]\Big)(k),$$

where $\mathrm{F}_-(\hat{f})(x)$ is an inverse and $\mathrm{F}_+(f)(k)$ a direct Fourier transform. Thus, in order to calculate the integral I from discrete lattice propagators one proceeds as follows:

1. calculate $\{f_i\}(p)$ and $\{h_i\}(p)$ as functions of $F(p), G(p), p^2$ for all i
2. apply the inverse Fourier transform F_- to all these functions and get $f_i(x)$ and $h_i(x)$
3. compute the product at the same point $f_i(x)\cdot h_i(x)$
4. apply the direct Fourier transform F_+ to $f_i(x)\cdot h_i(x)$

The calculation of Fourier transforms involves a Hankel transformation which is numerically evaluated by means of a Riemann sum

$$f(r) = (2\pi)^{-2}\|r\|^{-2}\sum_{i=1}^{N} J_1(r\rho_i)\rho_i^2\frac{\hat{f}[\rho_i] + \hat{f}[\rho_{i-1}]}{2}(\rho_i - \rho_{i-1}), \qquad \rho_0 = 0. \tag{43}$$

The inverse transformation is done in the similar way. In practice, because of the lattice artefacts which become important at large ρ the summation has to be restricted to $\rho < \rho_{max} \simeq 2.2$ instead of the "ideal" value 2π.

Errors There are three important sources of errors : statistical Monte-Carlo errors for $F(q^2)$ and $G(q^2)$, the bias due to the integral discretization and the truncation of the ρ-summation to values lower than ρ_{max}. The second one is dominated by the neglected contribution coming from the UV cut-off of the integral (the integration is performed on some ball $B(0,L)$ instead of $\mathbb{R}^4$). Let us estimate the error on the Fourier transform of the product in such a case:

$$\mathrm{F}_+(f(x)g(x))(k) = \int_{B(0,L)} d^4p d^4q \delta_\epsilon(k-p-q)\hat{f}(p)\hat{g}(q), \tag{44}$$

where the $\epsilon-$approximation to delta function is $\delta_\epsilon(p) = \int_{B(0,L)} d^4x e^{i(x,p)}$. Considering ϵ small enough we can integrate on q around the point $(k-p)$, obtaining finally:

$$(f \star g)_L \approx (f \star g)_\infty + \mathrm{Vol}(B(0,\epsilon(L))) \cdot (f \star \nabla g)_\infty$$

This gives us an estimation of the error coming from the UV cut-off. As for the last source of error, it may be neglected because of the following argument : the integral is logarithmically divergent, therefore the neglected behaves as $\log\left(\frac{2\pi}{La}\right) - \log\left(\frac{\rho_{max}}{La}\right) = \log(\frac{2\pi}{\rho_{max}})$. Thus it remains finite as a goes to zero and gets smaller and smaller as compared to the part actually computed.

Results: We still have to face the same problem we have already encountered in section (2.4.3), namely that the lattice Faddeev-Popov operator involves the non trivial discretisation Δ_U of the Laplacian operator. This is taken into account by means of the substitution of $\widetilde{\Delta_U}(p^2)/p^2$ to the "1" term in the l.h.s of equation (41) We present on (Fig. 6) the result of the numerical integration described above. We have chosen for this purpose the data set from the simulation with the gauge group $SU(3)$ at $\beta = 6.4, V = 32^4$. One sees that the equality is achieved at large momenta, but in the infrared the naive approximation of the ghost SD equation fails.

References

[1] J. C. Taylor, Nuclear Physics B Volume 33, Issue 2 , 1 November 1971, Pages 436-444
A. A. Slavnov, Theor. Math. Phys. **10** (1972) 99 [Teor. Mat. Fiz. **10** (1972) 153].

[2] Ph. Boucaud, J.P. Leroy, A. Le Yaouanc, A.Y. Lokhov , J. Micheli, O. Pène, J. Rodríguez-Quintero and C. Roiesnel [arXiv:hep-lat/0506031]

[3] R. Alkofer and L. von Smekal, Phys. Rept. **353** (2001) 281 [arXiv:hep-ph/0007355].

[4] D. Zwanziger, Phys. Rev. D **65** (2002) 094039 [arXiv:hep-th/0109224].

[5] J. C. R. Bloch, Few Body Syst. **33** (2003) 111 [arXiv:hep-ph/0303125].

[6] J. Kato, [arXiv:hep-th/0401068]

[7] K. Kondo, Nucl. Phys. Proc. Suppl. **129** (2004)715, [arXiv:hep-lat/0309142].

[8] K. Kondo, [arXiv:hep-th/0303251].

[9] L. Baulieu, Phys. Rept. **129** (1985) 1.

[10] T. Kugo and I. Ojima, Prog. Theor. Phys. Suppl. **66** (1979) 1.

[11] S. Furui and H. Nakajima, [arXiv:hep-lat/0410038.]

[12] H. Nakajima and S. Furui, Nucl. Phys. Proc. Suppl. **141** (2005) 34 [arXiv:hep-lat/0408001].

[13] S. Furui and H. Nakajima, [arXiv:hep-lat/0403021].

[14] A. Sternbeck, E.-M. Ilgenfritz, M. Mller-Preussker and A. Schiller, Nucl. Phys. Proc. Suppl. **140** (2005) 653 [arXiv:hep-lat/0409125].

[15] A. Sternbeck, E.- M. Ilgenfritz, M. Mueller-Preussker, A. Schiller AIP Conference Proceedings **756** (2005) 284 [arXiv:hep-lat/0412011].

[16] A. Sternbeck, E.- M. Ilgenfritz, M. Mueller-Preussker, A. Schiller [arXiv:hep-lat/0506007].

[17] T. D. Bakeev, E. M. Ilgenfritz, V. K. Mitrjushkin and M. Mueller-Preussker, Phys. Rev. D **69** (2004) 074507 [arXiv:hep-lat/0311041].

[18] P. Boucaud *et al.*, JHEP **0304** (2003) 005 [arXiv:hep-ph/0212192].

[19] K. G. Chetyrkin and A. Retey, [arXiv:hep-ph/0007088].

[20] A. I. Davydychev, P. Osland and O. V. Tarasov, Phys. Rev. D **54**, 4087 (1996) [Erratum-ibid. D **59**, 109901 (1999)] [arXiv:hep-ph/9605348].

[21] U. Ellwanger, M. Hirsch and A. Weber, Eur. Phys. J. **C1**, 1998, 563-578, [arXiv:hep-ph/9606468].

[22] D. Zwanziger, Nucl. Phys. B **364** (1991) 127.

[23] G. P. Lepage and P. Mackenzie, Phys. Rev. D48, (1993) 2250. [arXiv:hep-lat/9209022].

[24] C. S. Fischer and R. Alkofer, Phys. Rev. D **67** (2003) 094020 [arXiv:hep-ph/0301094].

[25] R. Alkofer, W. Detmold, C. S. Fischer and P. Maris, Phys. Rev. D **70** (2004) 014014 [arXiv:hep-ph/0309077].

[26] J. M. Pawlowski, D. F. Litim, S. Nedelko and L. von Smekal, Phys. Rev. Lett. **93** (2004) 152002 [arXiv:hep-th/0312324]; C. S. Fischer and H. Gies, arXiv:hep-ph/0408089.

[27] D. Zwanziger, Phys. Rev. D **69** (2004) 016002 [arXiv:hep-ph/0303028].

[28] C. Lerche and L. von Smekal, Phys. Rev. D **65** (2002) 125006 [arXiv:hep-ph/0202194].

[29] L. von Smekal, R. Alkofer and A. Hauck, Phys. Rev. Lett. **79** (1997) 3591, [arXiv:hep-ph/9705242]; Annals Phys. **267** (1998) 1 [Erratum-ibid. **269**, 182 (1998)] [arXiv:hep-ph/9707327].

[30] F. D. R. Bonnet, P. O. Bowman, D. B. Leinweber, A. G. Williams, J. M. Zanotti, Phys. Rev. D **64** (2001) 034501 [arXiv: hep-lat/0101013]

[31] J. Zinn-Justin and D. Zwanziger, Nucl. Phys. B **295** (1988) 297.

[32] A. Cucchieri, T. Mendes and A. Mihara, [arXiv:hep-lat/0408034]

[33] R. Alkofer, C. S. Fischer and F. J. Llanes-Estrada, Phys. Lett. B **611**, 279 (2005) [arXiv:hep-th/0412330].

[34] W. Schleifenbaum, A. Maas, J. Wambach and R. Alkofer, Phys. Rev. D **72**, 014017 (2005) [arXiv:hep-ph/0411052].

[35] Ph. Boucaud, Th. Brüntjen, J.P. Leroy, A. Le Yaouanc, A.Y. Lokhov , J. Micheli, O. Pène and J. Rodríguez-Quintero [arXiv:hep-ph/0604056], to appear in JHEP.

Annexe D

Scaling properties of the probability distribution of lattice Gribov copies

submitted to Phys. Rev. D

hep-lat/0511049

Scaling Properties of the Probability Distribution of Lattice Gribov Copies

A.Y. Lokhov[a], O. Pène[b], C. Roiesnel[a]

[a] Centre de Physique Théorique[1] de l'École polytechnique
F91128 Palaiseau cedex, France
[b]Laboratoire de Physique Théorique et Hautes Energies[2]
Université de Paris XI, Bâtiment 211, 91405 Orsay Cedex, France

Abstract

We study the problem of the Landau gauge fixing in the case of the $SU(2)$ lattice gauge theory. We show that the probability to find a lattice Gribov copy increases considerably when the physical size of the lattice exceeds some critical value $\approx 2.75/\sqrt{\sigma}$, almost independent of the lattice spacing. The impact of the choice of the copy on Green functions is presented. We confirm that the ghost propagator depends on the choice of the copy, this dependence decreasing for increasing volumes above the critical one. The gluon propagator as well as the gluonic three-point functions are insensitive to choice of the copy (within present statistical errors). Finally we show that gauge copies which have the same value of the minimisation functional ($\int d^4x (A^a_\mu)^2$) are equivalent, up to a global gauge transformation, and yield the same Green functions.

CPHT-RR 065.1105
LPT-Orsay/05-76

1 Introduction

The question of the quantisation in the infrared of a non-Abelian gauge theory is very important for the understanding of diverse non-perturbative phenomena. The main problem that arises while performing the quantisation in the covariant gauge is the problem of the non-uniqueness of the solution of the equation specifying the gauge-fixing condition, that was pointed out by Gribov [1]. In fact, the solution is unique for fields having small magnitude. A solution proposed in [1] consists in restricting the (functional) integration over gauge fields in the partition function to the region inside the so called Gribov horizon (the surface, closest to the trivial field $\mathcal{A}_\mu = 0$, on which the Faddeev-Popov determinant vanishes).

The Gribov's quantisation prescription is explicitly realised in the lattice formulation. Indeed, the procedure of Landau gauge fixing on the lattice (see [2] for a review) constraints all the eigenvalues of the Faddeev-Popov operator to be positive. Thus lattice

[1]Unité Mixte de Recherche 7644 du Centre National de la Recherche Scientifique
[2]Unité Mixte de Recherche 8627 du Centre National de la Recherche Scientifique

gauge configurations in Landau gauge are located inside the Gribov region, and all calculations on the lattice are done within the Gribov's quantisation prescription. But we also know that this is not enough - the gauge is not uniquely fixed even in this case, and there are secondary solutions (Gribov copies) inside the Gribov region ([3],[4]). The smaller region free of Gribov copies is called the fundamental modular region ([3],[5], [6]). On a finite lattice the gauge may be fixed in a unique way, but that reveals to be technically difficult (cf. the following section).

The quantities that are sensitive to the choice of the infrared quantisation prescription are Green functions. A lot of work regarding the influence of Gribov copies on lattice ghost and gluon propagators in the case of $SU(2)$ and $SU(3)$ gauge groups has already been done ([7],[8],[9],[10],[11],[12],[13]). Summarising the results, the infrared divergence of the ghost propagator is lessened when choosing Gribov copies closer to the fundamental modular region, and the gluon propagator remains the same (within today's statistical precision). In this paper we confirm these results in the case of the $SU(2)$ gauge group, and present a study of the influence of Gribov copies on the three-gluon vertex in symmetric and asymmetric kinematic configurations. We also discuss in details the structure of minima of the gauge-fixing functional. The authors of [8] reported that the number of minima of the gauge-fixing functional decrease with the β parameter (the bare lattice coupling). We perform a thorough analysis of the volume dependence of this phenomenon. We define a probability to find a lattice Gribov copy, and our computation shows that this probability increases considerably when the physical size of the lattice exceeds some critical value, around $2.75/\sqrt{\sigma}$, where σ is the string tension.

2 Non-perturbative Landau gauge fixing on the lattice

A lattice gauge configuration $U_{\mathcal{C}_0}$ generated during the simulation process is not gauge-fixed. One has to perform a gauge transformation $\{u(x)\}$ on it in order to move it along its gauge orbit up to the intersection with the surface $f_L\left[U_\mu(x)\right] = 0$ specifying the Landau gauge-fixing condition. But there is no need to have an explicit form of $\{u(x)\}$. Instead we do an iterative minimisation process that starts at $U_{\mathcal{C}_0}$ and converges to the gauge fixed configuration $U^{(u)}_{\mathcal{C}}$ Let us first illustrate it on the example of the Landau gauge in the continuum limit. For every gauge field $\mathcal{A}$ one defines a functional

$$F_{\mathcal{A}}[u(x)] = -\mathrm{Tr}\int d^4x \mathcal{A}^{(u)}_\mu(x)\mathcal{A}^{(u)}_\mu(x) = -||\mathcal{A}^{(u)}||^2, \quad u(x) \in SU(N_c). \tag{1}$$

Expanding it up to the second order around some group elements $\{u_0(x)\}$ we have (writing $u = e^X u_0$, $X \in \mathfrak{su}(N_c)$)

$$F_{\mathcal{A}}[u(x)] = F_{\mathcal{A}}[u_0(x)] + 2\int d^4x \mathrm{Tr}\left(X\partial_\mu \mathcal{A}^{(u_0)}_\mu\right) + \int d^4x \mathrm{Tr}\left(X^\dagger \mathcal{M}_{\mathrm{FP}}\left[\mathcal{A}^{(u_0)}\right] X\right) + \dots . \tag{2}$$

Note that the quadratic form defining the second order derivatives is the Faddeev-Popov operator. Obviously, if u_0 is a local minimum we have a double condition

$$\begin{cases} \partial_\mu \mathcal{A}^{(u_0)}_\mu = 0 \\ \mathcal{M}_{\mathrm{FP}}\left[\mathcal{A}^{(u_0)}\right] \quad \text{is positive definite.} \end{cases} \tag{3}$$

Hence, the minimisation of the functional (1) allows not only to fix the Landau gauge, but also to obtain a gauge configuration inside the Gribov horizon (cf. Figure 1). On the

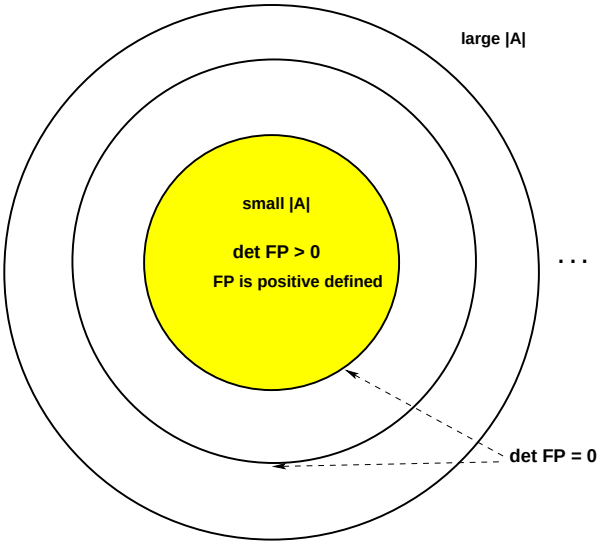

Figure 1: Restriction of the integration domain in the partition function to the Gribov region (hatched), and the Gribov horizon. “FP" is the Faddeev-Popov operator.

lattice, the discretised functional (1) reads

$$F_U[u] = -\frac{1}{V}\mathfrak{Re}\mathrm{Tr}\sum_{x,\mu} u(x)U_\mu(x)u^\dagger(x+e_\mu), \tag{4}$$

where $U_\mu(x)$ is the standard gauge link variable. Then at a local minimum u_0 we have a discretised Landau gauge fixing condition

$$\sum_\mu \left(\mathcal{A}_\mu^{(u_0)}\left(x+\frac{e_\mu}{2}\right) - \mathcal{A}_\mu^{(u_0)}\left(x-\frac{e_\mu}{2}\right)\right) = 0. \tag{5}$$

that we write in a compact form $\nabla_\mu \mathcal{A}_\mu^{(u_0)} = 0$. Here

$$\mathcal{A}_\mu\left(x+\frac{e_\mu}{2}\right) = \frac{U_\mu(x) - U_\mu^\dagger(x)}{2}. \tag{6}$$

The second derivative (the equivalent of the second-order term in (2)) can be written as

$$\frac{d^2}{ds^2}F_U\left[u(s,x)\right] = -\frac{1}{V}\left(\omega, \nabla_\mu \mathcal{A}'_\mu\right) \tag{7}$$

where

$$\mathcal{A}'_\mu = \frac{1}{2}\left(-\omega(x)U_\mu^{(u)}(x) + U_\mu^{(u)}(x)\omega(x+e_\mu) + \omega(x+e_\mu)U_\mu^{(u)\dagger}(x) - U_\mu^{(u)\dagger}(x)\omega(x)\right). \tag{8}$$

This defines a quadratic form $\left(\omega, \mathcal{M}_{FP}^{\mathrm{lat}}[U]\omega\right)$ where the operator $\mathcal{M}_{FP}^{\mathrm{lat}}[U]$ is the lattice version of the Faddeev-Popov operator ([14]). It reads

$$\begin{aligned}\left(\mathcal{M}_{FP}^{\mathrm{lat}}[U]\omega\right)^a(x) = \frac{1}{V}\sum_\mu \Bigg\{ & S_\mu^{ab}(x)\left(\omega^b(x+e_\mu) - \omega^b(x)\right) - (x \leftrightarrow x-e_\mu) + \\ & + \frac{1}{2}f^{abc}\left[\omega^b(x+e_\mu)A_\mu^c\left(x+\frac{e_\mu}{2}\right) - \omega^b(x-e_\mu)A_\mu^c\left(x-\frac{e_\mu}{2}\right)\right]\Bigg\},\end{aligned} \tag{9}$$

where

$$S_\mu^{ab}(x) = -\frac{1}{2}\mathrm{Tr}\left(\left\{t^a, t^b\right\}\left(U_\mu(x) + U_\mu^\dagger(x)\right)\right). \tag{10}$$

It is straightforward to check that in the continuum limit $a \to 0$ one finds the familiar expression of the Faddeev-Popov operator.

For the Landau gauge fixing in our numerical simulation we have used the Overrelaxation algorithm with $\omega = 1.72$. We stop the iteration process of the minimising algorithm when the following triple condition is fullfield:

$$\begin{aligned}
\frac{1}{V(N_c^2-1)}\sum_{x,\mu}\mathrm{Tr}\left[\left(\nabla_\mu \mathcal{A}_\mu^{(u_0)}\right)\left(\nabla_\mu \mathcal{A}_\mu^{(u_0)}\right)^\dagger\right] &\leq \Theta_{\max_x |\partial_\mu A_\mu^a|} = 10^{-18} \\
\frac{1}{V(N_c^2-1)}\left|\sum_x \mathrm{Tr}\left[u^{(n)}(x) - \mathbb{I}\right]\right| &\leq \Theta_{\delta u} = 10^{-9} \\
\forall a, t_1, t_2 \quad \left|\frac{\mathrm{A}_0^a(t_1) - \mathrm{A}_0^a(t_2)}{\mathrm{A}_0^a(t_1) + \mathrm{A}_0^a(t_2)}\right| &\leq \Theta_{\delta \mathrm{A}_0} = 10^{-7}.
\end{aligned} \tag{11}$$

where $u^{(n)}(x)$ is the matrix of the gauge transformation $u(x)$ at the iteration step n, and the charge

$$\mathrm{A}_0^a(\vec{x}, t) = \int d^3\vec{x} A_0^a(\vec{x}, t) \tag{12}$$

must be independent of t in Landau gauge when periodical boundary conditions for the gauge field are used. The choice of numerical values for the stopping parameters is discussed at the end of the next section.

3 The landscape of minima of the functional F_U

The functional F_U (4) has a form similar to the energy of a spin glass. The last is known to posses a very large number of metastable states, i.e. spin configurations whose energy increases when any spin is reversed. Typically, the number of these states grows exponentially with the number of spins.

Let us consider the landscape of the functional F_U. One of its characteristics is the distribution of values at minima $F_{\min}$ of F_U. We know that for small magnitudes of the gauge field all the link matrices $U_\mu(x)$ (they play the role of couplings between the "spin" variables) are close to the identity matrix, and thus the minimum is unique. Their number increases when the bare lattice coupling β decreases, because the typical magnitude of the phase of $U_\mu(x)$ grows in this case and thus link matrices move farther from the identity matrix. The number of minima also increases with the number of links (at fixed β) because in this case there are more degrees of freedom in the system. At Figure 2 we present typical histograms of the distribution of $F_{\min}$ for one given gauge configuration, as a function of the β parameter. We see that when β is large ($\beta \gtrsim 2.5$ for the volume $V = 8^4$ considered at Figure 2), we typically find only one value of $F_{\min}$. On the contrary, for very small values of β we find many different minima (cf. Figure 3). These values of β correspond to almost random links $U_\mu(x)$. In the following section we show that field configurations having the same $F_{\min}$ are in fact equivalent up to a global gauge transformation.

The probability to find a secondary minimum depends on the value of the β parameter. We can calculate this probability in the following way. For each orbit we fix the gauge

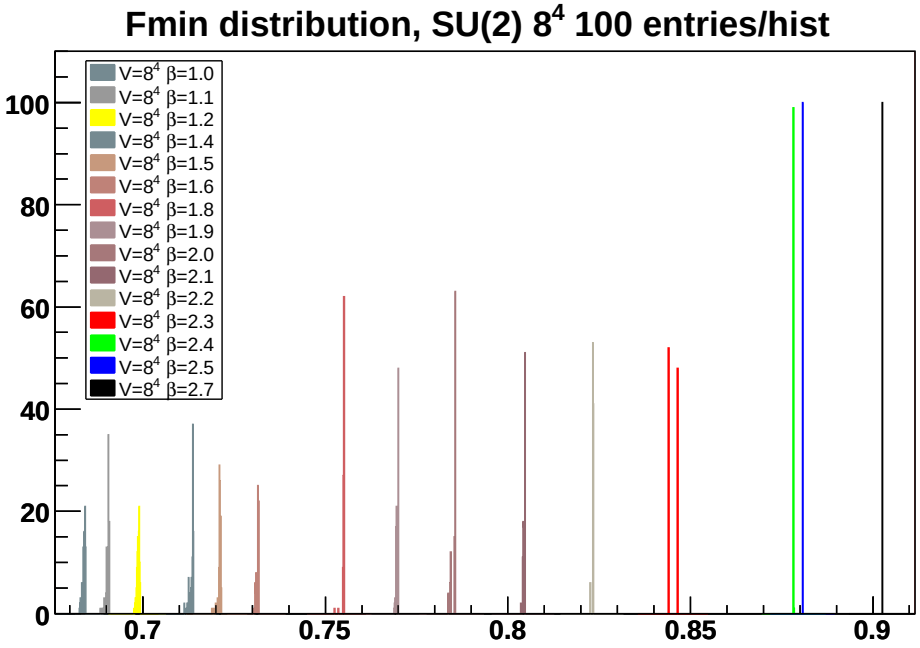

Figure 2: Histogram of minima values $F_{\min}$ for different β for *one particular* gauge-field configuration, $|\partial_\mu A^a_\mu(x)| \leq 10^{-9}$. Here $N_{\rm GF} = 100$. The histograms are ranged in the order the increase of the β parameter.

$N_{\rm GF}$ times, each gauge fixing starts after a random gauge transformation of the initial field configuration. We thus obtain a distribution of minima $F_{\min}$. This distribution gives us the number of minima $N(F^i)$ as a function of the value of $F^i \equiv F^i_{\min}$. The relative frequency of a minimum F^i is defined by

$$\omega_i = \frac{N(F^i)}{\sum_i N(F^i)}, \tag{13}$$

where $\sum_i N(F^i) = N_{\rm GF}$. Then the weighted mean number of copies per value of $F_{\min}$ is given by

$$\overline{N} = \sum_i \omega_i N(F^i). \tag{14}$$

This allows us to define a probability to find a secondary minimum when fixing the Landau gauge for a gauge field configuration :

$$p_{\rm 1conf} = 1 - \frac{\overline{N}}{\sum_i N(F^i)}. \tag{15}$$

If one finds the same value of $F_{\min}$ for all $N_{\rm GF}$ tries then this probability is zero. On the contrary, if all F_i are different then p is close to one.

Having the probability to find a secondary minimum when fixing the gauge for *one particular* configuration we can calculate the Monte-Carlo *average* $\langle\star\rangle$ on gauge orbits, i.e. on "spin couplings" $U_\mu(x)$. We obtain finally the overall probability to find a secondary minimum during a numerical simulation:

$$P(\beta) \equiv \langle p_{\rm 1conf}\rangle = 1 - \left\langle \frac{\overline{N}}{\sum_i N(F^i)} \right\rangle. \tag{16}$$

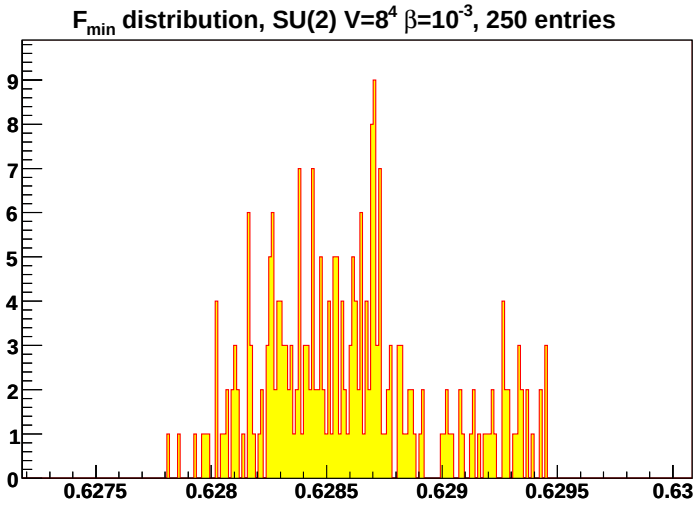

Figure 3: Histogram of minima values $F_{\min}$ for very a small value of $\beta = 10^{-3}$, $|\partial_\mu A^a_\mu(x)| \leq 10^{-9}$.

We have performed simulations in the case of $SU(2)$ latice gauge theory at volumes $V = \{8^4, 10^4, 12^4, 16^4\}$ for β varying from 1.4 to 2.9. For each value of β we generated 100 independent Monte-Carlo gauge configurations, and we fixed the gauge $N_{\rm GF} = 100$ times for every configuration. Between each gauge fixing a random gauge transformation of the initial gauge configuration was performed, and the minimising algorithm stops when the triple condition (11) is satisfied. The resulting probability to find a secondary minimum is presented at (Figures 4-7).

As expected, the probability is small when β is large, and it is close to one when β is small. The dispersion was calculated using the Jackknife method. The physical meaning of this dispersion is the following: when the error is small, all gauge configurations have a similar number of secondary minima. On the contrary, this dispersion is large if there are some exceptional gauge configurations having a different number of copies. At small β almost all gauge configurations have many secondary minima, that is why the dispersion of the probability is small. At large β almost all gauge configurations have a unique minimum, but some of them can have copies. This may considerably increase the dispersion of the probability. The appearance of exceptional gauge configuration possessing a large density of close-to-zero eigenvalues of the Faddeev-Popov operator has been recently reported [13]. Probably these fields are related with those having a lot of secondary minima at large β's, and this correlation deserves a separate study.

We can fit the data from Figures 4-7 with an empirical formula

$$P(\beta) = \frac{A}{1 + e^{B(\beta - \beta_c)}} \tag{17}$$

in order to define a characteristic coupling β_c when the probability to find a copy decreases considerably. One can define β_c as corresponding to the semi-heights of the probability function $P(\beta)$. At this value of β an *equally probable* secondary attractor of the functional F_U appears. The fit has been performed for the points between dashed lines at Figures 4-7, and the results for the fit parameters are given ibidem and in Table 1. We see that β_c depends on the volume of the lattice. Let us check whether these values correspond to some physical scale. According to works [15],[16] one has the following expression for the

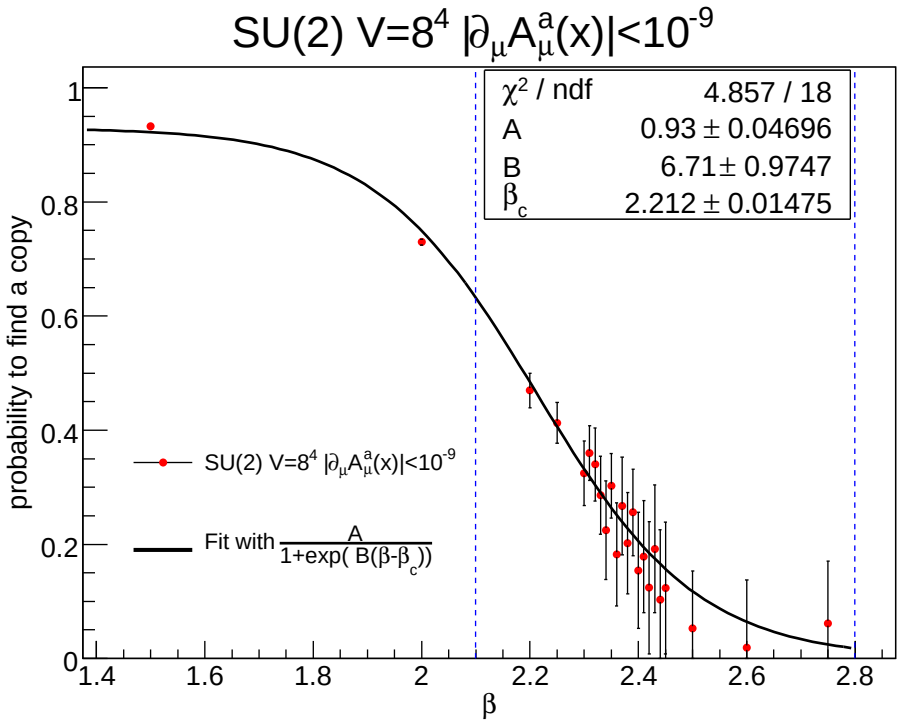

Figure 4: Probability (averaged over gauge orbits) to find a secondary minimum as a function of β at volume $V = 8^4$.

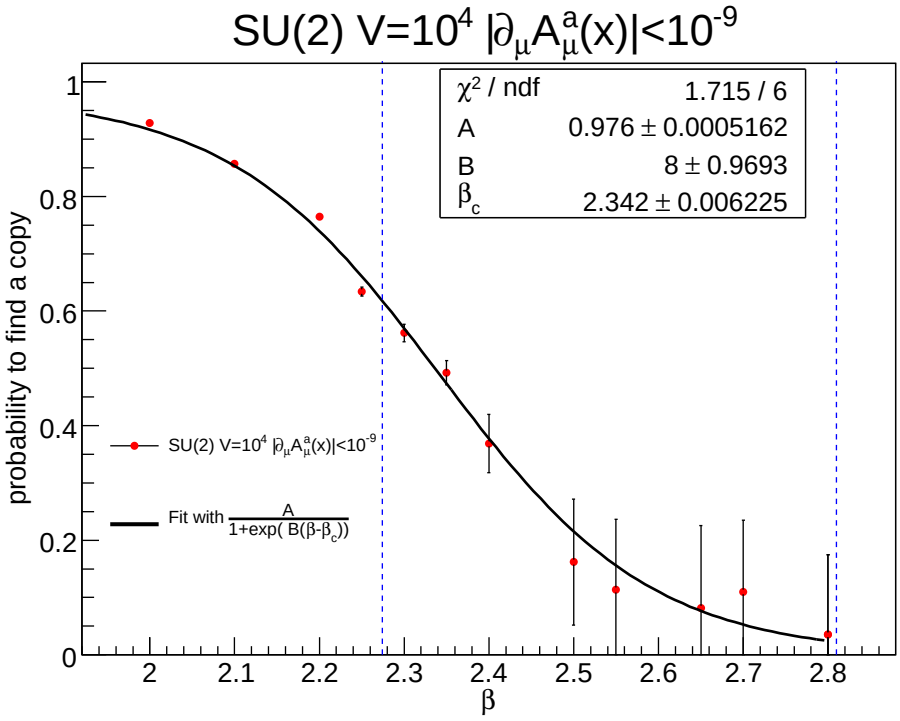

Figure 5: Probability (averaged over gauge orbits) to find a secondary minimum as a function of β at volume $V = 10^4$.

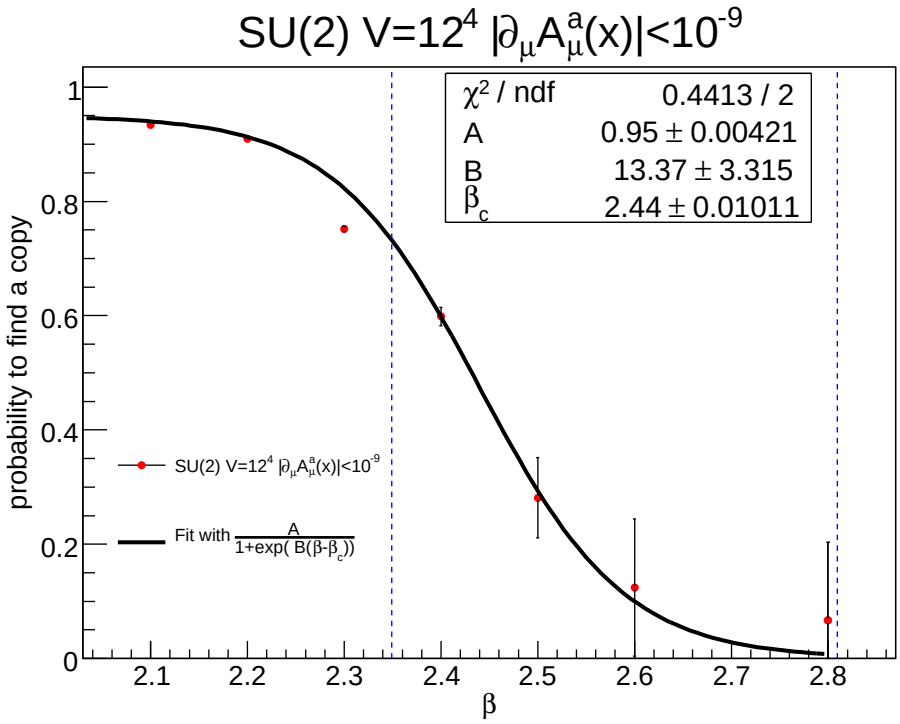

Figure 6: Probability (averaged over gauge orbits) to find a secondary minimum as a function of β at volume $V = 12^4$.

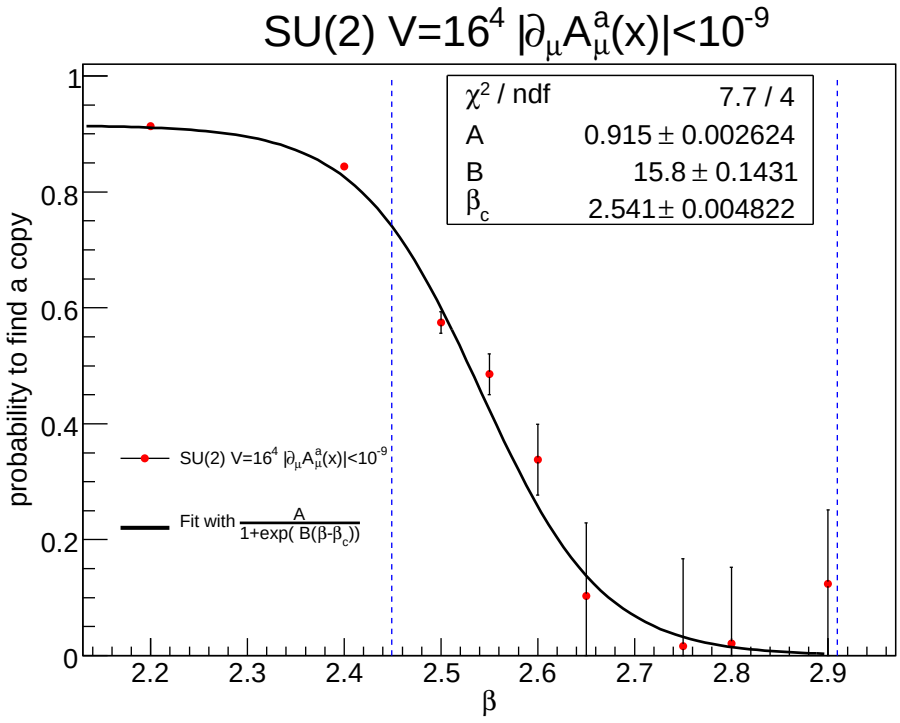

Figure 7: Probability (averaged over gauge orbits) to find a secondary minimum as a function of β at volume $V = 16^4$.

string tension σ for $\beta \geq 2.3$:

$$[\sigma a^2](\beta) \simeq e^{-\frac{4\pi^2}{\beta_0}\beta + \frac{2\beta_1}{\beta_0^2}\log\left(\frac{4\pi^2}{\beta_0}\beta\right) + \frac{4\pi^2}{\beta_0}\frac{d}{\beta} + c} \tag{18}$$

with $c = 4.38(9)$ and $d = 1.66(4)$. Using this formula, we define a characteristic scale corresponding to the critical values β_c from (Figures 4-7) :

$$\lambda_c = a(\beta_c) \cdot L$$

in the string tension units, L is the length of the lattice. In the last column of Table 1 we summarise the results. We see that for the values of β_c in the scaling regime when the

L	β_c	χ^2/ndf	λ_c, in units of $1/\sqrt{\sigma}$
8	2.221(14)	0.27	3.85(31)
10	2.342(6)	0.28	3.20(21)
12	2.44(1)	0.22	2.78(20)
16	2.541(5)	1.92	2.68(17)

Table 1: The characteristic length defining the appearance of secondary minima. The errors for λ_c include errors for d and c parameters, and the fitted error for β_c

formula (18) is applicable ($\beta \geq 2.3$) we obtain compatible values for the physical length λ_c.

This suggests that lattice Gribov copies appear when the physical size of the lattice exceeds a critical value of around $2.75/\sqrt{\sigma}$. At fist approximation λ_c is scale invariant, but a slight dependence in the lattice spacing remains.

In principle, the parameter β_c can be calculated with good precision. One should do it in the case of $SU(3)$ gauge group, because the dependence of the lattice spacing on the bare coupling is softer, and the scaling of the theory has been better studied than in the case of the $SU(2)$ theory.

Let us discuss the dependence of above results on the choice of the stopping parameters (11). In the Table 6 we present the probabilities $P(2.0), P(2.3), P(2.8)$, calculated on a 8^4 lattice with different values of the parameters (11). One can see that our choice of stopping parameters in (11) is strict enough to ensure the independence of our results on the further increase of the parameter $\Theta_{\max_x |\partial_\mu A^a_\mu|}$.

4 Green functions and the lattice Gribov copies

4.1 Two- and three-point lattice Green functions

Lattice Green functions are computed as Monte-Carlo averages over gauge-fixed gluon field configurations.

Gluonic Green functions are defined using the definition (6) of the gauge field. The ghost propagator $F^{(2)ab}(x-y)$ is computed, with the algorithm given in [17], by numerical inversion of the Faddeev-Popov operator (9), e.g.

$$F^{(2)}(x-y)\delta^{ab} \equiv \left\langle \left({\mathcal{M}^{\text{lat}}_{FP}}^{-1}[A] \right)^{ab}_{xy} \right\rangle . \tag{19}$$

The gluon propagator in Landau gauge may be parametrised as

$$G^{(2)ab}_{\mu\nu}(p,-p) \equiv \left\langle \widetilde{A}^a_\mu(-p)\widetilde{A}^b_\nu(p)\right\rangle = \delta^{ab}\left(\delta_{\mu\nu} - \frac{p_\mu p_\nu}{p^2}\right) G^{(2)}(p^2) \tag{20}$$

completed with

$$G^{(2)ab}_{\mu\nu}(0,0) = \delta^{ab}\delta_{\mu\nu}G^{(2)}(0). \tag{21}$$

The ghost propagator is parametrised in the usual way:

$$\widetilde{F}^{(2)ab}(p,-p) \equiv \left\langle \widetilde{c}^a(-p)\widetilde{\overline{c}}^b(p)\right\rangle = \delta^{ab}F^{(2)}(p^2) \tag{22}$$

The coupling constant can be defined non-perturbatively by the amputation of a three-point Green-functions from its external propagators. But this requires to fix the kinematic configuration of the three-point Green-function at the normalisation point. On the lattice one usually uses either a fully symmetric kinematic configuration (denoted MOM) or a zero point kinematic configuration with one vanishing external momentum (denoted generically $\widetilde{\text{MOM}}$). In what follows we only speak about gluonic three-point functions.

Symmetric case

There are only two independent tensors in Landau gauge in the case of the symmetric three-gluon Green function [18]:

$$\mathcal{T}^{[1]}_{\mu_1,\mu_2,\mu_3}(p_1,p_2,p_3) = \delta_{\mu_1\mu_2}(p_1-p_2)_{\mu_3} + \delta_{\mu_2\mu_3}(p_2-p_3)_{\mu_1} + \delta_{\mu_3\mu_1}(p_3-p_1)_{\mu_2} \tag{23}$$

$$\mathcal{T}^{[2]}_{\mu_1,\mu_2,\mu_3}(p_1,p_2,p_3) = \frac{(p_1-p_2)_{\mu_3}(p_2-p_3)_{\mu_1}(p_3-p_1)_{\mu_2}}{p^2}. \tag{24}$$

Then the three-gluon Green function in the MOM scheme ($p_1^2 = p_2^2 = p_3^2 = \mu^2$) can be parametrised as

$$\left\langle \widetilde{A}^a_{\mu_1}(p_1)\widetilde{A}^b_{\mu_2}(p_2)\widetilde{A}^c_{\mu_3}(p_3)\right\rangle = f^{abc}\Big[G^{(3)\text{sym}}(\mu^2)\mathcal{T}^{[1]}_{\mu_1',\mu_2',\mu_3'}(p_1,p_2,p_3)\prod_{i=1,3}\left(\delta_{\mu_i'\mu_i} - \frac{p_{i\mu_i'}p_{i\mu_i}}{\mu^2}\right) + \\ + H^{(3)}(\mu^2)\mathcal{T}^{[2]}_{\mu_1,\mu_2,\mu_3}(p_1,p_2,p_3)\Big] \tag{25}$$

The scalar function $G^{(3)\text{sym}}(\mu^2)$, proportional to the coupling g_0 at tree level, may be extracted by the following projection:

$$G^{(3)\text{sym}}(\mu^2) = \left(\mathcal{T}^{[1]}_{\mu_1',\mu_2',\mu_3'}(p_1,p_2,p_3)\prod_{i=1,3}\left(\delta_{\mu_i'\mu_i} - \frac{p_{i\mu_i'}p_{i\mu_i}}{\mu^2}\right) + \frac{1}{2}\mathcal{T}^{[2]}_{\mu_1',\mu_2',\mu_3'}(p_1,p_2,p_3)\right)\times \\ \times \frac{1}{18\mu^2}\frac{f^{abc}}{N_c(N_c^2-1)}\left\langle \widetilde{A}^a_{\mu_1}(p_1)\widetilde{A}^b_{\mu_2}(p_2)\widetilde{A}^c_{\mu_3}(p_3)\right\rangle. \tag{26}$$

Asymmetric case

The three-gluon Green function with one vanishing external propagator ([19],[18]) can be parametrised as

$$G^{(3)abc}_{\mu\nu\rho}(p,0,-p) \equiv \left\langle \widetilde{A}^a_\mu(-p)\widetilde{A}^b_\nu(p)\widetilde{A}^c_\rho(0)\right\rangle = 2f^{abc}p_\rho\left(\delta_{\mu\nu}-\frac{p_\mu p_\nu}{p^2}\right)G^{(3)\text{asym}}(p^2), \qquad (27)$$

and thus

$$G^{(3)\text{asym}}(p^2) = \frac{1}{6p^2}\frac{f^{abc}}{N_c(N_c^2-1)}\delta_{\mu\nu}p_\rho G^{(3)abc}_{\mu\nu\rho}(p,0,-p). \qquad (28)$$

Gauge coupling

Using the scalar functions $G^{(2)}$ and $G^{(3)}$ (the last stands for $G^{(3)\text{asym}}$ or $G^{(3)\text{sym}}$), the gauge coupling at the renormalisation scale μ^2 is defined by

$$g_R(\mu^2) = \frac{G^{(3)}(p_1^2,p_2^2,p_3^2)}{G^{(2)}(p_1^2)G^{(2)}(p_2^2)G^{(2)}(p_3^2)}Z_3^{3/2}(\mu^2) \qquad (29)$$

in the case of three-gluon vertices, where the choice of p_i determines the renormalisation scheme ($\widetilde{\text{MOM}}$ or MOM). In paper [20] it is shown that in the MOM schemes $g_R(\mu^2)$ vanishes in the zero momentum limit. It is interesting to investigate the possible influence of Gribov copies on this behaviour. We address this question in the following section.

4.2 Influence of the lattice gauge fixing

A natural question that arises after the study of the distribution of $F_{\min}$ is whether the gauge configurations having the same value of $F_{\min}$ are equivalent, i.e. they differ only by a global gauge transformation.

This can be checked by calculating the two-point gluonic correlation function on the gauge configuration . Indeed, according to the lattice definition of the gauge field that we used (6),

$$G^{(2)}_{1\text{ conf}}(x-y) \propto \text{Tr}\left[\left(U_\mu(x)-U^\dagger_\mu(x)\right)\cdot\left(U_\nu(y)-U^\dagger_\nu(y)\right)\right]. \qquad (30)$$

Applying a global gauge transformation $U_\mu(x) \to VU_\mu(x)V^\dagger$ we see that the gluon propagator remains unchanged. This is also the case of the ghost propagator scalar function. We have checked numerically that the values of the gluon and the ghost propagators in Fourier space are the same for gauge configurations having the same $F_{\min}$ (cf. Tables 2,3). For comparison, the data from a lattice Gribov copy (the same gauge configuration but having different value of $F_{\min}$) is also given. We see that the values are almost the same for gauge configurations having the same $F_{\min}$ contrarily to those coming from different minima. In fact, taking in account rounding errors appearing during the calculation, we may say that gauge configurations having the same $F_{\min}$ *are* equivalent.

The second question that has already been considered by ([7],[8],[9],[10],[11],[12],[13]) is the dependence of Green functions on the choice of the minimum. For this purpose we have performed the following simulation: for every of the 100 gauge configurations used to compute Green functions the gauge was fixed 100 times, and the Monte-Carlo average was computed with respect to the "first copy" (fc) found by the minimisation algorithm and the "best copy" (bc), having the smallest value of $F_{\min}$. We have calculated the gluon and the ghost propagators, and also the three-gluon Green functions in symmetric and

	$F_{\min}$	-0.871010810260	-0.871010810260	-0.870645877060
$V \cdot G^{(2)}(p^2):$	$p^2 = 0$	4249297	4249295	3322788
	$p^2 = 1$	2012518	2012516	2006186
	$p^2 = 2$	1215762	1215762	1362671
	$p^2 = 3$	834876.3	834876.4	798032
	$p^2 = 4_{\ p^{[4]}=16}$	620065.2	620067.3	434235.6
	$p^2 = 4_{\ p^{[4]}=4}$	521585.0	521585.2	556509.6
	$p^2 = 5$	410698.8	410698.5	440623.9

Table 2: Gluon correlator calculated on different gauge configurations having the same value of $F_{\min}$ (columns 2 and 3), compared to values from the "secondary" minimum (column 4). We present data for all H_4 group orbits for the momentum $p^2 = 4$ ([21],[17]). Notice that in all this paper the momenta are given in units of $2\pi/(aL)$. Simulation has been performed with parameters $V = 16^4, \beta = 2.4$

	$F_{\min}$	-0.871010810260	-0.871010810260	-0.870645877060
$F^{(2)}(p^2)$	$p^2 = 1$	14.06473	14.06473	14.82984
	$p^2 = 2$	6.278253	6.278253	6.736338
	$p^2 = 3$	3.757531	3.757531	3.939130
	$p^2 = 4_{\ p^{[4]}=16}$	2.929602	2.929602	2.705556
	$p^2 = 4_{\ p^{[4]}=4}$	2.599088	2.599088	2.775566
	$p^2 = 5$	2.071200	2.071200	2.011100

Table 3: Ghost correlator calculated on different gauge configurations having the same value of $F_{\min}$ (columns 2 and 3), compared to values from the "secondary" minimum (column 4). We present data for all H_4 group orbits for the momentum $p^2 = 4$ ([21],[17]). Simulation has been performed with parameters $V = 16^4, \beta = 2.4$

β	L	p^2	$F^{(2)}_{\rm fc}(p^2) - F^{(2)}_{\rm bc}(p^2)$	$\frac{F^{(2)}_{\rm fc}(p^2) - F^{(2)}_{\rm bc}(p^2)}{F^{(2)}_{\rm bc}}$
2.1	8	1	0.211	0.045
2.1	16	$4_{\ p^{[4]}=16}$	0.145	0.033
2.2	8	1	0.078	0.019
2.2	16	$4_{\ p^{[4]}=16}$	0.023	0.006
2.3	8	1	0.086	0.024
2.3	16	$4_{\ p^{[4]}=16}$	0.114	0.034

Table 4: Volume dependence of the ghost propagators, from Tables 7- 26

asymmetric kinematic configurations. The simulations have been performed on lattices of volumes 8^4 and 16^4 for $\beta = 2.1, 2.2, 2.3$. At these values of β we are sure to have lattice Gribov copies. The results are given in Tables 7-29. All data is given in lattice units. We present data for all H_4 group orbits ([21],[17]) for considered momenta, and we have checked that our results for two-point Green functions are consistent with numerical values given in [7],[8]. We conclude from Tables 7-29 that the ghost propagator is quite sensitive to the choice of the minimum - in the case of (bc) the infrared divergence is lessened. No systematic effect could be found for gluonic two- and three-point Green functions, the values in the cases of (fc) and (bc) being compatible within the statistical errors.

It is conjectured in [22] that in the infinite volume limit the expectation values calculated by integration over the Gribov region and the fundamental modular region become equal. However, the ghost propagator depends on this choice, even for volumes larger than the critical volume defined in section 3, see Table 19 where there is a four σ discrepancy for $p^2 = 1$. This dependence has been found to decrease slowly with the volume [12]. The results of section 3 indicate that the convergence can only happen beyond the critical size.

β	L	$\overline{\langle F_{\min}\rangle}_{\{U\}}$	$\delta\overline{\langle F_{\min}\rangle}_{\{U\}}$
2.2	8	-0.8236	0.003744
	10	-0.8262	0.002367
	12	-0.8272	0.001377
	16	-0.8279	0.000802
2.4	8	-0.8642	0.005270
	12	-0.8669	0.002739
	12	-0.8686	0.001849
	16	-0.8702	0.001003

Table 5: Volume dependence of the Monte-Carlo+gauge orbit mean value at minima $F_{\min}$ and the dispersion of this mean.

To check this we compare the fc-bc values of the ghost propagator, at one physical value of the momentum, for the orbit $p^2 = 1$ on a 8^4 lattice and the orbit $p^2 = 4, p^{[4]} = 16$ on the 16^4 lattice [3] at the same β (see Table 4). It happens indeed that the decrease is observed only at $\beta = 2.1$ and 2.2, in accordance with Table 1. However, these values of β are not in the scaling regime, and thus a study on larger lattices would be welcome. It is not surprising that the ghost propagator depends on the bc/fc choice: the bc corresponds to the fields further from the Gribov horizon where the Faddeev-Popov operator has a zero mode, whence the inverse Faddeev-Popov operator (ghost propagator) is expected to be smaller as observed. The correlation between the bc/fc choice and the gluon propagator is not so direct. Another quantity is obviously strongly correlated to the bc/fc choice: the value of $F_{\min}$. We tested the volume dependence of the Monte-Carlo+gauge orbit mean value of the quantity $F_{\min}$ (see Tab.5). According to the argument given in [22], all minima become degenerate in the infinite volume limit, and closer to the absolute minimum (in the fundamental modular region). We see from the Table 5 that their average value and dispersion decrease with the volume at fixed β, in agreement with [22].

5 Conclusions

Our study showed that

- Lattice Gribov copies appear and their number grows very fast when the physical size of the lattice exceeds some critical value $\approx 2.75/\sqrt{\sigma}$. This result is fairly independent of the lattice spacing.
- The configurations lying on the same gauge orbit and having the same $F_{\min}$ are equivalent, up to a global gauge transformation, and yield the same Green functions. Those corresponding to minima of F_U with different values of $F_{\min}$ differ by a non-trivial gauge transformation, and thus they are not equivalent.
- We confirm the result ([7],[8],[9],[10],[11],[12],[13]) that the divergence of the ghost propagator is lessened when choosing the "best copy" (corresponding to the choice of the gauge configuration having the smallest value of F_U). We also showed that gluonic Green functions calculated in the "first copy" and "best copy" schemes are compatible within the statistical error, no systematic effect was found. We conclude that gauge couplings that are defined by amputating the three-gluon vertices only

[3] Remember that the momentum in physical units is equal to $2\pi\, p/(La)$ in our notations.

slightly depend on the choice of the minimum of F_U. It implies that the infrared behaviour of $g_R(\mu^2)$ reported in [20] is not significantly influenced by lattice Gribov copies.

- We found that the influence of Gribov copies on the ghost propagator decreases with the volume when the physical lattice size is larger than the critical length discussed above. We also show that the quantity $F_{\min}$ decreases when the volume increases. These two points are in agreement with the argument on the equality of the averages over the Gribov's region and the fundamental modular region [22].

The fact that the abundance of lattice Gribov copies is mainly an increasing function of the physical size of the lattice is not too surprising. The existence of Gribov copies is a non-perturbative phenomenon and as such is related [1] to the infrared properties of the Faddeev-Popov operator and to the confinement scale. It should then dominantly depend on the infrared cut-off, the size (or volume) of the lattice in physical units. A milder dependence on the ultraviolet cut-off, the lattice spacing, is also expected but the limited accuracy concerning the lattice spacing did not allow us to identify it. In a recent paper [13] the lowest eigenvalues of the Faddeev-Popov operator have been computed. A dependence on the size of the lattice is seen. A detailed study of this dependence in connection with our findings in this paper would be useful.

More generally, the question of extracting from lattice simulations informations about Gribov copies in the continuum limit is not a simple issue. However, bulk quantities, such as the one we propose in this paper, may be traced down to the continuum limit and provide precious information about continuum Gribov copies. The total number of lattice Gribov copies in a given gauge orbit may be large. All the minima of the functional $F_{\mathcal{A}}[u(x)]$ (1) are possible end-points of the Landau gauge fixing algorithm, but their probability to be selected by the algorithm depends on the size of their domain of attraction and might vary significantly. This probability is therefore expected to depend on the attractor pattern and not on the choice of algorithm, which should be checked.

The explosion of the number of Gribov copies at larger volume does not contradict the statement that they a have decreasing influence on expectation values [22]. Even more, this influence decreases when the number of Gribov copies is large enough (cf. Tables 4,1), i.e. above the critical volume that we have outlined.

We wish to continue this research in a few directions: more refined quantities may be defined, a better accuracy is needed, larger volumes studied, in particular to check if the ghost propagatore dependence on the bc/fc choice fades away in the scaling regime. An extension of the study to $SU(3)$ and to unquenched gauge configurations will be welcome.

Note added in proof While this paper was being submitted, a preprint has appeared [23] which adds to the gauge group the extra global symmetry of the quenched lattice action with respect to the centre of the gauge group. This leads to an extension of the notion of Gribov copies and it results a sensitivity of the gluon propagator upon the latter. We note that the copy dependence is mainly observed at small lattice volumes, below the critical size found by us.

β	$\Theta_{\max_x \lvert\partial_\mu A^a_\mu\rvert}$	Θ_{A_0}	$\Theta_{\delta u}$	$P(\beta)$	$\delta P(\beta)$	$\langle F_{\min}\rangle$	$\delta_{\mathrm{RMS}} F_{\min}$
2.0	10^{-10}	10^{-5}	10^{-5}	0.729620	0.004738	0.78416564213526	0.00260692007045
2.0	10^{-14}	10^{-5}	10^{-9}	0.729606	0.004984	0.78416564421249	0.00260692062016
2.0	10^{-14}	10^{-7}	10^{-9}	0.729606	0.004985	0.78416564421259	0.00260692061867
$\rightarrow$ 2.0	10^{-18}	10^{-7}	10^{-9}	0.729606	0.004985	0.78416564421258	0.00260692062307
2.0	10^{-24}	10^{-7}	10^{-9}	0.729606	0.004985	0.78416564421258	0.00260692062150
2.0	10^{-28}	10^{-7}	10^{-9}	0.729606	0.004985	0.78416564421258	0.00260692062134
2.3	10^{-10}	10^{-5}	10^{-5}	0.324636	0.056660	0.84466892598808	0.00415444722060
2.3	10^{-14}	10^{-5}	10^{-9}	0.324636	0.056660	0.84466892602737	0.00415444721015
2.3	10^{-14}	10^{-7}	10^{-9}	0.324636	0.056660	0.84466892602833	0.00415444720619
$\rightarrow$ 2.3	10^{-18}	10^{-7}	10^{-9}	0.324636	0.056660	0.84466892602843	0.00415444720513
2.3	10^{-24}	10^{-7}	10^{-9}	0.324636	0.056660	0.84466892602847	0.00415444720356
2.3	10^{-28}	10^{-7}	10^{-9}	0.324636	0.056660	0.84466892602847	0.00415444720356
2.8	10^{-10}	10^{-5}	10^{-5}	0.024946	0.155566	0.89393978935534	0.00777035608940
2.8	10^{-14}	10^{-5}	10^{-9}	0.024946	0.155567	0.89393978936422	0.00777035609273
2.8	10^{-14}	10^{-7}	10^{-9}	0.024946	0.155567	0.89393978936434	0.00777035609111
$\rightarrow$ 2.8	10^{-18}	10^{-7}	10^{-9}	0.024946	0.155567	0.89393978936448	0.00777035608963
2.8	10^{-24}	10^{-7}	10^{-9}	0.024946	0.155567	0.89393978936449	0.00777035608962
2.8	10^{-28}	10^{-7}	10^{-9}	0.024946	0.155567	0.89393978936449	0.00777035608962

Table 6: The influence of different stopping parameters (11) on the value of the probability $P(\beta)$. Simulations done for the lattice size $V = 8^4$, 100 Monte-Carlo configurations (we uses the same set of configurations for every value of β) $\times$ $N_{\mathrm{NF}} = 100$ gauge fixings. The last two columns give the average value of $F_{\min}$ and the standard dispersion of this average. The arrow indicates our choice of stopping parameters (11).

$SU(2)$, $V = 8^4$ and $\beta = 2.1$, 100 Monte-Carlo configurations $\times$ 100 gauge fixings

Two point functions

p^2	$F_{\rm fc}^{(2)}(p^2)$	$\delta F_{\rm fc}^{(2)}(p^2)$	$F_{\rm bc}^{(2)}(p^2)$	$\delta F_{\rm bc}^{(2)}(p^2)$
1	4.898	0.099	4.687	0.071
2	2.046	0.039	1.959	0.043
3	1.210	0.021	1.168	0.023
$4_{\ p^{[4]}=16}$	0.961	0.023	0.925	0.021
$4_{\ p^{[4]}=4}$	0.834	0.019	0.801	0.013
5	0.696	0.007	0.680	0.014

Table 7: Ghost propagator, $V = 8^4$ $\beta = 2.1$

p^2	$G_{\rm fc}^{(2)}(p^2)$	$\delta G_{\rm fc}^{(2)}(p^2)$	$G_{\rm bc}^{(2)}(p^2)$	$\delta G_{\rm bc}^{(2)}(p^2)$
0	11.161	0.438	10.894	0.418
1	6.225	0.129	6.248	0.135
2	4.089	0.035	4.095	0.043
3	2.883	0.033	2.868	0.023
$4_{\ p^{[4]}=16}$	2.329	0.043	2.305	0.031
$4_{\ p^{[4]}=4}$	2.129	0.023	2.147	0.015
5	1.773	0.009	1.785	0.008

Table 8: Gluon propagator, $V = 8^4$ $\beta = 2.1$

Three point functions

p^2	$G_{\rm fc}^{(3)\rm asym}(p^2)$	$\delta G_{\rm fc}^{(3)\rm asym}(p^2)$	$G_{\rm bc}^{(3)\rm asym}(p^2)$	$\delta G_{\rm bc}^{(3)\rm asym}(p^2)$
1	29.636	2.081	29.408	2.721
2	19.018	1.168	18.387	1.173
3	11.513	0.971	12.293	1.739
$4_{\ p^{[4]}=16}$	10.424	0.857	11.817	1.126
$4_{\ p^{[4]}=4}$	6.968	0.618	6.547101	0.471
5	5.164	0.264	4.697285	0.293

Table 9: Three-gluon vertex in asymmetric kinematic configuration, $V = 8^4$ $\beta = 2.1$

p^2	$G_{\rm fc}^{(3)\rm sym}(p^2)$	$\delta G_{\rm fc}^{(3)\rm sym}(p^2)$	$G_{\rm bc}^{(3)\rm sym}(p^2)$	$\delta G_{\rm bc}^{(3)\rm sym}(p^2)$
2	13.613	0.745	14.188	0.752
4	2.680	0.272	2.612	0.272

Table 10: Three-gluon vertex in symmetric kinematic configuration, $V = 8^4$ $\beta = 2.1$

$SU(2)$, $V = 8^4$ and $\beta = 2.2$, 100 Monte-Carlo configurations $\times$ 100 gauge fixings

Two point functions

p^2	$F_{\rm fc}^{(2)}(p^2)$	$\delta F_{\rm fc}^{(2)}(p^2)$	$F_{\rm bc}^{(2)}(p^2)$	$\delta F_{\rm bc}^{(2)}(p^2)$
1	4.178	0.103	4.100	0.070
2	1.749	0.045	1.735	0.037
3	1.042	0.027	1.032	0.024
$4_{\ p^{[4]}=16}$	0.835	0.030	0.821	0.024
$4_{\ p^{[4]}=4}$	0.720	0.016	0.715	0.014
5	0.614	0.017	0.609	0.014

Table 11: Ghost propagator, $V = 8^4$ $\beta = 2.2$

p^2	$G_{\rm fc}^{(2)}(p^2)$	$\delta G_{\rm fc}^{(2)}(p^2)$	$G_{\rm bc}^{(2)}(p^2)$	$\delta G_{\rm bc}^{(2)}(p^2)$
0	20.170	0.620	20.241	0.665
1	8.359	0.129	8.247	0.122
2	4.431	0.039	4.433	0.037
3	2.870	0.028	2.857	0.025
$4_{\ p^{[4]}=16}$	2.111	0.038	2.153	0.041
$4_{\ p^{[4]}=4}$	2.021	0.013	2.038	0.019
5	1.642	0.014	1.652	0.013

Table 12: Gluon propagator, $V = 8^4$ $\beta = 2.2$

Three point functions

p^2	$G_{\rm fc}^{(3)\rm asym}(p^2)$	$\delta G_{\rm fc}^{(3)\rm asym}(p^2)$	$G_{\rm bc}^{(3)\rm asym}(p^2)$	$\delta G_{\rm bc}^{(3)\rm asym}(p^2)$
1	78.913	4.405	81.523	5.131
2	36.170	1.393	35.784	1.809
3	17.851	2.147	18.475	1.860
$4_{\ p^{[4]}=16}$	20.516	1.064	20.621	1.115
$4_{\ p^{[4]}=4}$	13.097	0.645	13.382	0.595
5	8.920	0.336	8.985	0.383

Table 13: Three-gluon vertex in asymmetric kinematic configuration, $V = 8^4$ $\beta = 2.2$

p^2	$G_{\rm fc}^{(3)\rm sym}(p^2)$	$\delta G_{\rm fc}^{(3)\rm sym}(p^2)$	$G_{\rm bc}^{(3)\rm sym}(p^2)$	$\delta G_{\rm bc}^{(3)\rm sym}(p^2)$
2	21.099	1.212	20.483	1.148
4	2.494	0.185	2.512	0.189

Table 14: Three-gluon vertex in symmetric kinematic configuration, $V = 8^4$ $\beta = 2.2$

$SU(2)$, $V = 8^4$ and $\beta = 2.3$, 100 Monte-Carlo configurations $\times$ 100 gauge fixings

Two point functions

p^2	$F_{\rm fc}^{(2)}(p^2)$	$\delta F_{\rm fc}^{(2)}(p^2)$	$F_{\rm bc}^{(2)}(p^2)$	$\delta F_{\rm bc}^{(2)}(p^2)$
1	3.742	0.109	3.656	0.084
2	1.569	0.043	1.544	0.032
3	0.945	0.022	0.941	0.019
$4_{\ p^{[4]}=16}$	0.755	0.021	0.751	0.016
$4_{\ p^{[4]}=4}$	0.669	0.015	0.663	0.013
5	0.562	0.009	0.564	0.009

Table 15: Ghost propagator, $V = 8^4$ $\beta = 2.3$

p^2	$G_{\rm fc}^{(2)}(p^2)$	$\delta G_{\rm fc}^{(2)}(p^2)$	$G_{\rm bc}^{(2)}(p^2)$	$\delta G_{\rm bc}^{(2)}(p^2)$
0	35.140	1.555	34.659	1.597
1	9.7073	0.107	9.839	0.156
2	4.487	0.054	4.503	0.055
3	2.668	0.027	2.652	0.018
$4_{\ p^{[4]}=16}$	1.934	0.022	1.919	0.020
$4_{\ p^{[4]}=4}$	1.811	0.016	1.823	0.015
5	1.414	0.014	1.414	0.014

Table 16: Gluon propagator, $V = 8^4$ $\beta = 2.3$

Three point functions

p^2	$G_{\rm fc}^{(3)\rm asym}(p^2)$	$\delta G_{\rm fc}^{(3)\rm asym}(p^2)$	$G_{\rm bc}^{(3)\rm asym}(p^2)$	$\delta G_{\rm bc}^{(3)\rm asym}(p^2)$
1	614.254	42.333	641.328	47.008
2	165.962	7.456	161.354	7.730
3	65.054	2.786	63.734	2.734
$4_{\ p^{[4]}=16}$	33.456	3.787	32.685	3.535
$4_{\ p^{[4]}=4}$	33.770	1.801	35.883	2.099
5	20.471	0.9744	19.994	1.168

Table 17: Three-gluon vertex in asymmetric kinematic configuration, $V = 8^4$ $\beta = 2.3$

p^2	$G_{\rm fc}^{(3)\rm sym}(p^2)$	$\delta G_{\rm fc}^{(3)\rm sym}(p^2)$	$G_{\rm bc}^{(3)\rm sym}(p^2)$	$\delta G_{\rm bc}^{(3)\rm sym}(p^2)$
2	26.483	1.260	26.774	1.280
4	2.249	0.105	2.424	0.104

Table 18: Three-gluon vertex in symmetric kinematic configuration, $V = 8^4$ $\beta = 2.3$

$SU(2)$, $V = 16^4$ and $\beta = 2.1$, 100 Monte-Carlo configurations $\times$ 100 gauge fixings

Two point functions

p^2	$F_{\mathrm{fc}}^{(2)}(p^2)$	$\delta F_{\mathrm{fc}}^{(2)}(p^2)$	$F_{\mathrm{bc}}^{(2)}(p^2)$	$\delta F_{\mathrm{bc}}^{(2)}(p^2)$
1	23.930	0.304	22.615	0.226
2	10.538	0.200	10.188	0.113
3	6.372	0.159	6.257	0.087
$4_{\ p^{[4]}=16}$	4.551	0.116	4.405	0.103
$4_{\ p^{[4]}=4}$	4.489	0.119	4.421	0.062
5	3.437	0.086	3.344	0.053

Table 19: Ghost propagator, $V = 16^4$ $\beta = 2.1$

p^2	$G_{\mathrm{fc}}^{(2)}(p^2)$	$\delta G_{\mathrm{fc}}^{(2)}(p^2)$	$G_{\mathrm{bc}}^{(2)}(p^2)$	$\delta G_{\mathrm{bc}}^{(2)}(p^2)$
0	8.485	0.440	8.309	0.251
1	8.182	0.122	7.871	0.102
2	7.186	0.073	7.022	0.071
3	6.359	0.037	6.385	0.037
$4_{\ p^{[4]}=16}$	6.058	0.091	5.874	0.086
$4_{\ p^{[4]}=4}$	5.710	0.081	5.669	0.067
5	5.161	0.029	5.195	0.026

Table 20: Gluon propagator, $V = 16^4$ $\beta = 2.1$

Three point functions

p^2	$G_{\mathrm{fc}}^{(3)\mathrm{sym}}(p^2)$	$\delta G_{\mathrm{fc}}^{(3)\mathrm{sym}}(p^2)$	$G_{\mathrm{bc}}^{(3)\mathrm{sym}}(p^2)$	$\delta G_{\mathrm{bc}}^{(3)\mathrm{sym}}(p^2)$
2	19.861	3.809	27.689	5.911
4	14.769	2.586	18.952	2.937

Table 21: Three-gluon vertex in symmetric kinematic configuration, $V = 16^4$ $\beta = 2.1$

$SU(2)$, $V = 16^4$ and $\beta = 2.2$, 100 Monte-Carlo configurations $\times$ 100 gauge fixings

Two point functions

p^2	$F_{\rm fc}^{(2)}(p^2)$	$\delta F_{\rm fc}^{(2)}(p^2)$	$F_{\rm bc}^{(2)}(p^2)$	$\delta F_{\rm bc}^{(2)}(p^2)$
1	20.867	0.376	20.406	0.392
2	9.151	0.145	9.070	0.192
3	5.499	0.083	5.460	0.085
$4_{\ p^{[4]}=16}$	3.861	0.095	3.838	0.082
$4_{\ p^{[4]}=4}$	3.803	0.067	3.819	0.068
5	2.929	0.041	2.979	0.067

Table 22: Ghost propagator, $V = 16^4$ $\beta = 2.2$

p^2	$G_{\rm fc}^{(2)}(p^2)$	$\delta G_{\rm fc}^{(2)}(p^2)$	$G_{\rm bc}^{(2)}(p^2)$	$\delta G_{\rm bc}^{(2)}(p^2)$
0	14.473	0.676	15.380	0.635
1	12.614	0.255	12.330	0.184
2	10.564	0.066	10.531	0.097
3	8.813	0.081	8.769	0.061
$4_{\ p^{[4]}=16}$	7.760	0.162	7.577	0.089
$4_{\ p^{[4]}=4}$	7.447	0.052	7.429	0.073
5	6.393	0.052	6.395	0.044

Table 23: Gluon propagator, $V = 16^4$ $\beta = 2.2$

Three point functions

p^2	$G_{\rm fc}^{(3)\rm asym}(p^2)$	$\delta G_{\rm fc}^{(3)\rm asym}(p^2)$	$G_{\rm bc}^{(3)\rm asym}(p^2)$	$\delta G_{\rm bc}^{(3)\rm asym}(p^2)$
1	136.266	91.211	115.376	53.064
2	93.912	39.689	90.432	26.263
3	84.119	17.125	81.880	17.916
$4_{\ p^{[4]}=16}$	101.745	17.120	99.140	18.988
$4_{\ p^{[4]}=4}$	78.176	15.640	63.382	14.634
5	51.954	7.666	56.088	8.017

Table 24: Three-gluon vertex in asymmetric kinematic configuration, $V = 16^4$ $\beta = 2.2$

p^2	$G_{\rm fc}^{(3)\rm sym}(p^2)$	$\delta G_{\rm fc}^{(3)\rm sym}(p^2)$	$G_{\rm bc}^{(3)\rm sym}(p^2)$	$\delta G_{\rm bc}^{(3)\rm sym}(p^2)$
2	93.161	11.297	87.022	10.680
4	34.756	7.434	37.655	5.797

Table 25: Three-gluon vertex in symmetric kinematic configuration, $V = 16^4$ $\beta = 2.2$

$SU(2)$, $V = 16^4$ and $\beta = 2.3$, 100 Monte-Carlo configurations $\times$ 100 gauge fixings

Two point functions

p^2	$F_{\text{fc}}^{(2)}(p^2)$	$\delta F_{\text{fc}}^{(2)}(p^2)$	$F_{\text{bc}}^{(2)}(p^2)$	$\delta F_{\text{bc}}^{(2)}(p^2)$
1	18.326	0.297	17.157	0.172
2	7.993	0.150	7.645	0.089
3	4.824	0.086	4.684	0.060
$4_{\ p^{[4]}=16}$	3.431	0.053	3.317	0.052
$4_{\ p^{[4]}=4}$	3.364	0.054	3.338	0.048
5	2.581	0.025	2.533	0.036

Table 26: Ghost propagator, $V = 16^4$ $\beta = 2.3$

p^2	$G_{\text{fc}}^{(2)}(p^2)$	$\delta G_{\text{fc}}^{(2)}(p^2)$	$G_{\text{bc}}^{(2)}(p^2)$	$\delta G_{\text{bc}}^{(2)}(p^2)$
0	32.705	1.063	31.557	0.721
1	21.940	0.444	21.616	0.385
2	15.007	0.122	15.206	0.166
3	11.400	0.107	11.235	0.116
$4_{\ p^{[4]}=16}$	8.848	0.190	8.882	0.108
$4_{\ p^{[4]}=4}$	8.904	0.118	8.782	0.099
5	7.057	0.062	6.978	0.045

Table 27: Gluon propagator, $V = 16^4$ $\beta = 2.3$

Three point functions

p^2	$G_{\text{fc}}^{(3)\text{asym}}(p^2)$	$\delta G_{\text{fc}}^{(3)\text{asym}}(p^2)$	$G_{\text{bc}}^{(3)\text{asym}}(p^2)$	$\delta G_{\text{bc}}^{(3)\text{asym}}(p^2)$
1	1192.828	250.675	779.501	204.768
2	566.632	39.161	505.435	46.025
3	402.454	32.415	388.260	26.754
$4_{\ p^{[4]}=16}$	272.205	35.491	242.150	30.928
$4_{\ p^{[4]}=4}$	239.204	35.152	241.295	25.467
5	174.210	14.126	169.739	10.825
6	130.209	7.523	125.733	7.563

Table 28: Three-gluon vertex in asymmetric kinematic configuration, $V = 16^4$ $\beta = 2.3$

p^2	$G_{\text{fc}}^{(3)\text{sym}}(p^2)$	$\delta G_{\text{fc}}^{(3)\text{sym}}(p^2)$	$G_{\text{bc}}^{(3)\text{sym}}(p^2)$	$\delta G_{\text{bc}}^{(3)\text{sym}}(p^2)$
2	283.901	15.417	313.824	15.595
4	81.695	5.785	72.573	5.787

Table 29: Three-gluon vertex in symmetric kinematic configuration, $V = 16^4$ $\beta = 2.3$

References

[1] V. N. Gribov. Quantization of non-abelian gauge theories. *Nucl. Phys.*, B139:1, 1978.

[2] L. Giusti, M. L. Paciello, C. Parrinello, S. Petrarca, and B. Taglienti. Problems on lattice gauge fixing. *Int. J. Mod. Phys.*, A16:3487–3534, 2001, hep-lat/0104012.

[3] M. Semenov-Tyan-Shanskii and V. Franke. All gauge orbits and some gribov copies encompassed by the gribov horizon. *Zap. Nauch. Sem. Leningrad. Otdeleniya Matematicheskogo Instituta im. V. A. Steklova, AN SSSR*, vol. 120:159, 1982. (English translation:New York, Plenum Press 1986).

[4] G. Dell'Antonio and D. Zwanziger. All gauge orbits and some gribov copies encompassed by the gribov horizon. *In *Cargese 1989, Proceedings, Probabilistic methods in quantum field theory and quantum gravity* 107-130. (see HIGH ENERGY PHYSICS INDEX 29 (1991) No. 10571).*

[5] Pierre van Baal. More (thoughts on) gribov copies. *Nucl. Phys.*, B369:259–275, 1992.

[6] Daniel Zwanziger. Critical limit of lattice gauge theory. *Nucl. Phys.*, B378:525–590, 1992.

[7] Attilio Cucchieri. Gribov copies in the minimal landau gauge: The influence on gluon and ghost propagators. *Nucl. Phys.*, B508:353–370, 1997, hep-lat/9705005.

[8] T. D. Bakeev, Ernst-Michael Ilgenfritz, V. K. Mitrjushkin, and M. Mueller-Preussker. On practical problems to compute the ghost propagator in su(2) lattice gauge theory. *Phys. Rev.*, D69:074507, 2004, hep-lat/0311041.

[9] A. Sternbeck, E. M. Ilgenfritz, M. Muller-Preussker, and A. Schiller. The influence of gribov copies on the gluon and ghost propagator. *AIP Conf. Proc.*, 756:284–286, 2005, hep-lat/0412011.

[10] A. Sternbeck, E. M. Ilgenfritz, M. Muller-Preussker, and A. Schiller. The gluon and ghost propagator and the influence of gribov copies. *Nucl. Phys. Proc. Suppl.*, 140:653–655, 2005, hep-lat/0409125.

[11] P. J. Silva and O. Oliveira. Gribov copies, lattice qcd and the gluon propagator. *Nucl. Phys.*, B690:177–198, 2004, hep-lat/0403026.

[12] A. Sternbeck, E. M. Ilgenfritz, M. Mueller-Preussker, and A. Schiller. Towards the infrared limit in su(3) landau gauge lattice gluodynamics. *Phys. Rev.*, D72:014507, 2005, hep-lat/0506007.

[13] A. Sternbeck, E. M. Ilgenfritz, and M. Mueller-Preussker. Spectral properties of the landau gauge faddeev-popov operator in lattice gluodynamics. 2005, hep-lat/0510109.

[14] Daniel Zwanziger. Fundamental modular region, boltzmann factor and area law in lattice gauge theory. *Nucl. Phys.*, B412:657–730, 1994.

[15] Jacques C. R. Bloch, Attilio Cucchieri, Kurt Langfeld, and Tereza Mendes. Propagators and running coupling from su(2) lattice gauge theory. *Nucl. Phys.*, B687:76–100, 2004, hep-lat/0312036.

[16] J. Fingberg, Urs M. Heller, and F. Karsch. Scaling and asymptotic scaling in the su(2) gauge theory. *Nucl. Phys.*, B392:493–517, 1993, hep-lat/9208012.

[17] Ph. Boucaud et al. Asymptotic behavior of the ghost propagator in su3 lattice gauge theory. 2005, hep-lat/0506031.

[18] P. Boucaud, J. P. Leroy, J. Micheli, O. Pene, and C. Roiesnel. Lattice calculation of alpha(s) in momentum scheme. *JHEP*, 10:017, 1998, hep-ph/9810322.

[19] B. Alles et al. α_s from the nonperturbatively renormalised lattice three gluon vertex. *Nucl. Phys.*, B502:325–342, 1997, hep-lat/9605033.

[20] P. Boucaud et al. The strong coupling constant at small momentum as an instanton detector. *JHEP*, 04:005, 2003, hep-ph/0212192.

[21] D. Becirevic et al. Asymptotic scaling of the gluon propagator on the lattice. *Phys. Rev.*, D61:114508, 2000, hep-ph/9910204.

[22] Daniel Zwanziger. Non-perturbative faddeev-popov formula and infrared limit of qcd. *Phys. Rev.*, D69:016002, 2004, hep-ph/0303028.

[23] I. L. Bogolubsky, G. Burgio, M. Muller-Preussker, and V. K. Mitrjushkin. Landau gauge ghost and gluon propagators in su(2) lattice gauge theory: Gribov ambiguity revisited. 2005, hep-lat/0511056.

Annexe E

Short comment about the lattice gluon propagator at vanishing momentum

Short comment

hep-lat/0602006

Short comment about the lattice gluon propagator at vanishing momentum

Ph. Boucaud[a], Th. Brüntjen[a], J.P. Leroy[a], A. Le Yaouanc[a], A.Y. Lokhov[b], J. Micheli[a], O. Pène[a], J. Rodríguez-Quintero[c] and C. Roiesnel[b]

February 6, 2006

[a]Laboratoire de Physique Théorique et Hautes Energies[1]
Université de Paris XI, Bâtiment 211, 91405 Orsay Cedex, France
[b] Centre de Physique Théorique[2]de l'Ecole Polytechnique
F91128 Palaiseau cedex, France
[c] Dpto. Física Aplicada, Fac. Ciencias Experimentales,
Universidad de Huelva, 21071 Huelva, Spain.

Abstract

We argue that all evidences point towards a finite non-vanishing zero momentum renormalised lattice gluon propagator in the infinite volume limit. We argue that different simulations with different lattice setups end-up with fairly compatible results for the gluon propagator at zero momentum, with different positive slopes as a function of the inverse volume.

LPT Orsay 06-08
CPHT-RR 009.0106
UHU-FT/06-02

1 Introduction

The lattice gluon propagator at small or vanishing momentum in the Landau gauge has recently been frequently addressed as it is related to several studies in the small momentum regime using non-lattice methods. It is often advocated that the zero momentum gluon propagator should vanish, while we have [1] shown a Slavnov-Taylor based argument in favor of a divergence when the momentum goes to zero. Notwithstanding these extraneous arguments we observe that the

[1]Unité Mixte de Recherche 8627 du Centre National de la Recherche Scientifique
[2]Unité Mixte de Recherche 7644 du Centre National de la Recherche Scientifique

genuine lattice data point towards *a finite non-vanishing gluon propagator at zero momentum in the infinite volume limit*. Our second claim is that, once a well defined renormalisation procedure has been defined, the different available results are close enough, despite several systematic effects, to suggest an agreement.

Our aim in this note is simply to gather the arguments in favor of this claim, without discussing the relationship with any non-lattice claim. We will not present any new result but only quote published results and add a reanalysis of our old data. We concentrate on $SU(3)$ pure Yang-Mills theory in the Landau gauge.

There are two approaches to the problem.

- One is to simply compute the gluon propagator at zero momentum and perform a well defined renormalisation. It is well known that the result is a finite non-vanishing value. But it might happen that the vanishing only happens in the infinite volume limit. Therefore an extrapolation to infinite volume is needed.

- The second approach uses a set of small non-vanishing momenta and tries a fit of the propagator in terms of a power law $(p^2)^{\alpha_G - 1}$, or equivalently of the dressing function in terms of $(p^2)^{\alpha_G}$. The fit gives some range of value for α_G. The value $\alpha_G = 1$ – which corresponds to a non-vanishing of the gluon propagator at vanishing momentum – has obviously zero measure and it is thus impossible to be assertive with this second method. It is nevertheless important to check that $\alpha_G = 1$ is compatible with the result and to check that the gluon propagator at vanishing momentum is in continuity with the result at small non-vanishing momenta.

2 Definitions and notations

In Landau gauge the gluon propagator writes

$$G_{\mu\nu}(p) = (\delta_{\mu\nu} - \frac{p_\mu p_\nu}{p^2})\, G^{(2)}(p^2), \tag{1}$$

which implies

$$\begin{aligned} G^{(2)}(p^2) &= \frac{1}{3}\sum_\mu G_{\mu\mu}(p) \quad \text{for} \quad p \neq 0 \\ G^{(2)}(0) &= \frac{1}{4}\sum_\mu G_{\mu\mu}(0). \end{aligned} \tag{2}$$

The factor 1/4 for zero momentum is due to an additional degree of freedom (clearly the orthogonality to the momentum in Landau gauge does not provide

any constraint for $p_\mu = 0$) related to the fact that the Landau gauge fixing algorithm keeps unconstrained the global gauge transformations [3].

In order to be able to compare the results from different gauge actions and different lattice spacings one needs to renormalise the gluon propagator. The standard method on the lattice is the Momentum substraction scheme (MOM) which amounts to define the renormalised propagator $G_R^{(2)}$ from the bare one $G^{(2)}$ according to

$$G^{(2)}(p,a) = Z_3(\mu,a)\, G_R^{(2)}(p,\mu) \tag{3}$$

where the renormalisation condition is

$$G_R^{(2)}(\mu,\mu) \equiv \frac{1}{\mu^2}, \quad \text{whence} \quad Z_3(\mu,a) = \mu^2\, G^{(2)}(\mu,a) \tag{4}$$

where a is the lattice spacing, i.e. the ultraviolet cut-off.

This renormalisation can thus be done non perturbatively from lattice data provided that μ is in the available range for the given lattice spacing a. If this is not the case it is necessary to match the Z_3's with different lattice spacings. To illustrate this let us give an example: if we take $\mu = 4$ GeV it is not possible to compute directly Z_3 for the Wilson gauge action with $\beta = 6.0$ ($a^{-1} = 1.97$ GeV) [4]. We will thus use the results at $\beta = 6.4$ ($a^{-1} = 3.58$ GeV). We then need to compute $Z_3(\mu, 6.0)/Z_3(\mu, 6.4)$. This ratio is independent of μ at leading order. It can thus be computed non perturbatively for momenta in which both lattice spacings provide data. An analytic approach is to rely on the one loop perturbative formula

$$\frac{Z_3(\mu,a')}{Z_3(\mu,a)} = \left(\frac{\beta(a')}{\beta(a)}\right)^{13/22}, \tag{5}$$

which is valid for small enough lattice spacings (in the perturbative regime).

3 The gluon propagator at vanishing momentum

The Adelaide group has performed a systematic study [2] of the gluon propagator in the infinite volume limit. They use the mean-field (tadpole) improved version of the tree-level, $O(a^2)$ Symanzik improved gauge action. They choose a MOM renormalisation at $\mu = 4$ GeV i.e. $G_R^{(2)}(4\,\mathrm{GeV}, \mu = 4\,\mathrm{GeV}) = 1/(4\,\mathrm{GeV})^2$. They fit the volume dependence of the zero momentum gluon propagator on several lattice spacings and lattice volumes up to a volume of 2000 fm^4, with always a

[3] Notice that this theoretically justified 3/4 factor is numerically confirmed as it ensures the continuity of the gluon propagator at $p^2 \to 0$ which will be discussed later on.

[4] It is advisable to keep $p < (\pi/2)\, a^{-1}$.

spatial cubic lattice and a length in the time direction twice the spatial length. Their fitting formula is

$$G_R^{(2)}(0, \mu = 4\,\mathrm{GeV}) = G_{R\infty}^{(2)}(0, \mu = 4\,\mathrm{GeV}) + \frac{c}{V}, \tag{6}$$

and gives

$$G_{R\infty}^{(2)}(0, \mu = 4\,\mathrm{GeV}) = 7.95 \pm 0.13\,\mathrm{GeV}^{-2}, \quad c = 245 \pm 22\,\mathrm{fm}^4\,\mathrm{GeV}^{-2}. \tag{7}$$

This result clearly indicates a finite non vanishing $G_R^{(2)}(0, \mu)$. It is strange that nobody objects to this published result but that, nevertheless, one repeatedly reads that the zero momentum gluon propagator vanishes.

β	V in units of a	bare propagator $G^{(2)}(p, a)$	$1/L$ in GeV
5.7	16^4	16.81 ± 0.13	0.0672
5.7	24^4	15.06 ± 0.29	0.0448
5.8	16^4	19.12 ± 0.16	0.0841
5.9	24^4	18.12 ± 0.30	0.0685
6.0	32^4	17.70 ± 0.59	0.0615
6.0	24^4	19.67 ± 0.35	0.0821

Table 1: Physical lattice sizes and raw data for the gluon propagator at zero momentum $G^{(2)}(p, a)$ from our old data.

This is why, waiting for a systematic and extensive reanalysis, we have simply digged out our old results for the gluon propagator which have been obtained from simulations with the Wilson pure gauge action on hypercubic lattices [3, 4]. Table 1 lists the normalized raw data of the gluon propagator at zero momentum for our largest physical volumes (some of these data have never been published). No rescaling, perturbative (Eq. 5) or non-perturbative, has yet been applied to these data. Our volumes are not very large as this was not the aim of our simulations, and we do not claim our study to be an improvement over ref. [2] but simply an independent check. Using the same renormalisation as ref. [2] we find

$$G_{R\infty}^{(2)}(0, \mu = 4\,\mathrm{GeV}) = 9.1 \pm 0.2 \pm 0.2\,\mathrm{GeV}^{-2}, \quad c = 140 \pm 30 \pm 40\ \mathrm{fm}^4\,\mathrm{GeV}^{-2}. \tag{8}$$

where the first error is statistical and the second is a systematic one estimated from different choices of the fitting points.

More recently ref. [5] provides additional information on the same issue. In their table 2 the authors report fits of the zero momentum gluon propagator as a function of $1/V$, using only data at $\beta = 6.0$ with Wilson gauge action obtained on very anisotropic lattices [5]. The results are given in lattice units and concern bare propagators.

[5] The time length is typically 16 times the spatial one

reference	$G_R^{(2)}(0, \mu = 4\,\mathrm{GeV})$ in GeV^{-2}	c in GeV^{-2} fm^4	max vol in fm^4
[2]	7.95 ± 0.13	245 ± 22	2000
table 1	9.1 ± 0.3	140 ± 50	90
[5]	10.9 - 11.3	47 - 65	110

Table 2: Summary of the infinite volume zero momentum propagator and its slope in terms of $1/V$ for three different simulations. The largest volume used in the fit is also indicated. The statistical error is not quoted in ref [5].

We shall assume, as has been done up to now, that the volume dependence is polynomial in $1/V$ for large volumes. The very asymmetric shape is meant to provide very low values of the momentum ; it is interesting to check whether the zero momentum propagator depends on the geometry. We therefore convert the authors' fit of the 0-momentun propagator to physical units and perform a MOM renormalisation at 4 GeV for which we use $a^{-1}(\beta = 6.0) = 1.97\,\mathrm{GeV}$ and, from our non-perturbative fits :

$$Z_3(4\,\mathrm{GeV}, \beta = 6.0)) = 1.648, \tag{9}$$

and we get

$$\begin{aligned} G_{R\,\infty}^{(2)}(0, \mu = 4\,\mathrm{GeV}) \quad &= \quad 11.3\,\mathrm{GeV}^{-2} \text{ and } 10.9\,\mathrm{GeV}^{-2}, \\ c = 47\,\mathrm{fm}^4\,\mathrm{GeV}^{-2} \quad &\text{and} \quad 65\,\mathrm{fm}^4\,\mathrm{GeV}^{-2}. \end{aligned} \tag{10}$$

where the two results correspond to a linear/quadratic fit in $1/V$ [6]. We do not know the statistical errors.

The results of these three collaborations are summarised in table. 2. Concerning $G_{R\,\infty}^{(2)}(0, \mu = 4\,\mathrm{GeV})$ the three results are in the same ballpark and it may be conjectured that the systematic errors are not all taken into account: $O(a)$ effects, effect of the shape, insufficiently large volumes (for the second and third lines), uncertainty in the estimate of the lattice spacing in physical units, etc. Altogether it seems that, not only there is a clear indication in favor of a finite non vanishing zero momentum gluon propagator, but that different simulations agree on the value. Of course a more extensive study is necessary.

Concerning the slope c the numbers clearly differ, they only agree in order of magnitude and are all positive. We expect that the slope is much more sensitive to systematic effects such as the shape.

We turn now to the second approach, namely a fit of the p^2 dependence of the propagator at small momenta. We first claim that the gluon propagator is continuous and smooth at $p = 0$. This has been observed in several references (see for instance figure 17 in [2]) . This can also be seen in figure 2 in [7].

[6] We are aware that the authors of [5] also use non polynomial fits in $1/V$ which can lead to vanishing or infinite zero momentum propagators. But they have themselves noticed that this destroys the smoothness.

The latter paper also compares the gluon propagator with periodic or twisted boundary conditions and concludes that the twisted propagtor is smaller than the periodic one but that the difference vanishes in the large volume limit. Let us now comment on the fit as a power law ($G^{(2)}(p) \propto (p^2)^{\alpha_G - 1}$) which necessarily discards the zero-momentum. In section 3.1 of ref. [1] we have shown with similar fitting formulae that α_G is compatible with 1 on the examples of $SU(2)$ and $SU(3)$. But we have experienced instabilities and we do not know of any convincing results obtained with this method [7]. This instability may be due to the fact that, if such a power law applies in the small momentum limit, it can only be isolated at very small momenta which have not yet been reached.

4 Conclusions

The renormalised gluon propagator at zero momentum converges, in the infinite volume limit, towards a non vanishing finite value [2] if one uses a volume dependence which is polynomial in $1/V$ independently of the boundary conditions [7]. We have shown that different studies with different gauge actions, different parameters and different shapes of the volume agree rather well on the value of the renormalised gluon propagator while the slopes in $1/V$ agree only in sign and order of magnitude.

No discontinuity of the gluon propagator is seen when the momentum goes to zero. It results that the infrared exponent α_G (often named 2κ) must be equal to 1. We have stressed the instability of the fits of the propagator without the point at $p = 0$ assuming a power law dependence: different fitting functions, which are equivalent in the infrared limit, give incompatible results. If this is duly taken into account in the systematic errors the value $\alpha_G = 1$ lies within the error bars in agreement with the claim about a non vanishing finite gluon propagator at zero momentum.

References

[1] P. Boucaud *et al.*, arXiv:hep-ph/0507104.

[2] F. D. R. Bonnet, P. O. Bowman, D. B. Leinweber, A. G. Williams and J. M. Zanotti, Phys. Rev. D **64** (2001) 034501 [arXiv:hep-lat/0101013].

[3] D. Becirevic, P. Boucaud, J. P. Leroy, J. Micheli, O. Pene, J. Rodriguez-Quintero and C. Roiesnel,

Phys. Rev. D **60** (1999) 094509 [arXiv:hep-ph/9903364].

[7] We do not understand the fits of [6] and we obviously disagree with their conclusion that the zero momentum propagator vanishes.

[4] D. Becirevic, P. Boucaud, J. P. Leroy, J. Micheli, O. Pene, J. Rodriguez-Quintero and C. Roiesnel, Phys. Rev. D **61** (2000) 114508 [arXiv:hep-ph/9910204].

[5] O. Oliveira and P. J. Silva, PoS **LAT2005** (2005) 287 [arXiv:hep-lat/0509037].

[6] P. J. Silva and O. Oliveira,
arXiv:hep-lat/0511043.

[7] T. Tok, K. Langfeld, H. Reinhardt and L. von Smekal, PoS **LAT2005**, 334 (2005) [arXiv:hep-lat/0509134].

Annexe F

Is the QCD ghost dressing function finite at zero momentum ?

JHEP 0606 : 001, (2006)

hep-lat/0604056

Published by Institute of Physics Publishing for SISSA

Received: *April 7, 2006*
Accepted: *May 18, 2006*
Published: *June 5, 2006*

Is the QCD ghost dressing function finite at zero momentum ?

Philippe Boucaud,[a] **Thorsten Brüntjen,**[a] **Jean Pierre Leroy,**[a] **Alain Le Yaouanc,**[a] **Alexey Lokhov,**[b] **Jacques Micheli,**[a] **Olivier Pène**[a] **and Jose Rodriguez-Quintero**[c]

[a] *Laboratoire de Physique Théorique et Hautes Energies*[*]
Université de Paris XI
Bâtiment 211, 91405 Orsay Cedex, France
[b] *Centre de Physique Théorique*[†] *de l'Ecole Polytechnique*
F91128 Palaiseau cedex, France
[c] *Dpto. Física Aplicada, Fac. Ciencias Experimentales*
Universidad de Huelva, 21071 Huelva, Spain
E-mail: Philippe.boucaud@th.u-psud.fr, Thorsten.bruentjen@th.u-psud.fr, Jean-Pierre.Leroy@th.u-psud.fr, Alain.Le-Yaouanc@th.u-psud.fr, lokhov@cpht.polytechnique.fr, Jacques.Micheli@th.u-psud.fr, Olivier.Pene@th.u-psud.fr, jose.rodriguez@dfaie.uhu.es

Abstract: We show that a finite non-vanishing ghost dressing function at zero momentum satisfies the scaling properties of the ghost propagator Schwinger-Dyson equation. This kind of Schwinger-Dyson solutions may well agree with lattice data and provides an interesting alternative to the widely spread claim that the gluon dressing function behaves like the inverse squared ghost dressing function, a claim which is at odds with lattice data. We demonstrate that, if the ghost dressing function is less singular than any power of p, it must be finite non-vanishing at zero momentum: any logarithmic behaviour is for instance excluded. We add some remarks about coupled Schwinger-Dyson analyses.

Keywords: Lattice Gauge Field Theories, QCD, Lattice QCD.

[*] Unité Mixte de Recherche 8627 du Centre National de la Recherche Scientifique
[†] Unité Mixte de Recherche 7644 du Centre National de la Recherche Scientifique

JHEP06(2006)001

Contents

1. Introduction **1**

2. Notations and summary of up-to-date lattice results **2**

3. Ghost SDE: the case $\alpha_F = 0$ **4**

4. Remarks about coupled gluon and ghost SDE solutions **5**

5. Conclusions **6**

1. Introduction

The infrared behaviour of Landau gauge lattice gluon and ghost propagators is an interesting and hot subject. Two main methods are used: lattice QCD (LQCD) and Schwinger-Dyson equations (SDE) in which we include related methods as RGE, etc. In ref. [1] we have shown that a combination of both methods is extremely enlightening as it combines the advantages of lattice QCD's full control of errors and SDE's analytical character.

We only consider the particularly simple ghost propagator SDE :

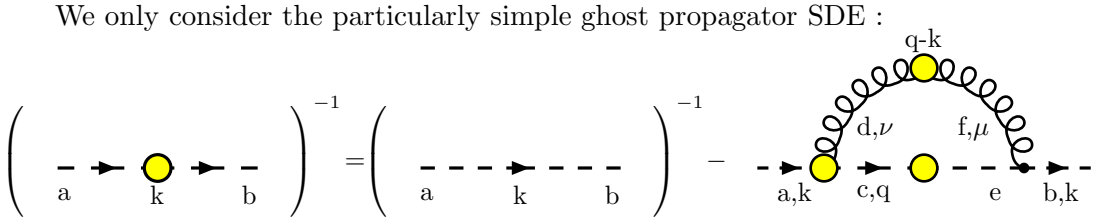

We have studied the discrepancy between LQCD data and a widely spread belief: the ghost propagator SDE is claimed to imply a gluon dressing function behaving like the inverse squared ghost one. In ref. [1] we have reconsidered the scaling properties of the SDE and found three possible ways out of this problem (which are summarised in table 1 of that paper). The first one is to assume a singular behaviour of the ghost-gluon vertex in the deep infrared. A second possibility implies a very singular ghost dressing function which is excluded by LQCD. The third one is to assume that the ghost dressing function is less singular in the infrared that any power of p. In view of the general belief that the ghost dressing function was strongly singular we had not paid in ref. [1] attention to the third one.

Very recently, Sternbeck et al. [2] have produced two new evidences: i) the ghost-gluon vertex seems not to be singular, ii) the ghost dressing function seems to behave at most like $\log p$ in the infrared. These two evidences, taken together, strongly encourage us to consider now seriously the third above-mentioned solution. This is the aim of the present letter.

JHEP06(2006)001

To our surprise we found that one can *demonstrate* from the scaling analysis of the ghost propagator SDE the impossibility of a $\log p$ behaviour or any other behaviour which is less divergent than any power of p: under these conditions, the ghost dressing function necessarily has a *finite non-vanishing* limit at zero momentum. This is at odds with a very general belief that the ghost dressing function is divergent. The proof will be displayed in section 3. We will shortly discuss published results about coupled gluon and ghost SDE in section 4.

2. Notations and summary of up-to-date lattice results

We use the following notations [1]:

$$\begin{aligned}
\widetilde{\Gamma}_\mu(-q,k;q-k) &= q_\mu H_1(q,k) + (q-k)_\mu H_2(q,k) \\
\left(F^{(2)}\right)^{ab}(k^2) &= -\delta^{ab}\,\frac{F(k^2)}{k^2} \\
\left(G^{(2)}_{\mu\nu}\right)^{ab}(k^2) &= \delta^{ab}\,\frac{G(k^2)}{k^2}\left(\delta_{\mu\nu} - \frac{k_\mu k_\nu}{k^2}\right),
\end{aligned} \tag{2.1}$$

where $G^{(2)}$ and $F^{(2)}$ are respectively the gluon and ghost propagators, G and F are respectively the gluon and ghost dressing functions and where $\widetilde{\Gamma}_\mu(-q,k;q-k)$ is the ghost-gluon vertex (k and q are the momenta of the incoming and outgoing ghosts and $q-k$ the momentum of the gluon) .

Following for simplicity the common, convenient, but not really justified, assumption of a power-law behaviour of the propagators in the deep infrared, we define

$$F(k^2) \sim \left(\frac{k^2}{\nu}\right)^{\alpha_F},\ G(k^2) \sim \left(\frac{k^2}{\lambda}\right)^{\alpha_G}. \tag{2.2}$$

In ref. [1] we have also defined an infrared exponent α_Γ for the vertex funtion H_1 ($\alpha_\Gamma < 0$ means a singular infrared behaviour).

Using the ghost propagator SDE equation it is often claimed that $2\alpha_F + \alpha_G = 0$. This belief is so strong that one often uses only one parameter $\kappa = -\alpha_F = \alpha_G/2$. However, as we will see in more details, everybody agrees that α_G is close [1] to 1 and it becomes now clear [2] that α_F is close to zero. Then *the relation* $2\alpha_F + \alpha_G = 0$ *is not satisfied [1, 2] and the arguments which support it have to be reconsidered.*

The lattice gluon propagator. Several SDE studies ([3] and references therein) predict a vanishing zero momentum propagator while, as discussed in ref. [4], a gluon propagator converging continuously to a non-zero value at vanishing momentum is a rather general

[1] For example, in many SDE approaches it is found [3] $\alpha_G \simeq 1.18$

[2] One may wonder why many power law fits have given negative α_F. Our own fit in ref.[1] (table 2) has produced negative values very close to zero, but the errors were clearly underestimated. Presumably the systematic one, due to the functional form chosen for the fit, has not been properly taken into account. This is also the case in several other published results.

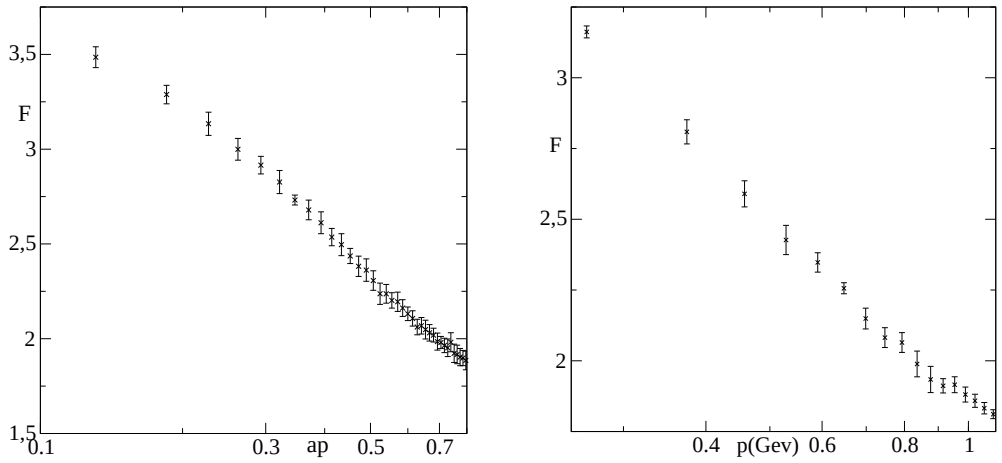

Figure 1: $F(p)$ from lattice simulations for SU(2) (left, $Vol = 48^4$, $\beta = 2.3$) and SU(3) (right,$Vol = 32^4$, $\beta = 5.8$). Logarithmic scales are used for x-axis in both plots. $\beta = 2.3$ for SU(2) has been chosen to guarantee that the string tension in lattice units is close to that of $\beta = 5.8$ for SU(3).

lattice result (in particular, the authors of ref. [5] obtain a non-vanishing infrared limit for the gluon propagator at a lattice volume of around 2000 fm^4). Therefore our preferred solution [3] is

$$\alpha_G = 1. \tag{2.3}$$

But, even if we relax this relation and assume a vanishing gluon propagator with $\alpha_G > 1$, the solution with a finite ghost dressing function at zero momentum remains possible as we shall see.

The lattice ghost propagator. The infrared behaviour of the ghost dressing function estimated from lattice simulations is a current controversial subject (see [7] and references therein). Very recent lattice estimates [2] seem to point towards a ghost dressing function rather close to the perturbative behaviour: the dressing function only shows, if any, a logarithmic dependence on the momentum (see ref. [2, figure 2]).

We confirm these results. In figure 1 the ghost dressing function is plotted as a function of $\log(p)$ for small values of the momenta. These plots were obtained from lattice simulations at $\beta = 5.8$ and a volume 32^4 in the SU(3) case and at $\beta = 2.3$ and a volume 48^4 in the SU(2) case. It is clear from these plots that $F(p)$ does not exhibit any power law: $\alpha_F = 0$. For SU(3) $F(p)$ is approximately linear in $\log(p)$ and for SU(2) it has even a smoother behavior (In this case one obtains a good fit of the data with a function $C(\log|p|)^\gamma$ and $\gamma \approx 0.4$).

The ghost-gluon vertex. In ref. [2], the authors did not find any evidence for a singularity in the case of a vanishing gluon momentum. Let us remark that this particular

[3] Let us recall however that there is still a problem coming from the Slavnov-Taylor identity for the three gluon-vertex: we have shown that, the vertices being regular when one momentum tends to zero, it implies $\alpha_G < 1$. Is it possible to avoid any contradiction by assuming, as done by Cornwall [6], a non-regular behaviour for the longitudinal part of the three-gluon vertex? This deserves more investigation.

kinematical configuration isolates the form factor H_1 (see Eq.(2.1)) which enters in the SD equation (It is worth recalling that in perturbation theory $H_1(q,0) + H_2(q,0)$ is equal to 1 although $H_1(q,0)$ is not [8]). Our dimensional analysis of the ghost SDE (see next section 3) invokes a different kinematical configuration for this form factor, $H_1(q, k \to 0)$ instead of $H_1(k,k)$. The non-singular behaviour they found as k tends to 0 excludes however the singularity of the ghost-gluon vertex that we proposed in ref. [1] as our favoured solution to reconcile the ghost propagator SDE and the lattice inspired relation $2\alpha_F + \alpha_G > 0$.

In conclusion lattice simulations show a strong evidence that $\alpha_G = 1$ and $2\alpha_F + \alpha_G > 0$, far from zero. Now we have a fair indication that $\alpha_F = 0$ and about the regularity of the vertex form factor involved in the ghost SDE. This leads us to revisit, in next section, the case in column 4 of table 1 in ref. [1] for ghost and gluon propagators and vertices satisfying the scaling properties of ghost SDE.

3. Ghost SDE: the case $\alpha_F = 0$

We will now demonstrate that $F(0)$ is finite non-vanishing for $\alpha_F = 0$. We will exploit the constraints, summarized in table 1 of ref. [1], between the infrared exponents α_F, α_G, α_Γ, from the ghost SDE. The IR convergence of the loop integral in the ghost SDE implies the two conditions:

$$\alpha_F + \alpha_\Gamma > -2 \ , \ \alpha_G + \alpha_\Gamma > -1 \ . \tag{3.1}$$

Then the dimensional consistency of ghost SDE at small momenta leads to only three allowed cases:

i) $\alpha_F \neq 0$ and $\alpha_F + \alpha_G + \alpha_\Gamma < 1 \Longrightarrow 2\alpha_F + \alpha_G + \alpha_\Gamma = 0$

ii) $\alpha_F \neq 0$ and $\alpha_F + \alpha_G + \alpha_\Gamma \geq 1 \Longrightarrow \alpha_F = -1$

iii) $\alpha_F = 0$ and $\alpha_G + \alpha_\Gamma \geq 1$ does not require any further constraint.

We shall look, in the following, at the consequences of the third case. It includes in particular $\alpha_G = 1$ and $\alpha_\Gamma = 0$ which is favoured by lattice simulations (see section (2)). Nevertheless we shall not suppose, in the following derivation, anything more than $\alpha_G + \alpha_\Gamma \geq 1$ and conditions (3.1). This leaves open, for example, the possibility that the gluon propagator goes to zero in the IR limit, the vertex remaining finite or singular.

Of course, even with $\alpha_F = 0$, we cannot exclude *a priori* the possibility that $F(k)$ diverges or tends to zero more slowly than any power of k when $k \to 0$. We shall however prove that this is not allowed: $F(k)$ remains finite in this limit provided that the two following conditions are satisfied:

$$\alpha_F = 0 \ , \ \alpha_G + \alpha_\Gamma \geq 1 \tag{3.2}$$

Writing the subtracted bare SD equation for two scales λk and $\kappa\lambda k$ (see ref. [1, eq. (14)]) one obtains:

$$\frac{1}{F(\lambda k)} - \frac{1}{F(\kappa\lambda k)} = g_B^2 N_c \int \frac{d^4q}{(2\pi)^4} \left(\frac{F(q^2)}{q^2} \left(\frac{(k\cdot q)^2}{k^2} - q^2 \right) \right.$$

$$\times\left[\frac{G((q-\lambda k)^2)H1(q,\lambda k)}{(q-\lambda k)^2}-\frac{G((q-\kappa\lambda k)^2)H1(q,\kappa\lambda k)}{(q-\kappa\lambda k)^2}\right]\Bigg)\,, \tag{3.3}$$

where λ is a parameter which we shall use to study the IR ($\lambda \to 0$) dimensional behaviour of F; κ is a fixed number, $0 < \kappa < 1$, needed to write a subtracted equation ensuring the UV convergence. It was shown in ref. [1] that the r.h.s. of eq. (3.3) is the sum of two terms behaving respectively as $\lambda^{2\mathrm{Min}(\alpha_F+\alpha_G+\alpha_\Gamma,1)}$ and λ^2 when $\lambda \to 0$. So it behaves as λ^2 when the conditions (3.2) are satisfied. For any κ there is a value of λ and c such that $\forall\lambda' \leq \lambda$ we have $|\frac{1}{F(\lambda' k)} - \frac{1}{F(\kappa\lambda' k)}| \leq c\lambda'^2$, thus:

$$\begin{aligned}\left|\frac{1}{F(\lambda k)}-\frac{1}{F(\kappa\lambda k)}\right| &\leq c\lambda^2\\ &\vdots\\ \left|\frac{1}{F(\kappa^{n-1}\lambda k)}-\frac{1}{F(\kappa^n\lambda k)}\right| &\leq c\lambda^2\kappa^{2(n-1)}\end{aligned} \tag{3.4}$$

which implies:

$$\left|\frac{1}{F(\lambda k)}-\frac{1}{F(\kappa^n\lambda k)}\right| \leq c\frac{1-\kappa^{2n}}{1-\kappa^2}\lambda^2. \tag{3.5}$$

So $F \to \infty$ when $\lambda \to 0$ is excluded because taking the limit of the above expression when $n \to \infty$ we should have $|\frac{1}{F(\lambda k)}| \leq c\frac{1}{1-\kappa^2}\lambda^2$ and F would diverge as or more rapidly than $\frac{1}{\lambda^2}$ implying $\alpha_F \leq -1$ in contradiction with the hypothesis $\alpha_F = 0$. Let us remark that $F \to 0$ is also excluded: Eq. (3.5) implies $|\frac{1}{F(\kappa^n\lambda k)}| \leq |\frac{1}{F(\lambda k)}| + c\frac{1-\kappa^{2n}}{1-\kappa^2}\lambda^2$ and $\frac{1}{F(\kappa^n\lambda k)}$ cannot tend to infinity when $n \to \infty$. This completes the proof. Notice that we have used bare Green functions and couplings, everything remains however exactly the same if we replace them by renormalized ones.

This is our main result: If $\alpha_F = 0$ the ghost dressing function has to be finite and $\neq 0$ in the IR limit. This solution is compatible with our knowledge from lattice simulations about the behavior of the ghost dressing function and ghost-gluon vertex. Of course, the current lattice simulations cannot yet exclude a smooth divergence which the preceding dimensional analysis forbids. A detailed numerical study of the ghost propagator in the deep IR is strongly needed.

4. Remarks about coupled gluon and ghost SDE solutions

The combination of the scaling analysis of ghost SDE and lattice predictions appears to be very restrictive concerning the low-momentum behaviour of gluon and ghost propagators. Such a behaviour must be a solution of the combined SDE for both gluon and ghost propagators. The schemes followed to solve the combined SDE's have often led to $2\alpha_F + \alpha_G = 0$ and $\alpha_G \gtrapprox 1$ (hence a strongly divergent ghost dressing function). However, a two-loop analysis [9] proves to be much less restrictive in constraining α_G. Our findings require to reconsider these approaches by taking into due account the special case $\alpha_F = 0$.

In a recent paper [10] Aguilar and Natale found $\alpha_G = 1$ and $\alpha_F = -0.04$, not far from our present conclusions and deserving a closer comparison. They followed the Cornwall [6]

lattice	m_0 (GeV)	$Z_b(a)$
5.6 (24^4)	0.523(2)	3.69(1)
5.7 (32^4)	0.527(1)	3.85(1)
5.8 (24^4)	0.493(7)	3.88(3)
6.0 (32^4)	0.503(4)	3.99(2)
6.0 (24^4)	0.461(16)	3.97(6)

Table 1: Best-fit parameters.

prescription for the trilinear gluon vertex and solved the coupled equations for the ghost and gluon propagators in the Mandelstam approximation [11]. Concerning the ghost dressing function, in spite of the fact that they find it slowly power-like divergent, it remains flat till very small momenta. This last point is in contradiction with the lattice results in ref. [2] and ours in figure 1, where $F(k)$ is not at all so flat and shows a logarithmic enhancement as the momentum decreases. Of course, if power-like divergences are excluded, the arguments presented in section 3 imply a flat dressing function in a small momentum range presumably not yet reached by current lattice analyses.

To compare quantitatively their gluon propagator with LQCD [12], we have applied the simple parametrization they proposed:

$$G^{(2)}_{\rm bare}(q^2;a,L) = \frac{Z_b(a)}{q^2 + \frac{m_0(L)^4}{q^2+m_0(L)^2}} + \mathcal{O}(a,1/L) \ , \tag{4.1}$$

where a stands for the lattice spacing and L for the lattice length. In refs. [12], the gluon propagator was estimated from 24^4 lattices at $\beta = 5.6, 5.8, 6.0$ and 32^4 lattices at $\beta = 5.7$ and $\beta = 6.0$ and analyzed through OPE or instanton liquid models that failed in describing the very low momentum range ($q < 0.4$GeV). In figure 2, we plot the curves corresponding to the best-fit parameters m_0 and Z_b collected in table 1. The parametrization eq. (4.1) matchs pretty well the lattice data [4]. Moreover one knows that, at the leading log,

$$d(\log(Z_b(a)) = \frac{13}{22} d(\log\beta) \ . \tag{4.2}$$

Performing a linear fit of $\log(Z_b)$ as a function of $\log(\beta)$ for $\beta \geq 5.7$ we obtain a slope approximately equal to 0.69 which has to be compared to $\frac{13}{22} = 0.59$. That result is unexpectedly good for the large lattice spacings we take in consideration.

5. Conclusions

The main result we presented in this brief note was to emphasize the interest of a general class of SDE solutions where $\alpha_F \approx 0$. This solution has the advantage of being compatible with other convincing lattice results namely: $\alpha_G = 1$ and $2\alpha_F + \alpha_G > 0$. It is also

[4] The masses we obtain differ from the one quoted in ref. [10] but these depend on a parameter, Λ, which in their approach can be varied.

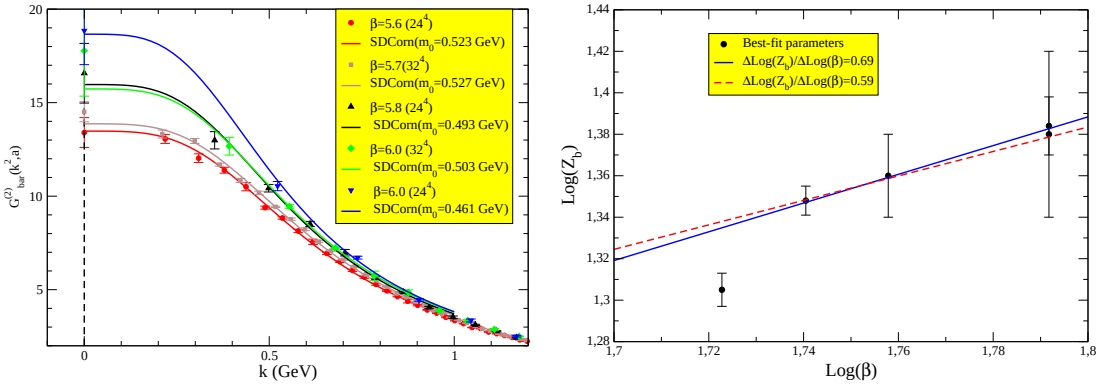

Figure 2: Best fits to the lattice data (left) and Log-log plot of Z_b in terms of the lattice bare gauge coupling parameter β (right). The solid blue (dotted red) line shows a fit to a linear formula where the slope is free to be fitted (fixed by one-loop perturbation theory in eq. (4.2)).

compatible with a still uncertain result concerning the regularity of the ghost-gluon vertex. We have proven that if $\alpha_F = 0$ the ghost dressing function must be finite in the IR limit. Of course one would need measures on larger volumes in order to test the finiteness of the ghost propagator in the limit $k \to 0$.

We have discussed some results from published coupled ghost and gluon SDE solutions and also shown that the lattice gluon propagator data at low momenta can be well described by the very simple parametrisation eq. (4.1) inspired by a recent gluon SDE analysis.

Acknowledgments

J.R.Q. is indebted to C. Aguilar and J. Papavasssiliou for illuminating discussions. This work was partially supported by spanish regional research program FQM-318 and CICYT FPA-2003-05598.

References

[1] P. Boucaud et al., *The infrared behaviour of the pure Yang-Mills green functions*, `hep-ph/0507104`;
A.Y. Lokhov et al., *Non-perturbative approach to the Landau gauge gluodynamics*, `hep-lat/0601007`.

[2] A. Sternbeck, E.M. Ilgenfritz, M. Muller-Preussker and A. Schiller, *Landau gauge ghost and gluon propagators and the Faddeev-Popov operator spectrum*, *Nucl. Phys.* **153** *(Proc. Suppl.)* (2006) 185 [`hep-lat/0511053`].

[3] R. Alkofer and L. von Smekal, *The infrared behavior of QCD Green's functions: confinement, dynamical symmetry breaking and hadrons as relativistic bound states*, *Phys. Rept.* **353** (2001) 281 [`hep-ph/0007355`].

[4] P. Boucaud et al., *Short comment about the lattice gluon propagator at vanishing momentum*, `hep-lat/0602006`.

[5] F.D.R. Bonnet, P.O. Bowman, D.B. Leinweber, A.G. Williams and J.M. Zanotti, *Infinite volume and continuum limits of the Landau-gauge gluon propagator*, *Phys. Rev.* **D 64** (2001) 034501 [hep-lat/0101013].

[6] J.M. Cornwall, *Dynamical mass generation in continuum quantum cromodynamics*, *Phys. Rev.* **D 26** (1982) 11453;
J.M. Cornwall and J. Papavassiliou, *Gauge-invariant three-gluon vertex in QCD*, *Phys. Rev.* **D 40** (1989) 3474.

[7] S. Furui and H. Nakajima, *Effects of the quark field on the ghost propagator of lattice Landau gauge QCD*, *Phys. Rev.* **D 73** (2006) 094506 [hep-lat/0602027].

[8] K.G. Chetyrkin and A. Retey, *Three-loop three-linear vertices and four-loop MOM beta functions in massless QCD*, hep-ph/0007088.

[9] J.C.R. Bloch, *Two-loop improved truncation of the ghost-gluon dyson- schwinger equations: multiplicatively renormalizable propagators and nonperturbative running coupling*, *Few Body Syst.* **33** (2003) 111–152 [hep-ph/0303125];
J.C.R. Bloch, A. Cucchieri, K. Langfeld and T. Mendes, *Propagators and running coupling from* SU(2) *lattice gauge theory*, *Nucl. Phys.* **B 687** (2004) 76 [hep-lat/0312036].

[10] A.C. Aguilar and A.A. Natale, *A dynamical gluon mass solution in Mandelstam's approximation*, *Int. J. Mod. Phys.* **A 20** (2005) 7613 [hep-ph/0405024]; *A dynamical gluon mass solution in a coupled system of the Schwinger-Dyson equations*, *JHEP* **08** (2004) 057 [hep-ph/0408254].

[11] S. Mandelstam, *Approximation scheme for QCD*, *Phys. Rev.* **D 20** (1979) 3223.

[12] P. Boucaud et al., *Evidences for instantons effects in Landau lattice green functions*, *Phys. Rev.* **D 70** (2004) 114503 [hep-ph/0312332];
P. Boucaud et al., *Testing Landau gauge ope on the lattice with a* $\langle a^2 \rangle$ *condensate*, *Phys. Rev.* **D 63** (2001) 114003 [hep-ph/0101302].

Resumé

Une étude non-perturbative des corélateurs en QCD est présentée. La méthode principale employée est la simulation numérique sur réseau. Cet outil a été largement utilisé en phénoménologie, mais il peut aussi servir pour étudier les paramètres fondamentaux de la théorie (tels que la constante de couplage) et ses propriétés fondamentales. Ceci est le but principal de la présente thèse. Nous avons étudié les fonctions de corrélation de la théorie Yang-Mills pure en jauge de Landau, notamment les propagateurs du gluon et du fantôme. Nous nous sommes particulièrement intéressés au paramètre $\Lambda_{\rm QCD}$ qui est extrait à l'aide des prédictions de la théorie des perturbations (jusqu'à l'ordre NNNLO). Les corrections dominantes en puissance sont aussi considérées, nous montrons qu'elles sont importantes même à des énergies assez grandes (de l'ordre de 10 GeV). Une méthode de soustraction de ces termes correctifs est proposée, ce qui permet une meilleur estimation de $\Lambda_{\rm QCD}$. Notre résultat final est $\Lambda_{\overline{\rm MS}}^{nf=0} = 269(5)^{+12}_{-9}$ MeV. Une autre question que nous considéons est celle du comportement infrarouge des fonctions de Green (aux énergies de l'ordre de ou inférieur à $\Lambda_{\rm QCD}$). A ces énergies le comportement des fonctions de Green change de manière radicale, et cela est probablement lié au confinement. Nous cherchons à clarifier la nature de ces changements afin de comprendre ses origines. Beaucoup de questions se posent: l'ambiguïté de Gribov, la portée de diverses relations non-perturbatives entre les fonctions de Green, la cohéence de l'approche nuérique aux petites énergies. Les simulations sur réseau permettent de vérifier les prédicitons analytiques, elles donnent accès aux corrélateurs non-perturbatifs. Notre analyse suggère que le propagateur du gluon est fini et non nul dans l'infrarouge, et que le comportement en puissance du propagateur du fanôme est le même que dans le cas libre.

Mots-clés: Chromodynamique quantique en jauge de Landau - méthodes non-perturbatives - constante de couplage - fonctions de Green - equations de Schwinger-Dyson

Abstract

This PhD dissertation is devoted to a non-perturbative study of QCD correlators. The main tool that we use is lattice QCD. Lattice QCD has been successfully used in phenomenology, but it can also be used to study the fundamental parameters (like the coupling constant) and properties of the theory itself. This is the main goal of the present dissertation. We concentrated our efforts on the study of the main correlators of the pure Yang - Mills theory in the Landau gauge, namely the ghost and the gluon propagators. We are particularly interested in determining the $\Lambda_{\rm QCD}$ parameter -the fundamental scale of the pure Yang-Mills theory. It is extracted by means of perturbative predictions available up to NNNLO. The related topic is the influence of non-perturbative effects that show up as appearance of power-corrections to the low-momentum behaviour of the Green functions. We shall see that these corrections are quite important up to energies of the order of 10 GeV. A new method of removing these power corrections allows a better estimate of $\Lambda_{\rm QCD}$. Our result is $\Lambda_{\overline{\rm MS}}^{n_f=0} = 269(5)^{+12}_{-9}$ MeV. Another question that we address is the infrared behaviour of Green functions, at momenta of order and below $\Lambda_{\rm QCD}$. At low energy the momentum dependence of the propagators changes considerably, and this is probably related to confinement. We try to clarify the laws that govern the infrared gluodynamics in order to understand the radical nature of the changes in the infrared behaviour. Many questions arise: the Gribov ambiguity, the impact of different non-perturbative relations at low momenta, self-consistency of the lattice approach in this domain. The lattice approach allows to check the predictions of analytical methods because it gives access to non-perturbative correlators. According to our analysis the gluon propagator is finite and non-zero at vanishing momentum, and the power-law behaviour of the ghost propagator is the same as in the free case.

Keywords: Quantum chromodynamics in Landau gauge - non-perturbative methods - coupling constante - Green functions - Schwinger-Dyson equations